

RESERVOIR CHARACTERIZATION OF THE HIBERNIA
FORMATION, JEANNE D'ARC BASIN,
GRAND BANKS, NEWFOUNDLAND

CENTRE FOR NEWFOUNDLAND STUDIES

**TOTAL OF 10 PAGES ONLY
MAY BE XEROXED**

(Without Author's Permission)

ERKAN FIDAN



**RESERVOIR CHARACTERIZATION OF THE HIBERNIA FORMATION,
JEANNE D'ARC BASIN, GRAND BANKS, NEWFOUNDLAND**

by

ERKAN FIDAN

**A thesis submitted to the
School of Graduate Studies
in partial fulfilment of the
requirements for the degree of
Master of Science**

**Department of Earth Sciences
Memorial University of Newfoundland**

July 1996

St. John's

Newfoundland



National Library
of Canada

Acquisitions and
Bibliographic Services Branch

395 Wellington Street
Ottawa, Ontario
K1A 0N4

Bibliothèque nationale
du Canada

Direction des acquisitions et
des services bibliographiques

395, rue Wellington
Ottawa (Ontario)
K1A 0N4

Your file - votre référence

Our file - Notre référence

The author has granted an irrevocable non-exclusive licence allowing the National Library of Canada to reproduce, loan, distribute or sell copies of his/her thesis by any means and in any form or format, making this thesis available to interested persons.

L'auteur a accordé une licence irrévocable et non exclusive permettant à la Bibliothèque nationale du Canada de reproduire, prêter, distribuer ou vendre des copies de sa thèse de quelque manière et sous quelque forme que ce soit pour mettre des exemplaires de cette thèse à la disposition des personnes intéressées.

The author retains ownership of the copyright in his/her thesis. Neither the thesis nor substantial extracts from it may be printed or otherwise reproduced without his/her permission.

L'auteur conserve la propriété du droit d'auteur qui protège sa thèse. Ni la thèse ni des extraits substantiels de celle-ci ne doivent être imprimés ou autrement reproduits sans son autorisation.

ISBN 0-612-17593-6

Canada

ABSTRACT

The offshore Hibernia oil field, discovered in 1979, 315 km (195 mi) southeast of St. John's, Newfoundland, has estimated recoverable oil of 83 million m³ (525 million bbl). Sediments of the Hibernia oil field occur within the northeast trending Jeanne d'Arc rift basin (JDB), which records two rift phases, each followed by a period of post-rift thermal subsidence. Reservoir sands in the Hibernia oil field were deposited during the second intense episode of rifting between Callovian and Early Aptian times.

The Hibernia Formation is Berriasian to Valanginian age and accommodates 85% of the recoverable oil in the Hibernia oil field. The formation is encountered within the average depth interval of 3,400 and 4,200 m. Sandstones of the Hibernia Formation were deposited in a fluvially-dominated deltaic complex and are composed of very fine- to coarse-grained, partially argillaceous quartzarenites and sublitharenites. Porosities (ϕ) range between 4% and 24.2% and permeabilities (k) between 0.01 mD to 9860 mD.

This study, of petrographic lithofacies, log character and response, and engineering data, evaluates Core Lab statistical analysis of porosity and permeability to define "hydraulic flow units" and Canadian Hunter's methodology of petrographic analysis to relate to flow units. Development of drainage character is a crucial process for maximizing hydrocarbon production. Permeability is a crucial parameter which defines the rate of fluid flow, and separate flow units in a reservoir. Permeability is highly variable as

a complex function of petrophysical and depositional properties which must be identified on the scale of microscopic lithofacies and macroscopic facies associations. "Hydraulic flow units" of the Hibernia Formation reflect highly variable plug permeability data. Definition of flow units by means of k - ϕ cross plots distinguish broad variations.

Three general k - ϕ clusters can be defined using k - ϕ cross plots. A concept of "*Enhanced Textural Maturity Index (ETMI)*" relating sorting and roundness is developed. The *ETMI* shows strong correlation with permeability. "*Reservoir Quality Zones (RQZ)*" are defined based on facies analysis, SEM/EDS, thin section petrography, and k - ϕ attributes. Anomalies contributing to a scattered data pattern are addressed. It is shown that facies architecture of the reservoir (i.e., the "mix" of lithofacies) is critical to effective interpretation. Integrated log suites and *RQZ* permit estimation of average horizontal permeability ranges in uncored sections when the availability of drill cuttings is restricted or non-existent. By using *RQZ* as a template in the Hibernia Formation a multi-parameter reservoir modelling and cell characterization in the model can be achieved.

Individual depositional models have inherent k - ϕ relationships. The assemblage models in the stratigraphic package and overprinting of diagenetic effects serve notice that neither geological nor engineering data can be left out of the equation if accurate characterization is to be expected.



ACKNOWLEDGEMENTS

I would like to extend my sincere thanks and appreciation to my supervisor, Dr. John Harper. His continuous encouragements, wisdom, and insight motivated me to earn my degree. He was constructive, helpful, and available at all times.

I am grateful to Hibernia Management and Development Company for their generous help and continuous support throughout this study. I also wish to thank the administration of Canada-Newfoundland Offshore Petroleum Board for providing me with unlimited access to the core storage facility, and wish to thank Canadian Hunter for allowing Mr. Howard King to assist me on reservoir analysis procedures.

The completion of this study would not have been possible without love and support of my son, Arman, my wife Sandra, and my family in Türkiye. That's why, this thesis is dedicated to them.

Table of Contents

	Page
Abstract	ii
Acknowledgements	iv
List of tables	viii
List of figures	ix
I <u>Introduction</u>	1
I.1- Thesis objectives	4
I.2- Methodology	5
I.3- Previous work	7
I.3.1- Statement of the problem	7
I.3.2- Analytical hydraulic flow unit zonation	9
II <u>Regional geology</u>	15
II.1- Tectonic setting	15
II.1.1- Tectonic history and stratigraphy of the Jeanne d'Arc basin	15
II.1.2- Geologic setting of the Hibernia oil field	18
II.2- Depositional characteristics of the Hibernia Formation	23
III <u>Conventional core descriptions</u>	25
III.1- Introduction	27
III.2- Facies groups in Hibernia sandstones	27
III.2.1- Sandstone-dominated facies	27
III.2.2- Interstratified shale, siltstone, and sandstone facies	33
III.2.3- HF4 - Loose and carbonaceous shales/soil zones	34

III.2.4- HF5 - Shelly, churned, and well-burrowed shales	35
III.3- Interpretation of all lithofacies	35
IV SEM microphotography and EDS elemental analysis	48
IV.1- Methodology	48
IV.2- Standardless SEMI-Quantitative Analysis (SSQ)	49
IV.2.1- Analyzing irregularly-shaped bulk specimens and geometric effects	49
IV.2.2- Non-detectables and pseudo-detections	50
IV.2.3- The analysis	51
V Thin section petrography	93
V.1- Introduction and objectives	93
V.2- Descriptions	95
V.2.1- Petrography of the sand-based lithofacies	95
V.2.2- Petrography of the interstratified shale/silt/sandstone facies	103
V.3- Summary and interpretation of thin sections	105
V.3.1- Summary of thin section petrography	105
V.3.2- Interpretation and conclusions of thin section petrography	105
VI Interpretations and application	121
VI.1- Interpretations	121
VI.1.1- Assessment of flow capabilities in hydraulic flow units and lithofacies	121
VI.1.2- Assessment of k-reduction by k-vertical (k_v) vs k-horizontal crossplots (k_h)	128
VI.1.4- Si/Al ratio-permeability relationship	130
VI.1.5- ETMI-permeability relationship	131

VI.1.6- Evaluation of the lithofacies and hydraulic flow unit (HU)	
distribution	131
VI.2- Interpretation of reservoir quality based on multi-parameter	
integration	134
VI.2.1- Identification of the Reservoir Quality Zones (RQZ) in the composite core	
plug data	134
VI.2.2- Comparison of the RQZ to the HMDC hydraulic flow units (HU)	140
VI.2.3- Estimation of the RQZ in the uncored sections	143
VII <u>Summary Interpretation and Implications</u>	145
VIII <u>Conclusions</u>	148
IX <u>References</u>	151
Appendix I. Core analyses and grain size logs of Hibernia B-08,	
B-27, C-96, K-18, and K-14	157
Appendix II. Gamma ray - lithofacies correlation and core depth-log	
depth corrections	183
Appendix III. Beam-spot mode analyses of SEM/EDS-coupled technique	205
Appendix IV. Porosity/permeability/facies distribution graphs of	
Hibernia B-08, B-27, K-18, K-14, and C-96	211
Appendix V. 3D crossplots of hydraulic flow unit - lithofacies, and	
hydraulic flow unit - RQZ distribution in Hibernia B-08,	
B-27, K-18, K-14, and C-96	217
Enclosure	227

List of Tables

	Page
Table 1. Wells in the Hibernia oil field	3
Table 2: Hibernia lithofacies and their descriptive features	26
Table 3. Elemental detections of X100 mag. surface-scan mode analyses	52
Table 4: Chemical compositions of minerals detected in the SEM/EDS analysis	58
Table 5: ETMI calculations based on sorting and roundness	94
Table 6a&b: Relationship between ETMI and other rock characteristics of facies	97-98
Table 7a&b: Hibernia lithofacies and some of their descriptive features	125
Appendix 4: Distinct mineralogies determined by the beam-spot mode analyses during the EDS process	205-210

Table of Figures

Figure	Page
1. The Hibernia oil field and sediment thickness map of the Jeanne d'Arc Basin	2
2. Composite porosity/permeability/facies relationship of Hibernia C-96	8
3. Histogram of the FZI distribution in the Hibernia Formation	13
4. HU-superimposed distribution of the porosity/ permeability data in the Hibernia Formation	14
5. Generalized stratigraphy of the Jeanne d'Arc Basin	17
6. Basement structure of the Hibernia oil field	19
7a. SW-NE cross-section of the Hibernia oil field	20
7b. S-N cross-section of the Hibernia oil field	21
7c. W-E cross-section of the Hibernia oil field	22
8. Facies associations in the Hibernia Formation	28
9a - 9p. Core photographs of lithofacies in the Hibernia Formation	40-47
10a. Composite porosity-permeability relationship of the SEM/EDS-treated specimens	53
10b. Si/Al ratio-permeability graph of SEM/EDS-treated specimens	53
10c. Al-permeability relationship of the SEM/EDS-treated specimens	54
10d. Mg-permeability relationship of the SEM/EDS-treated specimens	54

10e	K-permeability relationship of the SEM/EDS-treated specimens	55
10f	Ca-permeability relationship of the SEM/EDS-treated specimens	55
10g	Fe-permeability relationship of the SEM/EDS-treated specimens	56
10h	Na-permeability relationship of the SEM/EDS-treated specimens	56
10i	Cl-permeability relationship of the SEM/EDS-treated specimens	57
10j	Ti-permeability relationship of the SEM-EDS-treated specimens	57
11a - 11d	Typical spectra of mineralogies detected in the EDS analyses	59-62
12	SEM/EDS-derived mineralogic and diagenetic attributes on composite porosity/permeability data	69
13 - 35	SEM photomicrographs of the lithofacies in the Hibernia Formation	70-92
36 - 47	Thin section photograph of the lithofacies in the Hibernia Formation	112-120
48	Enhanced Textural Maturity Index- Permeability crossplot	110
49	Results of thin section analyses on composite porosity, permeability, facies crossplot	111
50	Integrated results on composite porosity/ permeability/facies crossplot	124
51	Vertical permeability - horizontal permeability relationship and crossplots	129
52	Composite 3D hydraulic flow unit - lithofacies distribution	133
53	Reservoir quality zones in the composite porosity/permeability/facies crossplot .	136
54	Hydraulic flow unit - RQZ relationship	141
55	Composite 3D hydraulic flow unit - RQZ distribution	142

	vi
56. RQZ template of the Hibernia Formation	144
Appendix I: Legend and grain size logs of Hibernia wells described in the related cores	158-182
Appendix II: Gamma-ray log-lithofacies correlations	184-204
Appendix IV: Core porosity/permeability/lithofacies distribution crossplots of the 5 Hibernia wells (B-27, B-O8, C-96, K-18, and K-14)	212-216
Appendix V: Va1-Va5: Hydraulic unit - lithofacies distribution crossplots of the 5 Hibernia wells	218-222
Vb1-Vb5: Hydraulic unit - reservoir quality zone (RQZ) distribution crossplots of the 5 Hibernia wells	223-227
Enclosure (SW - NE cross section with adjusted core intervals).....	228

I - INTRODUCTION

The Hibernia oil field was discovered offshore in 1979 approximately 315 km (195mi) east-southeast of St John's in the Grand Banks (Figure 1).

Following the discovery of Hibernia P-15 by Chevron, nine subsequent wells were drilled between 1980 and 1984 to delineate the field (Table 1). Information from those ten wells revealed that 58 metres of oil-bearing Upper Jurassic/Lower Cretaceous-aged sands were estimated to contain 83 million m³ (525 million bbl) of recoverable crude oil (Hurley *et al.* 1992). Primary reservoir sands containing 85% of the recoverable oil are in the Berriasian-to Valanginian-aged Hibernia Formation (Hurley *et al.* 1992). Conventional core descriptions indicate that the Hibernia Formation occurs at an average depth of 3,700 m (12,200ft) and was deposited through fluvially-dominated distributary channels in a deltaic complex (Hurley *et al.* 1992).

The Hibernia oil field is located in the Jeanne d'Arc basin (JDB) which is one of the several Mesozoic rift basins along the west Atlantic passive margin. The JDB is a north-northeast trending asymmetric half-graben (Driscoll and Hogg 1995). Intense drilling activity in the basin has resulted with the acquisition of 465 km² (180 mi²) three-dimensional seismic data (Hurley *et al.* 1992). Core plugs of the Hibernia Formation were analysed and the reservoir has been differentiated into hydraulic flow units by Core Laboratories for the Hibernia Management and Development Company (HMDC).

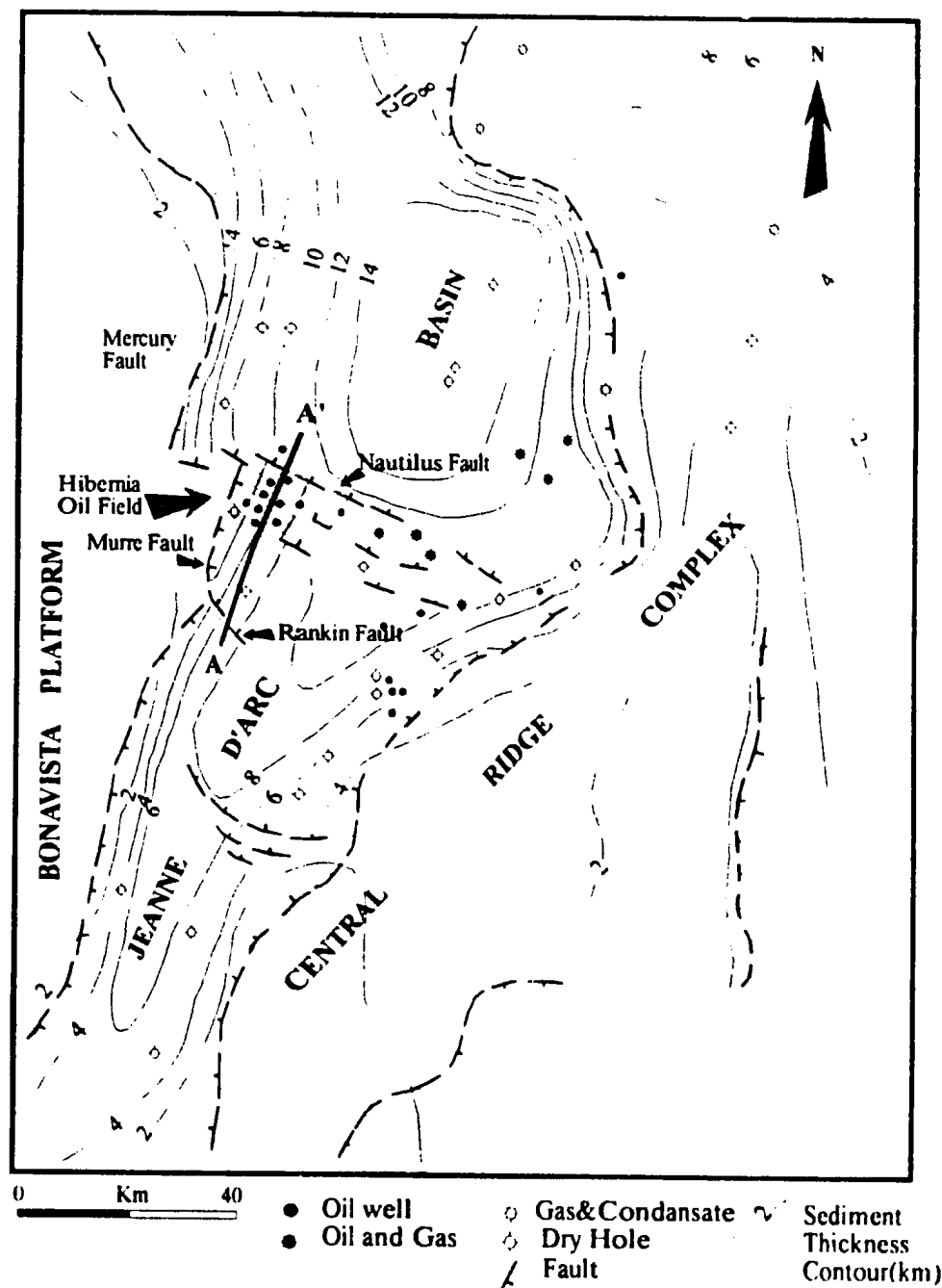


Figure 1: The Hibernia oil field and sediment thickness map of Jeanne d'Arc Basin (JDB) (modified after Brown *et al.* 1986). Note the northeast extending geometry of the JDB.

Well	Location	Spud Date	Total Depth (m)	Water Depth (m)	Clssfc.	Describ.	Penetration Interval into Hib Form. (m)	Shale Equivalent of Upper Zone (m)	Cored Interval (m)	DST Analysis
P-15(#60)	46 44'59.98"N 48 46'51.18"W	1979-05-27	4,406.8	80.2	Expl.*	Abndn.* disc. well	3,439-3,939	3,439-3,743	None from Hibernia F.	Yes
O-35(#65)	46 44'54.92"N 48 49'53.74"W	1980-01-01	4,788.5	79.6	Del.*	Abndn.* oil well	3,326-4,210	3,326-3,913	None from Hibernia F.	None in Hib.F.
B-08(#67)	46 47'06.36"N 48 45'29.87"W	1980-03-19	4,435.5	82.9	Del.	Abndn. oil well	3,185-3,651	3,185-3,477	3,479.6-3,497.8 3,554.2-3,559.2 3,606.0-3,613.5 3,613.5-3,628.0	Yes
G-55(#74)	46 44'17.07"N 48 53'10.75"W	1980-12-11	3,460.1	76.5	Del.	Abndn. oil well	None	None	-	-
K-18(#76)	46 47'34.69"N 48 47'17.05"W	1981-02-26	5,039.3	78.3	Del.	Abndn. oil well	3,413-3,859	3,413-3,686	3,796.9-3,819.4 3,820.0-3,866.7	Yes
J-34(#82)	46 43'33.84"N 48 50'13.00"W	1981-11-29	3,711.8	78.3	Del.	Abndn. oil well	3,630-3,711.8	3,630-3,711.8	None from Hibernia F.	None in Hib.F.
I-46(#87)	46 45'40.74"N 48 51'17.20"W	1982-12-18	3,435.7	78.7	Del.	Abndn. oil well	None	None	-	-
B-27(#92)	46 46'11.21"N 48 48'28.34"W	1983-08-08	4,380.0	80.5	Del.	Abndn. oil well	3,467-3,977	3,467-3,781	3,841.0-3,854.0 3,854.5-3,914.8	Yes
K-14(#93)	46 43'39.83"N 48 47'36.18"W	1983-08-09	4,462.0	79.9	Del.	Abndn. oil well	?-4,089	?-3,840	3,848.4-3,973.7	Yes
C-96(#95)	46 45'10.19"N 48 44'35.77"W	1984-01-21	4,420.0	80.8	Del.	Abndn. oil well	3,467-3,984	3,467-3,784	3,865.2-3,868.5 3,869.7-3,958.9	Yes

*Expl.: Exploration, Del.: Delineation, Abndn. Disc. well: Abandoned discovery well

Table 1: Wells in The Hibernia Oil Field (CNOBP 1990).

1.1- THESIS OBJECTIVES

Different stages of deposition and burial, physical compaction, deformation, and cementation result in varying degrees of internal petrophysical inhomogeneity in all types of hydrocarbon reservoirs (Finley and Tyler 1986). Vavra *et al.* (1991) stated that in many clastic reservoirs pore structure and reservoir quality are primarily controlled by grain size and textural maturity (sorting&roundness) of sediments. Furthermore, diagenetic processes such as quartz cementation and formation of pore-lining and pore-bridging clays also modify pore structure and decrease reservoir quality.

The term "permeability" in this study always refers to horizontal permeability unless stated otherwise.

Conceptually, "*flow zones*" in a given reservoir are definable flow paths with measurable drainage characteristics. Drainage capability and fluid flow rates in reservoirs are controlled by permeability. Permeability, as described by Koederitz *et al.* (1989) "*is a measure of the ease with which fluid can flow through [a rock].*" Permeability is an end product of porosity, pore connectivity grain size distribution, textural maturity, sedimentary structures, abundance of cements and carbonaceous material, clays and accessory mineral attributes, and diagenetic influences. Evaluation of the permeability-controlling mechanisms is a crucial process for hydrocarbon production. Therefore, the objectives of this study are:

1. Evaluate permeability-controlling mechanisms in the Hibernia Formation by core, log, SEM-EDS, and thin section analyses.
2. Describe zones having internal resemblance and potential similarity for fluid flow.

- 3 Assess the reservoir delineation of hydraulic flow units defined for HMDC by Core Laboratories, Calgary.
4. Assess lithofacies and pore characterization by the procedures of Canadian Hunter Ltd. (Sneider *et al.* 1984).
5. Integrate the engineering data, lithofacies descriptions, SEM/EDS processes, thin section petrography and log responses in order to create a high resolution model of geological attributes and actual reservoir quality zones in the Hibernia Formation.

1.2- METHODOLOGY

Five of the ten wells in the Hibernia oil field were cored in the Hibernia formation (Table 1). The cores are archived in the Canada Newfoundland Offshore Petroleum Board's (CNOPB) core storage in St. John's, Newfoundland.

Characterization of lithofacies in this study is based on the Canadian Hunter approach (Sneider *et al.* 1984, Hietala 1991) which combines core descriptions, log interpretations, thin section petrography and SEM/EDS-coupled processes. The first phase of this study involved thorough examination of 386 m (1266 ft) of core. Grain size logs were recorded, lithofacies and palaeo-environments were described and interpreted for each of the five Hibernia wells; Appendix 1). Core depth corrections and correlations were performed between gamma ray and grain size logs in order to identify the exact locations of core plugs on log suites (Appendix 2). Facies associations were then superimposed on the gamma ray logs. A field cross section was drawn in order to display the dominance of channel

successions in the framework of the reservoir. Core plug-lithofacies distributions were determined. Porosity-permeability windows of each lithofacies were graphed in semi-log format (Appendix 3).

A set of facies-representative rock chips were collected from the walls of core plugs where permeability and porosity values were available. These cuttings were subjected to Scanning Electron Microscopy imaging. Along with the SEM microphotographs, elemental analyses in point and surface scanning modes were performed by an energy dispersive x-ray spectrum analyzer (EDS)(Appendix 3). Mean elemental percentages were calculated and plotted against permeabilities (horizontal)

Dye-impregnated thin sections of the cuttings were provided by HMDC. Only minor additional thin section preparation was required. Petrographic analyses were performed under transmitted and reflected lights. Mineralogical framework and diagenetic attributes were described as well as pore/pore throat plugging, permeability-reducing features.

Finally, complete thin section descriptions, SEM microphotographs, EDS elemental analyses, core and log descriptions, and porosity/permeability data were combined in order to determine reservoir quality zones within the reservoir. These results were compared and correlated with the analytically-determined hydraulic flow unit determinations by HMDC so that optimum delineation of reservoir could be assessed (Appendix 5).

1.3- PREVIOUS WORK

1.3.1- Statement of the problem:

For many years, porosity-permeability distributions in a reservoir system were characterized by the following equation (Slingerland *et al* 1994):

$$\log k = a\phi + b \dots\dots\dots 1$$

Prediction of permeability in eq. 1 is not always reliable (Amaefule *et al.* 1993; Gardner and Albrechtsons 1995). By regression analysis, only the mean values of permeability are obtained. Lower values are overestimated and higher values are underestimated (Rogers *et al.* 1995).

Permeability is a unique parameter which principally determines the rate of flow into the bore hole. In order to understand how a reservoir will drain into a well, delineation of separate flow paths has to be performed. Although porosity is a primary factor in the generation of permeability, perplexing influences of other petrophysical properties can have control over fluid flow through porous media. Figure 2 is the cross plot of porosity-permeability distribution in Hibernia C-96. It is evident that for any specific porosity, permeabilities cover a broad range. Such drastic permeability variations within the range of a single porosity value may reflect the effects of rock properties in addition to grain size. Therefore, for effective reservoir characterization, relationships between rock properties and permeability have to be addressed.

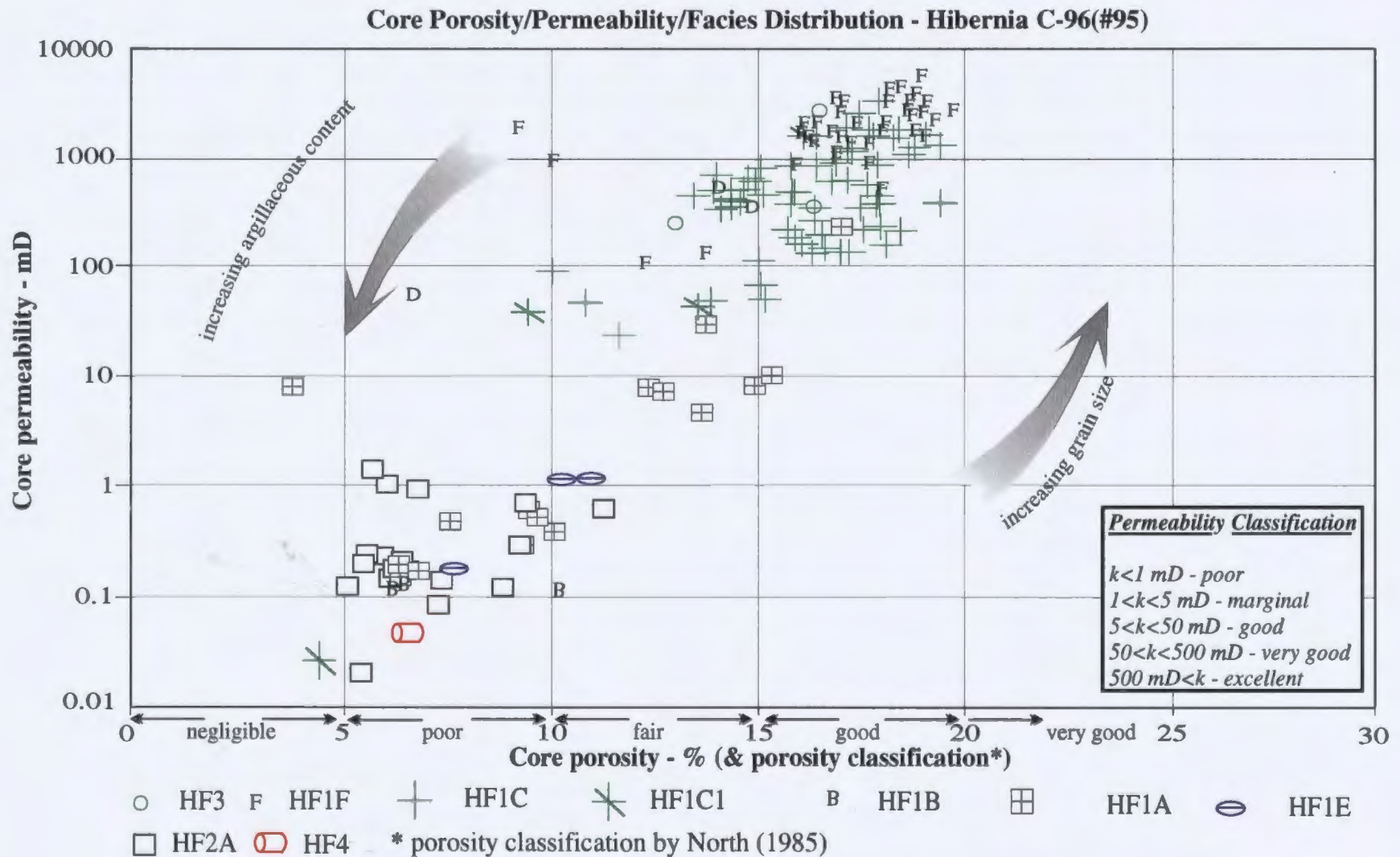


Figure 2: Composite porosity/permeability/facies relationship in the plugged sections of the cored interval of Hibernia C-96(#95).

1.3.2- Analytical hydraulic flow unit zonation:

1.3.2.1- Modification of Kozeny-Carman equation (KCE) by Amaefule *et al.* (1993)

Amaefule *et al.* (1993) stated that the mean hydraulic flow unit radius (r_{mh}) concept is crucial to correlate porosity, permeability, and capillary pressure with the hydraulic unit.

Kozeny (1927) and Carman (1937) initially assumed that reservoir rock is formed as a bundle of capillary tubes which have a common mean hydraulic radius, r_{mh} . The r_{mh} can be addressed as

$$r_{mh} = \frac{\text{Volume Open to Flow}}{\text{Wetted Surface Area}} = \frac{\pi r^2 h}{2\pi r h} = \frac{r}{2} \quad \dots\dots\dots 2$$

where r is the radius and h is the height of the capillary tube.

Kozeny (1927) and Carman (1937) combined the Hagen-Poiseuille and Darcy equations in order to define single phase laminar flow in a capillary tube,

$$k = \frac{r^2 \phi_e}{8\tau} \quad \dots\dots\dots 3$$

where k is permeability; ϕ_e is effective porosity; τ is tortuosity. In order to match tortuosity properties of "the representative elementary volume (REV)" of reservoir rock with flow in the proposed capillary tube, Lake (1989) assumed that "the travel time of a fluid element in a capillary tube is equal to that in a REV". Tortuosity by Lake's definition (1989) is equal to "the squared ratio of the capillary tube length to REV length; $(L_c/L)^2$." The value of tortuosity is variable, being between 1 and 10 in most permeable media, and is most frequently encountered in the range of 2-5.

Substitution of r_{mh} in equation 3 gives

$$k = \frac{\phi_e}{2\tau^2} \left(\frac{r}{2} \right)^2 = \frac{\phi_e r_{mh}^2}{2\tau^2} \quad \dots \dots \dots 4$$

The relationship between the r_{mh} and the surface area per unit grain volume (S_{gv}) and ϕ_e can be addressed as

$$S_{gv} = \frac{2}{r} \left(\frac{\phi_e}{1-\phi_e} \right) = \frac{1}{r_{mh}} \left(\frac{\phi_e}{1-\phi_e} \right) \quad \dots \dots \dots 5$$

Substitution of equation 5 in equation 4 yields

$$k = \frac{\phi_e^3}{(1-\phi_e)^2} \left(\frac{1}{2\tau^2 S_{gv}} \right) \quad \dots \dots \dots 6$$

2 is the value of the shape factor (F_s) for a circular cylinder in the equation 6, $F_s \tau^2$ is described as *Kozeny constant* which is "a variable constant which varies between hydraulic units, but is a constant in a given unit" (Amaefule *et al.* 1993). Value of the Kozeny constant may change from 5 to 100. Redefinition of eq 6 in terms of the Kozeny constant results in *the Kozeny Carman Equation (KCE)*:

$$k = \frac{\phi_e^3}{(1-\phi_e)^2} \left(\frac{1}{F_s \tau^2 S_{gv}} \right) \quad \dots \dots \dots 7$$

Rearrangement of eq.7 gives

$$\sqrt{\frac{k}{\phi_e}} = \frac{\phi_e}{1-\phi_e} \times \frac{1}{(\sqrt{F_s})\tau S_{gv}} \quad \dots \dots \dots 8$$

where permeability is in μm^2 and effective porosity is a fraction. From this equation, Amaefule *et al.* (1993) defines a "Reservoir Quality Index" (RQI) as

$$RQI = 0.0314 \sqrt{\frac{k}{\phi_e}} \quad (mD) \quad \dots \dots \dots 9$$

* 0.0314 = conversion factor of permeability from μm^2 to mD.

Amaefule *et al.* (1993) designated the porosity component of equation 8, which is the ratio of pore volume-to-grain volume, to be normalized porosity (ϕ_z)

$$\phi_z = \frac{\phi_c}{1 - \phi_c} \dots\dots\dots 10$$

and defined the component $1/(\sqrt{F_z})\tau S_{gw}$ as "Flow Zone Indicator" (FZI). Substituting FZI, RQI and ϕ_z in eq.8 gives $RQI = \phi_z \times FZI$ or as a logarithmic function:

$$\log RQI = \log \phi_z + \log FZI \dots\dots\dots 11$$

FZI is the y-intercept of a 45° angle line to the x-axis on a $\log RQI / \log \phi_z$ crossplot when ϕ_z equates to 1. Points that lie on a line having the same FZI are interpreted to have the same flow zone ϕ/k characteristics and are therefore defined as being part of a single hydraulic flow unit. Thus, determination of FZI in cored intervals allows the identification of lithologies with similar FZI values. However, FZI is a parameter which represents rock properties other than porosity. Since a reliable calculation of FZI is not possible in equation 8, the RQZ- ϕ_z cross plot permits the assignment of an FZI value to a given unit. Lithologies with similar FZI are then grouped as separate zones of flow by using univariate FZI frequency histograms.

1.3.2.2. Application of KCE to the Hibernia Formation

Gardner and Albrechtsons (1995) reported that FZI values of core plugs were calculated for cored sections of the Hibernia Formation by using the $RQI = \phi_z \times FZI$ relationship. A univariate frequency histogram of calculated FZI values (Figure 3) identified FZI clusters which were subdivided into five groups (hydraulic flow units = HU) with the following cutoffs:

FZI range: 15.27-23.25 (HU1)
" : 7.52-15.27 (HU2)
" : 3.43-7.52 (HU3)
" : 1.887-3.43 (HU4)
" : 0-1.887 (HU5)

All data points occurring within each of these FZI intervals are assigned to the corresponding hydraulic units. The highest FZI range (HU1) represents the best reservoir quality and HU5 corresponds to the poorest quality. A composite crossplot of core porosity and permeability from all of the cored Hibernia wells (Figure 4; HU-superimposed) displays wide permeability ranges within each of the hydraulic units.

As this present study will show, this HU zonation process by means of mathematical and statistical applications reflects the geological rock properties of the system. Each HU defines porosity and permeability ranges which are too large in effective reservoir description

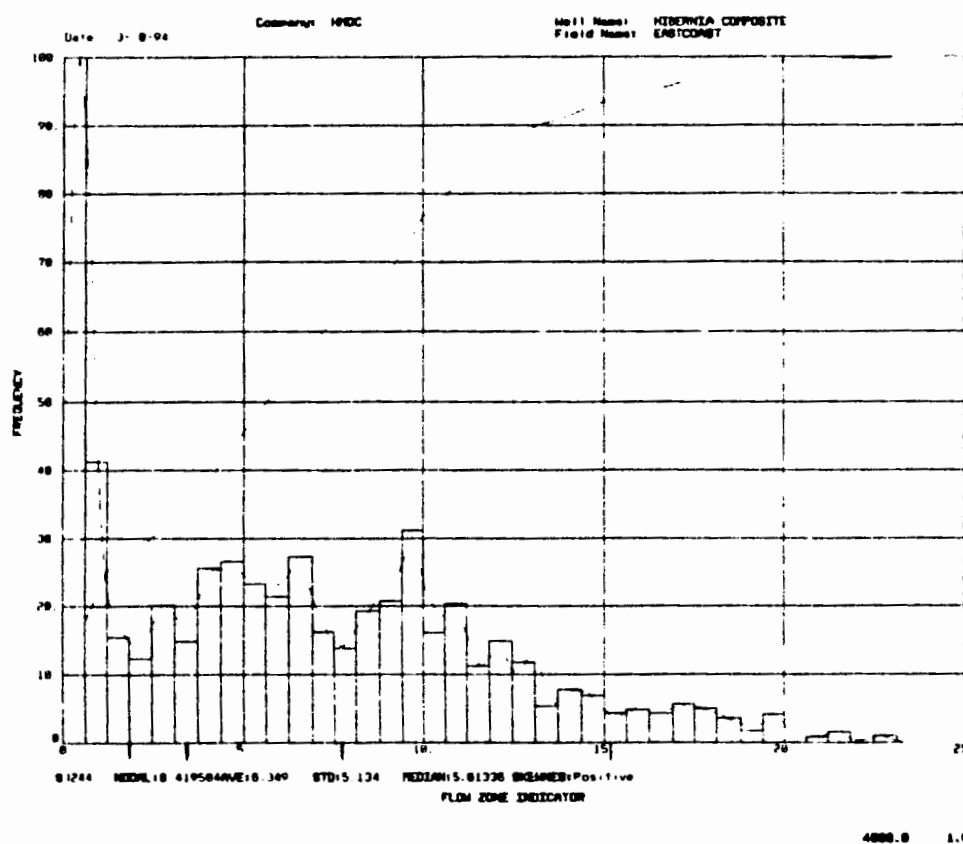


Figure 3: Univariate FZI frequency histogram showing five major FZI cut-offs assigned to different hydraulic units (HU) in the Hibernia Formation (From Gardner and Albrechtsons 1995).

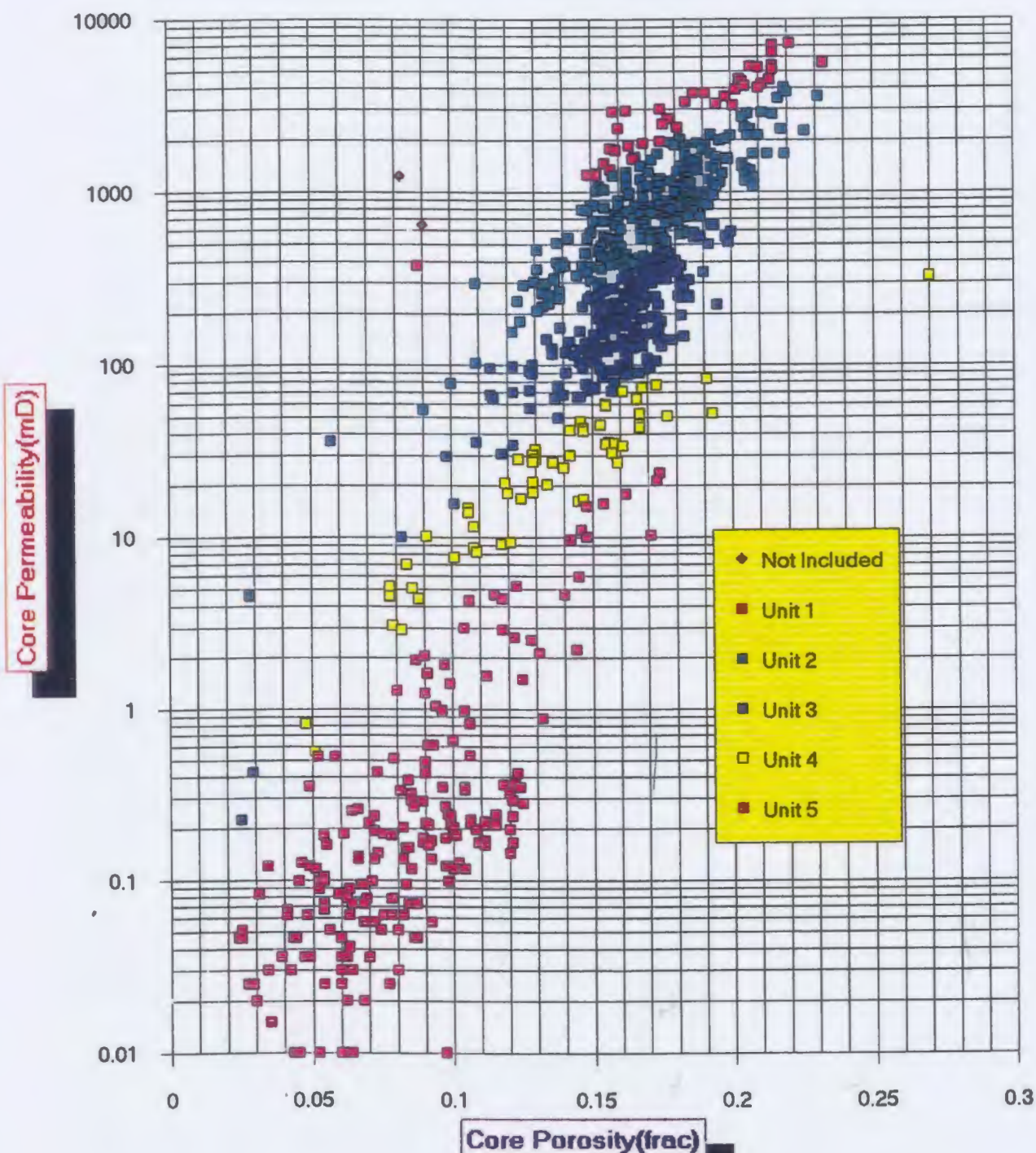


Figure 4: HU-superimposed distribution of the ϕ/k data in the Hibernia Formation. Note the wide porosity and permeability ranges within each of the HU (From Gardner and Albrechtsons 1995).

II - REGIONAL GEOLOGY

II.1- TECTONIC SETTING:

II.1.1. Tectonic History and Stratigraphy of the Jeanne d'Arc Basin:

The Hibernia oil field is located on the Grand Banks, offshore Newfoundland in the Jeanne d'Arc Basin (JDB). The eastern coast of Canada underwent convergent tectonism during the Paleozoic when the Avalon basement was deformed during the Caledonian and the Hercynian orogenies (Welsink *et al.* 1989, Tankard and Welsink 1989; Tankard and Balkwill 1989). Consolidation of the Pangean supercontinent took place in the Permian. The JDB lies within those Precambrian to Paleozoic metasedimentary and crystalline rocks of the Avalon basement (Tankard *et al.* 1989). The geology of the JDB was primarily controlled by pre-Mesozoic basement structure

According to Tankard *et al.* (1989) the opening of the North Atlantic from south to north started with a Triassic rifting episode and lasted for over 100 million years. The entire rifting cycle occurred within four main phases. The stratigraphic record of the JDB highlights all of the four rifting episodes (Figure 5) (Sinclair 1988; Hiscott *et al.* 1990; Abid 1996).

1. Rift climax in the Late Triassic and the culmination of rifting during the Early Jurassic (Deposition of the Eurydice, Argo, and Iroquois Formations).
2. Deceleration of the subsidence rate during the Middle Jurassic. Separation of Africa from Nova Scotia started in this episode and lasted until the Late Jurassic (Deposition of the Downing, Voyager, and Rankin Formations). Organic-rich calcareous

Kimmeridgian shales of the Egret Member deposited during this phase of rifting are the source of hydrocarbon in the Hibernia oil field (Powell 1984, Fitzgerald 1987, von der Dick 1989).

3. A second intense rifting phase lasted about 45 million years between the Late Jurassic and the Early Aptian. Reservoir sediments of the Jeanne d'Arc, Hibernia, Catalina, Ben/Nevis and Avalon Formations were deposited during this intense rifting activity. Separation of the Grand Banks and the Iberian crustal plates also took place within this episode.
4. A post rift thermal subsidence phase started during the Late Aptian and has lasted to present day during which time Tertiary sediments were deposited (McAlpine 1990). Decrease of thermal energy resulted in the vertical and horizontal sagging of the sediments. Within this last episode Dawson Canyon and Banquereau Formations were deposited. Europe separated from Greenland and North America in the Late Cretaceous. The combined thickness of the syn-rift and post-rift sediments (Figure 1) is approximately 14 km. in deep portions of the basin (Grant *et al.* 1986)

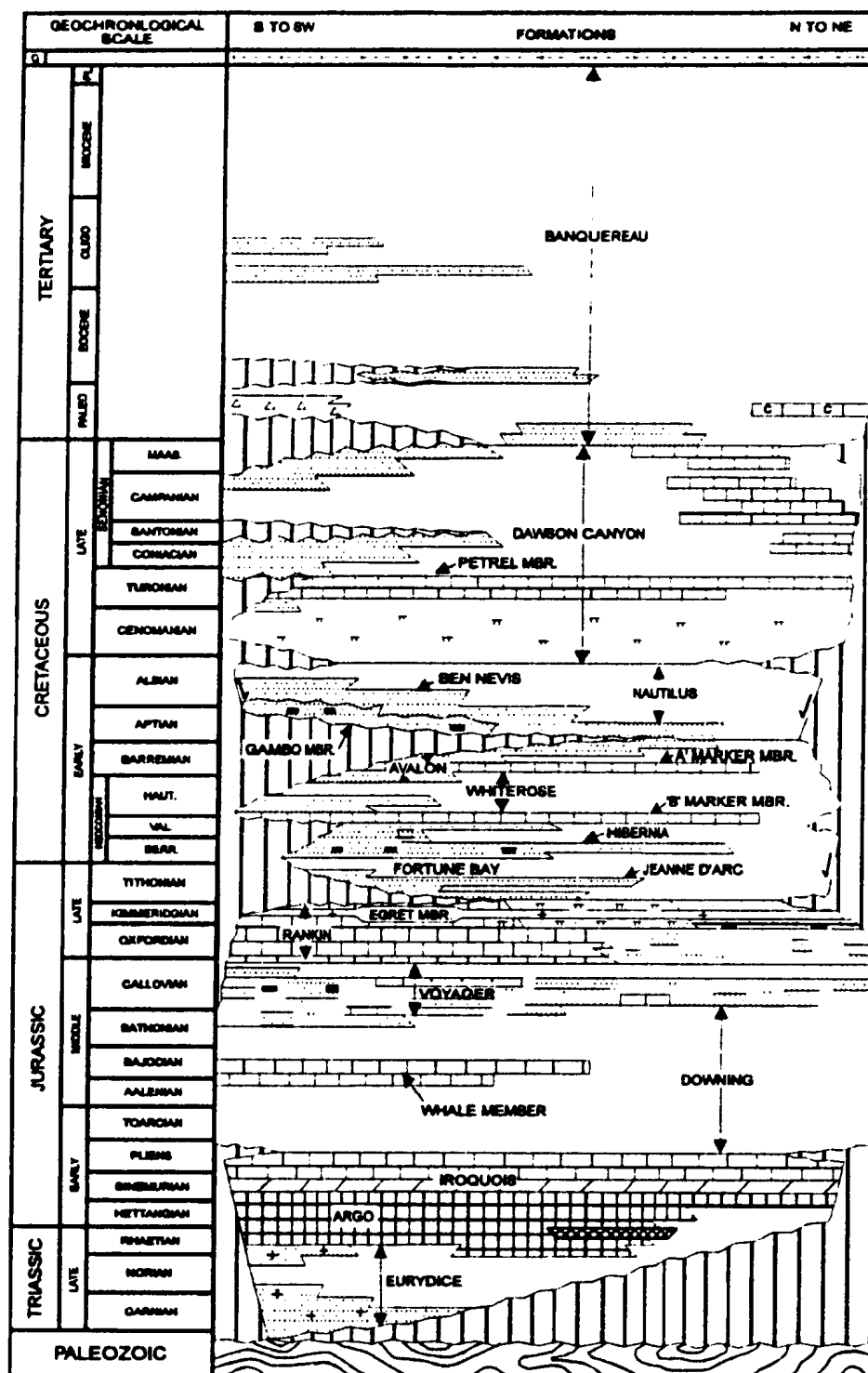


Figure 5: Generalized stratigraphy of the Jeanne d'Arc Basin. Early Cretaceous sands are the hydrocarbon reservoirs. The white intervals represent shale/mudstone (Sinclair 1993 and Abid 1996).

II.1.2. Geologic setting of the Hibernia Oil Field:

The JDB is a north-northeast extending rift basin formed by a complex listric fault geometry (Figure 1). The basin is surrounded by the Bonavista Platform to the west, the Avalon uplift to the south, and the Central Ridge Complex to the east and the northeast

The Hibernia oil field is located at the western margin of the basin, and as Soliman (1995) points out, it formed as a roll-over anticline of the Rankin growth fault (Figure 6). The oil field is constrained by the Murre fault to the west and by the Nautilus transform fault to the north (CNOPB 1986). The Hibernia Formation occurs at depths varying between 3,477 m and 4210 m (Figure 7a,b,&c). The structural character of the oil field is controlled by complex fault geometries. Ten wells were drilled in the oil field of which eight penetrated the Hibernia Formation (Table 1). G-55 to the southwest and the western well I-46 did not penetrate the Hibernia Formation. B-08 is structurally the highest well where a gas-oil interface was encountered at 3,544 m. depth. Since the remaining wells are structurally lower than B-08, this gas-oil interface was initially accepted as a field-wide contact (Hurley *et al.* 1992). However, oil-water contacts have since been determined to occur at various depths. Multiple hydrostatic relationships reflect the complex fault block structure of the JDB (CNOPB 1986). Fluid properties in the oil field are also controlled by the fault block structure. According to Handyside and Chipman (1983), reservoir fluid properties are separated into two non-communicating fluid zones:

- 1- B-08 fault block: Saturated crude oil (API 40.0°) with a gas condensate cap containing a liquid content of ~180 STB/MMSCF overlaying the oil layer.
- 2- P-15 fault block: Undersaturated crude oil (API ~35.0°)

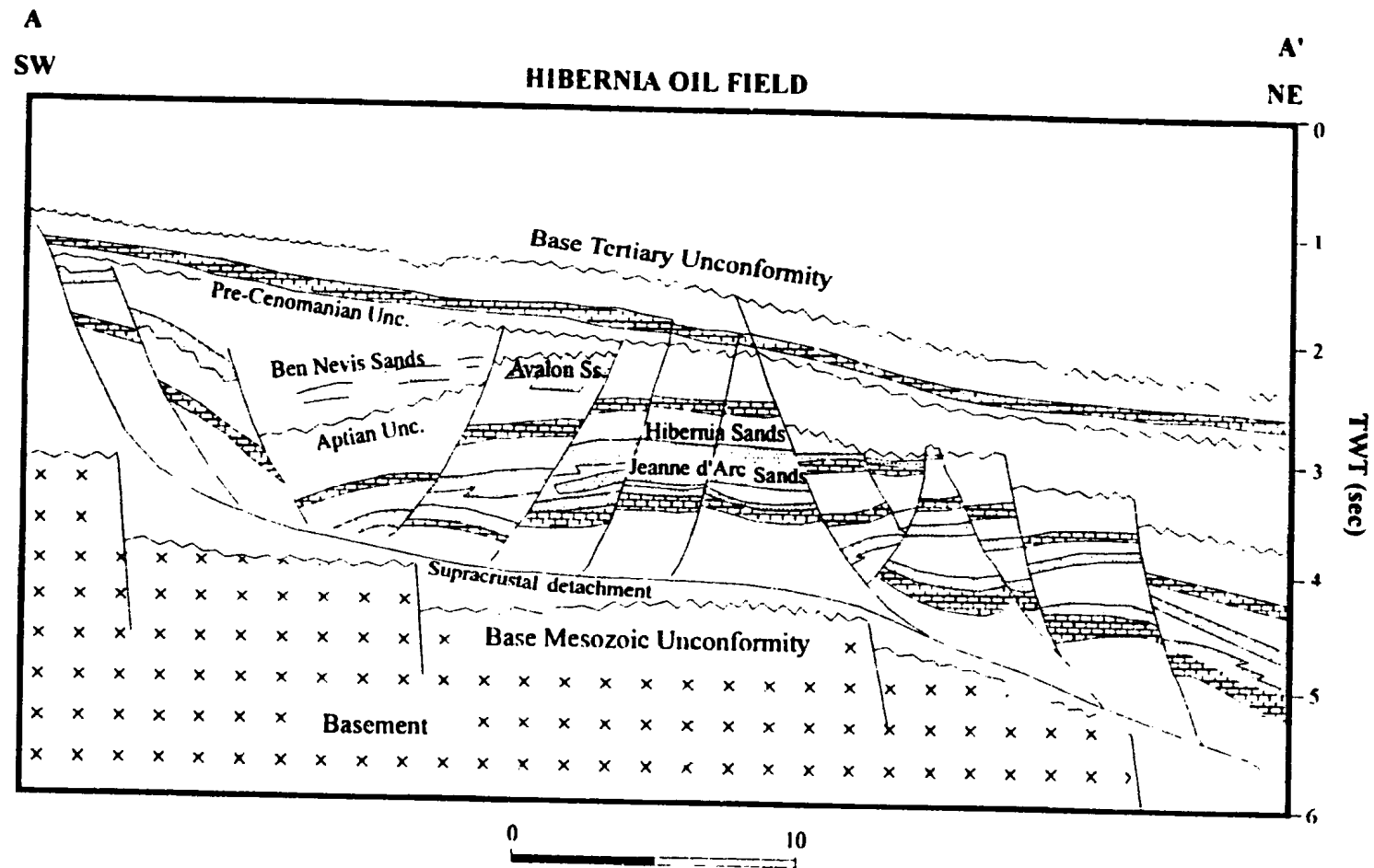


Figure 6: Basement structure and post-Mesozoic evolution of the Hibernia oil field. Supracrustal detachment was generated by the basin-bounding Rankin fault. For the location of the seismic line, see figure 1 (from Tankard *et al.* 1989).

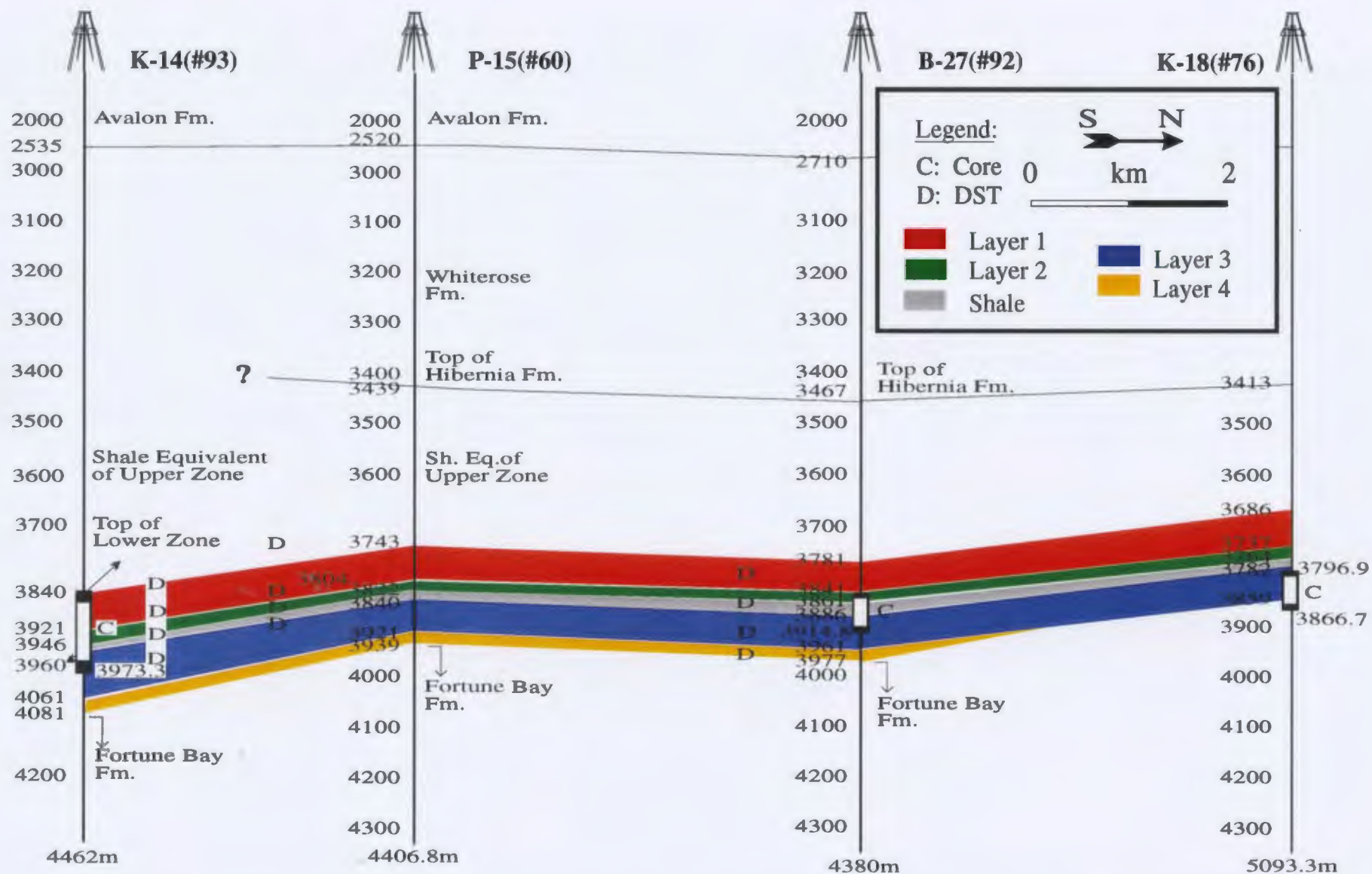


Figure 7b: South-north cross-section of Hibernia oil field. Zonation and geologic tops are adopted from CNOBP (Schedule of Wells 1990). Depths (meters) are measured from K.B.

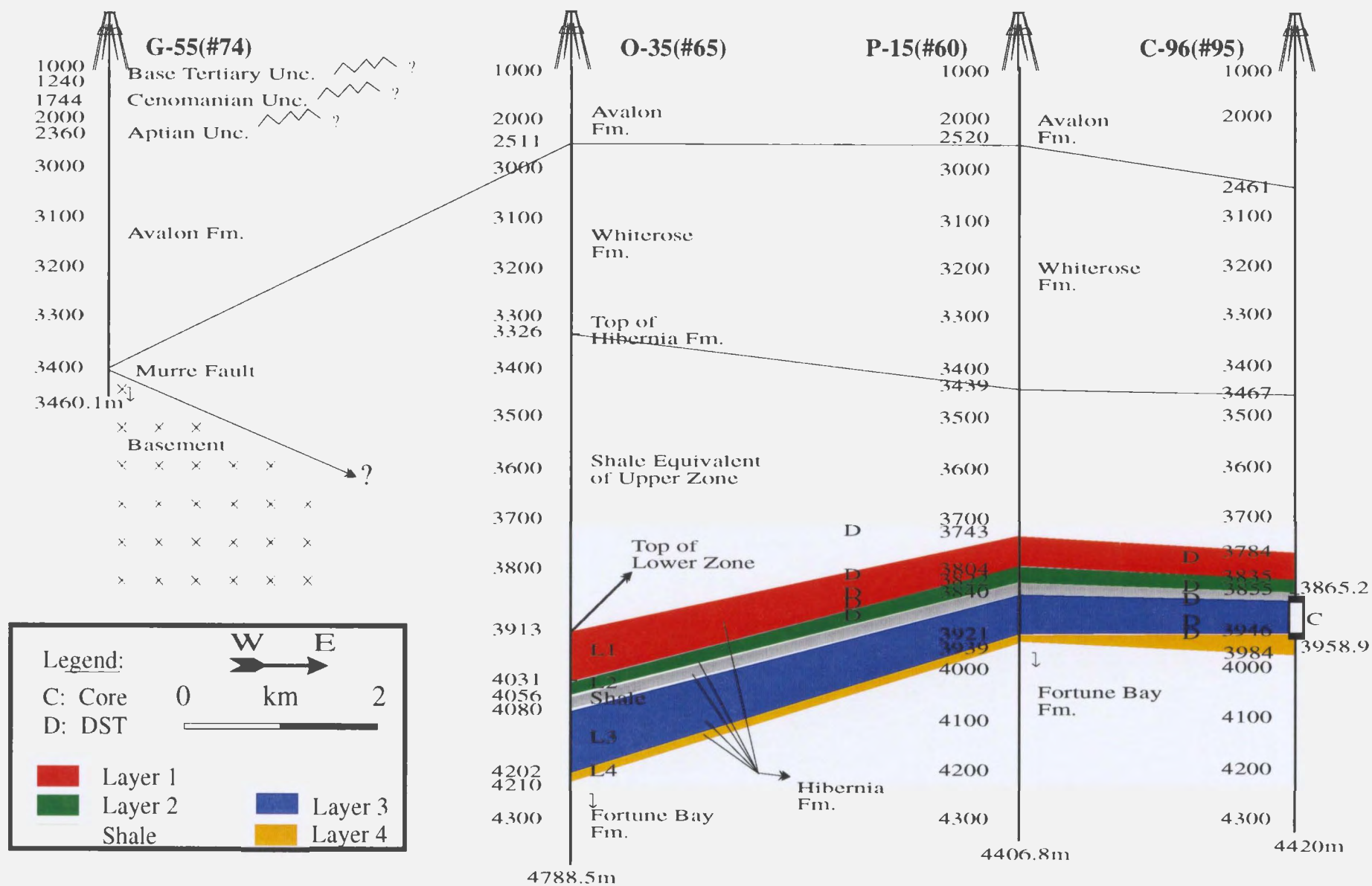


Figure 7c: West-east cross-section of Hibernia oil field. Zonation and geologic tops are adopted from CNOPB (Schedule of Wells 1990). Depths (meters) are measured from K.B.

II.2- DEPOSITIONAL CHARACTERISTICS OF THE HIBERNIA FORMATION

Interpretations of the conventional cores in the Hibernia Formation, integrated with wire-line log suites, reveal that the sandstones of the Hibernia formation were deposited in a fluvial-deltaic distributary channel system with minimal tidal and marine influence (Hurley *et al.* 1992). During fault-controlled subsidence, the Avalon Uplift rose on the southern side of the oil field (Sinclair *et al.* 1994). Clastic detritus in the Hibernia Formation was derived in part from the Avalon Uplift which rose on the southern side of the JDB during the fault-controlled subsidence (Arthur *et al.* 1982; Brown *et al.* 1986; Hurley *et al.* 1992; Sinclair *et al.* 1994). A secondary sediment source is the western Bonavista Platform (Figure 1) (Brown *et al.* 1986). Since tectonically-induced slopes and the faults that formed along individual asymmetric blocks are the major forces inducing sediment transfer, Murre fault within the Hibernia oil field had profound influence on sediment transportation and deposition of the Hibernia Formation (Brown *et al.* 1986).

Hibernia Formation lithologies, Berriasian to Valanginian in age, are composed dominantly of very fine to coarse-grained, argillaceous sandstones containing local rafted carbonaceous material (Arthur *et al.* 1982). The average sediment thickness of the Hibernia Formation is approximately 200 metres. Calculated core porosities range from 4% to 24.2% while core permeabilities vary between 0.01 and 9860 millidarcies. The best reservoir quality displaying the highest porosity/permeability distribution, occurs in thick, sandstone lithofacies of distributary channels. Interstratified silty and shaly sandstones, mudstone and shales formed in crevasse splay, levee, overbank, flood plain, abandoned channel, marsh and marine bay

palaeo-environments which possess poorer reservoir quality with very low permeabilities (average 1 mD). Hurley *et al.* (1992) suggested that the major vertical components of deposition reflect repetitive cycles of fluvial sedimentation starting with channel sands at the base, upward-fining grain size and finally drowning of the delta complex, where mudstone, interstratified silty and shaly sandstone lithologies become dominant

III - CONVENTIONAL CORE DESCRIPTIONS

III.1- INTRODUCTION

Finley and Tyler (1986) described a facies as "a three-dimensional body of rock having an environmental origin that can be inferred from a set of characteristics including external geometry, internal geometry, sedimentary structures, lithology, organic content, stratigraphic relations, and associated sedimentary facies." Sedimentary lithofacies containing vertical and lateral heterogeneities should be analyzed in small successive intervals (Hurst and Rosvoll 1991). Lithofacies, as used in this study, are based on the physical, textural, structural, mineralogic, organic, and petrographic elements of the core, in the context of Finley and Tyler's definition. **There is no depositional environment interpretation involved in the designation of these lithofacies.** Emphasis has been put on describing those features of lithofacies which control the flow properties of rocks. Locations of the cored sections and correlation of gamma ray log responses are presented on the cross section of the field (Pocket).

A summary of the distinguishing features of the Hibernia lithofacies, and the lithofacies coding system, is presented in table 2.

Facies	Definition	Av. Grain Size	Bedding
HF1A	Convolute & wavy bedded ss*	very fine	
HF1B	Crossbedded & carbonaceous ss	fine	
HF1C	Crossbedded & oil-stained ss	medium lower	
HF1C1	Medium-grained sands with high clay & rip-up clasts	medium lower	
HF1D	Poorly-consolidated sands	medium-coarse	
HF1F	Coarse-grained basal ss	coarse	
HF3	Conglomeratic bimodal ss	pebbly medium-coarse	
HF1E	Rippled & wavy bedded carbonaceous ss	very fine-fine	
HF1E1	Horizontally-laminated carbonaceous ss	very fine-fine	
HF1G	Argillaceous slightly-cemented ss	silt-very fine	
HF6	Coaly & carbonaceous ss	fine	
HF2A	Slightly-burrowed silty/shaly ss	silt-clay	
HF2B	Lenticular bedded, moder.-burrowed silty/shaly ss	silt-clay	
HF2C	Well-burrowed silty/shaly ss	clay-silt	
HF4	Loose carbonaceous shales & soil zones	clay	
HF5	Shelly/churned & well-burrowed shales	clay	

Facies Coding System

- 1 "as in HF1A" stands for ss-dominated facies
- 2 "as in HF2A" stands for interstratified silt/sand/shale facies
- 3 "as in HF3" stands for conglomeratic sands
- 4 "as in HF4" stands for loose shales & soil zones
- 5 "as in HF5" stands for shelly/churned shales
- 6 "as in HF6" stands for coaly/carbonaceous sands

Grain Size Scale

vcU = 1410-2000 μ	mL = 250-350 μ
vcL = 1000-1410 μ	fl = 177-250 μ
cU = 710-1000 μ	fl = 125-177 μ
cL = 500-710 μ	vfU = 88-125 μ
mU = 350-500 μ	vfL = 62-88 μ

Burrowing

	Slightly-burrowed
	Moderately-burrowed
	Well-burrowed

Sedimentary Structures

	Horizontal bedding		Coal growth
	Crossbedding		Quartzitic
	Convolute bedding		Ripple xbedding
	Load cast		Climbing ripples
	Normal grading		Lenticular bedding
	Wavy bedding		Shell fragments
	Arkosic		Rafted carb.* material
	Pyrite growth		Vertical carb. material
	Siderite growth		Churned
	Ball & pillow structure		Plant root tube
	Rip-up clast		

* ss sandstone, carb carbonaceous, moder moderate

Table 2: Hibernia lithofacies and some of their descriptive features For detailed facies successions, refer to the grain size logs in Appendix ??.

III.2- FACIES GROUPS IN HIBERNIA SANDSTONES

III.2.1- Sandstone-dominated facies:

III.2.1.1. Lithofacies HF1A - Convolute and wavy-bedded, very fine-grained sands

HF1A (Figure 8 and 9a) consists of very fine-grained (62-125 μ), consolidated, and light grey quartz sandstone. None to trace amounts of carbonaceous stringers and rare quartz veins are observed. Trough and lenticular crossbedded units are commonly described. Convolute bedding and wavy bedding are sporadically encountered. The sands of HF1A contain rare siderite nodules.

HF1A is commonly encountered in association with coarser-grained sandstones; usually occurring at the upper portion of fining-upward sequences in all of the cored Hibernia wells.

III.2.1.2. Lithofacies HF1B - Carbonaceous fine-grained sands

HF1B (Figure 8 and 9b) is composed of very fine- to fine-grained (62-125 μ) quartz sandstones containing carbonaceous material. The lithology is well-consolidated and slightly oil-stained. The hydrocarbon content of the HF1B sands prevents precise identification of faintly crossbedded sections. Local rafted carbonaceous material is rare but present.

Sandstones of HF1B are encountered in all five of the cored Hibernia wells and are found in association with coarser medium-grained HF1C sands and very fine-grained HF1A sands producing typical fining-upward log cycles.

III.2.1.3. Lithofacies HF1C - Crossbedded and oil-stained medium-grained sands

HF1C is composed of upper fine- to lower medium-grained (125-350 μ), well-consolidated quartz sandstones containing faint and locally-concentrated ripple crossbeds, and

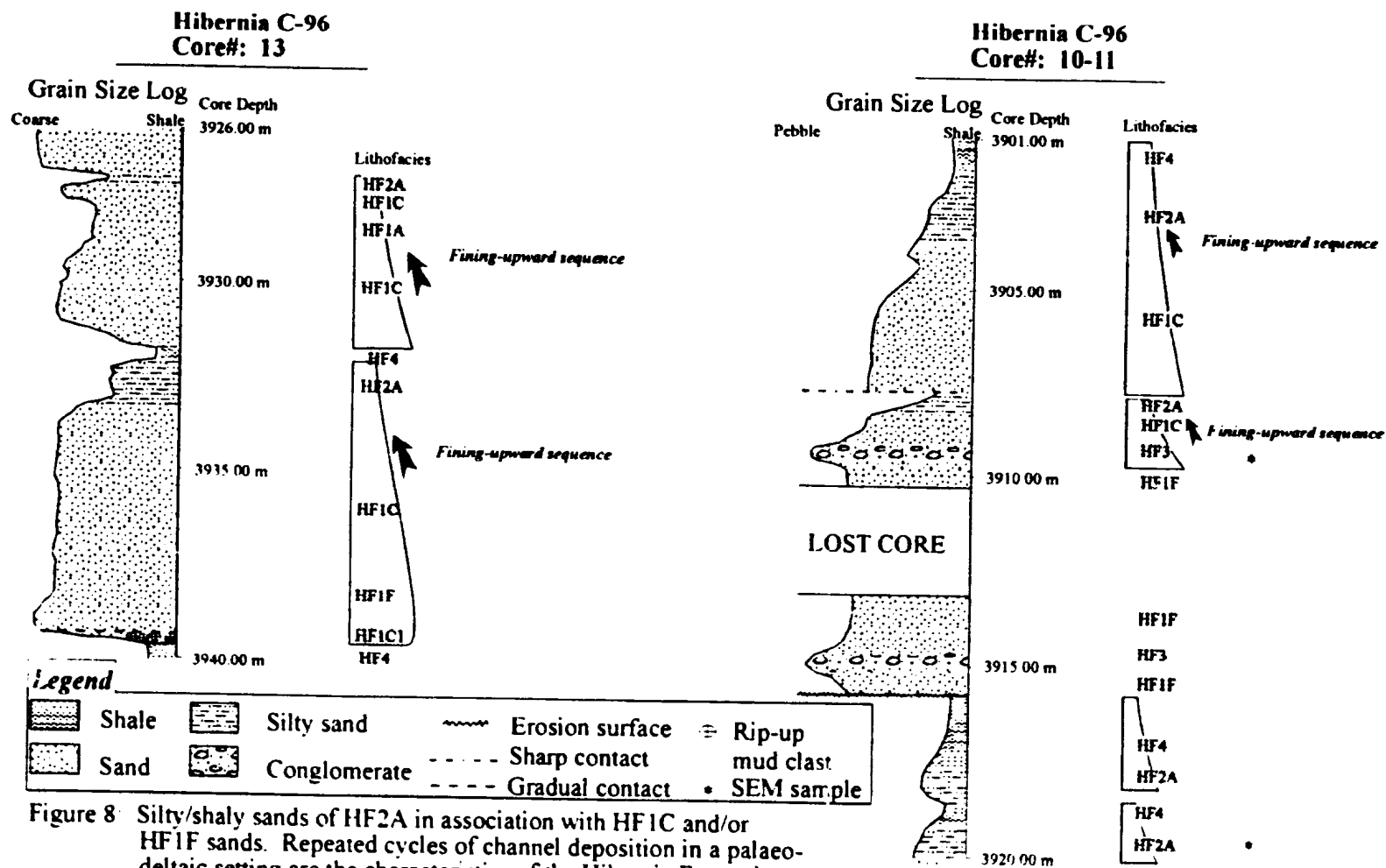


Figure 8 Silty/shaly sands of HF2A in association with HF1C and/or HF1F sands. Repeated cycles of channel deposition in a palaeo-deltaic setting are the characteristics of the Hibernia Formation. Channel sands are at the base. Floodplain muds, associated with the drowning of the channel, are commonly at the top of channel sands.

rare horizontally-laminated sections commonly disguised by the dark-brown coloured hydrocarbon component of the lithology (Figure 9c). Locally-concentrated carbonaceous rafted material is present.

The lithofacies HF1C represents the most commonly encountered lithology within the examined sections. All of the cored Hibernia wells contain HF1C in association with the other sandstone-dominated facies (Appendix 1, grain size logs). Figure 8 shows that the HF1C sands are either a part of a sand-dominated body stacked in a fining-upward trend or occur with sharp and erosive boundary with the underlying strata.

III.2.1.4. Lithofacies HF1C1 - Medium-grained sands with rip-up clasts

Lithofacies HF1C1 (Figure 9d) is composed of upper fine-grained to lower medium-grained quartz sandstones (125-350 μ). Although HF1C1 sandstones are encountered in association with HF1C and their grain sizes are very similar, abundant mudstone rip-up clasts distinguish HF1C1 from HF1C (Figure 8). Sands in this facies are sideritic, hydrocarbon-odoured, well-consolidated and rarely contain carbonaceous material. No bedding type, except a few faint crosslaminated intervals, is observed.

HF1C1 sands are few and are always encountered in association with HF1C sands and HF4 shales (refer to grain size logs, appendix 1).

III.2.1.5. Lithofacies HF1D - Poorly-consolidated medium- to coarse-grained sands

Quartz sandstones of HF1D (Figure 9e) are upper medium upper- to coarse-grained (350-2000 μ), light to dark grey in colour, poorly-consolidated, carbonaceous, and hydrocarbon-odoured but not oil-stained. Due to their very loose texture, no depositional features and

structure characteristics were preserved

Facies HF1D is encountered in most of the cored wells. In almost all cases, HF1D sands produce a grain size log pattern with an upward-fining trend where grain size decreases to the size of HF1C sands (grain size logs, appendix 1).

III.2.1.6. Lithofacies HF1F - Coarse-grained basal sands

HF1F (Figure 9f) is composed of coarse-grained quartz sands (500-2,000 μ). The lithology is grey to dark brown coloured depending on the degree of hydrocarbon saturation. The lithology is poorly- to moderately-consolidated with local zones of very loose texture. Therefore, sedimentary structures are very poorly-preserved. Only a few faint crosslaminated intervals are recognizable. The HF1F sands have low clay content.

HF1F sandstones are observed only in Hibernia B-O8 and C-96 at the base of sand bodies (Figure 8). They represent the coarsest fraction observed in the fining-upward trends which produce associations with finer-grained sands of HF1C or basal channel lag conglomeratic sands of HF3.

III.2.1.7. Lithofacies HF3 - Conglomeratic bimodal sands

Lithofacies HF3 (Figure 9g) consists of pebbles and medium- to coarse-grained quartz sandstones that are thinly-bedded and commonly found as the basal lithology in channel sequences where they form sharp lower boundaries with the underlying strata (Figure 8). They are bimodal with sand size and pebble size components. The sand size mode is the supporting interpebble matrix of the lithology. Rare and locally-concentrated sideritic nodules, poor sorting, poor-to moderate consolidation and rare rafted organic material are

evident characteristics of HF3. HF3 sands and conglomerates contain no visible hydrocarbons and do not exhibit any depositional bedding structure. However, they are distinctively separated from underlying shales and soil zones by scoured and erosive sharp interfaces (see the grain size log of Hibernia K-14; depth interval=3863-3858m; appendix 1).

HF3 was identified only in Hibernia C-96 and Hibernia K-14 in association with overlying coarse-grained sands of HF1F or crossbedded sands of HF1C.

III.2.1.8. Lithofacies HF1E - Carbonaceous, rippled and wavy-bedded sands

Very fine- to fine-grained (62-250 μ) quartz sandstones constitute the facies HF1E (Figure 9h). The lithology is well-consolidated, and hydrocarbon-odoured. Ripple-cross-laminated, lenticular, wavy and horizontally-bedded intervals are sporadic. Horizontally-concentrated organic material is present.

The facies HF1E is encountered at various depths in Hibernia B-08, C-96, K-18 and B-27 (grain size logs, appendix 1). In general, the thickness of the facies is variable between 10 cm. to 1-2 m. In grain size logs, HF1E sediments commonly generate associations with medium-grained sands of HF1C or interstratified sand, silt and shaly facies of slightly-burrowed HF2A or flaky and organic matter-rich shales of HF4.

III.2.1.9. Lithofacies HF1E1 - Horizontally-laminated, carbonaceous sands

Very similar to the facies HF1E, HF1E1 (Figure 9i) is composed of well-consolidated and very fine- to fine-grained quartz sandstones. Some ripple crosslamination, lenticular and convolute bedding are evident. The most abundant structure is horizontal lamination. Regular coupling of dark grey/light grey-coloured laminae is distinctive. Darker laminae are

very rich in organic material. Sideritic nodules in the sediment are rarely encountered.

Facies HF1E1 is observed in four cored Hibernia wells other than K-14. The carbonaceous sands of HF1E1 are always found in association with medium-grained reservoir sands as shown in the grain size log for core 9 of Hibernia B-27 (Appendix 1). In general, thickness of the facies does not exceed one metre. The upper contact of facies HF1E1 produces sharp interfaces with the overlying relatively coarser-grained sands.

III.2.1.10. Lithofacies HF1G - Argillaceous&slightly carbonate-cemented very fine-grained sands

HF1G (Figure 9j) is argillaceous and very fine-grained quartz sandstone (<62 microns) with <10% silt content. Rare carbonate cementation and bioturbation, locally-concentrated faint burrowing, well consolidation and rare rafted wood material are the main features of HF1G. In addition, vertical plant root casts and a 3-4 cm. thick coal zone are observed. Except for a few convoluted beds and wavy bedding, no other sedimentary structure is evident.

HF1G is one of the most rarely encountered facies occurring only in Hibernia B-27 between the core depths of 3,865.10 and 3,874.00 m (see appendix 1). HF1G formed gradational contacts with the underlying HF2A and overlying HF2C interbedded sand, silt, and shales.

III.2.1.11. Lithofacies HF6 - Coaly fine-grained sands

Fine-grained quartz sands of HF6 are poorly-consolidated and very carbonaceous. Coal constitutes approximately <20% of the facies (Figure 9k). Slight oil stain, abundant rafted

organic material, normal-graded beds, and very rare convoluted and wavy bedding are recorded. HF6 coaly sands are encountered solely in Hibernia B-27 (core depth interval: 3,846.73-3,849.34 m; appendix 1). They form associations with the medium-grained, oil-bearing sands of the facies HF1C.

III.2.2- Interstratified sandstone, siltstone and shale facies:

III.2.2.1. Lithofacies HF2A - Slightly-burrowed silty/shaly sands

Lithofacies HF2A (Figure 9l) consists of well-consolidated interbedded shaly siltstone and very fine-grained quartz sandstone. The lithology is slightly-burrowed/bioturbated, highly-contorted and poorly-sorted. Convolute and wavy bedding are the most common deformation-related structures. Load casts, climbing ripples and lenticular bedding are sporadically observed.

HF2A is found in contact with either medium-grained oil-wetted sands of HF1C and coarse-grained sands of HF1F or carbonaceous soft, flaky shales of HF4 (Figure 8). The HF2A lithologies generally occur at the top fraction of the fining upward sequence.

Interbedded shaly silt and sandstones of HF2A are observed in all five cored wells of the Hibernia formation (grain size logs; appendix 1).

III.2.2.2. Lithofacies HF2B - Lenticular-bedded and moderately-burrowed silty/shaly sands

Well-consolidated, very fine-grained quartz sands, shales and siltstones are the major lithological constituents of HF2B (Figure 9m). The main difference of this facies from HF2A is that the lenticular beds and horizontal lamination are the abundant features of HF2B.

Moderate burrowing is sporadic. Wavy and convolute bedding, rare ripple lamination are present. Locally-concentrated and well-developed horizontal lamination becomes distinctive in parts of HF2B (grain size log of Hibernia K-18; appendix 1). Interstratified sediments of HF2B are generally found in association with coarser-grained sands of the fining-upward trends, HF4 shales and interstratified sediments of HF2A and/or HF2C.

III.2.2.4. Lithofacies HF2C - Heavily-burrowed, bioturbated muddy/silty sands

Shaly and silty very fine-grained quartz sandstones of HF2C are well-consolidated, bioturbated and well-burrowed (Figure 9n). Rare shell fragments are locally clustered in some sections of the facies. Horizontally-laminated layers are rarely occurring. Some carbonaceous material is present. Deformation structures such as convolute bedding and wavy bedding are widespread.

III.2.3- HF4 - Loose and carbonaceous shales/soil zones:

Soft and flaky shales of facies HF4 are commonly encountered in all five of the Hibernia wells. They are carbonaceous, occasionally sideritic and dark grey to black in colour (Figure 9o). There is no indication of rafted carbonaceous material. The lithology rarely possesses a coaly texture. HF4 is encountered in association with interstratified claystones and/or channel sands (Figure 8). Associated soil zones in HF4 shales are commonly found as zones of "subaerial exposure" where well-preserved plant roots also occur (see grain size logs; appendix 1). HF4 shales display gradational contacts with underlying strata whereas the upper contact is frequently sharp and erosional where HF1C and HF1F sands or HF3 conglomerates erosively overlay the boundary.

III.2.4- HF5 - Shelly, churned and well-burrowed shales:

Well-burrowed, churned, slightly- and locally-sideritic, grey-coloured shales of the facies HF5 (Figure 9p) are well-consolidated as opposed to the loose texture of the HF4 shales. Clusters of shell fragments sporadically encountered in this facies indicate the lithology was deposited under a marine influence.

HF5 shales were encountered only within Hibernia B-O8 and K-14 cores (refer to grain size logs; appendix 1). They occur over thirteen metres of a continuous interval in K-14 where the lower contact is gradational with interstratified claystones and the upper contact is very sharp and erosional with the sands of the fining-upward cycles.

III.3- INTERPRETATION OF ALL LITHOFACIES

Palaeo-environmental interpretations of the Hibernia formation have been contributed by Brown *et al.* (1986).

Brown *et al.* (1986) separated the Hibernia Formation into two main zones: the Main Hibernia Zone (MHZ) and the Upper Hibernia Zone (UHZ) separated by a gradational boundary. The MHZ consists of sand-dominated and stratified lithologies. MHZ sandstones are divided into three lithofacies "the M-sandstone facies", "the M-sandstone/mudstone facies" and "the M-mudstone facies". The UHZ is composed of quartzarenites interbedded with mudstone and siltstones which are recorded as serrate gamma ray log patterns and are grouped in two main facies; "the U-sandstone facies" and "the U-mudstone facies".

Brown *et al.* (1986) described the crossbedded, very coarse to very fine-grained M-sandstone facies as distributary channel deposits (DCD). DCD sandstones possess fining-upward trends with sharp and sometimes erosional basal and gradational upper contacts. Interbedded sandstone, siltstone and mudstone facies of M-sandstone/ mudstone facies are interpreted as (flood plain) crevasse splay, crevasse channel fill and natural levee deposits, due to the presence of abundant rippled beds, soft sediment deformation structures, common horizontal bedding and laminated sands. The M-sandstone/mudstone facies displays a serrated log pattern and is always found associated with the M-sandstone facies. The M-mudstone facies contains a high degree of bioturbation, sideritic nodules, local carbonaceous stringers, local shell fragments and common soft sediment deformation are described as "interdistributary bay or lacustrine" deposits. The M-mudstone are always overlain by either DCD or flood plain facies.

Brown *et al.* (1986) also observed fining-upward cycles in U-sandstones. However, U-sandstones are more thinly-bedded than M-sandstones. Local coarsening-upward trends are also visible. In addition, crossbedding occurs in smaller scale. Bioturbated, shelly and locally-laminated U-mudstone facies is interbedded with the U-sandstone lithofacies. Therefore, the upper zone is described as "deposits of shallow, upper delta front environment, on the seaward sloping margin, adjacent to a lower deltaic plain" produced under increasing marine influence.

In a very similar sense, Hurley *et al.* (1992) interpreted the palaeo-environments of the Hibernia Formation and the adjacent strata. In their interpretation, deposition started with

delta front sedimentation at the base of the formation overlying prodeltaic shales of the Fortune Bay Formation. A complex thick delta plain sequence consisting of distributary channel, levee, crevasse splay, flood plain, bay, marsh and abandoned channel deposits and a medial shale marker overlie delta front deposits. These delta plain deposits correspond to the Main Hibernia Zone classification of Brown *et al.* (1986). Thinly-bedded sandstones of small scale coarsening-upward cycles overlying the delta plain sequence are interpreted as a bay and thin crevasse splay sequence. This latter sequence represents the increased influence of marine sedimentation and therefore corresponds to the Upper Hibernia Zone of Brown *et al.*

Three cross sections of the Hibernia Formation (southwest-northeast, south-north, and west-east (Figure 7a,b,&c) in the Hibernia oil field) illustrate another approach to subdivision of the unit into 4 layers. Zonation and geologic tops are adopted from the interpretation of CNOPB (Schedule of Wells 1990). The thinnest layer (4) is the deepest zone in the Hibernia formation and was only cored in Hibernia C-96. Examination of layer 4 cores indicates that shales and slight coarsening-upward trends constitute this zone (see grain size log of Hibernia C-96 at 3939.7-59 m, appendix 1).

Layer 3 of the Hibernia formation was intensively cored. Therefore, the greatest range of visual evidence derived through core analyses are present in this segment of the reservoir. Layer 3 mainly contains the fining-upward cycles of the channel deposition consisting of thick bodies of sandstones and rare basal conglomerates. Interstratified sandstone/ siltstone/ shales, mudstone and shale lithofacies are rarely described in this section.

Cores of the medial shale, layer 2 and layer 1 reflect a decreasing influence phase of the delta deposition, where sandy channel bodies begin to get thinner and the interstratified lithologies and the shales become more abundant (grain size log of K-14; appendix 1)

Lithofacies HF3, HF1F, HF1D, HF1C1, HF1C, HF1B, and HF1A provide greater detail to the lithologic variation and form fining-upward trends in all of the five cored Hibernia wells. These facies form and regular log responses with very sharp, either erosive (see Hibernia K-18 at 3830-3860m; appendix 1) or gradational basal contacts with the underlying strata and usually produce gradational boundaries with overlying lithologies. The very coarse to very fine-grained sandstones in this group of facies corresponds to the distributary channel deposits (DCD) of Brown *et al.* (1986) produced in a delta plain environment. Although the high hydrocarbon content of DCD facies prevents precise identification of the characteristic sedimentary structures, high angle cross stratification, including trough and lenticular crossbedding, is observed. Migrating channels can produce large-scale crossbedded signatures during the migration of channel bars (Hurley *et al.* 1992). HF3 conglomerates overlying scoured and eroded surfaces are probably coarse-grained lag deposits formed at the base of the distributary channel system. Rip-up mud clasts encountered within the HF1C1 sands are commonly observed in association with the underlying shales of HF4 from where the mud clasts were originated. Zones of rip-up mud clasts are reported to form tight zones in sandstones (Kramers *et al.* 1989) where the magnitude of permeabilities are reduced. Therefore significant permeability reductions in the HF1C1 sands are expected.

Very fine to fine-grained sandstones of lithofacies HF1E and HF1E1 containing ripple

crosslamination, horizontal, convolute and wavy bedding overlie DCD sandstones. The sedimentary structures and the sequence of deposition indicate that the HF1E and HF1E1 sands mark fluvial levee deposition.

Slightly-burrowed, highly-deformed and-thinly interbedded sandstone, siltstone and shales of HF2A generally overlie crossbedded, upward-fining sandstones of the delta plain deposits and underlie soft, flaky, and carbonaceous shales of HF4 which occasionally contain rootlets and soil zones. HF2A, therefore, can be described as floodplain deposits formed by channel abandonment (Hurley *et al.* 1990) and corresponds to the M-sandstone/mudstone facies of Brown *et al.* (1986), whereas the HF4 shales represent marsh/swamp deposition with occasional soil zones where subaerial exposure zones were identified. Increasing bioturbation and degree of burrowing, the interstratified character of the sands, silts, and shales, and abundant soft deformation structures of HF2B, HF2C, and HF5 record interdistributary marine bay deposition. Lithofacies HF2B and HF2C are commonly found in association with DCD sands, HF4 shales and interbedded HF2A sediments.

Reineck and Singh (1973) described fine rhythmically-laminated sandy and muddy sediments separated by sharp contacts as "rhythmic bedding produced from tidal changes." The rhythmic bedding in HF2B records the effects of tidal working. Moderate burrowing provides evidence for marine influence in the related sections of the cores. However, rhythmites are solely encountered in K-18 in a thickness of <2 m (gr. size log of K-18; app. 1). Thus a restricted tidal influence in the northeast portion of the oil field can be concluded.



Figure 9a: Very fine-grained sands of HF1A are encountered with the fine-grained sands of HF1B in fining-upward sequences (3,797.25 m, Hibernia K-18).



Figure 9b: Well-consolidated, fine-grained quartz sandstones of HF1B are slightly oil-stained (3,807.50 m, Hibernia K-18).



Figure 9c: Oil-wetted, upper fine- to lower medium-grained reservoir sands of HF1C constitute the main pay in the formation (3,935.70 m, Hibernia K-14).



Figure 9d: Elongate rip-up mud clasts are abundant in the lower medium-grained sandstones of HF1C1 (3,939.50 m, Hibernia C-96).



Figure 9e: Carbonaceous, quartzitic, medium- to coarse-grained sands of HF1D. Sedimentary structures are not preserved (3,869.70 m, Hibernia K-14).



Figure 9f: Quartzitic basal sandstones of HF1F are coarse-grained. No evident structure other than a few faint crossbeds is observed in the lithology. HF1F sands are found in the bases of fining-upward cycles (3,923.2 m, Hibernia C-96).



Figure 9g: Pebbly and bimodal sands of HF3 are basal lag sediments which form the base of fining-upward cycles. The photo shows the HF3 lithology in association with medium-grained sands (3,909.40m, Hibernia C-96).



Figure 9h: Ripple cross lamination and abundant carbonaceous zones are evident in the very fine- to fine-grained sandstones of HF1E (3,622.18 m, Hibernia K-18).



Figure 9i: Coarbonaceous and horizontally-laminated sands of HF1E1 also contain ripple cross lamination and lenticular sand beds (3,820.1 m, Hibernia K-18).

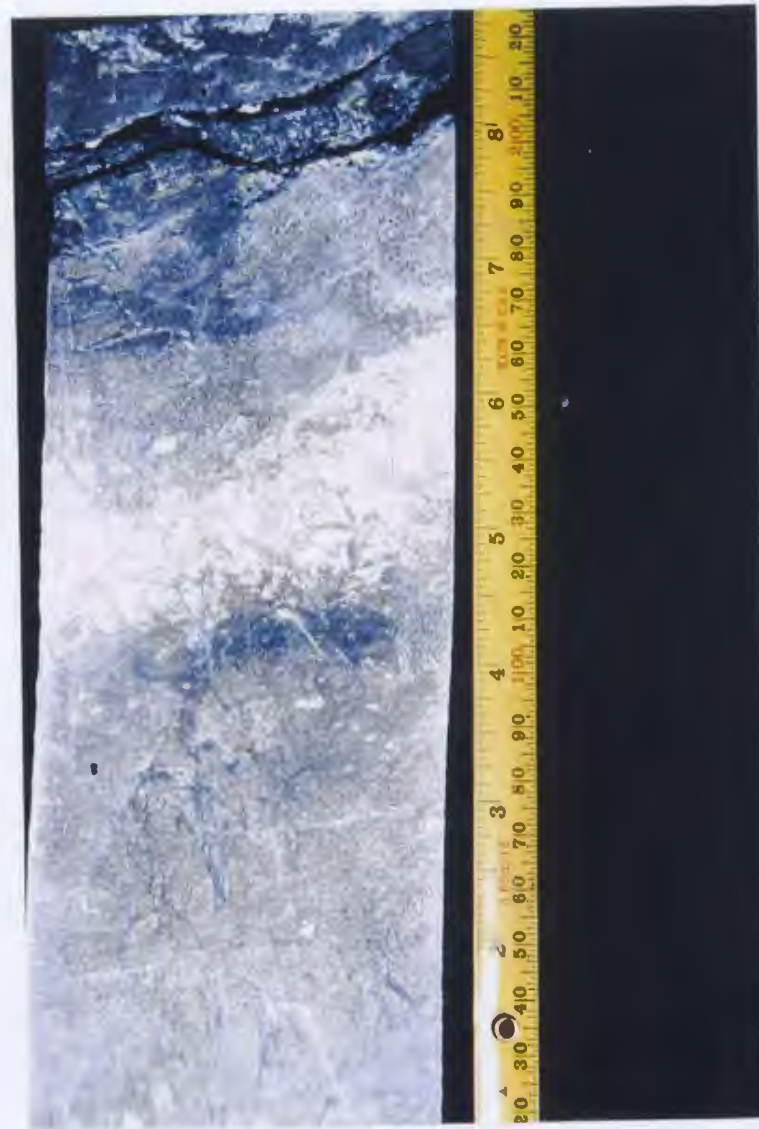


Figure 9j: Argillaceous very fine-grained sands of HF1G contain vertical plant roots. A coaly bed is present at the top of the section. HF1G occurs only in Hibernia B-27 (3,874.9 m).



Figure 9k: Very carbonaceous, poorly-consolidated fine-grained sands of HF6 are also recorded only in Hibernia B-27 (3,848.4 m).



Figure 9l: Slightly-burrowed, churned, contorted and interstratified sandstone, siltstone and clayshales of HF2A. The lithology is encountered in association with coarser sandstone facies as the top member of fining-upward cycles (3,919.2 m, Hibernia C-96).



Figure 9m: High shale content and lenticular sand lenses are characteristics of HF2B (3,624.9 m, Hibernia B-O8).



Figure 9n: Bioturbated, heavily-burrowed, and interstratified silt, shale and sandstone of HF2C (3,879.6 m, Hibernia B-27).



Figure 9o: Carbonaceous, loose shales of HF4 are frequently exposed as soil zones. Upper boundaries of HF4 shales are commonly truncated by coarse-grained sands ("soil zone", 3917.4 m, Hibernia C-96).



Figure 9p: Shales of HF5 contain shell fragments (3,950.8 m, Hibernia C-96).

IV - SEM MICROPHOTOGRAPHY AND EDS ELEMENTAL ANALYSIS

IV.1- METHODOLOGY

29 samples were selected for microphotography and elemental analyses of the 16 Hibernia lithofacies. Locations of the SEM/EDS-treated specimens are marked on the grain size logs of the cored intervals in appendix 1. Specimens with freshly broken rough surfaces are assumed to represent the actual reservoir rock and rock properties. Sample cuttings were initially carbon-coated and sealed along the stub-sample interface with silver paste and silver paint in order to prevent electrical overcharging which causes interference during the photography processes. The samples were then gold-coated in an Edwards S150A Sputter coater in order to increase the precision of the photography.

The double-coated cuttings were examined in a Hitachi S570 Scanning Electron Microscope at an accelerating voltage of 20 kV. X-ray analyses were performed in beam spot mode with a Tracor Northern 5500 Energy Dispersive X-ray analyzer equipped with a Microtrace silicon X-ray spectrometer, Model 70152. Spectral resolution was 145 eV. Detector positioning gave an effective take-off angle of 30 degrees (C. Emerson-MUN, personal communication 1995).

Element concentrations were calculated using Tracor Northern's software package "SSQ", Standardless Semi-Quantitative Analysis which modelled and subtracted the background, measured peak intensities, and then provided analysis of samples without standards, using a ZAF correction program to calculate element percentages. Secondary electron images were

recorded on Polaroid Type 665 Positive/Negative films. Standard X100 magnification was used for each sample. Suites of X100, X300, X700 and X2,000 times magnified images were used to identify mineral types, and porosity attributes. Elemental analyses acquired in surface-scan mode at X100 mag. were accepted as being representative of the whole specimen (Table 3) and were plotted against permeability in order to correlate the abundance of certain mineralogy with the flow properties of the reservoir (Figure 10a-10j). For the same purpose, Si/Al ratios were calculated and plotted against permeability.

The coding procedure of the samples in the analyses is as follows:

Plug Name-Facies segment#-magnification code-location of beam spot analysis (i.e., SP102-HF1A 1-A-1)

Magnification Codes: A=X300 mag. A1=X700 mag. A2=X2000 mag.

IV.2- STANDARDLESS SEMI-QUANTITATIVE ANALYSIS (SSQ)

IV.2.1- Analyzing irregularly-shaped bulk specimens and geometric effects:

Rock specimens that were used in SSQ analysis do not meet the geometrical requirements of ideal specimens. The ideal specimen concept is restricted to those that are flat and mounted at known angles to the electron beam and the spectrometer (Goldstein *et al.* 1981). Irregularly-shaped rock specimens are influenced by "geometrical effects" which are divided into three major groups as mass, absorption, and fluorescence effects (Goldstein *et al.* 1981). The fluorescence effect has relatively less influence on analysis.

In the mass effect, electrons may escape from the sides and the bottom of the specimen

resulting in decreased intensity of readings. In the absorption effect, the absorption of an electron beam proportionally increases with the length of the absorption path in the particle. For rough-surfaced bulk samples, the length of the absorption path can vary as a function of "electron beam placement" and "particle size" (Goldstein *et al.* 1981). The fluorescence effect is only significant when minor heavy elements in a light matrix composed of C, O, Al, Si are in the area of interest. Heavy elements in a specimen may produce x-ray lines that are close to the absorption edges of the surrounding elements. Therefore, up to 20% of detected intensities may be derived from the fluorescent x-rays.

In order to minimize geometrical and fluorescence effects, working distance, column voltage and gathering time were standardized by being kept the same. Standardized procedure and associated EDS analyses were used for comparative petrography that has defined relative petrophysical changes between analyzed targets (Gies *et al.* 1992). Clays, framework, and accessory grain mineralogies were identified by integrated examination of photomicrographs and spectrums. As Gies *et al.* (1992) stated, the advantage of the SEM/EDS combination over X-ray analysis is that the analyzed feature, its morphology and distribution can be observed and more precise mineral identifications can be acquired.

IV.2.2- Non-detectables and pseudo-detections:

An SEM/EDS analyzer is designed to obtain detections from the elements with atomic number (Z) above 11 (>Sodium)(Welton 1984).

Drilling fluids may contain dispersant polyphosphates (SAPP, Calgon, Barafos, TSPP - thinning agents) to control viscosity of mud (Chilingarian and Vorabutr 1983). Although the

components of the invaded drilling mud could have had effect on P detections. P, S, and Cd detections in the analyses are not real. Emission lines of coating agents, silver and gold overlap with P, S, and Cd energy levels and generate pseudo-detections of those elements.

IV.2.3- The analysis

Table 3 provides depth and porosity/permeability information about the samples which were elementally-analyzed and photographed by SEM/EDS combination. Locations of the samples are marked on grain-size logs of the five Hibernia wells (see appendix 1). Mineral identifications were performed by a comparative approach using Welton's (1984) petrography atlas.

IV.2.3.1. Standard comparator spectra

In order to avoid repetitious presentations of similar mineral detections, representative chemical compositions and typical spectra collected from the encountered mineralogies in the EDS analyses are presented in table 4 and figure 11a-e. These spectra represent standard EDS responses acquired from different spots in different specimens. Beam-spot mode analyses can acquire element concentrations from either a single or many different mineral types depending on the electron beam magnitude and the size of the crystals or grains in the analyzed surface. Estimates for dominant mineral type(s) were determined based on the spectra and atomic weight percentages of detected elements, and visual identification of mineral(s) in photomicrographs.

Sample Code	Well	Depth (m)	Por-%	k (mD)	Mg	Al	Si	K	Ca	Fe	Cr	Na	Cl	P*	Ti	S*	Cd*	S/Al
P269-HF1A	K-14	3,910.25-10.50	9.20	0.61	0.25	10.57	74.59	2.50	0.00	7.04	0.00	0.18	0.23	4.64	0.00	0.00	0.00	7.06
SP102-HF1A	K-18	3,797.12-97.34	12.80	15.30	0.56	4.77	69.41	0.51	0.22	6.23	0.03	1.26	0.11	10.15	0.96	5.81	0.00	14.66
P218-HF1B	K-14	3,874.78-75.08	14.60	44.00	1.68	6.96	62.95	1.94	3.37	2.10	0.07	1.99	1.03	11.63	0.12	8.04	0.04	10.38
SP102-HF1B	B-08	3,624.17-24.30	12.30	52.70	0.84	4.64	73.69	0.59	1.47	0.63	0.12	1.36	0.59	9.73	0.34	5.88	0.15	15.98
P85-HF1C	C-96	3,881.56-81.92	16.50	1,480.00	0.77	3.98	68.55	2.34	0.50	0.69	0.01	1.56	1.94	10.35	0.78	8.54	0.00	17.24
P315-HF1C	K-14	3,935.56-35.89	21.40	2,030.00	0.18	3.08	82.39	1.14	0.00	0.50	0.00	1.05	3.29	8.30	0.07	0.00	0.00	26.75
SP249-HF1C	K-18	3,855.75-55.94	18.60	615.00	0.45	6.49	80.02	1.41	0.55	1.77	0.01	0.60	0.63	7.19	0.88	0.00	0.00	12.33
SP99-HF1C1	C-96	3,894.55-94.80	4.60	0.03	0.45	11.97	68.40	1.44	0.00	4.45	0.06	0.79	0.25	6.08	0.02	6.10	0.00	5.71
P208-HF1C1	K-14	3,862.43-62.75	14.20	0.32	1.57	11.63	59.77	3.58	0.29	2.80	0.13	2.26	2.72	8.73	0.44	6.06	0.07	5.14
P347-HF1D	K-14	3,869.12-69.36	19.40	4,640.00	0.00	1.09	78.14	0.63	0.00	0.80	0.00	0.00	0.43	8.18	1.46	8.34	0.94	33.78
P349-HF1D	K-14	3,869.60-69.83	22.50	9,710.00	0.93	4.64	78.80	1.37	0.53	0.92	0.15	0.87	0.88	9.35	1.98	N/A	N/A	17.00
SP74-HF1F	B-08	3,606.18-06.29	19.30	1,290.00	0.00	2.94	68.38	0.00	0.00	1.85	0.00	0.00	0.00	13.57	1.10	11.23	0.94	23.26
P160-HF1F	C-96	3,923.08-23.44	18.50	2,780.00	1.52	4.02	59.55	0.71	0.95	0.11	0.07	2.52	0.97	16.46	0.03	8.10	3.84	14.80
P134-HF3	C-96	3,909.28-09.48	13.20	238.00	0.22	3.60	77.31	1.67	0.30	1.20	0.07	1.32	4.82	7.19	2.33	0.00	0.00	21.50
P345G-HF3	K-14	3,962.42-62.70	13.50	273.00	0.62	5.63	73.07	0.75	0.21	2.28	0.05	1.14	0.95	8.58	0.17	6.59	0.00	12.99
SP277-HF1E	B-27	3,905.76-05.85	13.30	8.85	0.50	5.88	70.05	1.77	0.70	1.67	0.00	0.69	2.30	9.34	0.43	6.57	0.10	11.91
P145-HF1E	K-18	3,822.18	13.00	29.60	2.87	6.18	59.23	1.00	0.48	0.90	0.21	3.48	1.41	13.85	0.37	9.45	0.59	9.59
P137-HF1E1	K-18	3,820.00-20.18	5.20	0.13	1.86	19.44	55.95	6.56	0.45	6.24	0.13	1.90	0.87	4.24	2.37	0.00	0.00	2.88
SP244-HF1E1	B-27	3,893.12-93.32	7.90	0.14	0.15	5.46	55.01	10.73	8.14	1.73	0.00	0.00	12.98	5.95	N/A	0.00	0.00	10.07
SCA29-HF1G	B-27	3,873.06-73.20	11.70	0.42	1.60	9.94	67.15	2.65	0.05	4.29	0.07	1.51	0.65	6.74	0.53	4.66	0.15	6.76
SP162-HF6	B-27	3,847.53-47.66	13.80	145.00	0.61	4.78	71.16	0.80	0.08	2.39	0.00	1.39	0.70	10.31	0.37	7.31	0.10	14.89
P147-HF2A	C-96	3,919.15-19.44	11.40	0.62	2.20	15.31	56.18	3.85	0.21	2.80	0.10	2.70	1.30	8.60	1.03	5.44	0.30	3.79
P219-HF2A	B-27	3,874.19-74.40	10.90	0.45	3.28	8.36	46.89	1.83	0.39	2.30	0.40	4.25	1.37	17.44	1.03	12.46	0.00	5.61
SP235-HF2B	B-27	3,884.64-84.86	7.50	0.06	0.61	9.88	79.58	2.88	0.05	2.55	0.00	0.00	0.18	3.68	1.22	0.00	0.00	8.05
SP103-HF2B	B-08	3,624.83-25.00	3.50	0.09	0.60	18.49	65.24	3.34	0.08	3.03	0.10	0.99	0.18	6.48	1.11	0.00	0.00	3.53
3,806.3-HF2C	K-18	3,806.38	N/A	N/A	0.87	17.96	54.47	4.27	0.42	5.68	0.00	1.19	0.00	8.14	1.21	2.81	0.00	3.03
SP228-HF2C	B-27	3,879.57-79.67	9.0	0.93	0.87	19.89	56.19	7.23	0.29	7.01	0.05	0.73	0.00	5.20	2.54	0.00	0.00	2.83
3,912.9-HF4	B-27	3,912.90	N/A	N/A	1.22	13.56	61.46	3.56	1.19	2.42	0.00	1.55	0.42	8.09	0.68	5.85	0.00	4.53
3,945.45-HF5	K-14	3,945.45	N/A	N/A	0.48	14.91	54.64	3.97	0.00	4.88	0.00	4.43	8.14	4.72	0.74	3.09	0.00	3.66

N/A = Not Available, Mag. = Magnification, Por. = Porosity, * = "not real"-pseudo-reading.

Table 3. Element detections (%) were acquired in surface-scan mode at standard X100 magnification

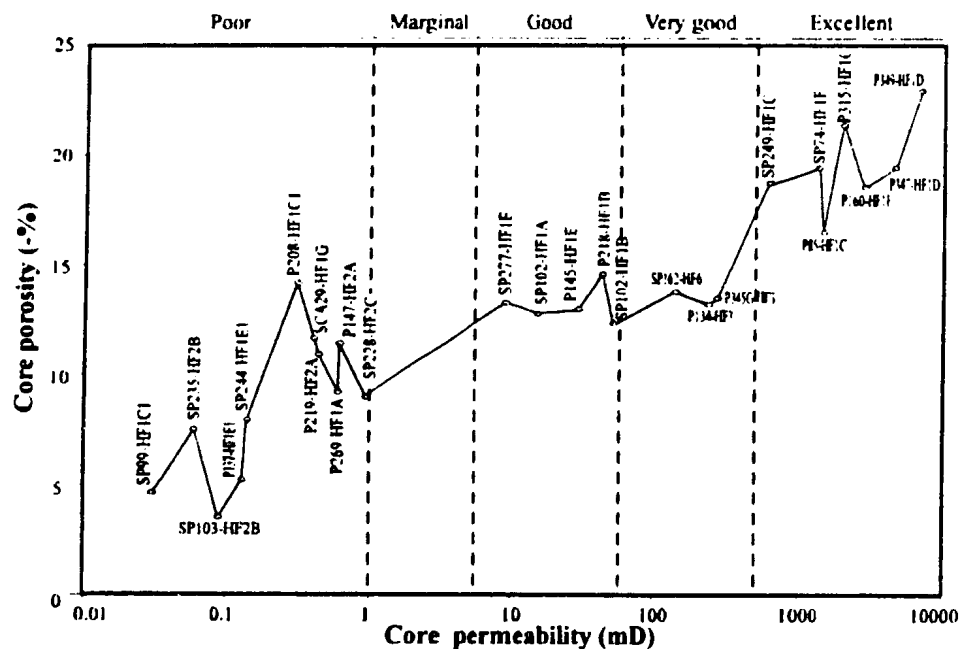


Figure 10a: Composite porosity-% - permeability relationship of the SEM/EDS-treated specimens.

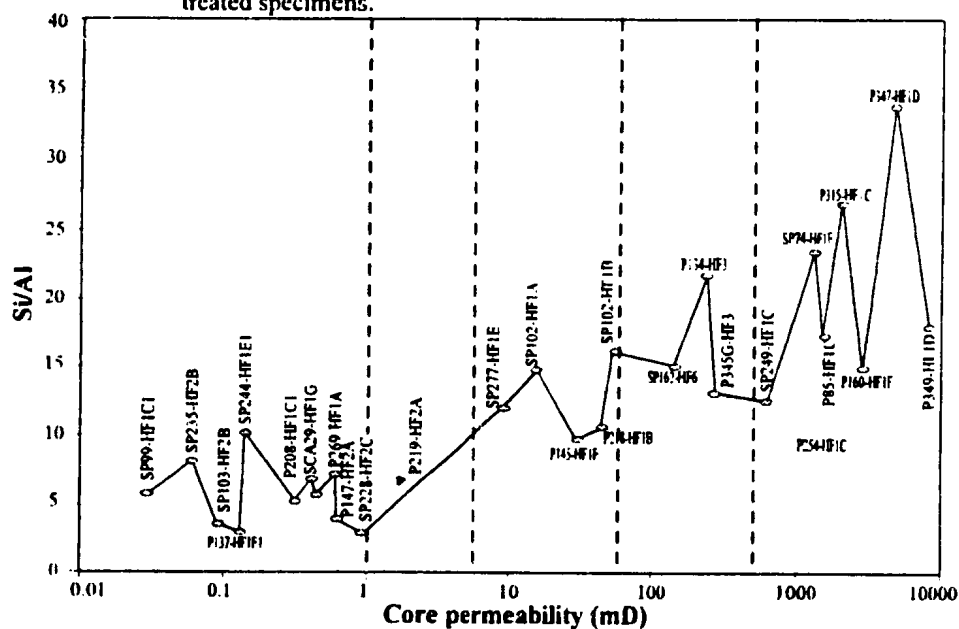


Figure 10b: Composite Si/Al ratio - permeability relationship of the SEM/EDS-treated specimens.

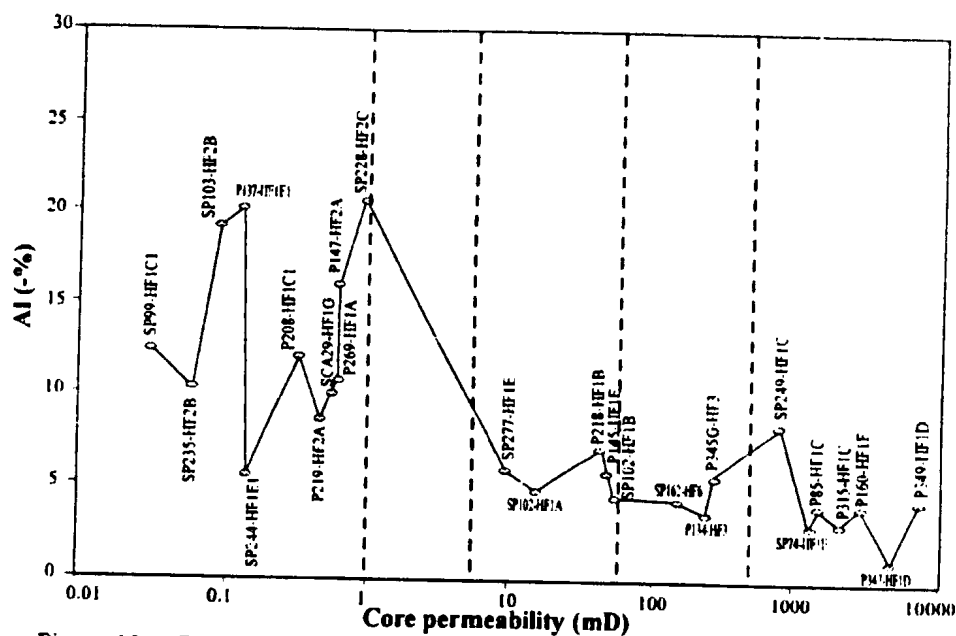


Figure 10c: Composite Al (%) - permeability relationship for the SEM/EDS-treated specimens.

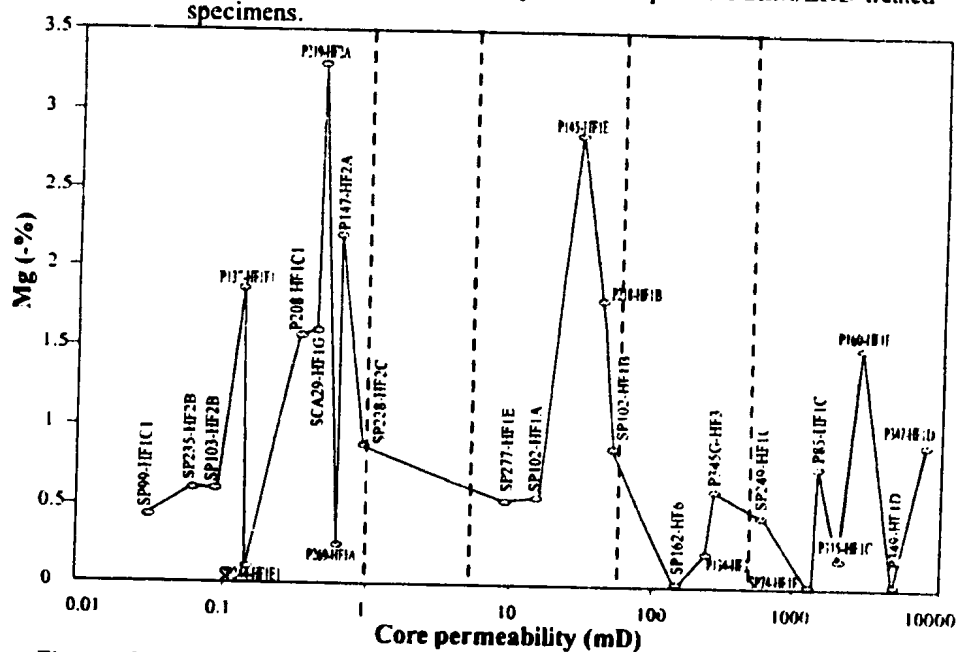


Figure 10d: Composite Mg (%) - permeability relationship for the SEM/EDS-treated specimens.

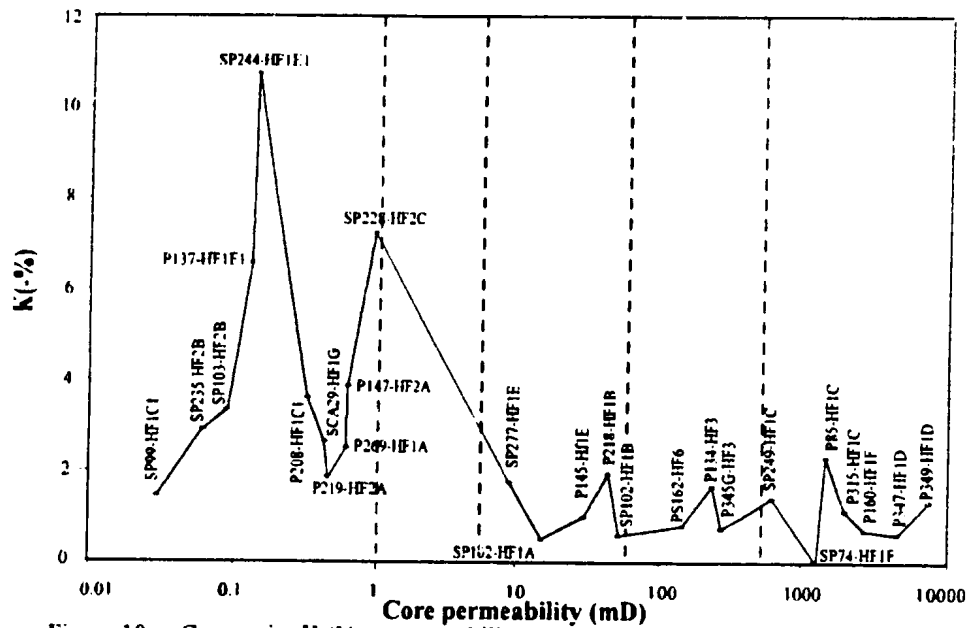


Figure 10c: Composite K (%) - permeability relationship of the SEM/EDS-treated specimens.

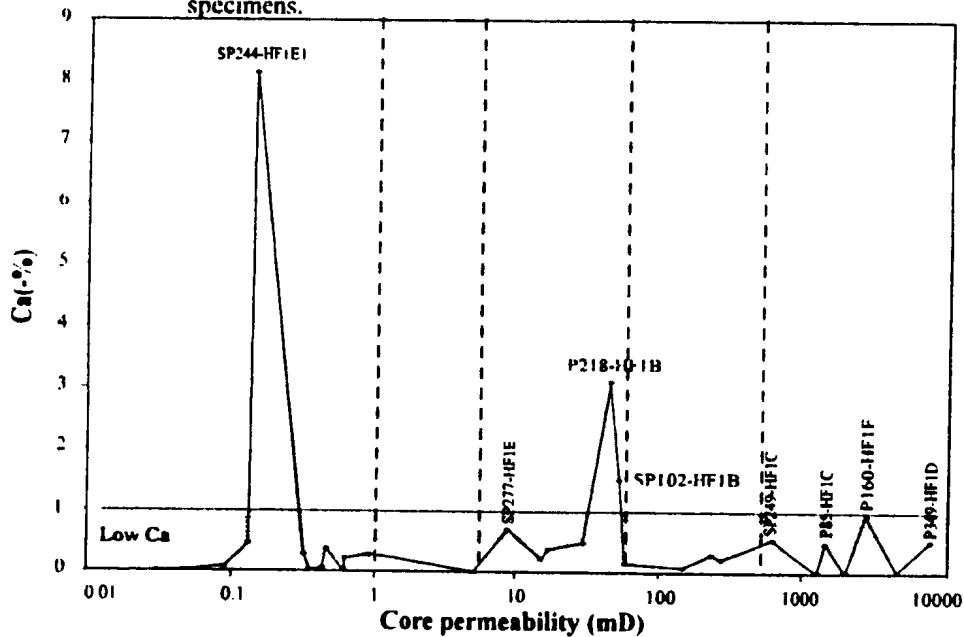


Figure 10f: Composite Ca (%) - permeability relationship of the SEM/EDS-treated specimens.

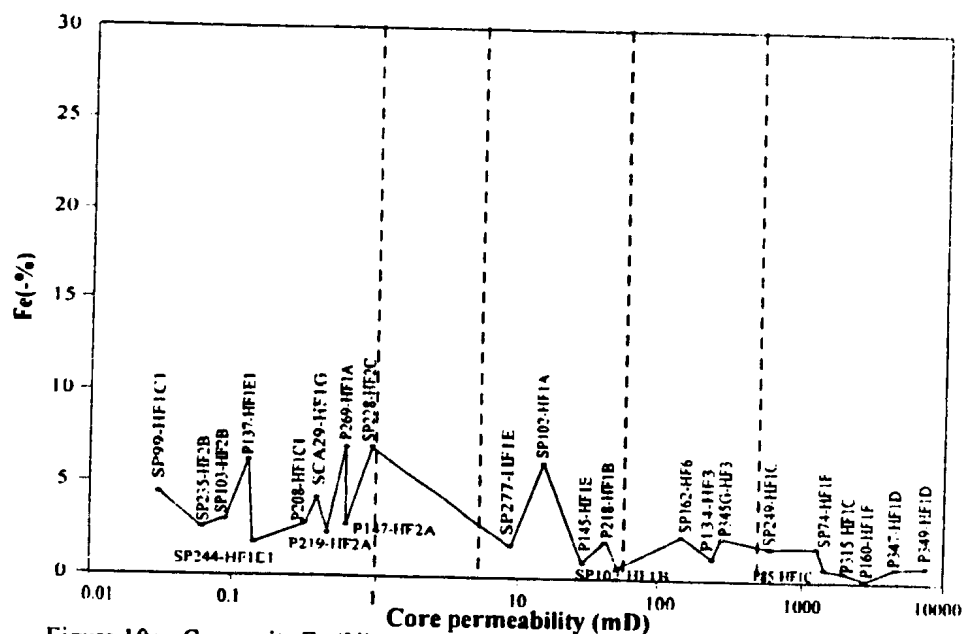


Figure 10g: Composite Fe (%) - permeability relationship of the SEM/EDS-treated specimens.

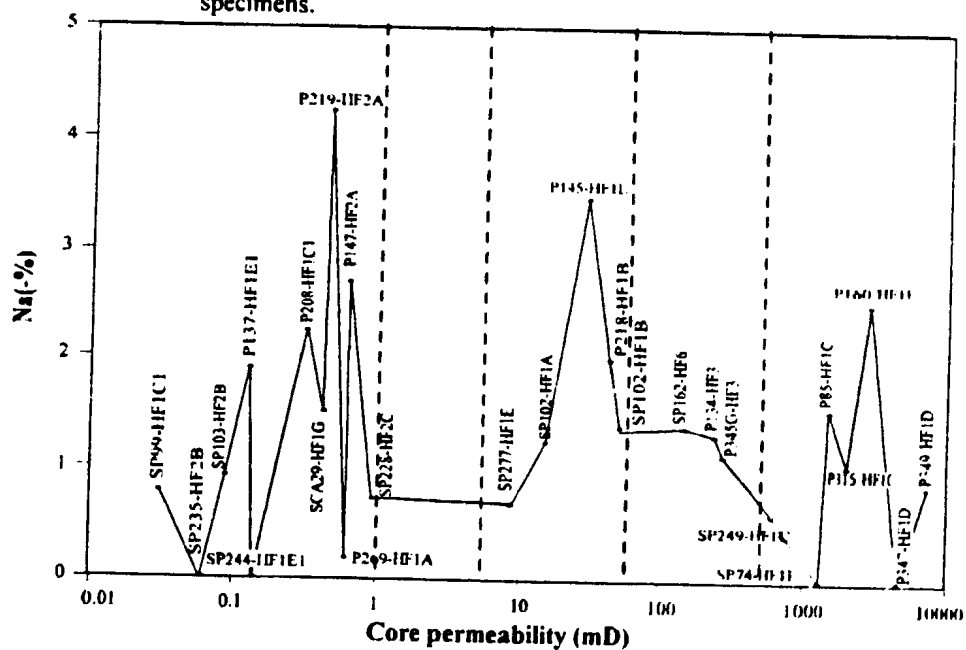


Figure 10h: Composite Na (%) - permeability relationship of the SEM/EDS-treated specimens.

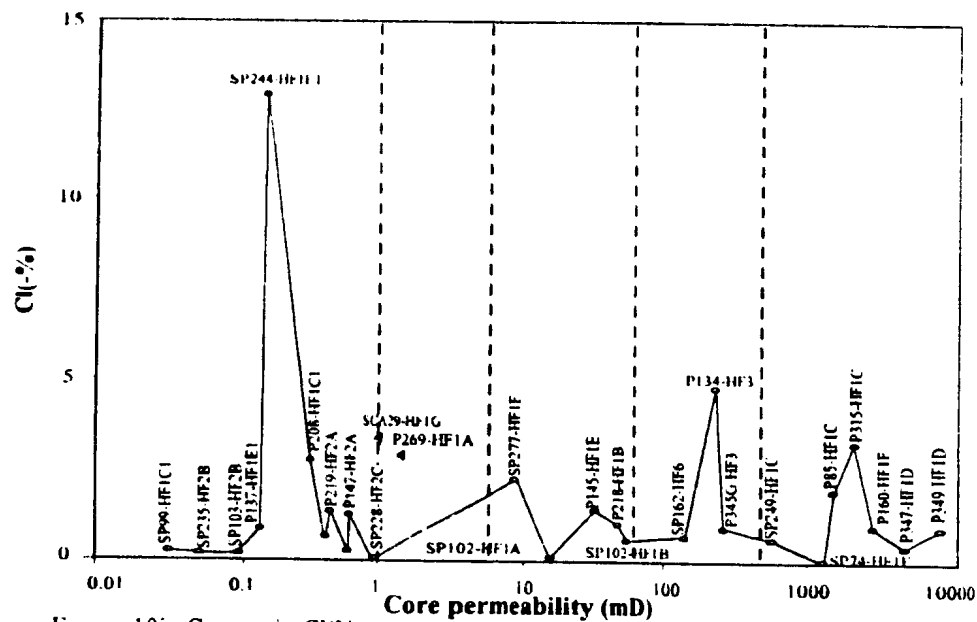


Figure 10i: Composite Cl(%) - permeability relationship of the SEM/EDS-treated specimens.

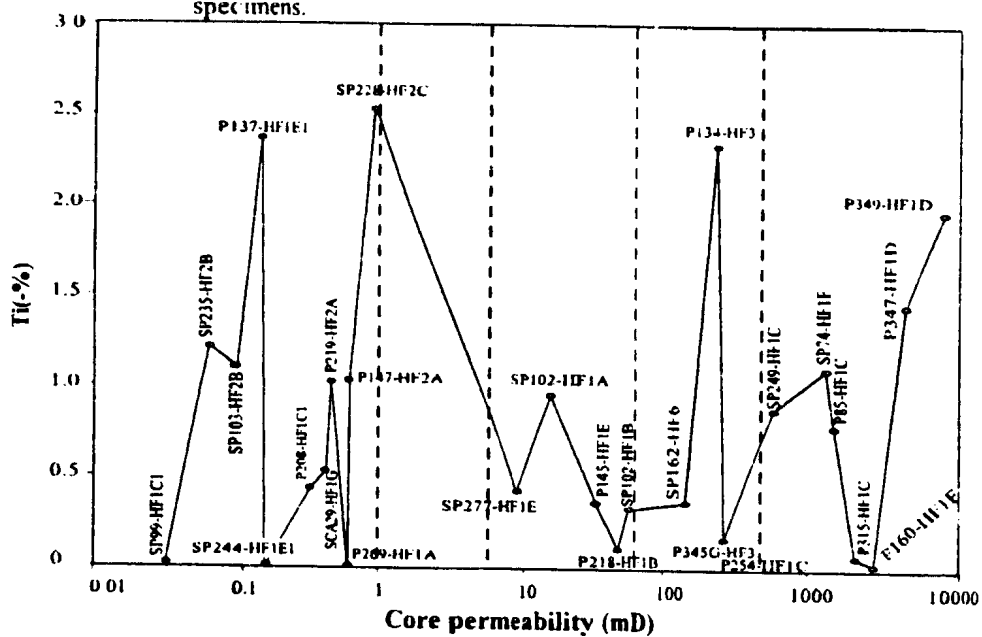
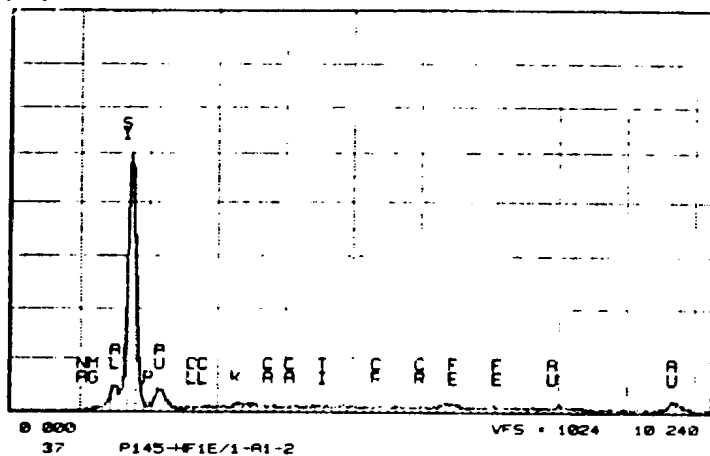


Figure 10j: Composite Ti(%) - permeability relationship of the SEM/EDS-treated specimens.

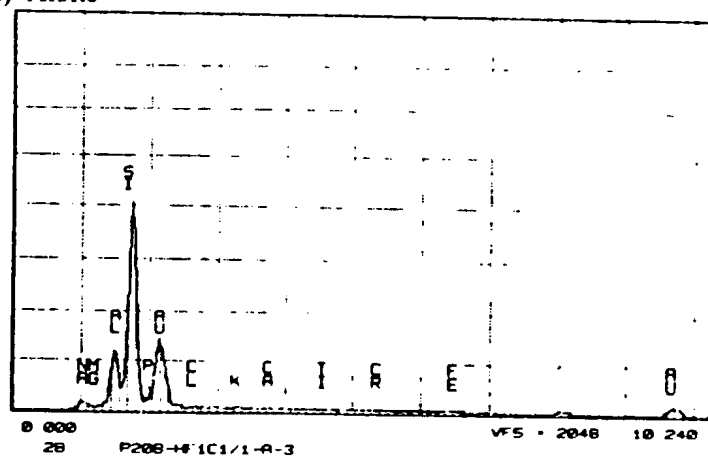
Table 4: Chemical groups and formulas of the EDS-detected minerals during SEM/EDS coupled processes. Standard spectra of the following elemental combinations are presented in figure 11a-e.

SILICATES/Silica	
Quartz	SiO_2
Feldspars	
Albite	$\text{Na}(\text{AlSi}_3\text{O}_8)$
K-Feldspar	KAlSi_3O_8
Plagioclase feldspar	$\text{Na}(\text{AlSi}_3\text{O}_8) - \text{Ca}(\text{Al}_2\text{Si}_2\text{O}_8)$
Clays	
Chlonte	$(\text{Mg}, \text{Al}, \text{Fe})_{12}[(\text{Si}, \text{Al})_8\text{O}_{20}](\text{OH})_4$
Illite	$\text{K}_{1-2}\text{Al}_2[\text{Si}_{3-4}\text{Al}_{1-2}\text{O}_{20}](\text{OH})_4$
Kaolinite	$\text{Al}_2[\text{Si}_2\text{O}_5](\text{OH})_4$
Smectite	$(1/2\text{Ca}, \text{Na})_n(\text{Al}, \text{Mg}, \text{Fe})_2[(\text{Si}, \text{Al})_4\text{O}_{20}]$
Corrensite	Chlonte - Smectite
Micas	
Biotite	$\text{K}_2(\text{Mg}, \text{Fe})^{+2}_{2-3}(\text{Fe}^{+3}, \text{Al}, \text{Ti})_2[\text{Si}_6\text{Al}_2\text{O}_{20}](\text{OH}, \text{F})_4$
Muscovite	$\text{K}_2\text{Al}_2[\text{Si}_4\text{Al}_2\text{O}_{20}](\text{OH}, \text{F})_4$
CARBONATES Calcite	CaCO_3
Dolomite	$\text{CaMg}(\text{CO}_3)_2$
Ferroan Dolomite/Ankerite	$\text{Ca}(\text{Mg}, \text{Fe}^{+2}, \text{Mn})(\text{CO}_3)_2$
Siderite	FeCO_3
SULPHIDES Pyrite	FeS_2
OXIDES Rutile	TiO_2
Ilmenite	FeTiO_3

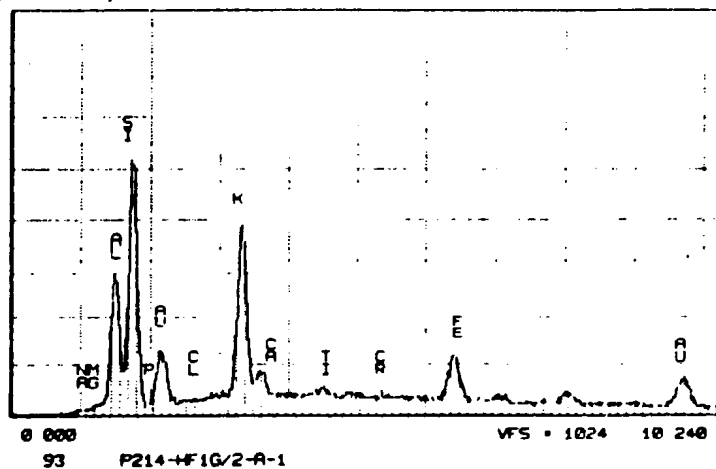
1) Quartz



2) Albite



3) K-feldspar



4) Corrensite/Mica

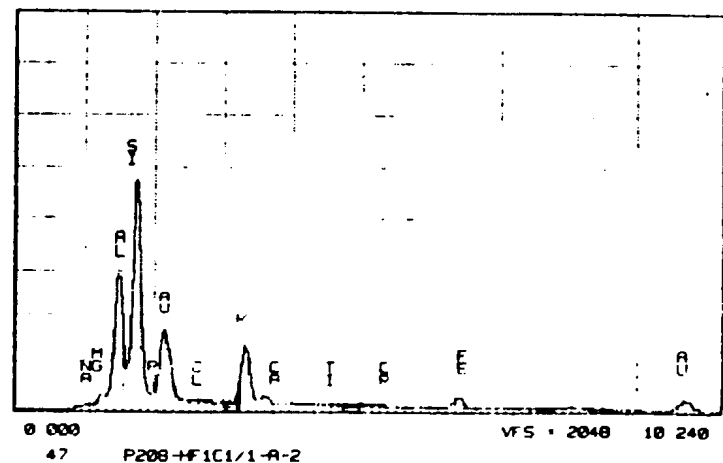
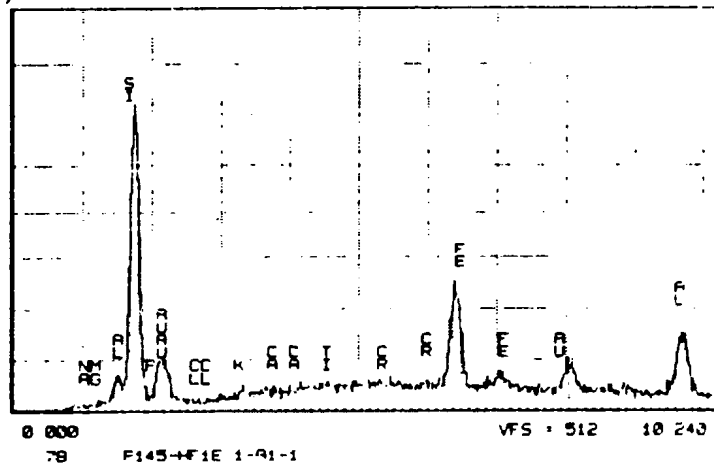
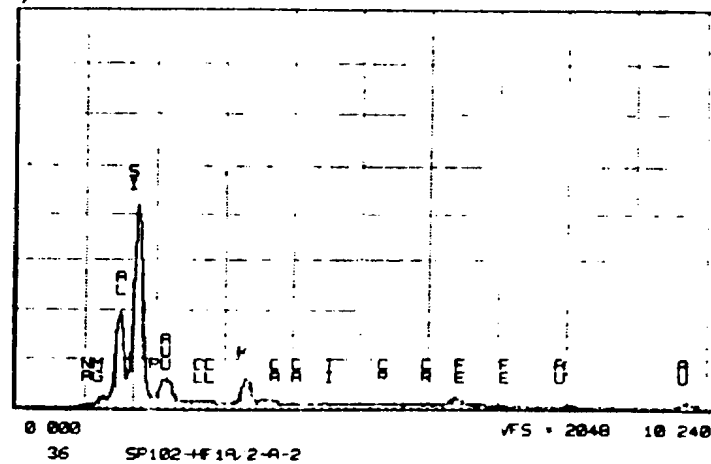


Figure 11a: Typical spectra of quartz, feldspar, and corrensite/(mica) analyses (beam spot mode)

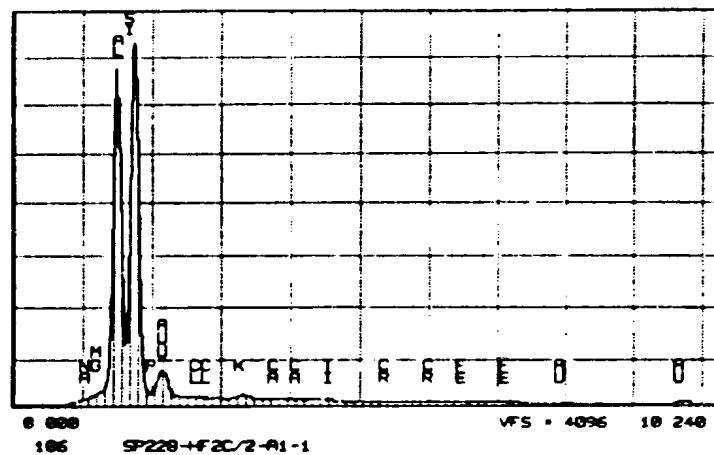
5) Chlorite



6) Illite



7) Kaolinite



8) Smectite

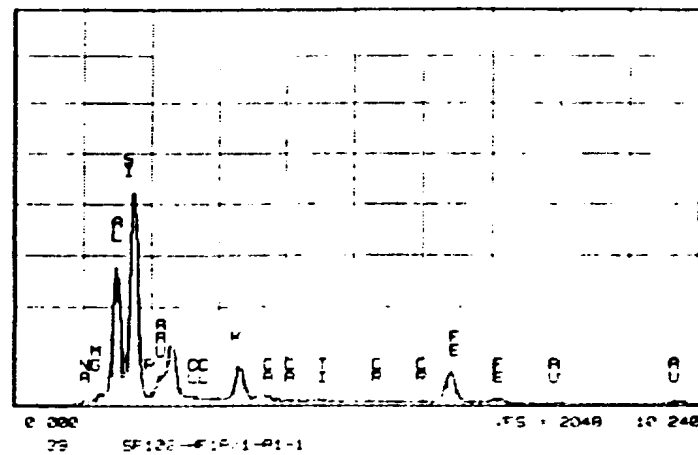
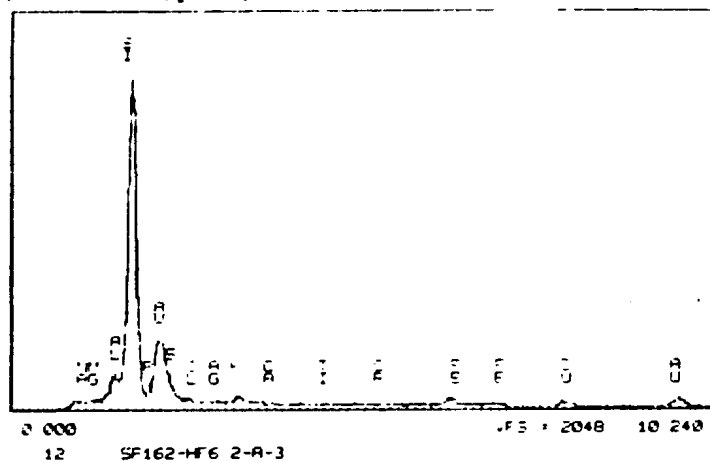
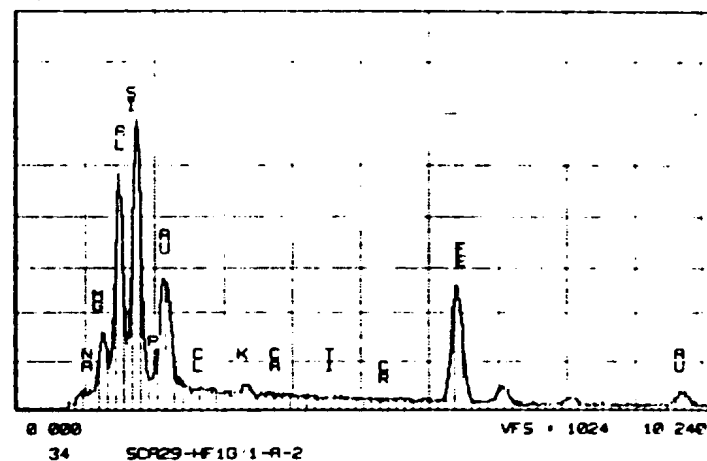


Figure 11b: Typical spectra of clay analyses (beam-spot mode) (also see corrensites in figure 11c).

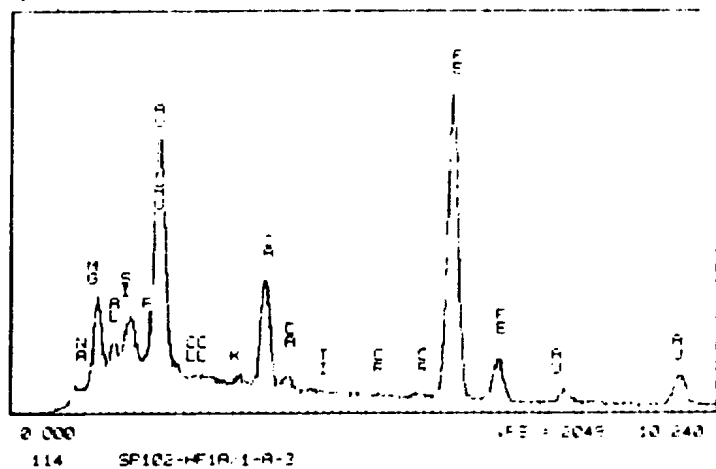
9) Muscovite/(quartz)



10) Biotite



11) Ferroan Dolomite



12) Calcite

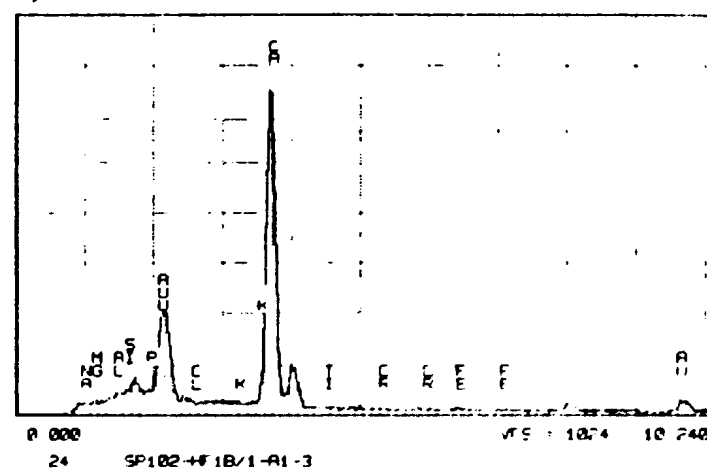
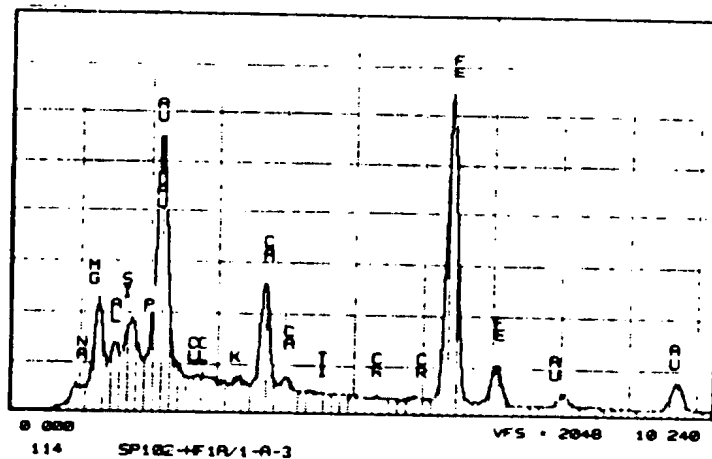
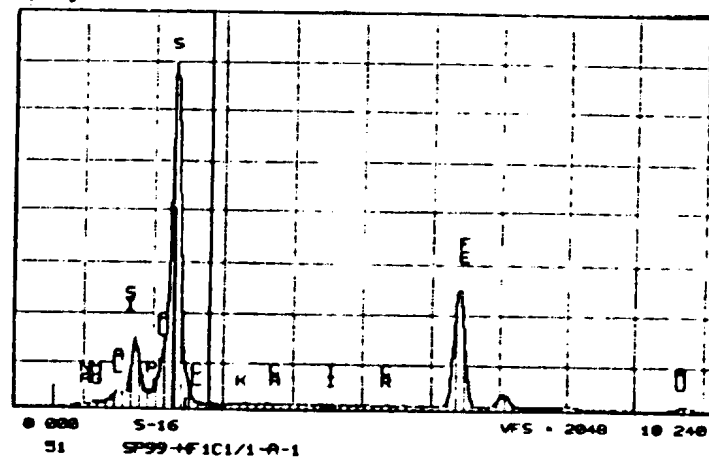


Figure 11c: Typical spectra of corrensite micas, ferroan dolomite, and calcite (beam-spot mode).

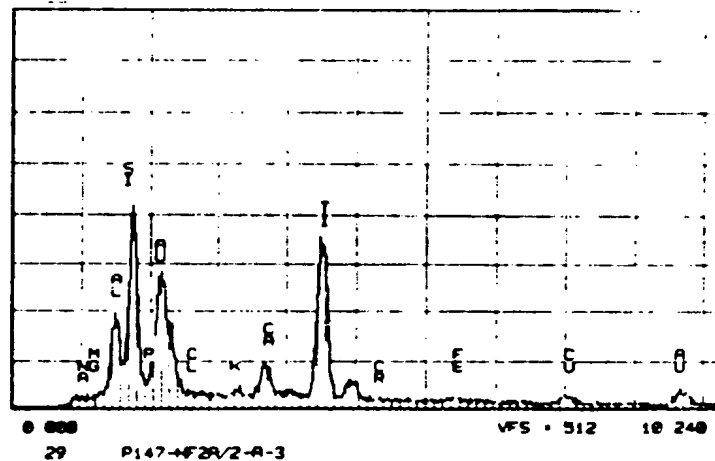
13) Siderite



14) Pyrite



15) Rutile



16) Ilmenite

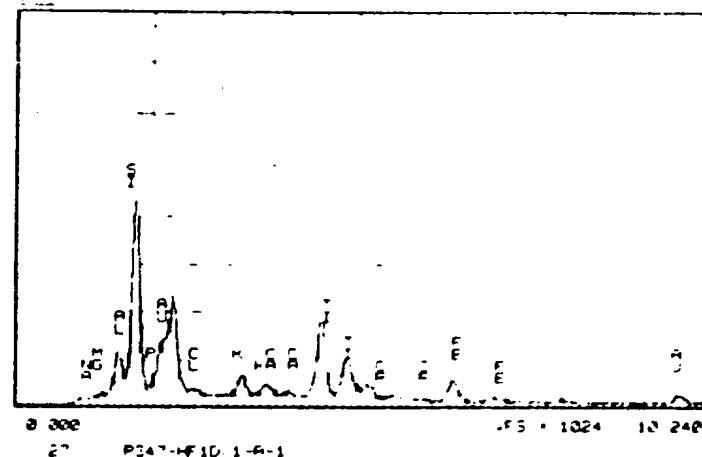


Figure 11d: Typical spectra of siderite, pyrite, and oxides (S peak in pyrite is magnified by metal contamination)

IV.2.3.2. SEM/EDS analyses of the Hibernia lithofacies

IV.2.3.2.1. Introduction

The objectives of performing high magnification SEM photomicrography and EDS elemental analyses on the Hibernia lithologies are as follows:

1. Identification of complex clay mineralogy, cement materials, diagenetic attributes, and minor additional mineralogy.
2. Visual assessment of pore morphologies, pore space, and connectivity relationships.
3. Determining relationships between the abundance and distribution of pore-controlling mechanisms and lithofacies groups.

Representative SEM photomicrograph suites referred of the Hibernia lithofacies are presented in figure 13-35 at the end of this chapter. Geochemical descriptions are performed based on Degen's (1965) interpretations. In order to see the described minerals in the beam spot mode analyses, use the coding system (numbers show the locations of beam-spot analysis) introduced in the section "IV.1-" and refer to the appendix 3.

IV.2.3.2.2. Pore space/connectivity-controlling mechanisms

IV.2.3.2.2a. Quartz overgrowths

The most commonly observed, pore-reducing component within the sand-dominated lithofacies is the authigenic quartz overgrowths. Abundances of quartz overgrowth crystals display a distinct distribution pattern within those lithofacies:

1. In the less argillaceous and porous sands in the fine to coarser grain sizes (HF1B, HF1C, HF1D, HF1F, HF3, and HF6) larger crystal forms (~width=100 μm ; figure 16b&19c)

and individual grain and crystal surfaces maintain their smoothness

2. In the argillaceous sands of very fine to lower medium grain size (HF1C1, HF1G, HF1E, HF1E1) micro size (~width 3-4 μm ; figure 20d), but numerous crystals coalesce to produce overgrowths, and overgrowth rims forming stepped pore surfaces. The micro quartz overgrowths display a honey comb-like structure in HF2A sample formed by the dimpling effect of bunched crystal terminations (Figure 33c). The smoothness of the framework grain surfaces was significantly disrupted.

Authigenic pore-lining and grain-coating clays, especially smectite, blocked quartz nucleation in some instances resulting in partially-grown quartz overgrowths (HF1B and HF1C) (Figure 15c and 19c). Similar results were reported earlier by Pittman *et al.* (1992)

IV.2.3.2.2b. Authigenic kaolinite

Authigenic kaolinite booklets were observed to occur in two major forms:

1. Isolated, discontinuous booklets
2. Pore-lining and pore-filling, continuous rims.

Isolated booklets were identified in porous, lower medium (mL)- to coarse-grained sands of HF1C (Figure 17), HF1D (Figure 23) and HF3 (Figure 27) where they formed discontinuous clusters without disrupting pore connectivity. SP249-HF1C, P349-HF1D, and P345G-HF3 exhibit lower Si/Al ratios as a result of the presence of the clays but permeability is not diminishing.

Pore-filling (Figure 21d) and pore-lining kaolinite (Figure 32c&d) were observed as continuous clay rims which effectively reduced the visual pore connectivity of the HF1A,

HF1C1, HF1E, HF1E1 and HF6 lithofacies.

IV.2.3.2.2c. Authigenic chlorite

Chaotic texture of authigenic chlorite in the form of blades perpendicular to the underlying grains was identified in the argillaceous sands of HF1C1(Figure 20), HF1E1 (Figure 30), and HF1G (Figure 31). Authigenic chlorite was observed to form grain coats and ragged/irregular grain surfaces and rough pore walls in the HF1C1, HF1E1, and HF1G specimens where high permeability reductions can be expected.

Authigenic chlorite was not identified in the interstratified shale facies (HF2A, 2B, and 2C) and shales of HF4 and HF5 in association with poor porosity.

IV.2.3.2.2d. Authigenic smectite and illite

Smectite was commonly described in all of the porous, very fine to coarse-grained sandstone lithofacies and was not detected in tighter (less porous) argillaceous sands and interstratified shale lithologies. Authigenic smectite was identified in the form of pore-lining (Figure 17d) and pore-bridging structures (16b) where pore connections and available pore space were reduced.

Relative to smectite, authigenic illite was less frequently encountered in the sample examinations. Solely HF1B and HF1E (Figure 29d) specimens yielded illite detections in the beam-spot mode. Illite formed in fine clay rims around pores in HF1B and HF1E where pore space reductions remain insignificant.

IV.2.3.2.2e. Carbonate cements

Calcareous cement is not common in the Hibernia sandstones. Two major carbonates

were determined in the specimens.

1. **Siderite cement and nodules:** Siderite was detected in the beam-spot mode analyses performed on intergranular, pore-blocking cement (Figure 32b). Detection of siderite cement is sporadic in HF1A, HF1B, HF1C and HF6. The presence of low abundance siderite cement is restricted to the very fine- to lower medium-grained sands. Rare siderite nodules were only identified in the very fine-grained sands of HF1A (Figure 13c).
2. **Calcite and dolomite cement:** Calcite cement was detected only in the fine-grained lithofacies of HF1B and HF1E1 (Figure 16b). Surface scan analyses of these samples yielded overall higher Ca detections (Table 3&Figure 10f) than background levels of the other lithofacies. Dolomite cement was detected only in lithofacies HF1B, in a minor fraction.

IV.2.3.2.2f. Detrital micas

Detrital muscovite and biotite were determined as two common constituents of the fine- to very fine-grained argillaceous sands and interstratified shales of HF2A, HF2B, and HF2C (Figure 14c). HF1C1 specimens were identified as exceptions to this grain size-abundance of mica pattern where the overall argillaceous material content of the HF1C1 specimens is greater. Other than this exception, the coarser-grained sands of HF1B, HF1C, HF1D, HF1F, HF3, and HF6 contained trace amounts of mica.

IV.2.3.2.2g. Additional minor mineralogy in argillaceous content

Feldspars, anhydrite, halite, rutile, ilmenite, sylvite were sporadically determined without

any specific pattern in the lithofacies. Rare sylvite detections were obtained in local and isolated forms in the specimens from Hibernia K-14 (P208-HF1C1; appendix 3; figure 20c). Well records report KCL-gel polymer mud systems were used in the drilling of the Hibernia Formation in K-14 (Well Summary 1983). This mud probably account for the sylvite occurrence. Secondary anhydrite laths and well-developed halite cubes were identified solely in P85 of the facies HF1C (Figure 18c). Anhydrite was described in aggregate form with intergranular clays which could be precipitated from the invaded mud, as well. Trace amount of rutile and ilmenite were detected only in the coarse-grained sands and conglomerates of HF1D, HF1F, and HF3.

IV.2.3.2.3. Interpretation of the SEM/EDS acquisitions by using ϕ/k crossplot

A combined lithofacies, core porosity, and permeability crossplot of core plug data display distinct data clusters, as well as scattered data points (Figure 12). The findings of the SEM/EDS-coupled analyses superimposed on this cross plot highlight the influence of certain diagenetic attributes on porosity and permeability. This crossplot allows us to determine different data packages possessing specific textural and diagenetic properties. The following conclusions can be drawn from the crossplot:

1. Argillaceous material including mica increases with the decreasing grain size.
2. Quartz overgrowths are larger and form individual grains in fine-to coarser-grained sandstones. The abundance of large overgrowths increases with the increasing grain size and decreasing argillaceous content.
3. Small (micro) quartz overgrowths are abundant in very fine- to fine-grained

lithologies and their abundance decreases with the increasing grain size and decreasing argillaceous content.

4. Authigenic kaolinite booklets are in an isolated and discontinuous form in the coarser-grained sands and do not significantly affect the flow properties of the related lithologies. Pore-filling and continuous authigenic kaolinite booklets are more commonly observed in the very fine-to fine-grained sandstones and are effective in pore reduction.
5. Authigenic chlorite is a significant component of those specimens in the porosity range of 10-15 % and the permeability range of 0.1-1 mD. The abundance of chlorite does not reflect a distribution related to grain size. Chlorite bearing specimens have fair porosities, yet they remain tight. This shows that authigenic chlorite can principally disrupt pore connections and cause significant permeability reductions while the overall absolute porosity does not change. Moreover, chaotic-textured authigenic chlorite increases surface friction and the resistance of the pore surfaces because the blade-like crystals grow perpendicular to the underlying grains.
6. Siderite cement and authigenic illite appears to decrease the porosity of the very fine- to lower medium-grained sandstone lithofacies.
7. Calcite cement is observed in fine-grained sands of HF1B and HF1E1.
8. Authigenic smectite was determined to be scattered without any distribution pattern. Therefore, smectite component of the lithofacies is not presented in the crossplot.
9. The identified features and patterns represent only the findings of the SEM/EDS analyses. Resolution and extrapolation of the patterns and trends identified in figure 12 can be improved by increasing sampling density over the whole range of lithofacies.

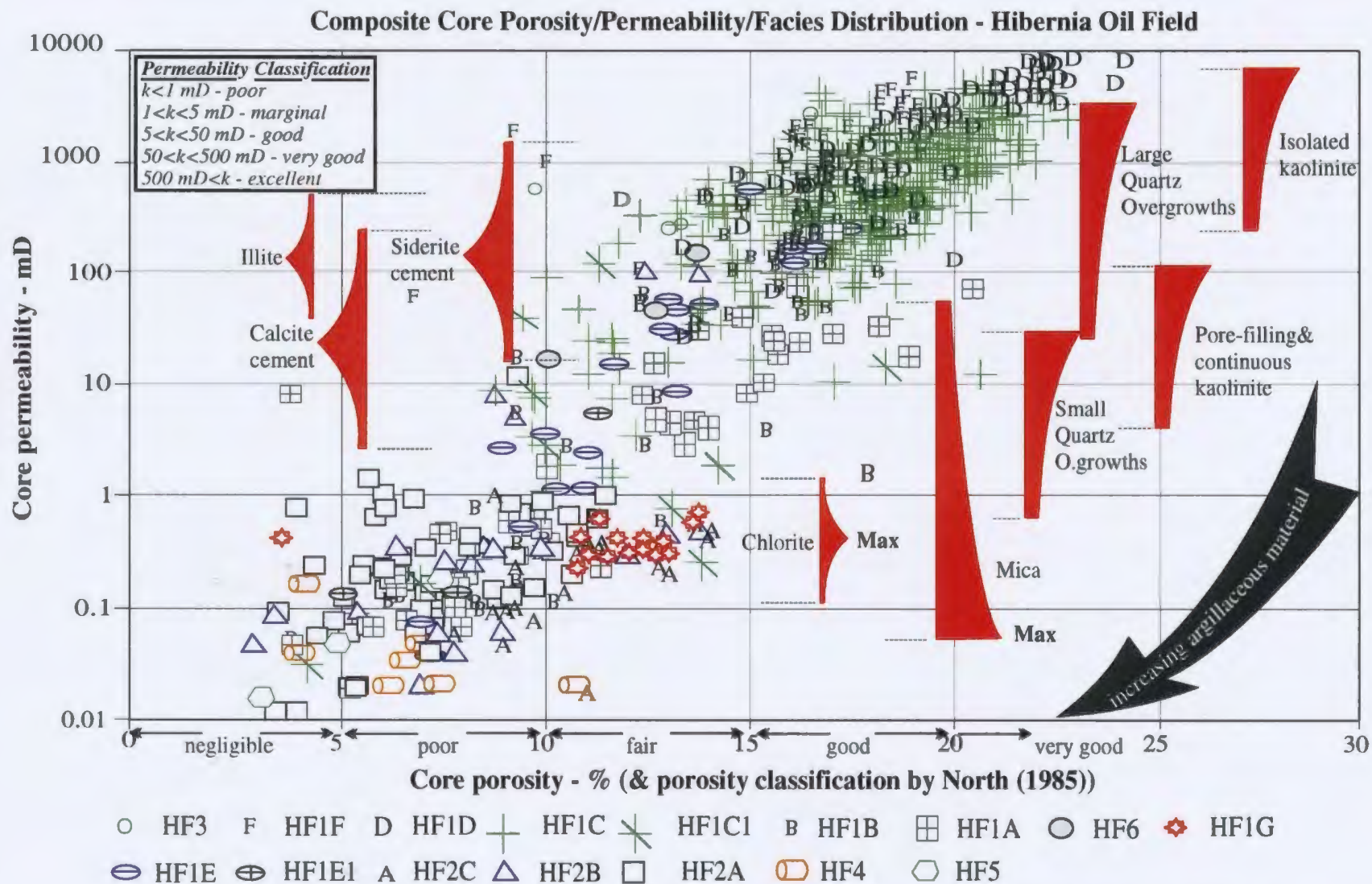


Figure 12: SEM/EDS-derived mineralogic and diagenetic attributes show relative abundances of porosity & permeability-influencing factors. Thickest part of each bar indicates relative maximums (Max).



Figure 13: This specimen of HF1A is more argillaceous than SP102-HF1A. Elongated flaky minerals are muscovite. Siderite cement and smectite are the primary constituents as well as detrital quartz (Appendix 3).

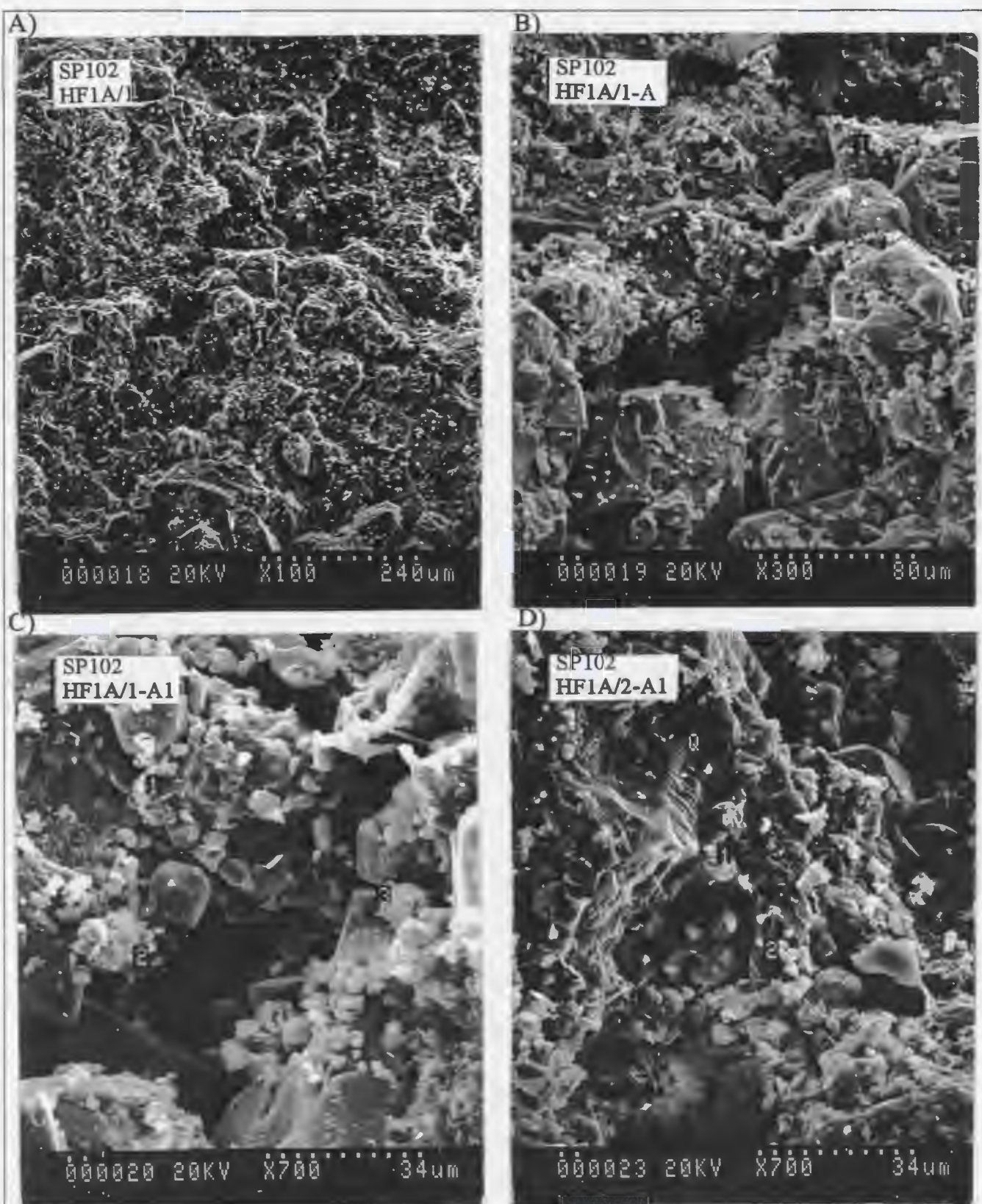


Figure 14: Very fine-grained sands of HF1A contain micro quartz overgrowths and pseudo hexagonal kaolinite booklets (14D). Smectite was also detected in point "1" in 14D.

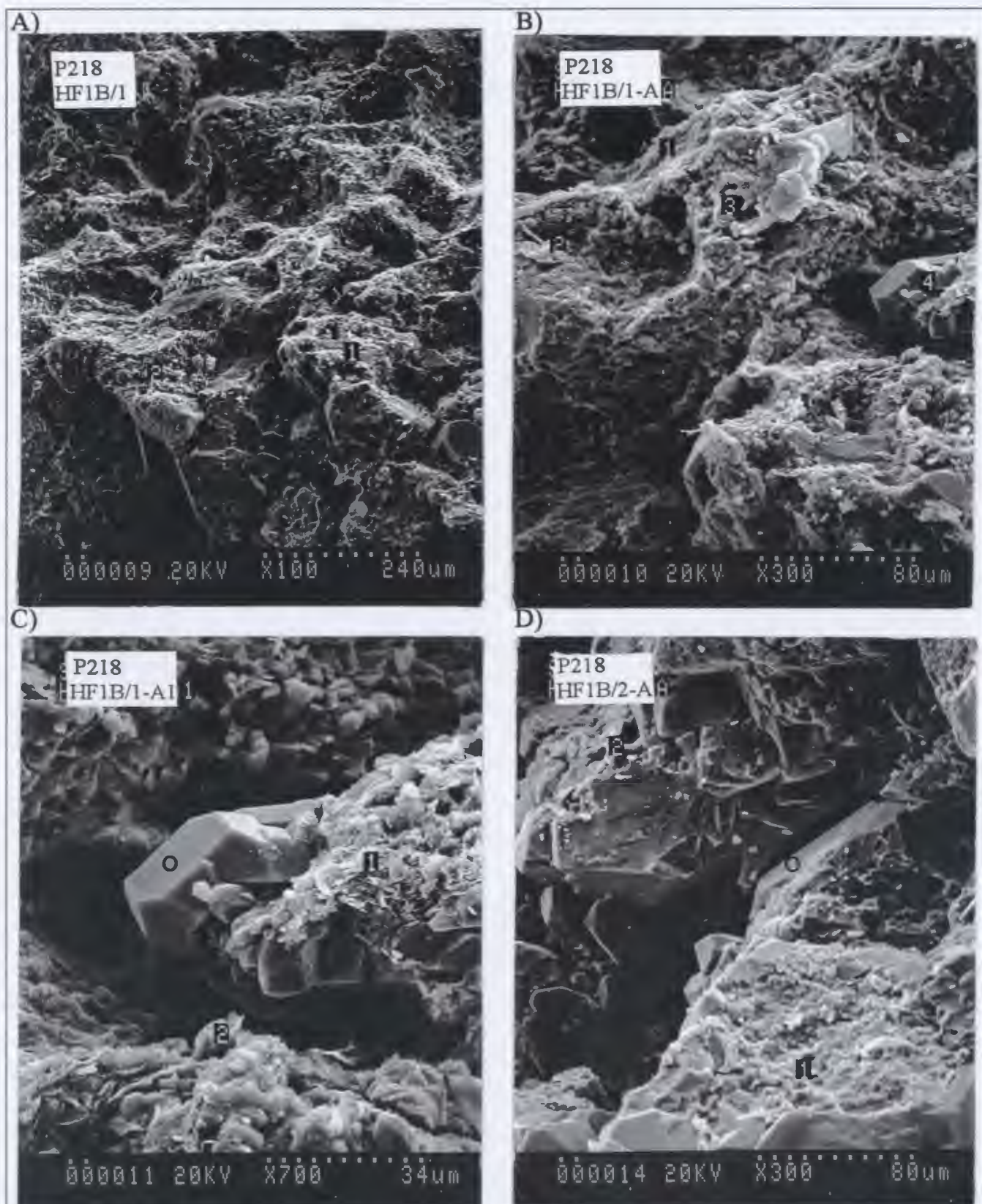


Figure 15: 15b and 15c are the magnified surfaces marked with arrows on 15a. 15d is taken from a different location. Quartz overgrowths (O) can be readily recognized at any magnification. Smec./Illite cluster is identified by the EDS of P218-HF1B/1-A1/1 (Appendix 3).

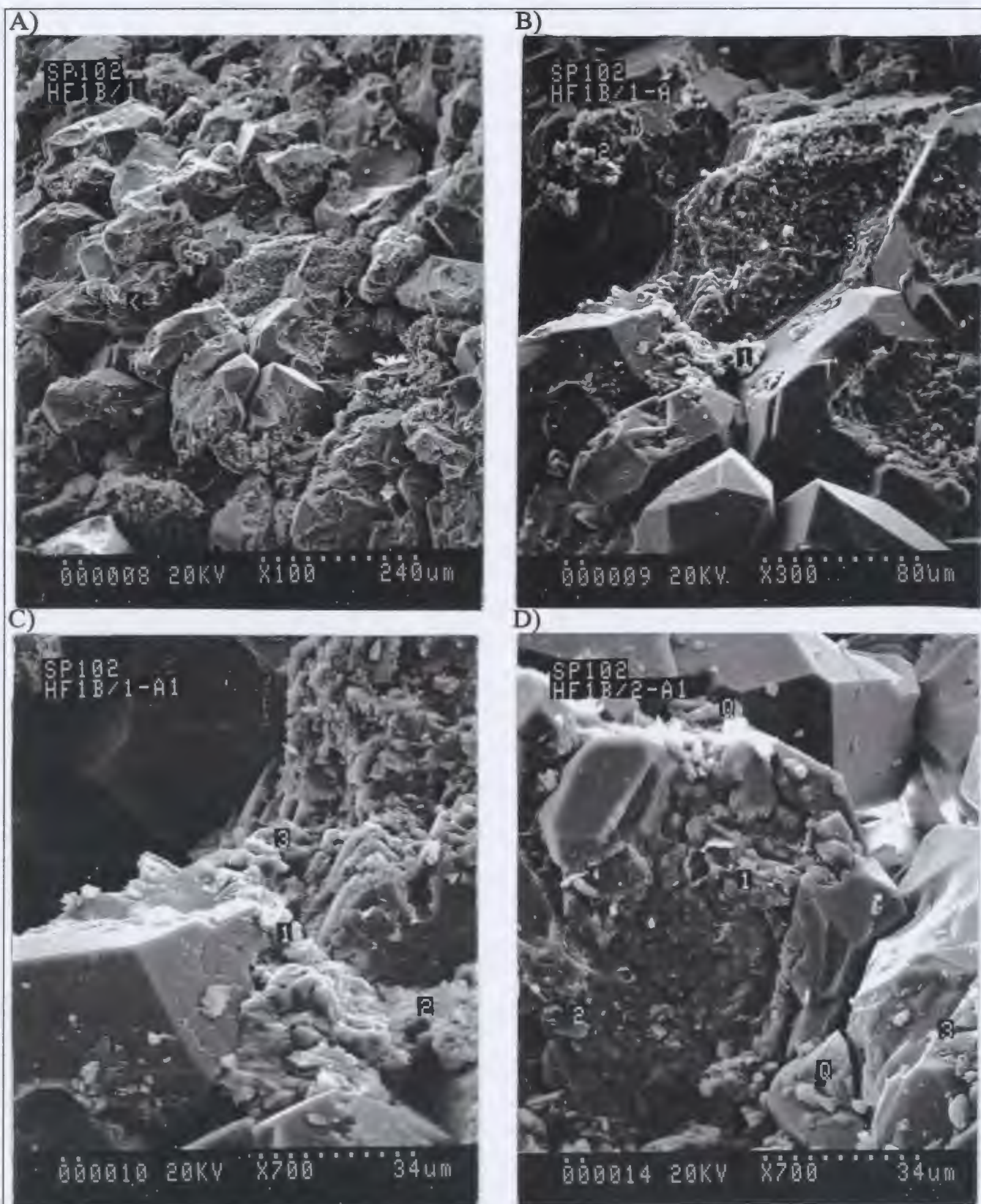


Figure 16: Euhedral quartz overgrowths can be readily observed at any magnification. Calcite was distinctively defined by the analyses 1-A-1, 1-A-3, 1-A1-1, 1-A1-2, and 1-A1-3 (refer to appendix 3). A smectitic cluster marked with 1 in 16b was also identified.

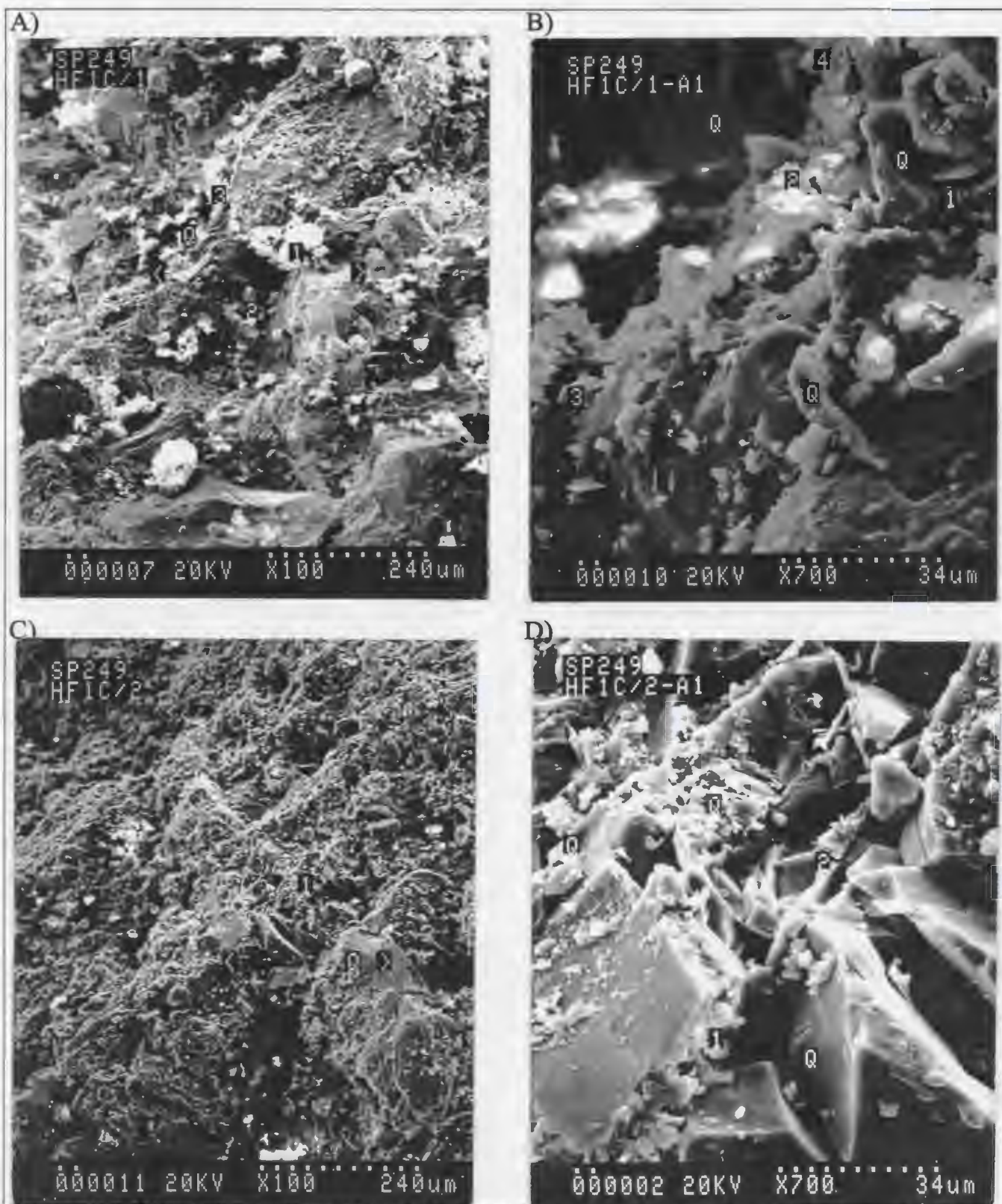


Figure 17: Quartzitic texture of the specimen is identified by most of the point analyses (Appendix 3). Siderite cement is detected in 17a, at the spot marked with "2". Quartz overgrowths are well-developed. Authigenic smectite is determined at the rim of detrital grain in 17d ("1"). Well-preserved pores are evident in 17d.

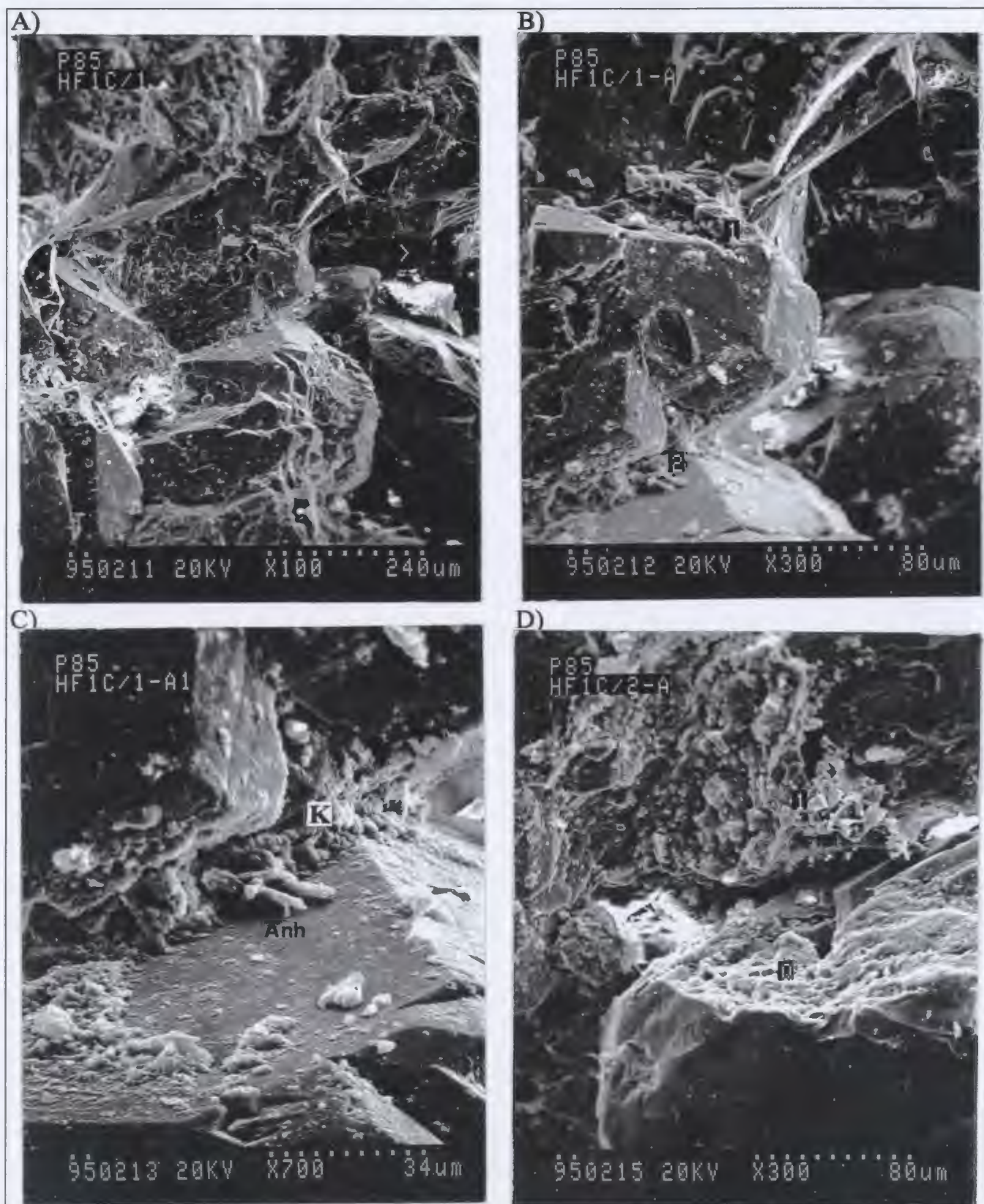


Figure 18: P85 of HF1C, precipitated anhydrite centre of 18c) and cubic halite crystal ("1" in 18d) are identified in this specimen. Anhydrite (Anh.) is in aggregate form with kaolinite (K) producing intergranular cement. The cement is local and ineffective on permeability (Table 3)(Drilling mud invasion (?)).

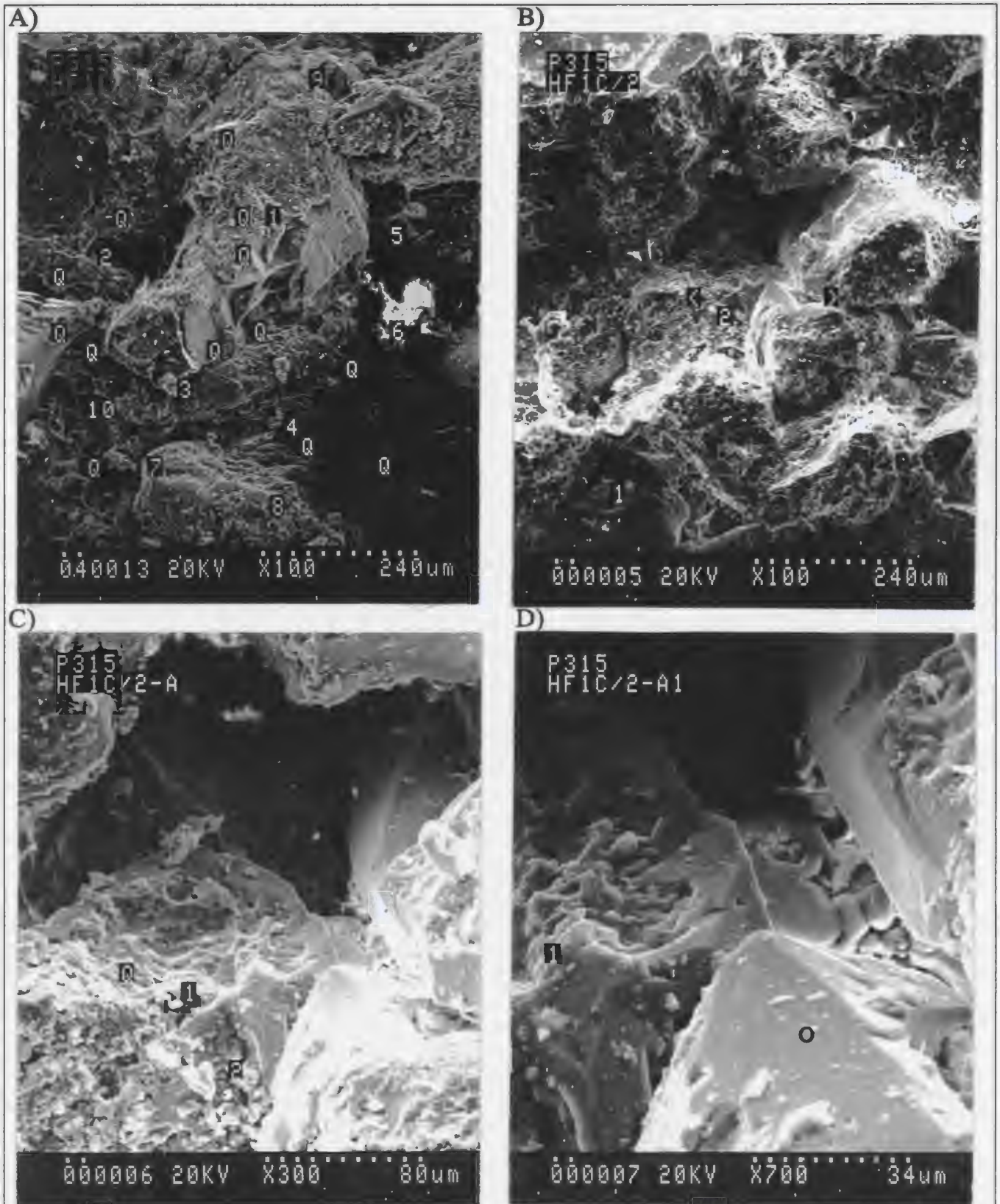


Figure 19: Argillaceous material content of P315 is minimal. Kaolinite is the most common clay spotted in 19A (/1-3, /1-5, /1-6, /1-7, /1-8 and /1-10; table 7& app.3). Smectite is also defined in the second surface segment at X300 mag. ("1" and "2" in 19c) (O=Overgrowth)

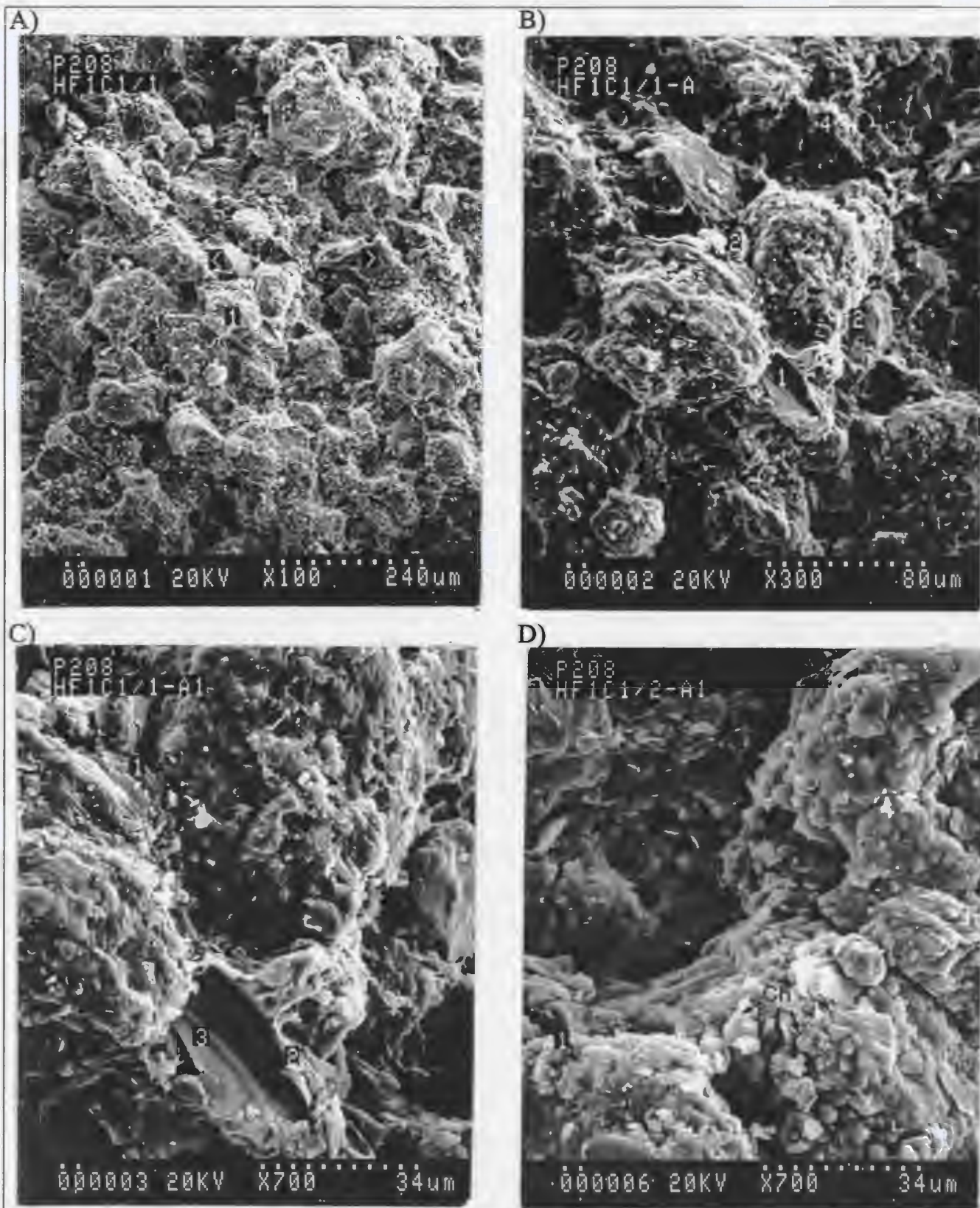


Figure 20: X100, X300, and X700 mag. SEM photomicrographs of P208-HF1C1. Depression surface marked with "3" in 20c is the surface of a sylvite mineral precipitated from invaded drilling fluids. Micro size quartz overgrowths (O) are common (20d). Chlorite (CH) is evident (20c).

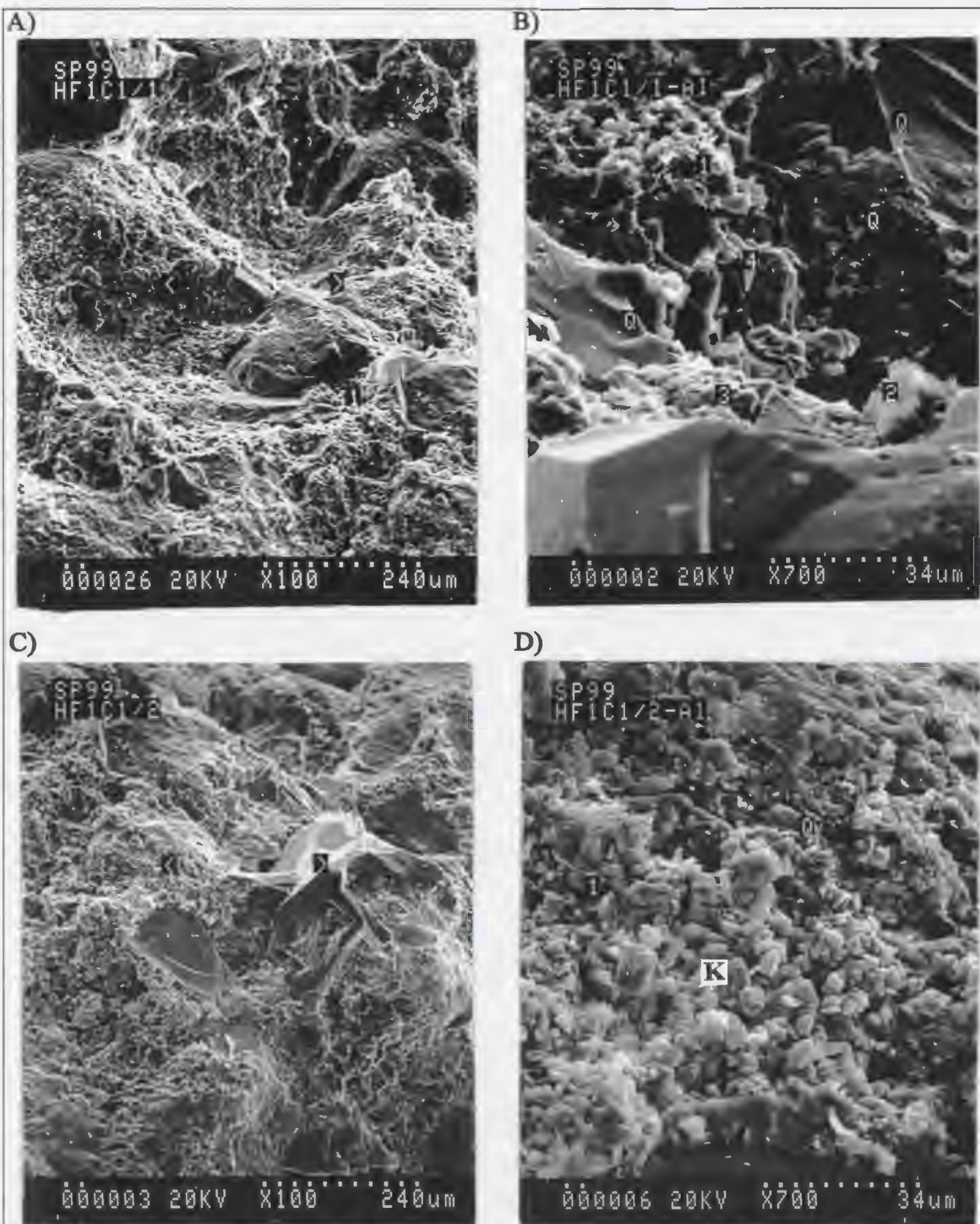


Figure 21: SP99 is more argillaceous than P208-HF1C1. Quartz overgrowths are larger in size (width > 34 μm ; 21b) than in P208. Well-developed kaolinite booklets (K) are readily recognized in 21d. Clay clusters also contain minor smectite. Spot "3" in 21b yielded pyrite detection (Appendix 3).

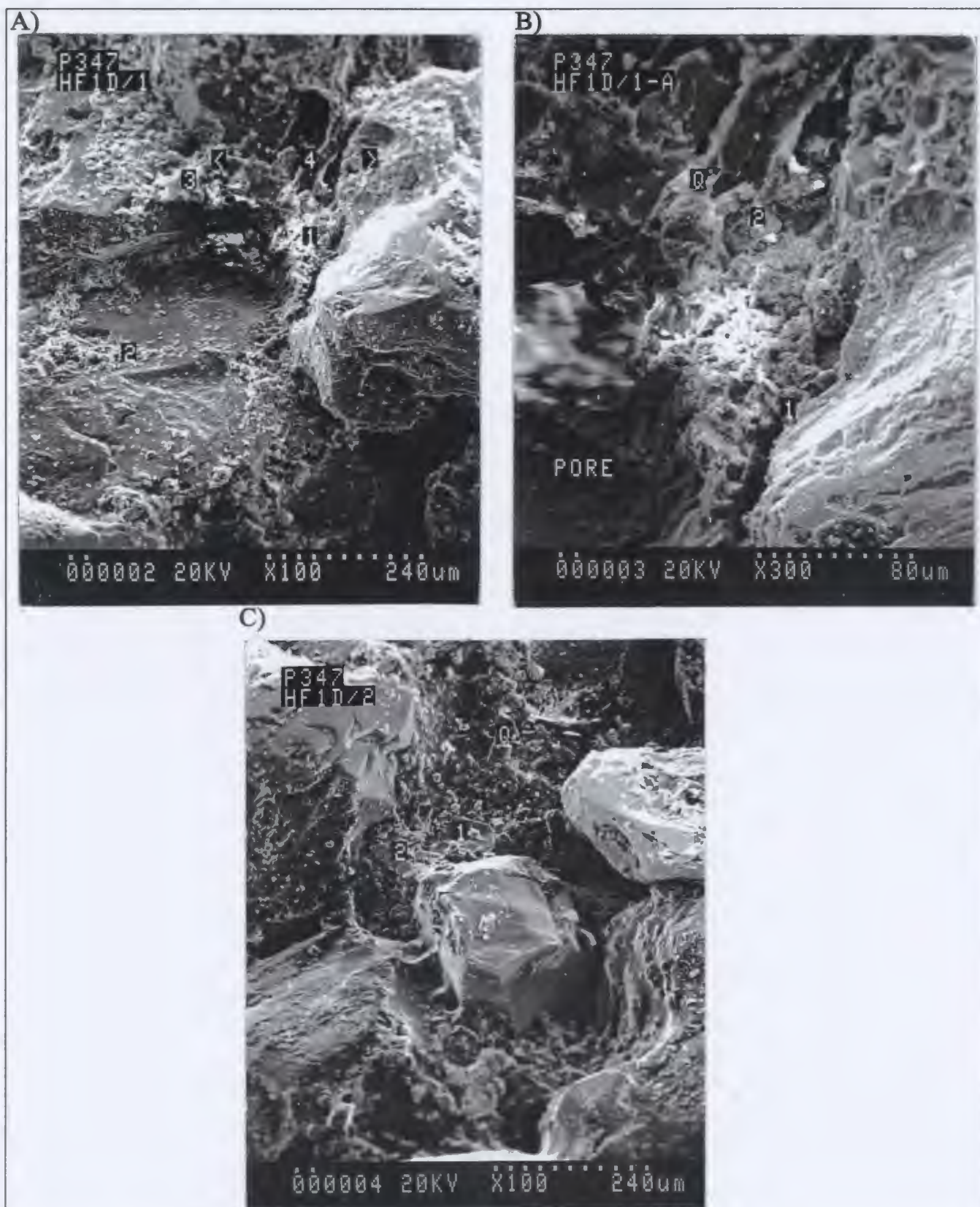


Figure 22: Ilmenite is determined at point "1" in 21b where cluster of clay-sized material obstructs pore connections. Two shades of gray on the central grain in 22c shows quartz overgrowth boundary (Appendix 3).

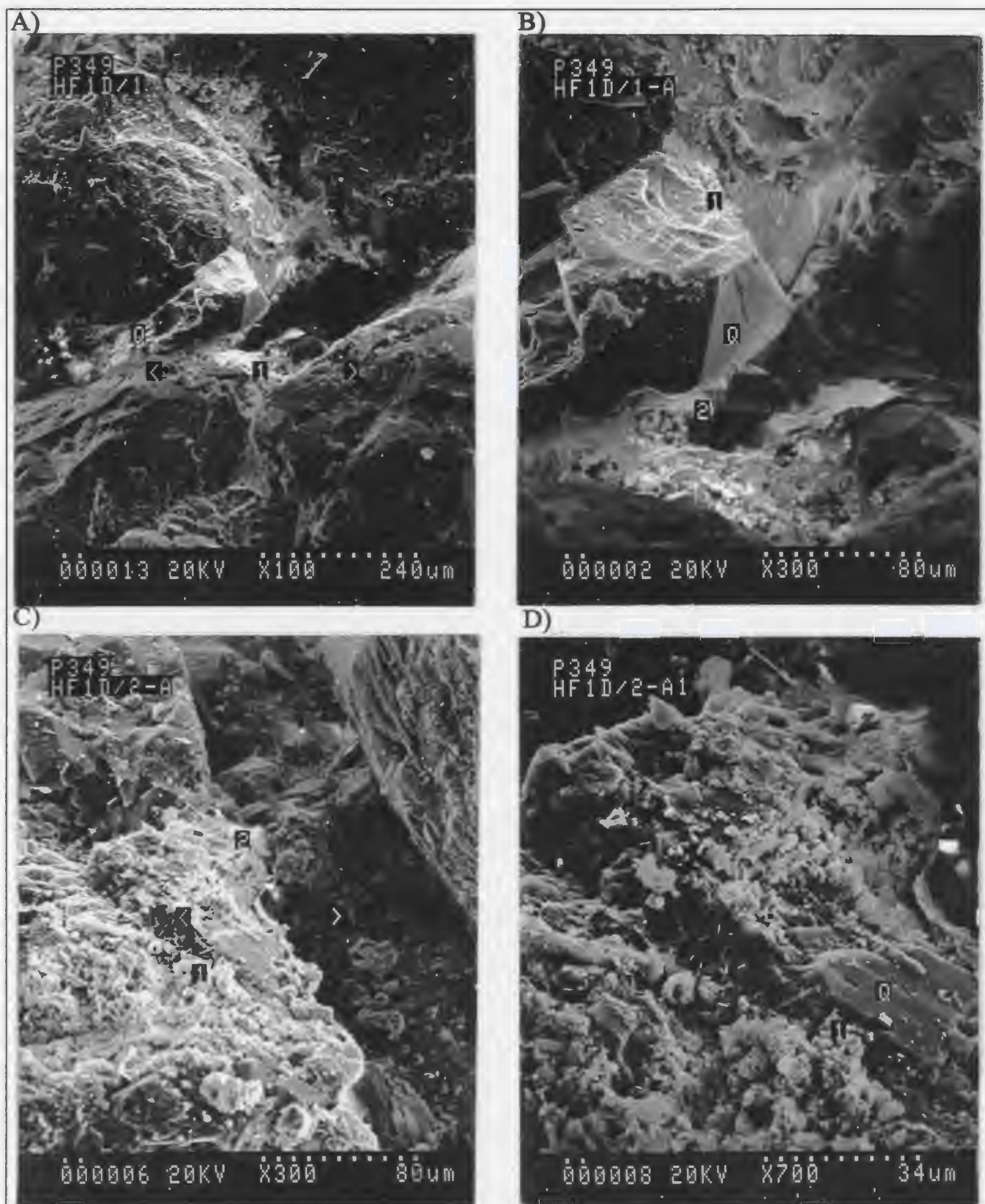


Figure 23: Quartz overgrowths and isolated kaolinite booklets are the evident features of P349-HF1D. Neither of these features are effective reducing the available pore-space and pore connections. Permeability of the specimen is maximum among the lithologies ($k=9710$ mD; table 3; appendix 3).

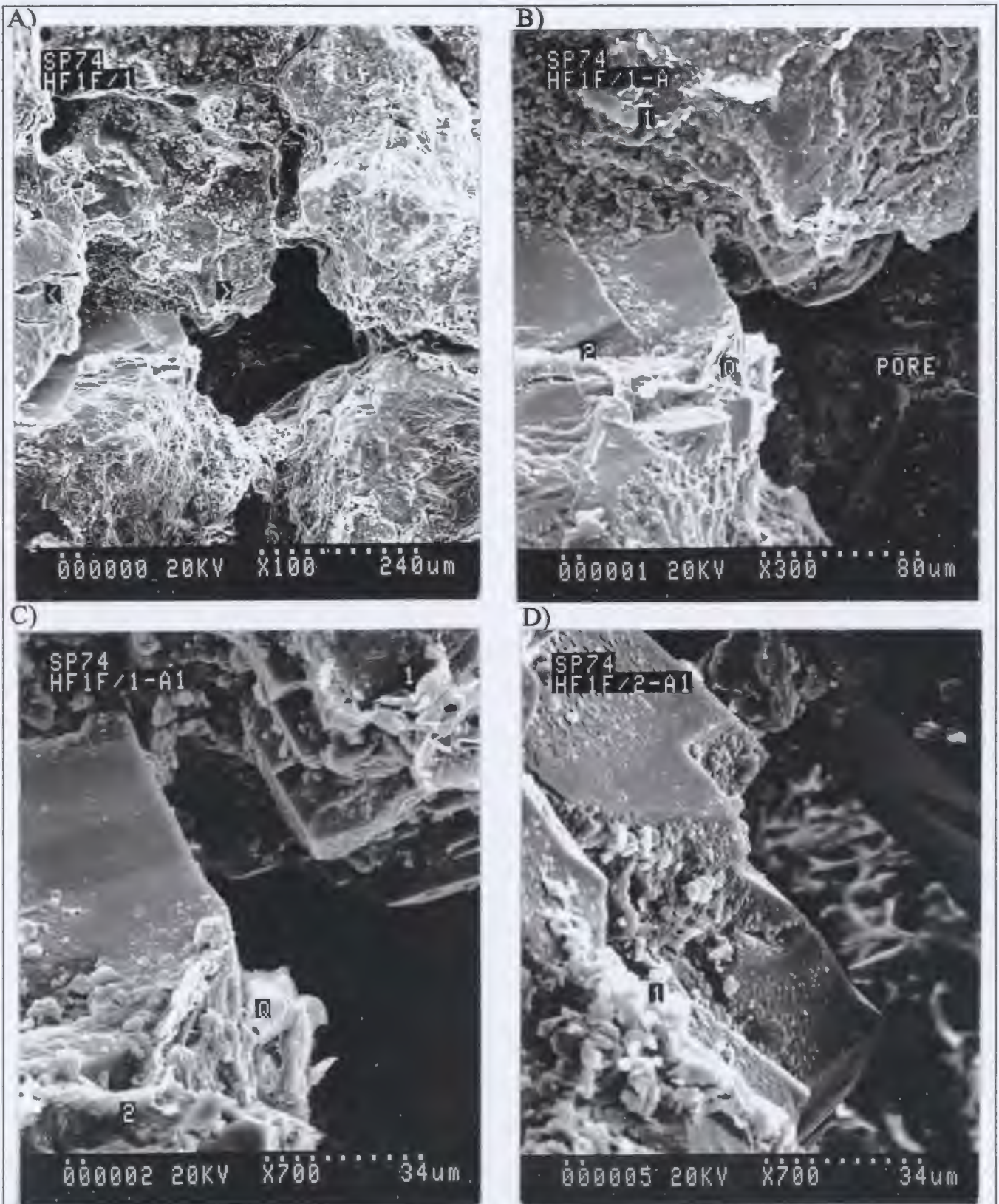


Figure 24: In all four photographs, well-developed and large quartz overgrowths are the major permeability-reducing component. Ilmenite is detected at point "1" in 24b. Other beam-spot analyses yielded quartz, biotite and smectite responses (Appendix 3).

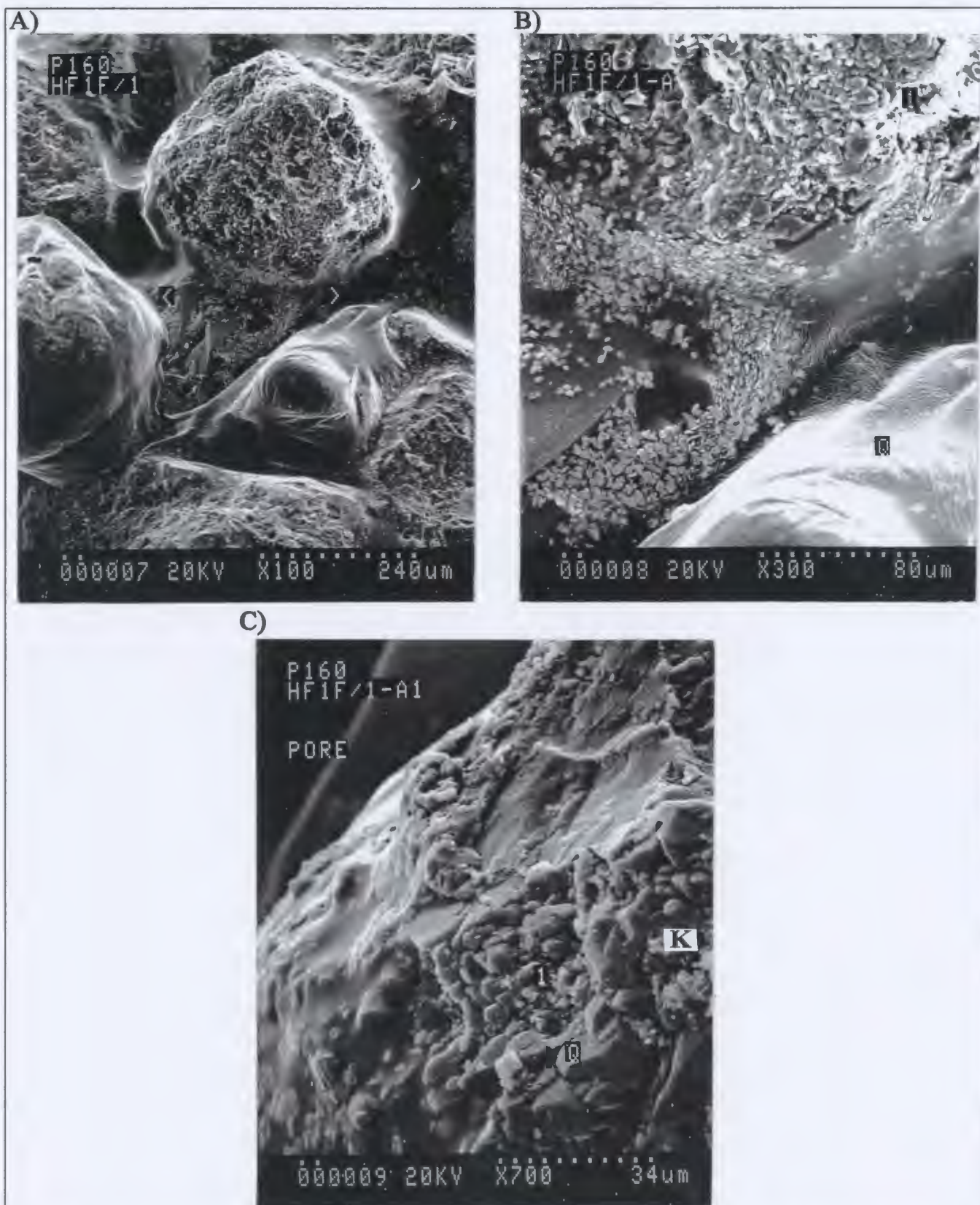


Figure 25: Smoky sections are due to silver contamination. Very fine-grained material in the centre of 25b is sputtered gold coat. Quartz overgrowths (O) are pore-occupying features in 25a and 25c. Sample was rotated before taking 25c in order to avoid electrical charging. *K*=Kaolinite (Appendix 3)

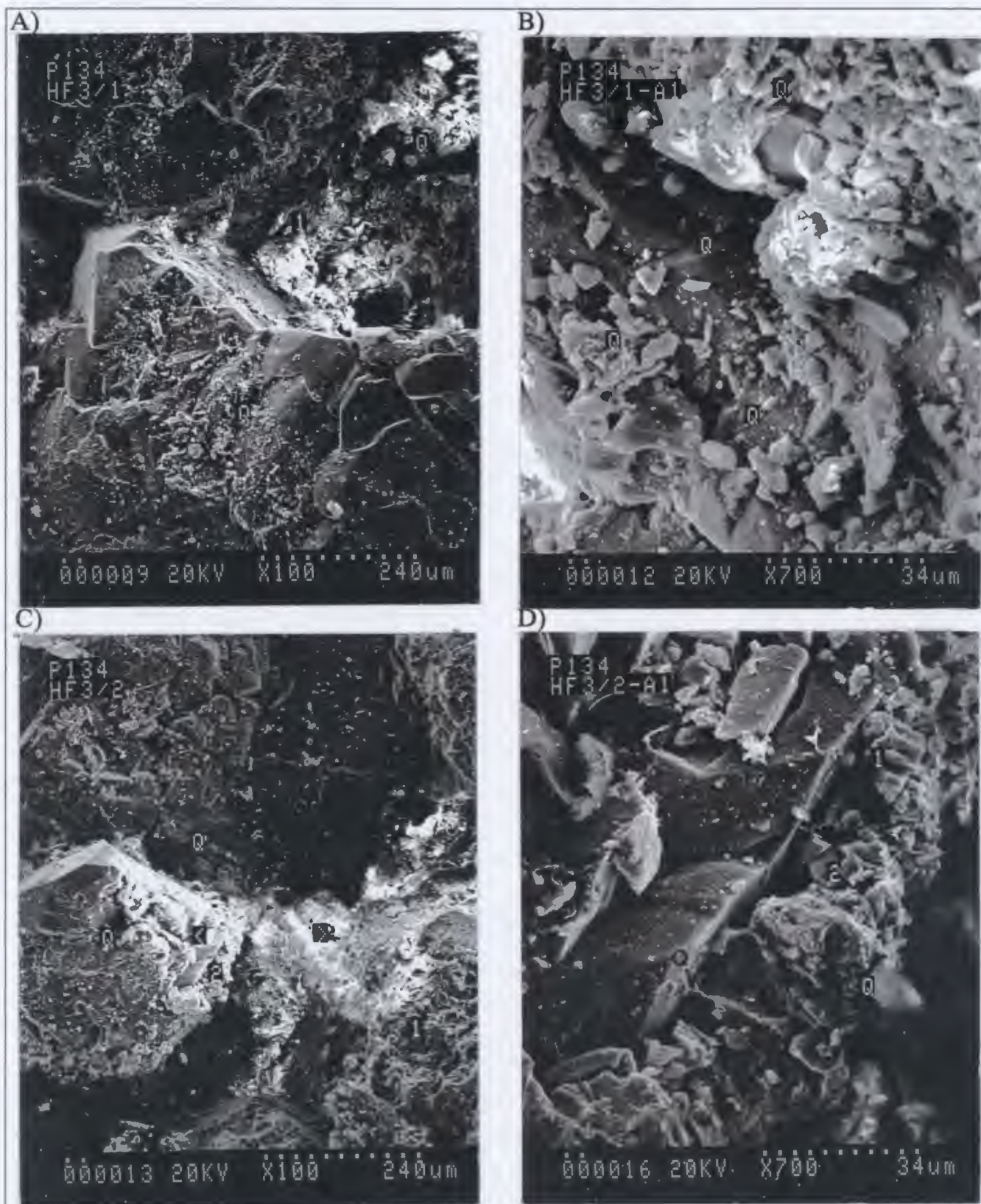


Figure 26: Smectite-rich clay mineralogy is observed in 26b (point "1"). Analysis of dust-sized particles in 26b yielded quartzitic detections (Q). Material surrounding the overgrowth in 26d consists of rutile, sylvite, and quartz. Bridge-like features in 26d are quartz silicifications (Q).

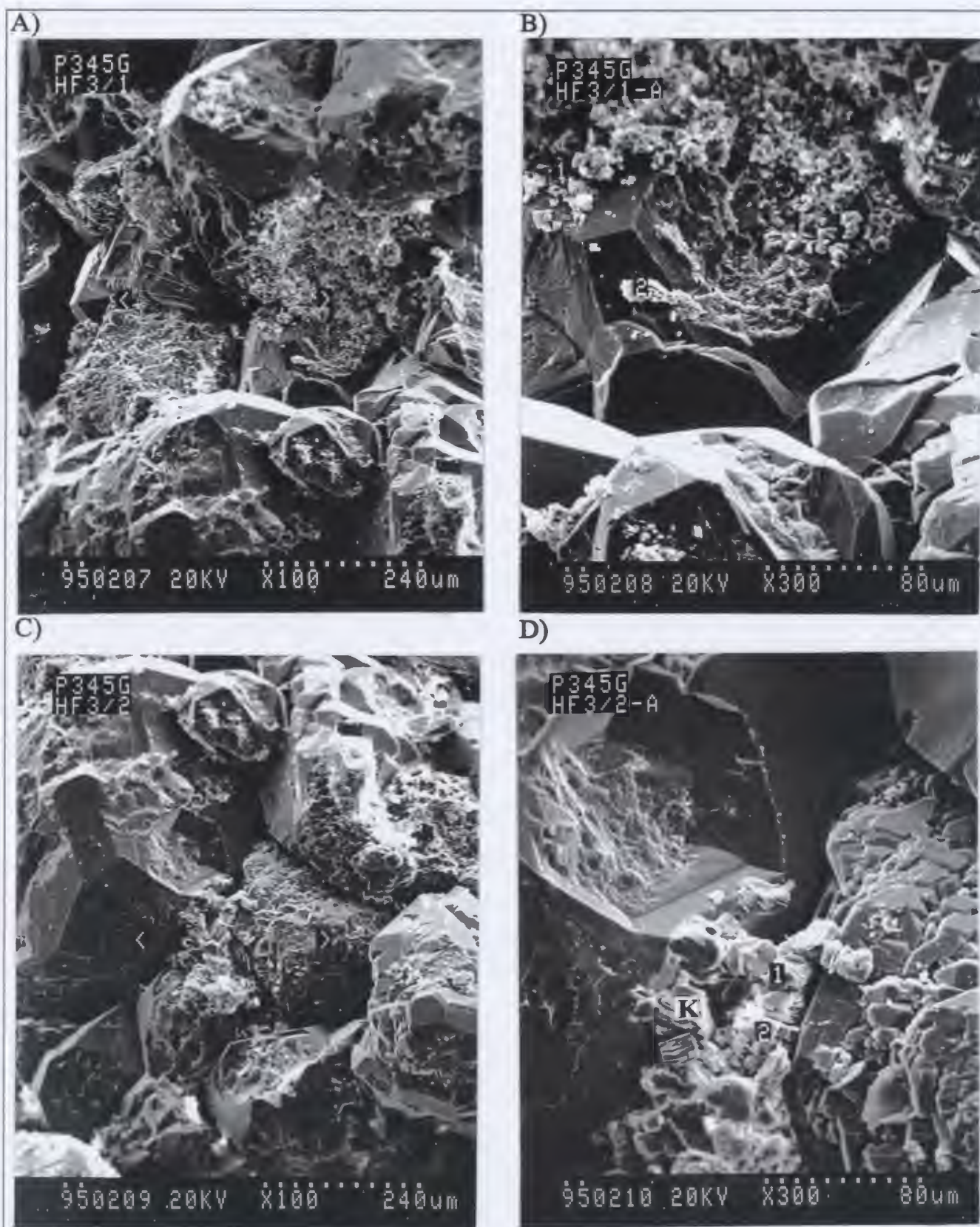


Figure 27: Quartz overgrowths and kaolinite booklets are well-developed. Blend of pyrite and smectite was determined at point "2" in 27b. Poorly-sorted texture of the lithology is evident in 27a and 27c (Appendix 3).

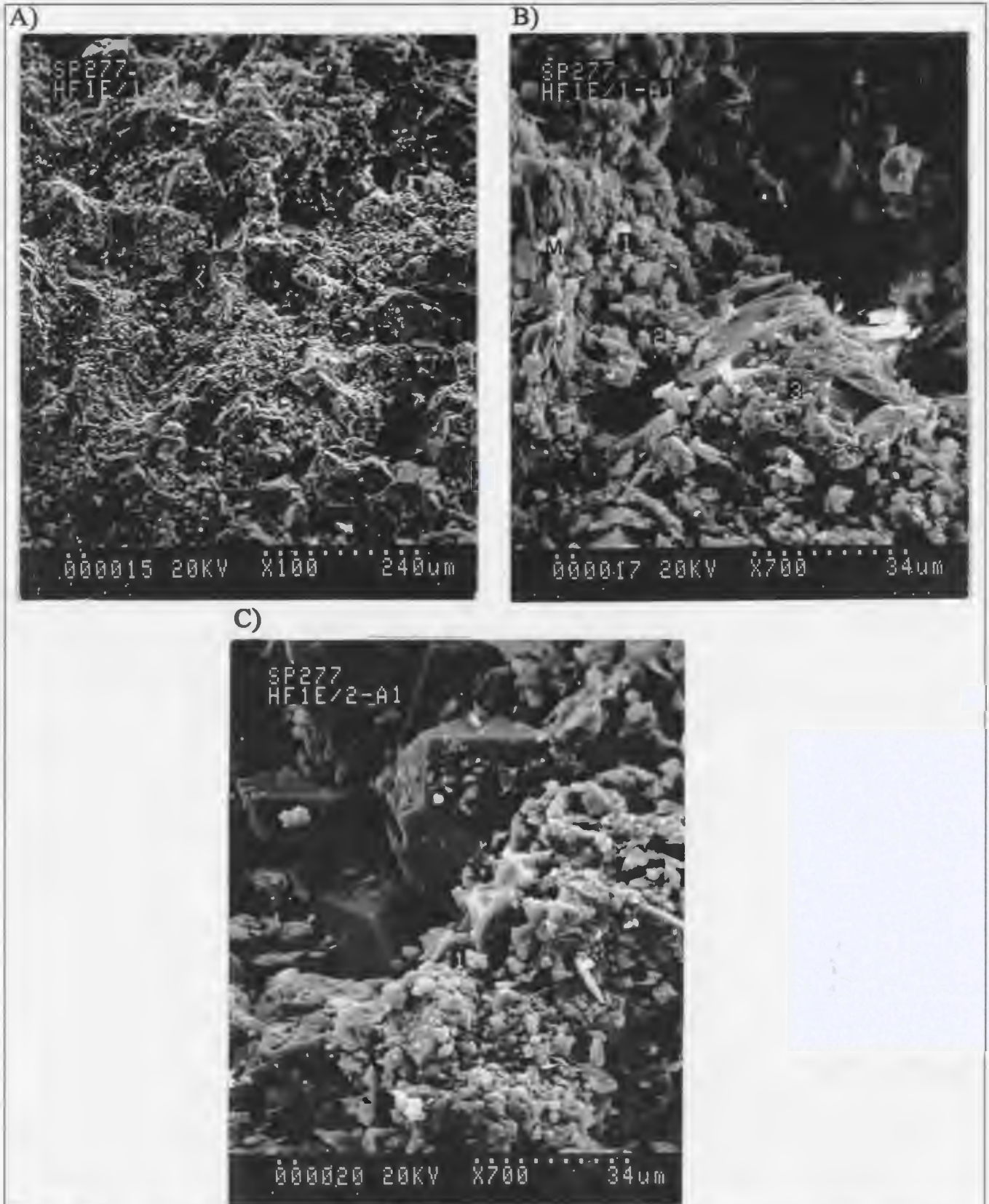


Figure 28: Argillaceous nature of the specimen is evident with rich clay-sized particle content (28a). Quartz silicification formed well-developed overgrowths (O) (28c). Detrital mica flakes (M) are seen at the left side of 28b. Biotite/smectite detection was acquired in "1" in 28c. (Appendix 3).

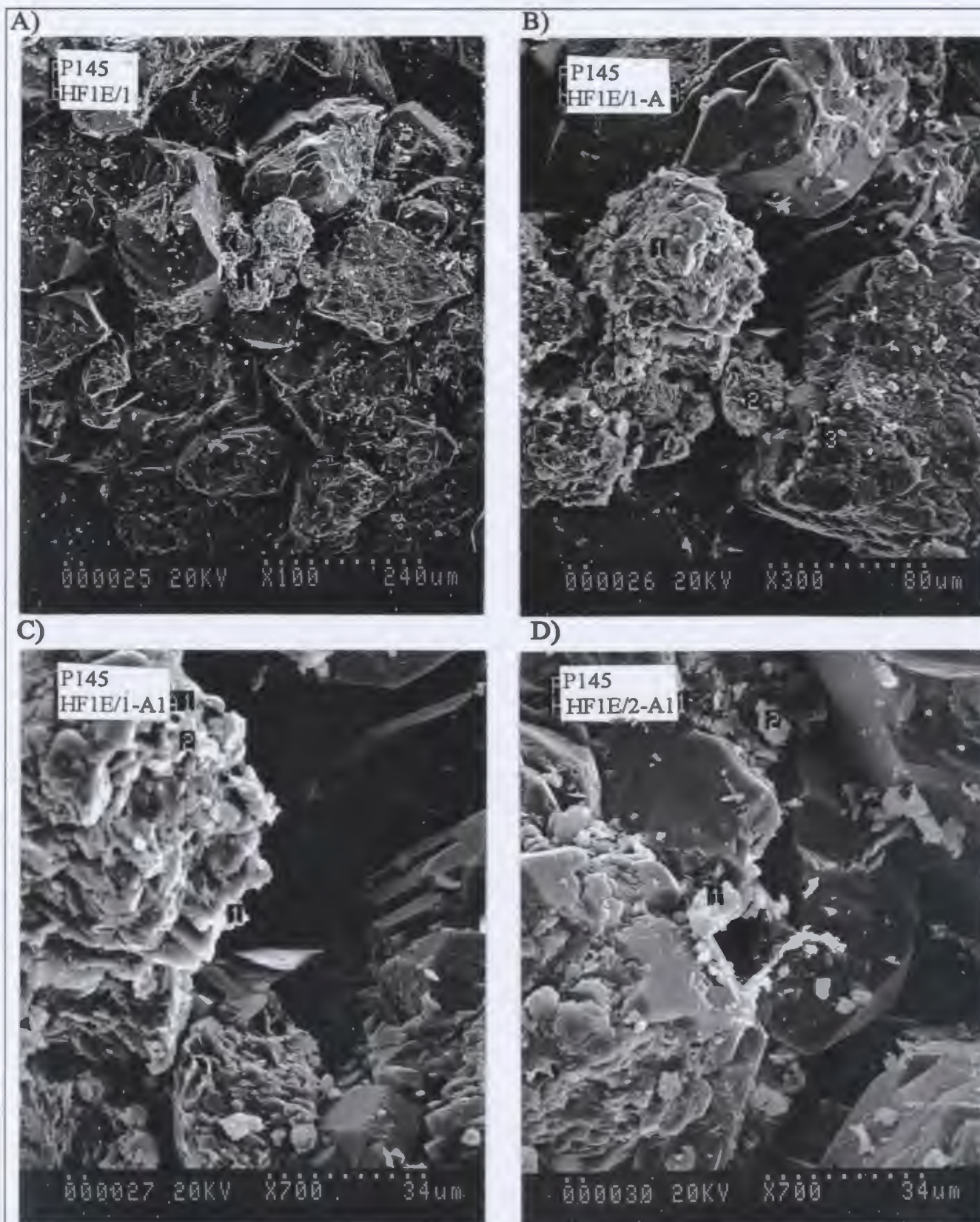


Figure 29: Pore connections are better developed and preserved than those in SP277-HF1E. Grain with ragged-surface in the centre of 29a is quartz. 29c shows that the irregular face of the grain is made up of various quartz overgrowths (O). Major clays are chlorite ("1" in 29c), and illite ("1" in 29d)(Appendix 3)

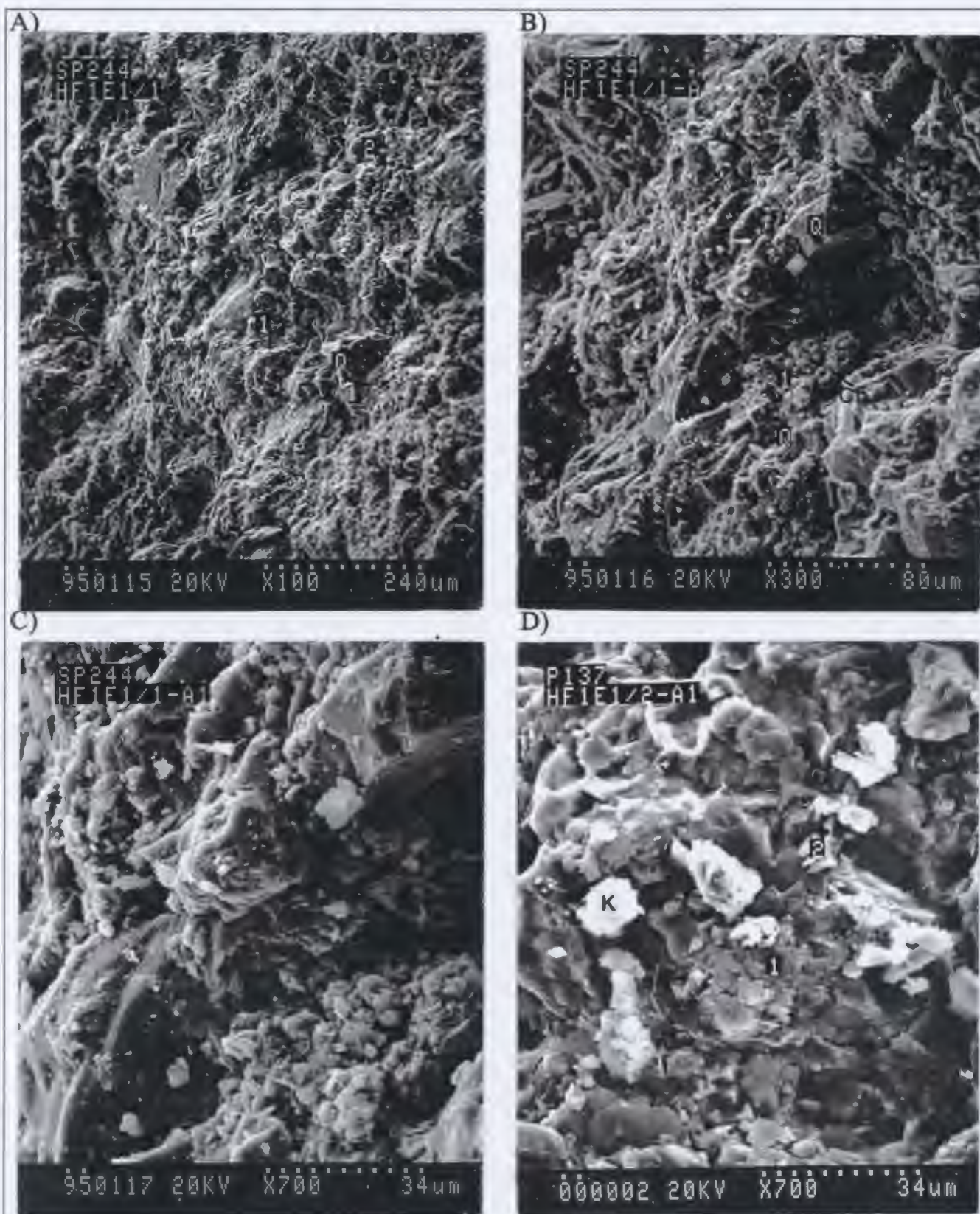


Figure 30: Diagonally-oriented bedding planes are evident in 30a. Argillaceous nature of the facies is complex. Clays and micas are the primary components of the argillaceous matrix. Pore connections and flow path in both of the specimens are disrupted (K=Kaolinite, Ch=Chlorite)(Appendix 3).

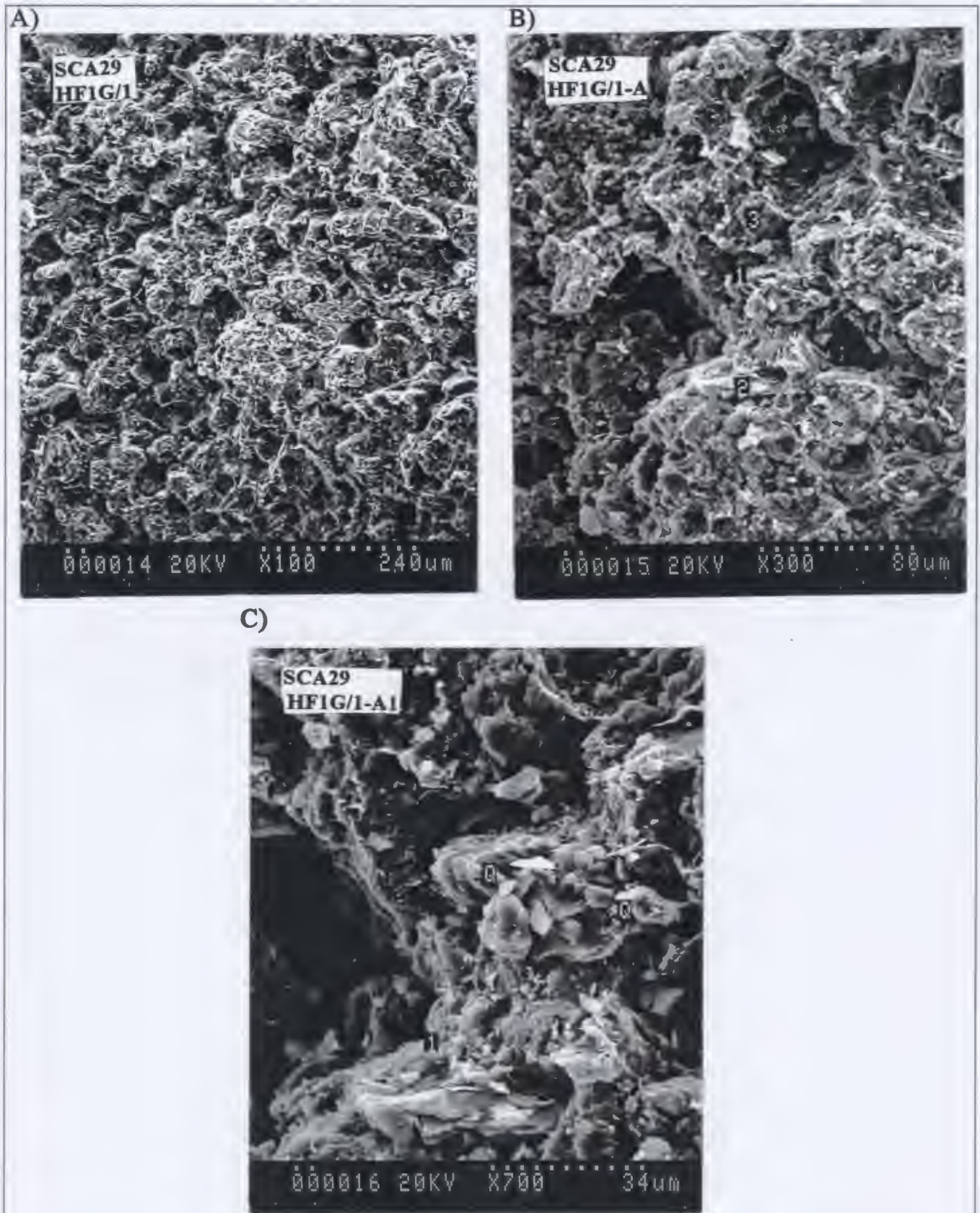


Figure 31: Grain-coating, pore-blocking chlorite (Ch) is the primary component of the clay-rich aggregates in the specimen. Detrital mica ("1" in 31b), albite ("1" in 31c) and rare quartz overgrowths are also observed (Appendix 3).

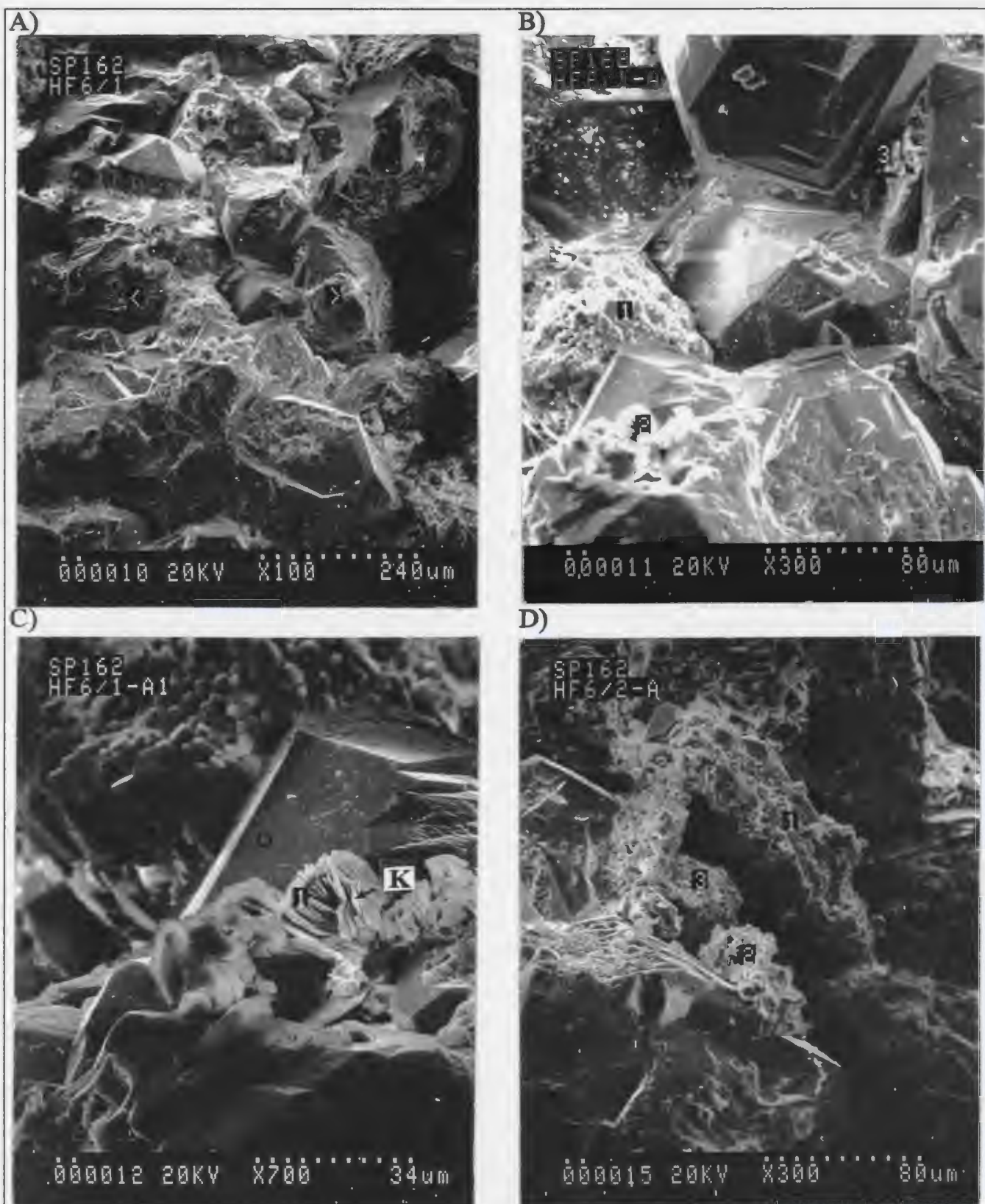


Figure 32: Detrital grains of SP162-HF6 are subrounded. Quartz overgrowths, kaolinite booklets and intergranular siderite cement are the primary features in 32b ("1", "2" and "3"). Arc-like feature in 32d is muscovite-rich also is composed of quartz and kaolinite (O=Overgrowth, K=Kaolinite) (Appendix 3).

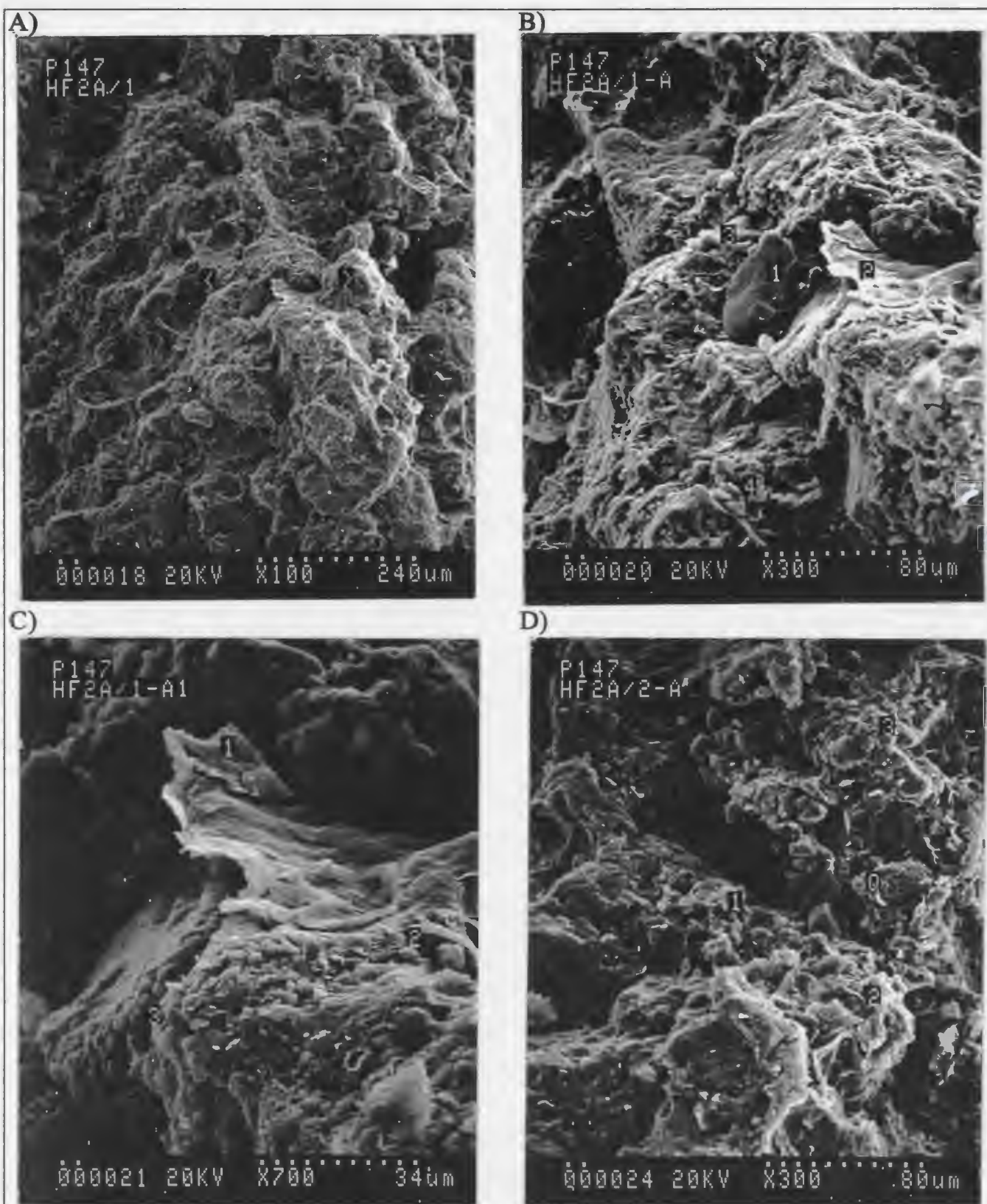


Figure 33: Argillaceous and micaceous nature of the specimen is evident in all photos. (Mica flake="1" in 33c). Well-developed micro quartz overgrowths (width~<5μm) are dominant in bottom-left portion of 33c. Chlorite is sporadically detected.



Figure 34: SP103-HF2B is more argillaceous than HF2A specimen. Clay- and mica-rich character of the specimen yielded very complex elements detections in the SSQ analysis. Kaolinite is identified at point "3" and "4" in 34b . X2,000 mag. helped to visually identify chlorite (Ch) in the argillaceous clusters (Kaolinite="3" in 34b, Muscovite="1" in 34c, Ch=Chlorite)(Appendix 3).

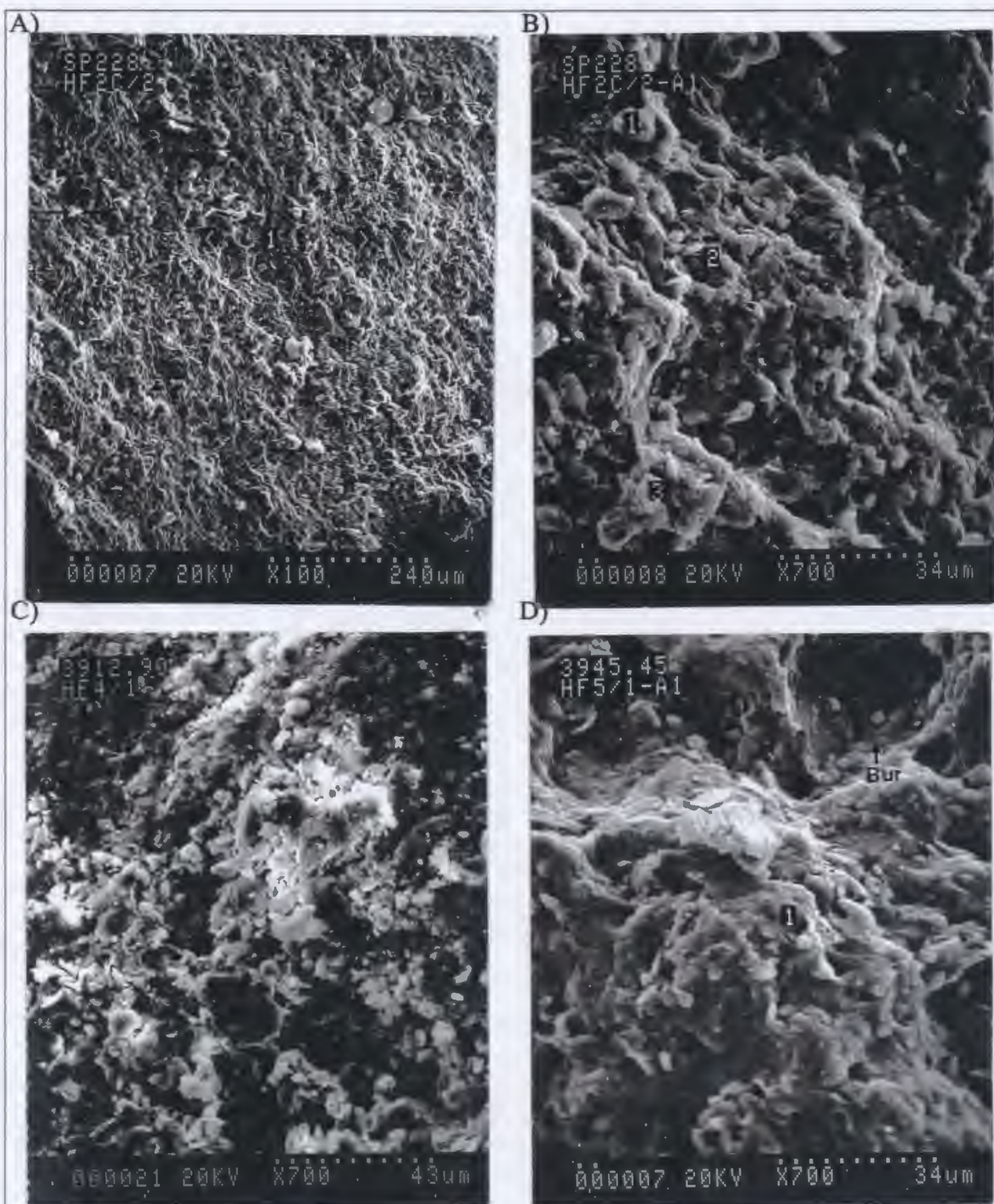


Figure 35: Argillaceous component is abundant in SP228-HF2C, 35a&b. Element detections have become extremely complex in this facies where only muscovite ("1" in 35a) and kaolinite ("1" in 35b) were identified. Loose texture of the HF4 and consolidated HF5 shales are in 35c&d. Burrows in HF5 (Bur) are well-documented in 35d (Upper right portion of 35d)(App.3).

V - THIN SECTION PETROGRAPHY

V.1- INTRODUCTION AND OBJECTIVES

Thin sections examined in this chapter were provided by HMDC. Sample locations are marked on the grain size logs in appendix 1. Examinations were performed under plane-polarized and cross-polarized lights. Depths, flow properties and petrographic characteristics identified in the analyses are presented in tables 18a and 18b.

The primary lithologies of the reservoir-forming rocks in the oil field are the sandstones of the Hibernia Formation. In this study, Folk's (1980) classification of sandstones and sediment maturity is used. A majority of the sandstones occur in quartz arenite-sub litharenite range. For sorting and roundness, comparators developed by Pettijohn *et al.* (1973) were accepted as reference material. Specific mineral identifications were performed on the basis of standard comparator photos of Adams *et al.* (1984).

The objectives of these thin section examinations are:

1. Describe grain size, sorting, and roundness attributes of the lithofacies
2. Identify major and minor mineralogies
3. Determine depositional and diagenetic attributes affecting pore structures
4. Address the relationships between the identified parameters and permeability.

Based on these objectives, the degree of sorting and roundness was determined for each sample. Numerical codes were assigned for every sorting and roundness level (Table 5). A concept of "*Enhanced Textural Maturity Index (ETMI)*" was developed and calculated as

a function of sorting and roundness. *ETMI*, when graphed against permeability, shows that the degree of sorting and roundness is proportional to permeability. The crossplot also highlights the relative influence of permeability-reducing factors (Figure 48)

Roundness Sorting	VA	VA-A	A	A-SA	SA	SA-SR	SR	SR-R	R	R-WR	WR
P	1 ₀	1.5 ₁₁	2 ₁₁	2.5 ₁₁	3 ₁₂	3.5 ₁₁	4 ₁₁	4.5 ₁₂	5 ₁₂	5.5	6 ₁₁
P-M	1.5 ₁₁	2.25 ₀	3 ₁₁	3.75 ₁₁	4.5 ₁₁	5.25 ₁₁	6 ₁₂	6.75	7.5 ₁₂	8.25	9 ₁₂
M	2 ₁₁	3 ₁₁	4 ₀	5 ₁₁	6 ₁₁	7 ₁₁	8 ₁₁	9 ₁₁	10 ₁₂	11 ₁₁	12 ₁₂
M-W	2.5 ₁₁	3.75 ₁₁	5 ₁₁	6.25 ₀	7.5 ₁₁	8.75 ₁₁	10 ₁₁	11.25	12.5	13.75	15 ₁₂
W	3 ₁₂	4.5 ₁₁	6 ₁₁	7.5 ₁₁	9 ₀	10.5 ₁₁	12 ₁₁	13.5	15 ₁₁	16.5	18 ₁₂
W-V.W	3.5 ₁₁	5.25 ₁₁	7 ₁₁	8.75 ₁₁	10.5 ₁₁	12.25 ₀	14 ₁₁	15.75	17.5	19.25	21
VW	4 ₁₁	6 ₁₂	8 ₁₁	10 ₁₁	12 ₁₁	14 ₁₁	16 ₀	18 ₁₁	20	22	24

Roundness: VA: Angular, VA-A: Angular to angular, A: Angular, A-SA: Angular to subangular, SA: Subangular, SA-SR: Subangular to subrounded, SR: Subrounded, SR-R: Subrounded to rounded, R: Rounded, R-WR: Rounded to well-rounded, Sorting: WR: Well-rounded, P: Poorly-sorted, P-M: Poorly to moderate, M: Moderate, M-W: Moderate to well, W: Well, W-V.W: Well to v.well, VW: V.well

Table 5: Calculated "*ETMI*" values by the numerical codes assigned for degrees of sorting and roundness. Duplicate numbers are separated from each other by subscripts. Subscript letters ("s" or "r") represent the dominance of sorting or roundness for a given specimen. Secondary subscript, as in 4.5₁₁, increases with the increasing dominance of either sorting or roundness. i.e. 4.5₁₁ represents well-sorted and VA-A while 4.5₁₂ stands for poorly-sorted and SR-R. Subscripts do not change the way *ETMI* values are plotted in figure 48.

V.2- DESCRIPTIONS

V.2.1- Petrography of the sand-based lithofacies:

V.2.1.1. Lithofacies HF1A

This lithology is very fine-grained sublitharenite (SP102, figure 36; table 6a). Major components of the lithology are mono-crystalline quartz, mud pellets rich in igneous particles, igneous and lithic rock fragments. Grain size variations highlight that the sample is poorly- to moderately-sorted and angular to sub angular, and is texturally mature to submature. Minor minerals are mica, plagioclase and detrital clays in the form of mud pellets. Intergranular clays are a pore-plugging factor but abundant quartz overgrowths cause the main grain interlock and pore space-reduction. Orientation of grains reflects the laminated nature of the specimen. Porosity is substantially primary. Very rare oversized pores are suspected to be secondary.

V.2.1.2. Lithofacies HF1B

The sandstones of HF1B (Table 6a; figure 37) are composed of fine-grained monocrystalline quartz which is slightly coarser than HF1A sandstones. In both thin sections the sandstones are sub-angular to sub-rounded, and moderately-sorted, and thus can be classified as texturally mature sublitharenites. Additional major constituents are monocrystalline quartz, lithic rock fragments and detrital clays. Minor components are mica, calcite, polycrystalline quartz, rare pyrite and plagioclase. The matrix is mainly composed of clays, however, calcite cementation becomes significant, especially in SP102. Widespread quartz overgrowths and pore-lining clays are also observed. Quartz overgrowths appear to

be more effective in SP102 than in P218 while grain-coating clays (chlorite?) are identified in P218

Secondary pores were rarely observed where corroded serrate edges of quartz grains produced oversized voids. Pore enlargement can be explained by dissolution of calcareous intergranular cement.

V.2.1.3. Lithofacies HF1C

Primary reservoir sandstones of facies HF1C were examined in 4 thin sections from three different wells (Table 6b).

Medium-grained sands of HF1C have a common mineralogical framework in all three specimens. The major rock forming mineral is monocrystalline quartz constituting an average of >95% in all four. Thus, HF1C mainly is a quartzarenite (Figure 38). Minor components of the mineral framework are mica grains, very little feldspar, calcite and lithic rock fragments.

HF1C quartzarenites are subrounded to rounded and moderately- to well-sorted. SP249 has relatively greater amount of quartz overgrowths than the other three. The least amounts of overgrowth was determined in P315 where the highest permeability among the four HF1C specimens was measured.

Very low percentages of kaolinite (~<1%) together with subtle amounts of pore-lining authigenic clays (~<1%) are observed in all four thin sections. The only variation is that the authigenic clay content in the pore system of SP249 is slightly higher than for the other remaining samples. In diagenetic evolutionary order of pore-plugging material, quartz

Facies & Plug#	Well	Depth (m)	ϕ - %	k-mD	Major minerals >95%	Minor minerals	Roundness	Sorting	ETMI
HF1A SP102	K-18	3797.12 - 97.34	12.8	15.30	Monocrys. qtz*+ LRF+IRF	Mica+plag.+ detrital clays	A-SA*	Poor - Moder.	3.75 ₁
HF1B SP102	B-08	3624.17 - 24.30	12.3	52.70	Monocrys. qtz+ LRF+kaolinite	Mica+calcite+ plag.+pyrite+ poly. qtz	SR*	Moder.	8.00 ₁
HF1B P218	K-14	3674.78 - 75.08	14.6	44.00	Monocrys. qtz+ LRF+kaolinite	Mica+calcite+ plag.+pyrite+ poly. qtz+chert	SA - SR	Moder.	7.00 ₁
HF1C1 P207	K-14	3861.62 - 61.92	5.4	17.10	Monocrys. qtz+ IRF+clays	Poly. qtz+mica+ chert+calcite+ feldspars	SR	Moder.	8.00 ₁
HF1C1 P208	K-14	3862.43 - 62.75	14.2	0.32	Monocrys. qtz+ IRF+clays	Poly. qtz+mica+ chert+calcite+ feldspars	SA	Poor - Moder.	4.50 ₁
HF1D P347	K-14	3869.12 - 69.36	19.4	4640	Monocrys. qtz	Poly. qtz+LRF+ pyrite	R*	Moder. - Well	12.50
HF1D P349	K-14	3869.60 - 69.83	22.5	9710	Monocrys. qtz	Poly. qtz+LRF+ pyrite	R - WR*	Well	16.50
HF1F P160	C-96	3923.08 - 23.44	18.5	2780	Monocrys. qtz	Poly. qtz+LRF+ matrix material	R	Moder. - Well	12.50
HF1F SP74	B-08	3606.18 - 06.29	19.3	1290	Monocrys. qtz	Poly. qtz+LRF+ rare detrital clays	SA - SR	Moder. - Well	8.75 ₁
HF3 P345G	K-14	3962.42 - 62.70	13.5	273	Mono/Poly. qtz+ LRF+chert	Mica+clays+ pyrite+IRF	SR	Poor - Moder.	6.00 ₁
HF3 134	C-96	3909.28 - 09.48	13.2	238	Mono/Poly. qtz+ LRF+chert	Mica+kaolin.+ pyrite+IRF	SR	Poor - Moder.	6.00 ₁
HF1E P145	K-18	3822.18	13.0	29.60	Monocrys. qtz	Detr. clays+mica LRF+IRF+Plag.	SA	Poor - Moder.	4.50 ₁
HF1E1 P137	K-18	3820.00 - 20.18	5.2	0.13	Monocrys. qtz+ LRF	Biotite+plag.+ clays	A	Poor	2.00 ₁
HF1G P203	B-27	3865.27 - 65.59	13.2	0.67	Monocrys. qtz+ LRF+clays	Mica+feldspar calcite cement	A-SA	Poor - Moder.	3.75 ₁
HF6 SP163	B-27	3847.80 - 47.99	12.8	49.30	Monocrys. qtz+ LRF+IRF	Chert+mud pellets+mica	SR	Moder.	8.00 ₁
HF6 SP164	B-27	3848.39 - 48.49	10.2	17.00	Monocrys. qtz+ LRF+IRF	Chert+mica (?) + Organic matter	R	Moder.	10.00 ₁
HF2A P97	C-96	3892.08 - 92.34	5.7	0.24	Silt with sand and abundant clays		VA*	Poor	1.00 ₁
HF2A P147	C-96	3919.15 - 19.44	11.4	0.62	Silt with sand and abundant clays		VA	Poor	1.00 ₁
HF2B SP103	B-08	3624.83 - 25.00	3.5	0.09	Silt with sand and abundant clays rare calcite cement+ pyrite		SA - SR	Poor	3.50 ₁
HF2C P198	B-27	3864.15 - 64.35	10.8	0.23	Silt with sand and abundant clays +plag.		SA	Poor	3.00 ₁

* A: Angular, SA: Subangular, SR: Subrounded, R: Rounded, WR: Well-rounded, Moder: Moderate, Monocrys. qtz: Monocrystalline quartz, LRF: Lithic rock fragments, IRF: Igneous rock fragments Poly. qtz: Polycrystalline quartz, plag: Plagioclase, kaolin: Kaolinite

Table 6a: Relationship between ETMI and other rock characteristics of facies other than HF1C. (For calculated ETMI values, see table 5)

Facies	Plug#	TS#	Well	Core Depth (m)	ϕ (%)	k(mD)	Type	Major Minerals >95%	Minor Minerals <5%	Roundness	Sorting	ETMI
HFIC	SP249	79	K-18	3855.75-55.94	18.6	615	QA	Monocryst. qtz	LRF+AC	SR-SA	Moderate	7.1
HFIC	85	812	C-96	3881.56-81.92	16.5	1480	QA	Monocryst. qtz	LRF+AC (kaol.) +mica+feldspar (<1%)	SR-SA	Moderate- well	8.75
HFIC	254	760	K-14	3804.70-04.90	19.4	1370	QA	Monocryst. qtz	Polycryst. qtz+ Lithic and igneous rock fragments	SR	Well	12.1
HFIC	315	773	K-14	3935.56-35.89	21.4	2030	QA	Monocryst. qtz	LRF and mica +calcite (<<1%)	R-SR	Well	13.5

* TS#: Thin section number, QA: Quartzarenite, LRF: Lithic rock fragments, AC: Authigenic clay, SR: Subrounded
SA: Subangular, R: Rounded, kaol.: Kaolinite, k: Permeability, ϕ : Porosity

Table 6b: Relationship between *ETMI* and other rock characteristics of HFIC specimens determined by thin section petrography. (For calculated *ETMI* values, see table 5)

$$ETMI = \text{Sorting constant} \times \text{Roundness constant}$$

overgrowths precipitated before pore-lining clays formed. Some over-sized pores, especially in P315, suggest that the dissolution of either grains or some of the fine matrix material might have produced secondary porosity. Rarely-occurring serrate edges of some of the quartz grains also mark the grain dissolution.

V.2.1.4. Lithofacies HF1C1

This lithology is fine- to lower medium-grained sublitharenite composed of monocrystalline quartz, metasedimentary rock fragments, and detrital, chlorite-rich mud pellets (Table 6a; figure 39). Hydrocarbon residue is locally found trapped in some isolated pores. Minor additional mineral components are polycrystalline quartz, mica, micro porous chert, rare calcite (<1%) and feldspars. The grains of plug 207 are subrounded and moderately-sorted, while 208 displays a more subangular and poorly- to moderately-sorted textural framework. Neither P207 nor P208 have substantial amounts of quartz overgrowth that would significantly affect the permeability. However, clay-rich and argillaceous matrix, and intergranular mud pellets disrupt the pore connections. Due to the highly complex assemblage of argillaceous material, identification of clay types is not possible by means of thin section analysis.

V.2.1.5. Lithofacies HF1D

Examined thin sections of the HF1D lithology have similar mineral framework (Table 6a). Medium- to coarse-grained sandstones of HF1D are dominantly clean quartzarenites composed of over 95% monocrystalline quartz grains (Figure 40). Minor constituents are polycrystalline quartz, very low percentage of lithic rock fragments (~1%), and trace amounts

of pore-lining clays and pyrite

Plug 347 is rounded and well-sorted. Although plug 349 is also well-sorted, its roundness is higher (well-rounded). Both sandstones are very porous and the pore connectivities have established high permeabilities.

Quartz overgrowths occur rarely. The pore system is partially hydrocarbon-stained. Preferential alignment of minor detrital clays within pores indicate infiltrated geopetal fill.

V.2.1.6. Lithofacies HF1F

Thin sections of P160 from Hibernia C-96 and SP74 of Hibernia B-O8 are examined as representatives of HF1F (Table 6a). Coarse- to very-coarse-grained quartzarenites are rounded, moderately- to well-sorted and composed mainly of monocrystalline quartz (Figure 41a&b). In addition, the remainder of the particles are polycrystalline quartz, lithic rock fragments and a matrix material composed of very fine-grained sands, kaolinite, mica, calcite, plagioclase and igneous rock fragments. Very fine-grained matrix material is always located on the same side of the pore system, just as geopetal fill would have formed after the infiltration of ground waters. Pore-lining authigenic clays are encountered in both samples. Pore-lining clays cause porosity reduction in both SP74 and P160. Quartz overgrowths are rare in both specimens

Identified pore-reducing mechanisms remain relatively ineffective in the quartzarenites of HF1F where both of the specimens possess high porosities and permeabilities.

V.2.1.7. Lithofacies HF3

Bimodal conglomeratic sandstones of HF3 are represented by plug 345G of Hibernia K-14

and plug 134 of Hibernia C-96 (Table 6a). Both samples are composed of poorly- to moderately-sorted and subrounded sublitharenites containing pebbles (Figure 42). Major constituents of the sand-sized component are monocrystalline and polycrystalline quartz, lithic rock fragments and chert. Minor constituents of the lithofacies are mica, clays, very rare pyrite crystals, and igneous rock fragments. Most of the clays are authigenic and occur in a pore-lining form.

The lithology is porous; however, pore connections are poorly-developed. Abundant quartz overgrowths have resulted in are significant grain interlocking. Intergranular lithic rock fragments, pore-lining clays and very fine-grained matrix material composed of mostly quartz grains also decrease pore interconnection.

V.2.1.8. Lithofacies HF1E

This lithology is a quartzarenite consisting mainly of very fine- to fine-grained monocrystalline quartz (Table 6a). Ripple cross lamination (Figure 43a) and horizontal laminae determined during core description are also evident in the thin section. Minor components of the mineral framework are lithic and igneous rock fragments and detrital clays. Intergranular matrix is micaceous (Figure 43b).

Sorting is poor to moderate and roundness is angular to sub-angular. Silicification on quartz grains exists but is not abundant. Intergranular detrital and pore-lining authigenic clays are the important pore space-reducing components, while precise identification of clay types is not possible.

V.2.1.9. Lithofacies HF1E1

HF1E1 is a sublitharenite which mainly contains monocrystalline quartz and lithic rock fragments (Table 6a). Parallel lamination is identified in the form of alternating very fine-grained/muddy and fine-grained (relatively coarser) layers (Figure 44a&b). Very fine-grained muddy laminae and quartz overgrowths occupy the intergranular system of the lithology. Overall, the monocrystalline framework grains are angular and poorly-sorted. No visual evidence for porosity is observed. The lithology is very carbonaceous and is intermixed within the clay-rich argillaceous laminae.

V.2.1.10. Lithofacies HF1G

This lithology is a silt sized to very fine-grained sublitharenite with the major mineral components of monocrystalline quartz, lithic rock fragments, and detrital clays mixtures (Table 6a; Figure 45a&b). Minor components are mica, feldspars, and calcite. Clay types are difficult to determine due to the highly-mixed abundant argillaceous texture. The lithology is poorly- to moderately-sorted, angular to sub angular. Carbonate cement identified during the core descriptions is readily observed as intergranular stained red patches. Quartz overgrowths are in negligible abundance. Rare pores are in isolated forms where they do not produce pore connections.

V.2.1.11. Lithofacies HF6

HF6 consists of organic material-rich, fine-grained sublitharenitic sandstones containing monocrystalline quartz, carbonaceous stringers, coal, micaceous igneous fragments, and detrital mud pellets (Table 6a; figure 46a&b). Minor additional constituents are chert,

polycrystalline quartz, rare mica flakes and detrital clays. Quartz overgrowths are present but not abundant. The lithology is moderately-sorted and subrounded. Pores are well-preserved. Organic nodules are ubiquitous and partially occupy the pore space. There is no evidence for any type of bedding.

V.2.2. Petrography of the interstratified sand/silt/claystone facies*:

** Due to the highly argillaceous, shaly and silty texture, thin section photographs of all three interstratified lithologies displayed close similarities. Therefore, only the photograph of HF2A specimen is presented as the representative of HF2A, HF2B, and HF2C.*

V.2.2.1. Lithofacies HF2A:

HF2A was examined in P97 and P147, both being from Hibernia C-96 (Table 6a). Both samples are composed of silt, shale and very fine-grained sandstones which are poorly-sorted and very angular (Figure 47). Observed highly contorted texture of both samples could be the result of the deformation structures or bioturbation determined during the core descriptions. Grain size variations fluctuate under the control of bedding structures. Due to the highly blended nature of the lithology identification of different types of detrital clay other than rare kaolinite booklets becomes difficult. No visual porosity is evident. The matrix is composed of mica-rich igneous rock fragments, clays, pyrite and rare calcitic cement.

V.2.2.2. Lithofacies HF2B

HF2B is characterized by a thin section of SP103 of Hibernia B-O8 (Table 6a). The lithology is very silty, shaly sublitharenite containing monocrystalline quartz, lithic and igneous rock fragments. Minor additional components forming the fine-grained matrix material are clays, mica, rare calcite and pyrite.

The sample is parallel-laminated. Two distinct laminae, one coarser than the other, were identified. The grains of the coarser-grained laminae are well-sorted and subangular to subrounded within the coarser lamination. However, in overall view, sorting is very poor and the degree of grain roundness is subangular to subrounded.

Quartz overgrowths are common and appear to reduce intergranular pore space in many parts of the specimen. Authigenic and pore-lining clays are not encountered. Most of the clays are in intergranular form, intermixed with silt particles..

V.2.2.3. Lithofacies HF2C

P198 of Hibernia B-27 was analysed for the lithofacies HF2C (Table 6a). The average grain size in the specimen is mostly clay and silt. Intergranular matrix is composed of clays and mica. Rare plagioclase crystals were identified. Grain size variations are high and thus the sorting is very poor. Visible grains are subangular. No visual porosity was identified.

Neither HF4 nor HF5 were examined by thin section petrography technique since both lithofacies are shale.

V.3- SUMMARY AND INTERPRETATION OF THIN SECTIONS

V.3.1. Summary of thin section petrography:

Summarized information of the analyzed specimens regarding depth, and flow properties, major and minor mineralogies, and textural maturity is presented in table 6a and 6b. X10 magnification was the standard in this study as long as the grain size attributes allow us to do so. Standard magnification provided visual and comparative understanding of textural maturity, as well as grain size distribution. Permeability-controlling mechanisms which were earlier introduced in the previous chapter are also evaluated.

V.3.2- Interpretation and conclusions of thin section petrography:

V.3.1.2. Permeability - Textural Maturity relationship

Enhanced Textural Maturity Index (ETMI) values (Table 6a&6b) were graphed against permeabilities of the examined specimens (Figure 48). Permeability proportionally increases with higher values of *ETMI*. An envelope of $k/ETMI$ ranges suggests that two separate trends may exist in the *ETMI*-permeability relationship. Specimens falling around *line A* have higher permeabilities than those around *line B* for a particular *ETMI* value. The upper portion of the graph is an area of low matrix, clay content, cements, diagenetic pore-reducing components, and permeability-reducing factors. Common permeabilities can range over approximately 4 *ETMI* units. For instance, the permeability of P254 ($k=1370$ mD, *ETMI*=12) is close to the permeability of P85 (1480 mD) which has an *ETMI* of 8.75. Both are in the same lithofacies (HF1C). The greater abundance of quartz overgrowths identified in P85 may

account for the permeability reduction

The window of "extremely high permeability" contains samples of coarse grained, clean, porous, well-sorted, and rounded to well-rounded quartzarenites. "The high permeability window" includes all samples of HF1C as well as two samples of HF3, the conglomeratic sandstones. Bimodal sands of HF3 possess a lower degree of *ETMI*.

"The intermediate permeability" window contains very fine-grained HF1A (15.3 mD), very fine- to fine-grained HF1E (29.60 mD) and HF1B (44.0 and 52.7 mD) samples. Two specimens of HF1C1 (P207, P208) reflect the correlation between the *ETMI* and permeability. An abundance of rip-up mud clasts can affect the quality of sorting. In spite of the lower medium (125-350 μ) grain size of the lithofacies, lower *ETMI* and high argillaceous content reduced HF1C1 permeabilities.

P145 of HF1E (rippled sands) with a permeability of 29.60 mD is grouped within "the intermediate permeability" zone together with the finer-grained sands of distributary channel deposits. P145 is poorly- to moderately-sorted and subangular. Thus it has a low *ETMI* (4.50). However, a lower degree of silicification (relative to HF1E1; laminated sands of HF1E1, of similar character) has maintained optimal permeability. Very low textural maturities (Table 6a), together with very fine to silt size grain attributes maintain lower permeabilities in samples of HF1E1, HF1G, HF2A, HF2B and HF2C.

By using the calculated *ETMI*, porosity and permeability values of the thin section-analyzed specimens, three major conclusions can be drawn from figure 49.

1. High *ETMI* correlates with increasing grain size, decreasing clay matrix, and

decreased influence of k-reducing diagenetic variables. Low ETMI correlates with decreasing grain size, increasing clay matrix and k-reducing diagenetic components.

2. *ETMI* increases proportionally with permeability.

3. The general grain size trend is for increase with increasing *ETMI*. However, contrary to this, the coarsest lithofacies have intermediate *ETMI* values (HF3, HF1F), as a result of their poorer sorting and roundness attributes (Table 6a) and tendency for higher clay content

Therefore, a high level of sorting and roundness such as will occur at the end of a transportation process long enough to eliminate less stable and finer-grained minerals is one of the major components of a unique permeability-producing system.

V.3.1.2. Nature of the quartz overgrowths; abundance of quartz overgrowth - permeability relationship in thin sections

The paragenetic sequence of diagenesis indicates that the first cementation episode involved the precipitation of silica from silica-rich pore fluids. Quartz overgrowths are reported to be one of the most significant pore space-blocking features in sand-dominated lithologies (McIlreath and Morrow 1990). As Boles and Franks (1979), Hayes (1979), Blatt (1980), Franks and Forester (1984), Galloway (1985), and Brown *et al.* (1986) have pointed out, silica-rich pore fluids can be generated from

1. "dewatering of muds during the initial burial and/or meteoric ground waters,"
2. "dewatering of deeply buried shales (3-4 km.; 60-120°C) which produce Si⁴⁺-rich waters released during the smectite-illite transition,"
3. "dissolution of siliceous microflora and microfauna," and

4. "pressure dissolution."

Sutured grain interfaces (HF1F) are less frequently observed than regular contacts between quartz grains.

Quartz overgrowths are observed as an important pore volume reducing factor in HF1A, HF1B, HF1C, HF3, HF1E, HF1E1, and HF6. This conclusion corresponds with the SEM/EDS findings recorded the previous chapter (Figure 12) where overgrowths occur in the intermediate ranges of the data set (Figure 49). However, information regarding the size of quartz overgrowths and their relative abundance in the composite graph can not be reliably obtained in two-dimensional resolution of thin section petrography.

V.3.1.3. Argillaceous material - permeability relationship in thin sections

Identification of clay types other than kaolinite, regardless of being detrital or authigenic is not possible in thin section. Therefore, the term "argillaceous material" has been used in the context of all the pore-occupying and textured materials including clays, feldspars, mica, mud pellets and aggregates, lithic and igneous rock fragments, and carbonaceous material.

Pore-lining authigenic clays in general are detected in most of the samples. Their abundances have not been quantitatively determined since the argillaceous material has a complex and chaotic character. Detrital clays are more abundantly observed in the lower-medium to fine-grained sands with the amount increasing proportionally to the decrease in grain size. Mica is most abundant within the silt to very fine-grained sand lithologies of HF1A, HF1E, HF1E1, HF1G, HF2A, HF2B, and HF2C. Overall, permeability decreases with the increasing argillaceous content (Figure 49)

V.3.1.4. Calcite cement - permeability relationship in thin sections

Pore-reducing calcite cement occurs in the intergranular matrix of HF1B, HF1C1, and HF1G lithologies consistent with the findings of the SEM/EDS analyses (Figure 49). The only difference is that the calcareous content of HF1G (refer to core descriptions, chapter III) is identified in thin sections and increased the resolution of the SEM/EDS findings. The most abundant calcite content is observed in HF1B lithologies.

Results of Thin Section Analysis on Composite Porosity/Permeability/Facies Distribution

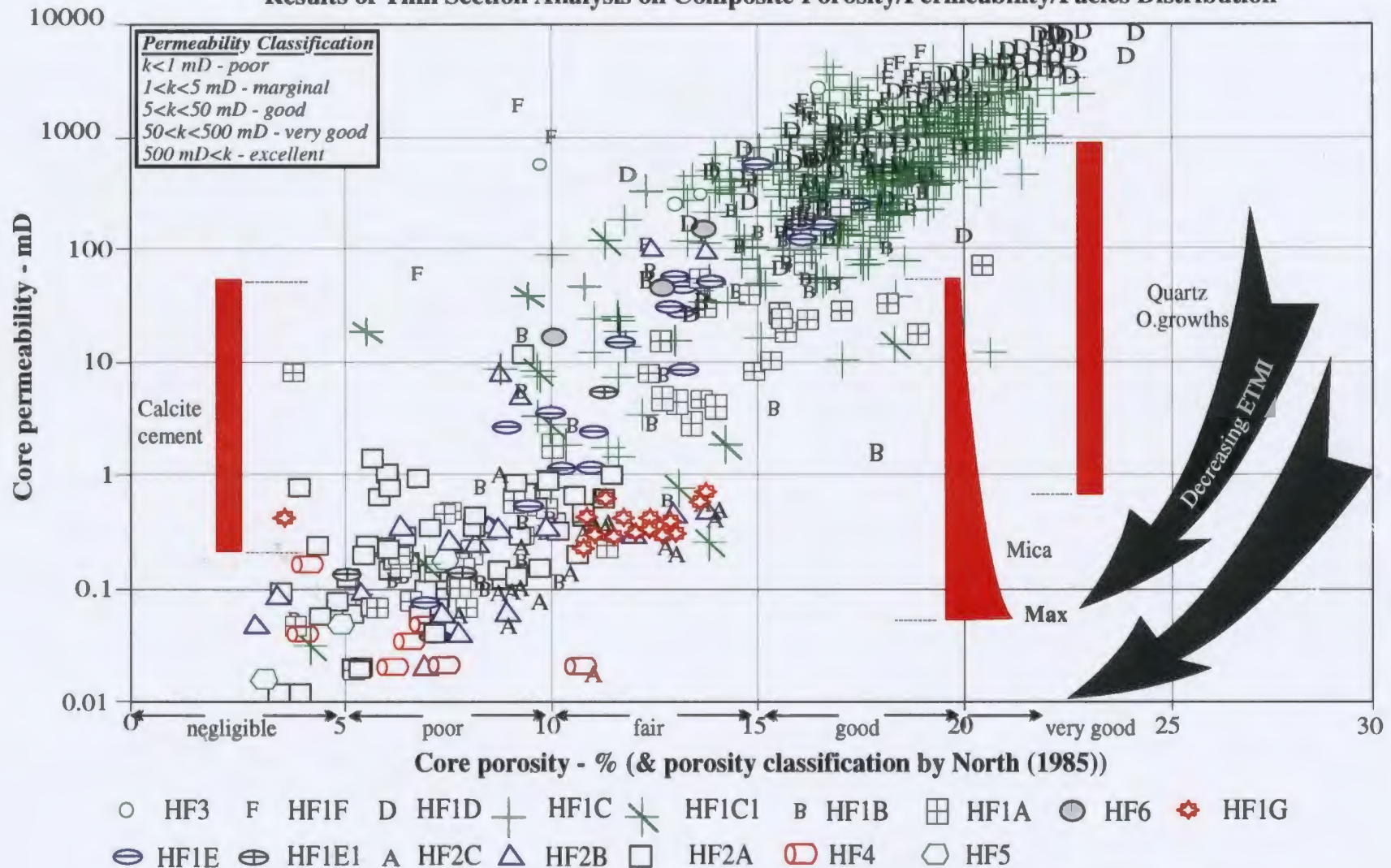


Figure 49: Analyzed HF1F and HF3 specimens have lower ETMI and porosities than HF1D. Two distinct clusters of HF1F and HF1D are evident and coinciding with the *ETMI* attributes (also refer to table 6a&b). Calcite cement is observed in a wider range relative to results of SEM/EDS in figure 12.

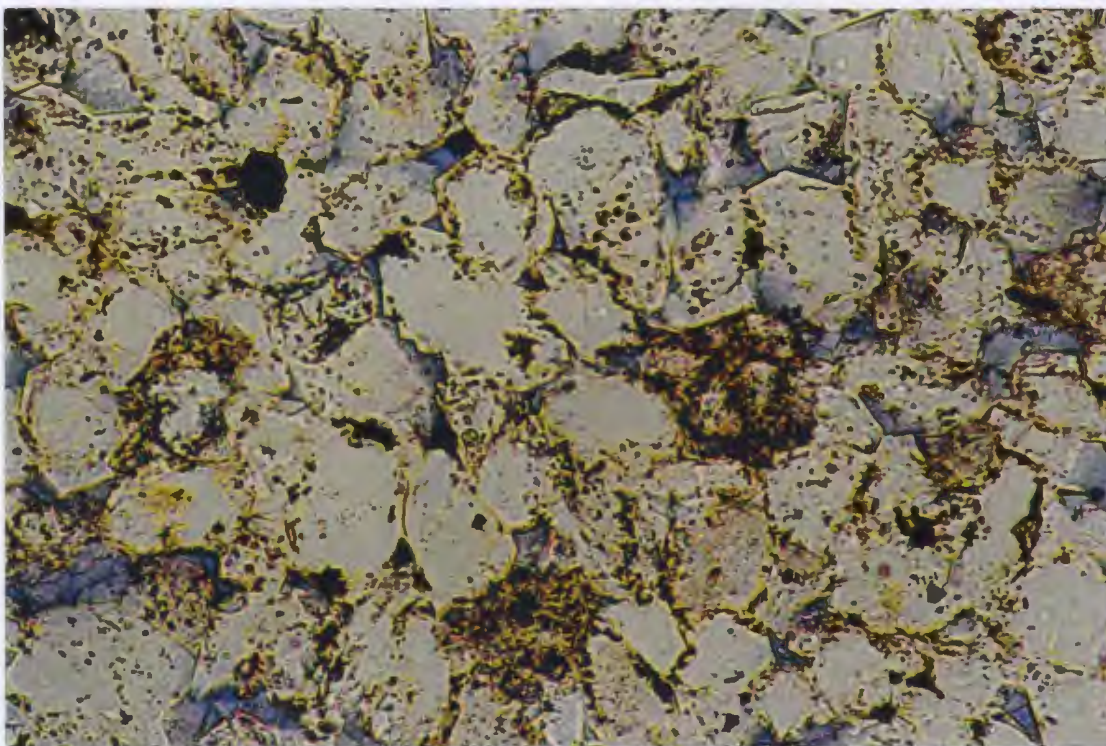


Figure 36: Poor to moderate sorting of subangular, fine-grained sands of HF1A. Widespread overgrowths are distinguished with clay rims on detrital grains. (SP102 (of HF1A); Mag=X10PP)($k=15.30$ mD; $\phi=12.8\%$)

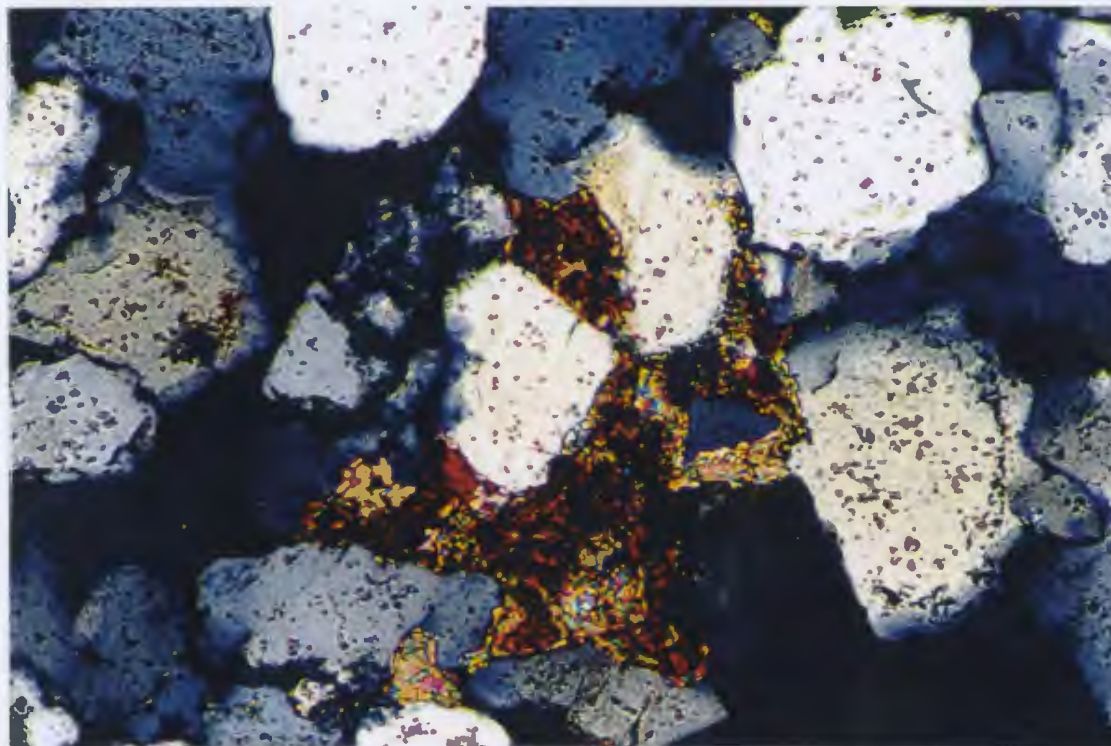


Figure 37: Intergranular calcite cement is locally-concentrated in HF1B. The lithology is fine-grained, moderately-sorted, subangular to subrounded. Overgrowths are common.

(Stained thin section of SP102 (HF1B); Mag=X10XP)($k=52.70$ mD; $\phi=12.3\%$)

(Width of both of the pictures=0.64mm ; PP=Plain-polarized, XP=Cross-polarized)

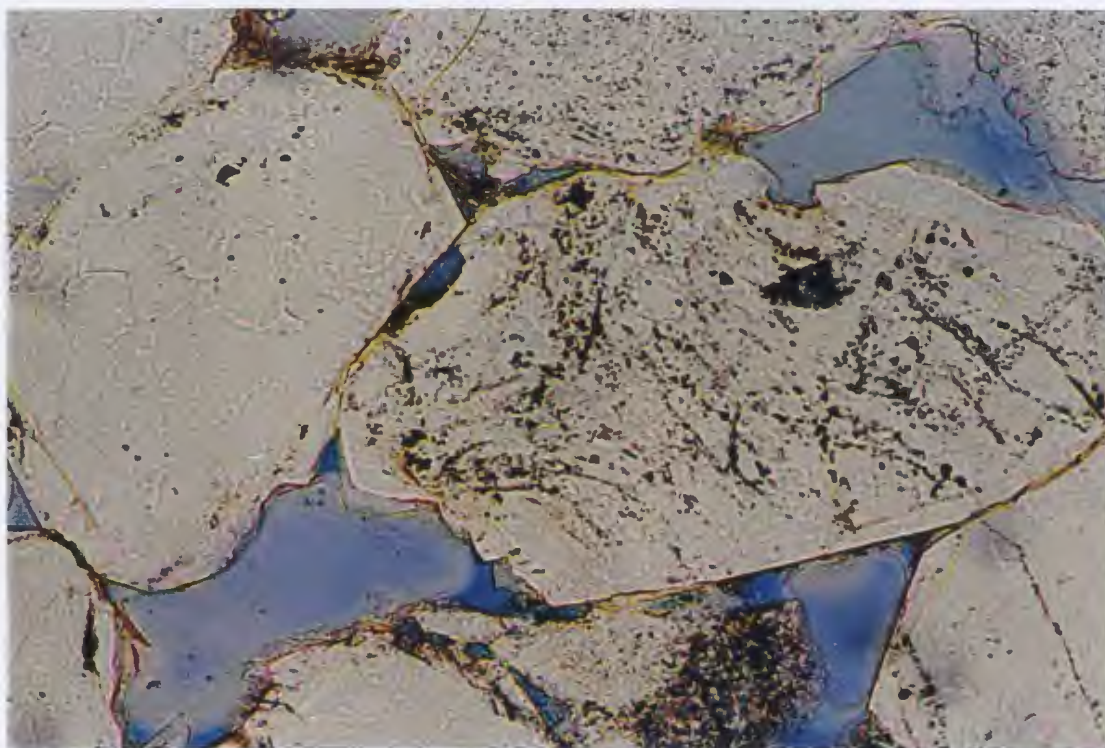


Figure 38: The lithology of **HF1C** is moderately-sorted, subrounded, and medium-grained. Quartz overgrowths are evident. Serrate grain edges are rare, presenting ϕ -increase by grain and/or matrix dissolution. (SP249; Mag=X10PP)($k=615$ mD; $\phi=18.6\%$)

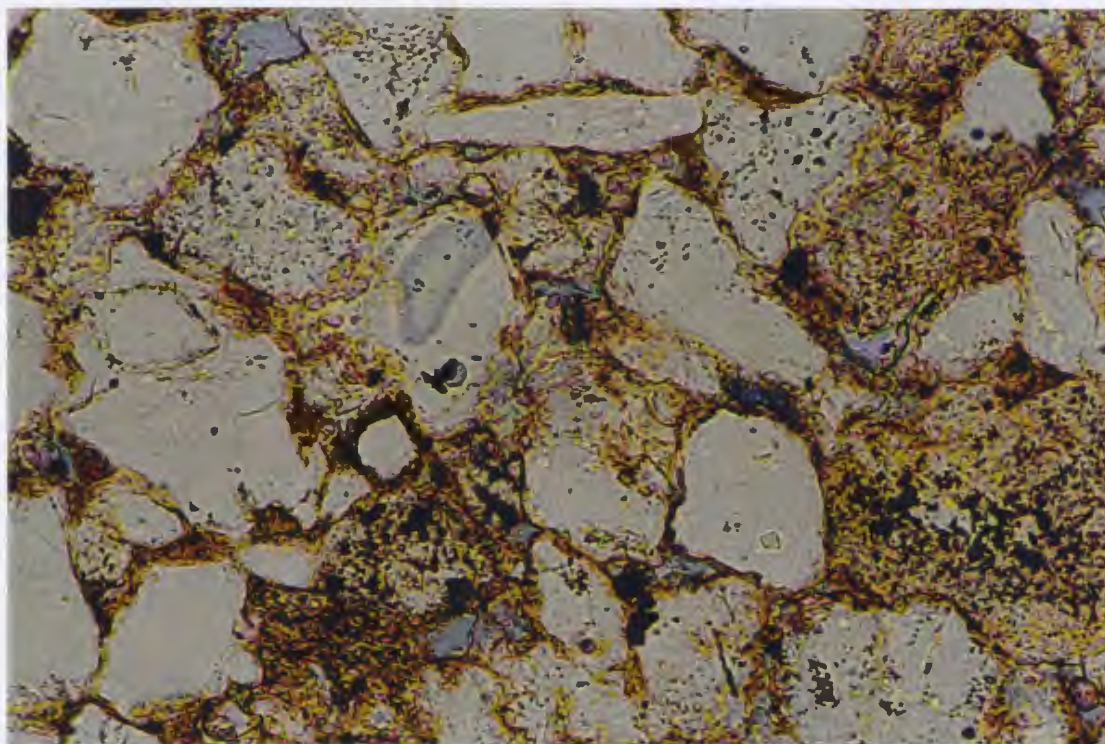


Figure 39: Upper fine-grained sands of **HF1C1** are argillaceous, poor to moderately-sorted, subangular to subrounded. Types of abundantly-occurring clays are not clear. Pores are isolated by the matrix. (P208; Mag=X10PP)($k=0.32$ mD; $\phi=14.2\%$)

(Width of both of the pictures=0.64mm)

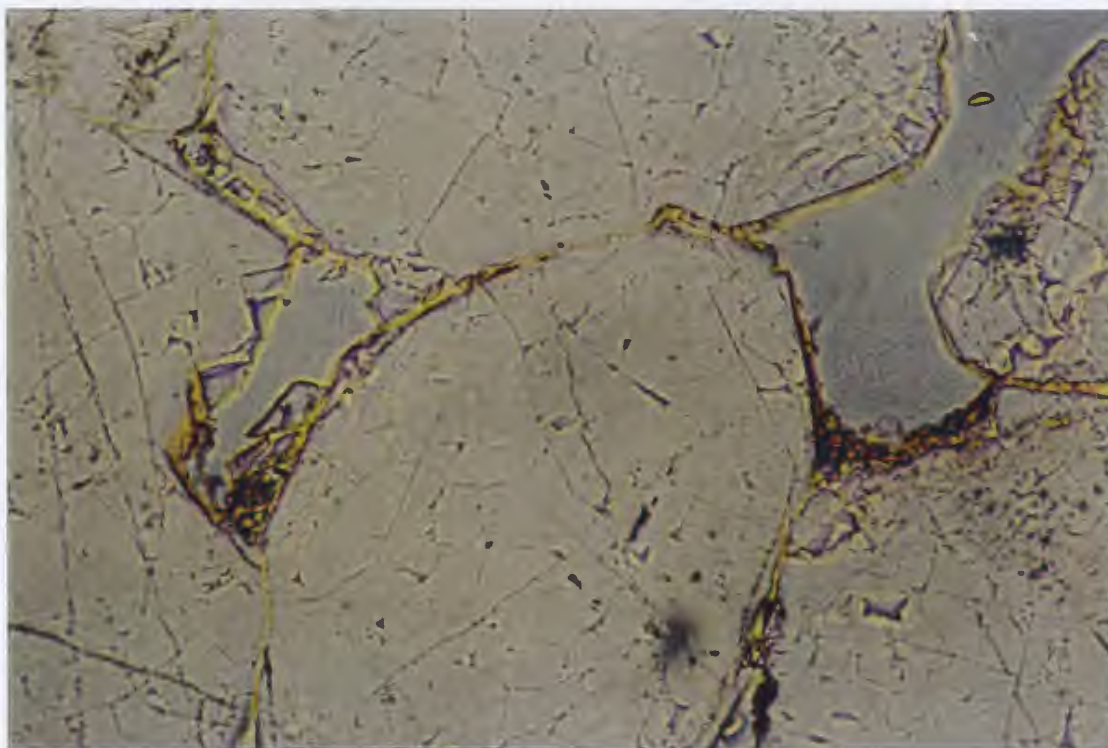


Figure 40: **HF1D**. High degree of roundness and clean texture of the coarse-grained sands are in favor of high porosity and permeability. Pore connections are well-preserved. Preferential alignment of geopetal fill in pores are ineffective on pore connectivity. (P347; Mag=X10PP) ($k=4640$ mD; $\phi=19.4\%$)

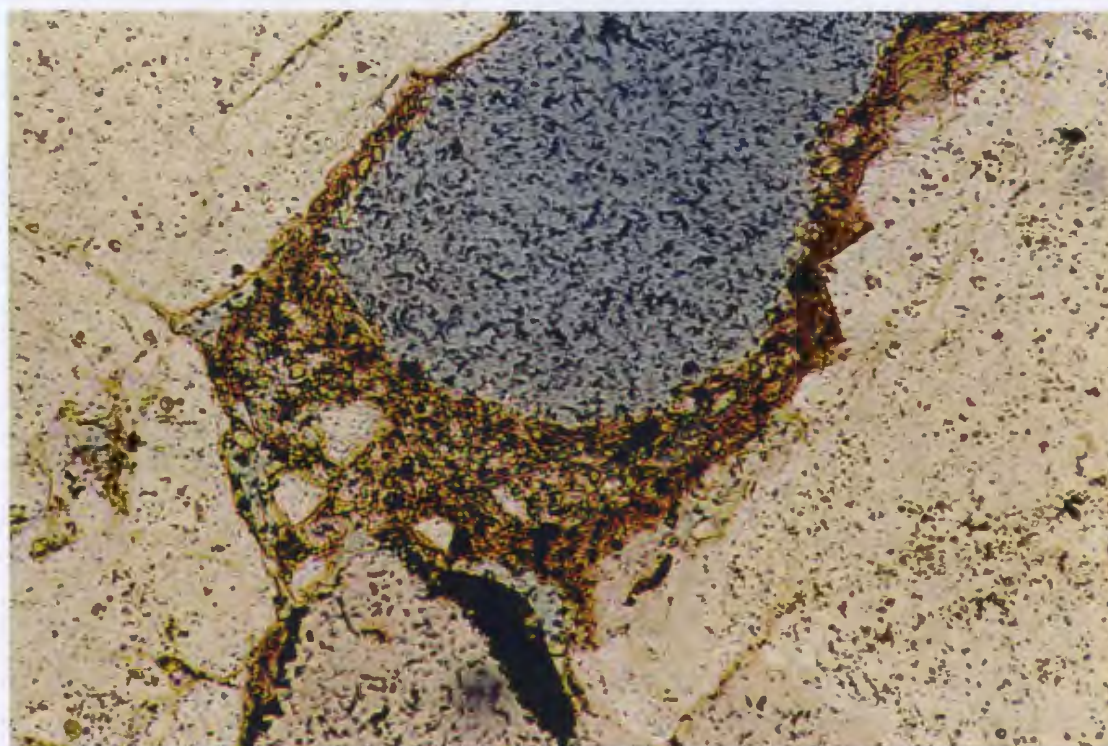


Figure 41a: **HF1F**. Possible geopetal fill in coarse-grained sands. (P74; Mag=X10PP) ($k=1290$; $\phi=19.3\%$)
(Width of both of the pictures=0.64mm)



Figure 41b: **HF1F**. Preferential alignment of possible geopetal fill, good porosity and pore connectivity of the lithology can be observed in lower magnification photo. The lithology is subangular to subrounded, and moderately-sorted. (P74; Mag=X2PP) ($k=1290$ mD; $\phi = 19.3\%$)

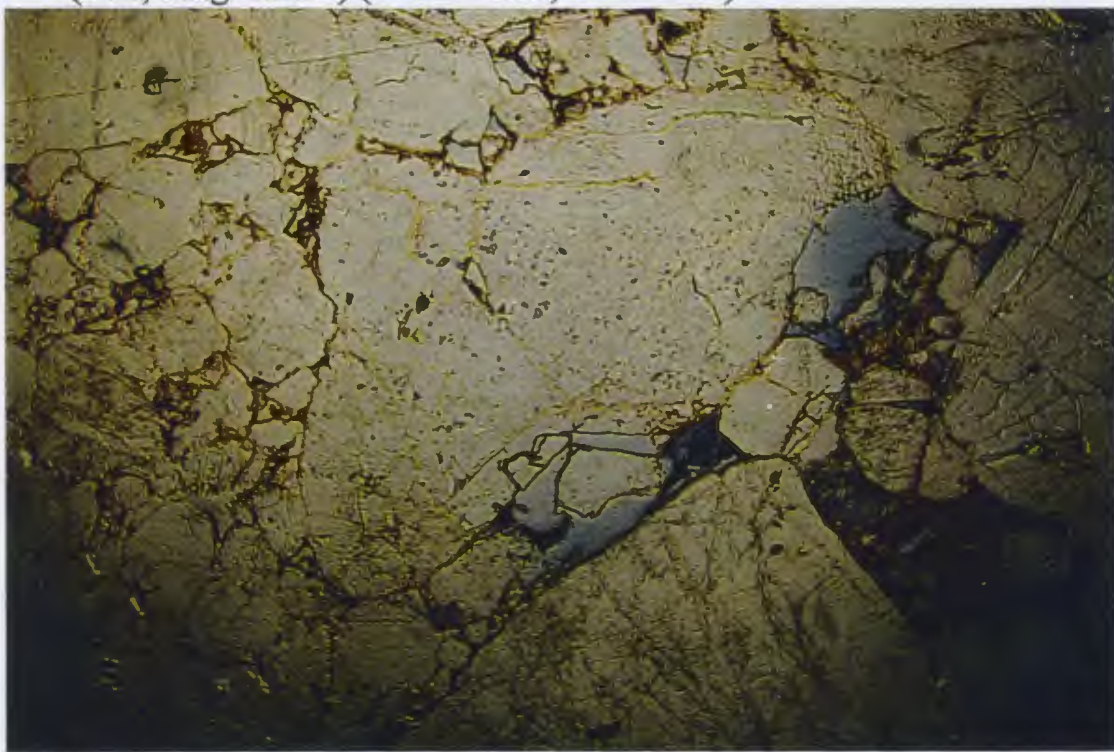
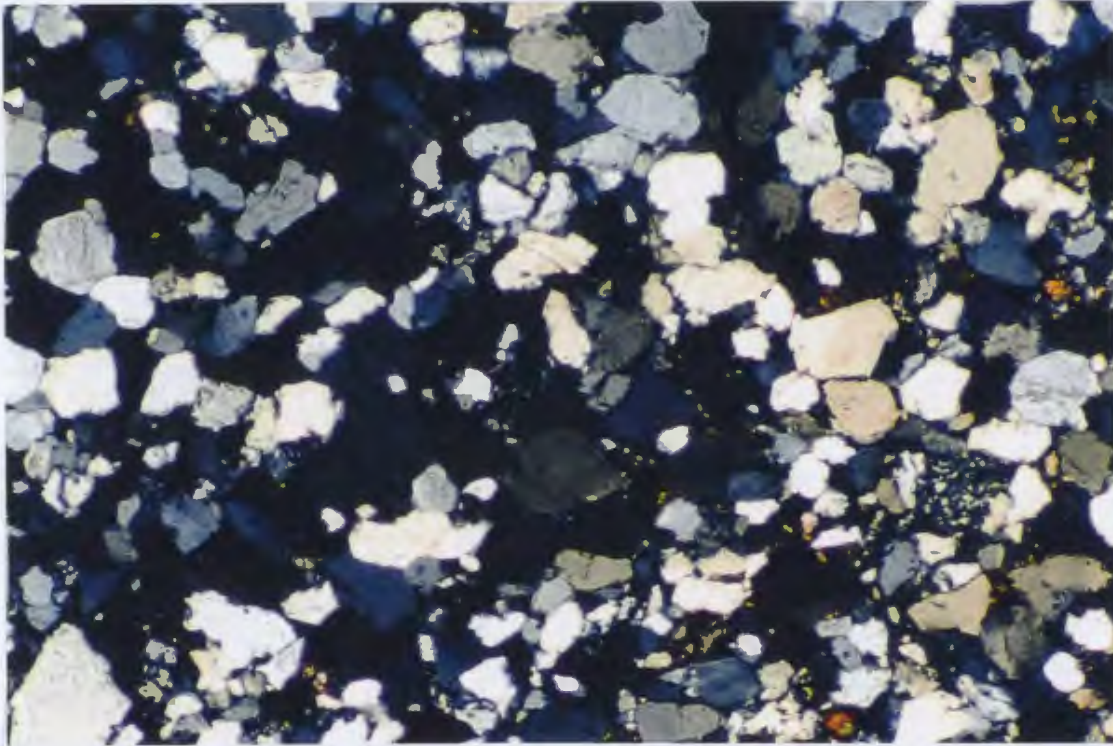


Figure 42: Bimodal character of the lithofacies **HF3** is presented with pebbles and very fine to fine grains. Intergranular, kaolinitic clays appear to be depositional. (P134; Mag=X2PP) ($k=238$ mD; $\phi=13.2\%$)

(Width of both of the pictures=3.2mm)

a)

116



b)

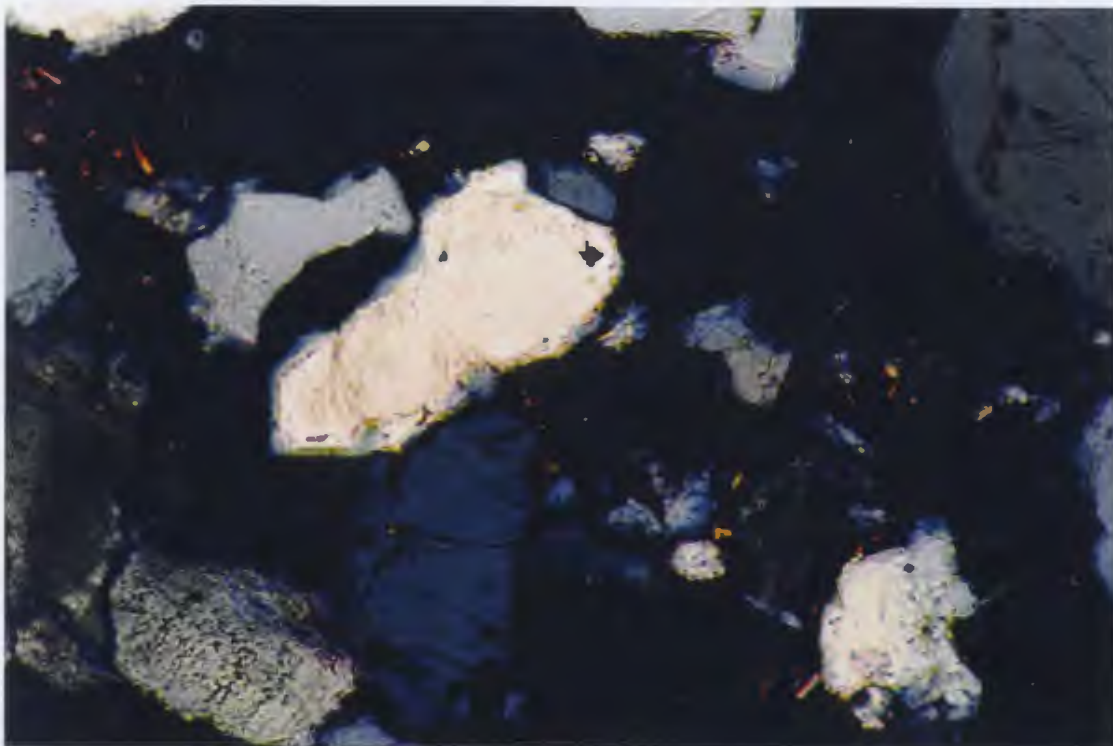


Figure 43a&b: Ripple cross laminated sands of **HF1E**. HF1E is very fine- to fine-grained, poor- to moderately-sorted, and subangular (43b). Quartz overgrowths and micaceous, clay-rich, and intergranular matrix reduce the porosity. (P145; a): Width of picture=3.2mm; Mag=X2XP: b): Width: 0.64mm; Mag=X10XP)($k=29.60$; $\phi=13.0\%$)

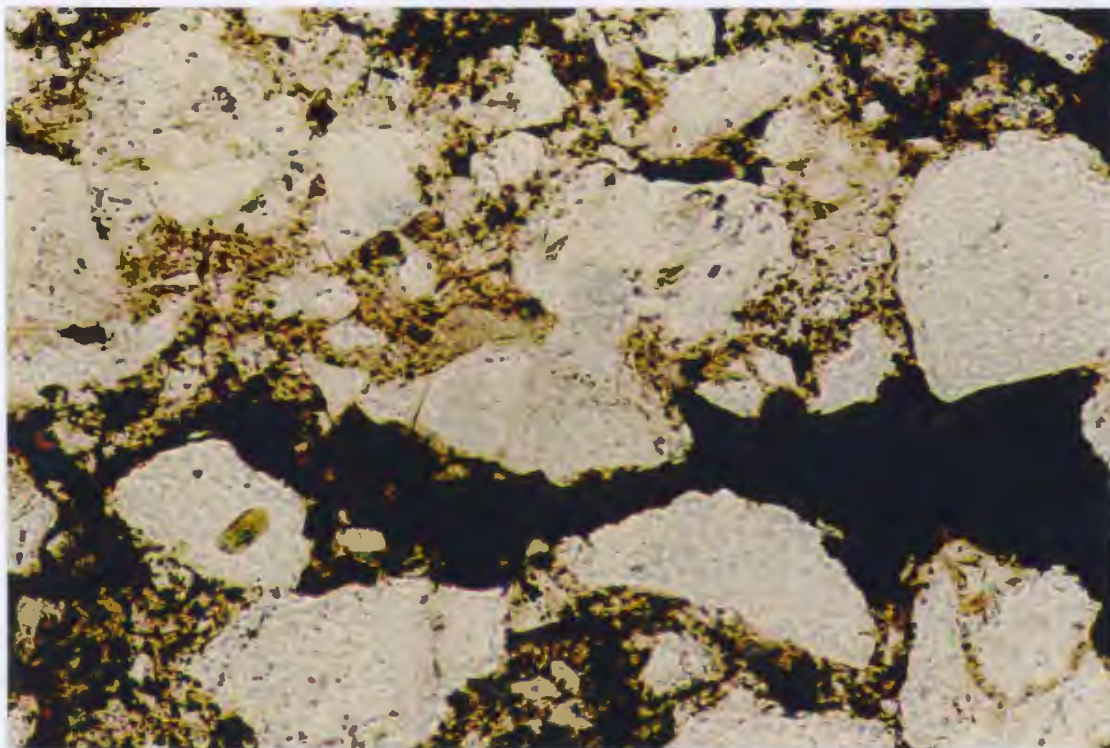
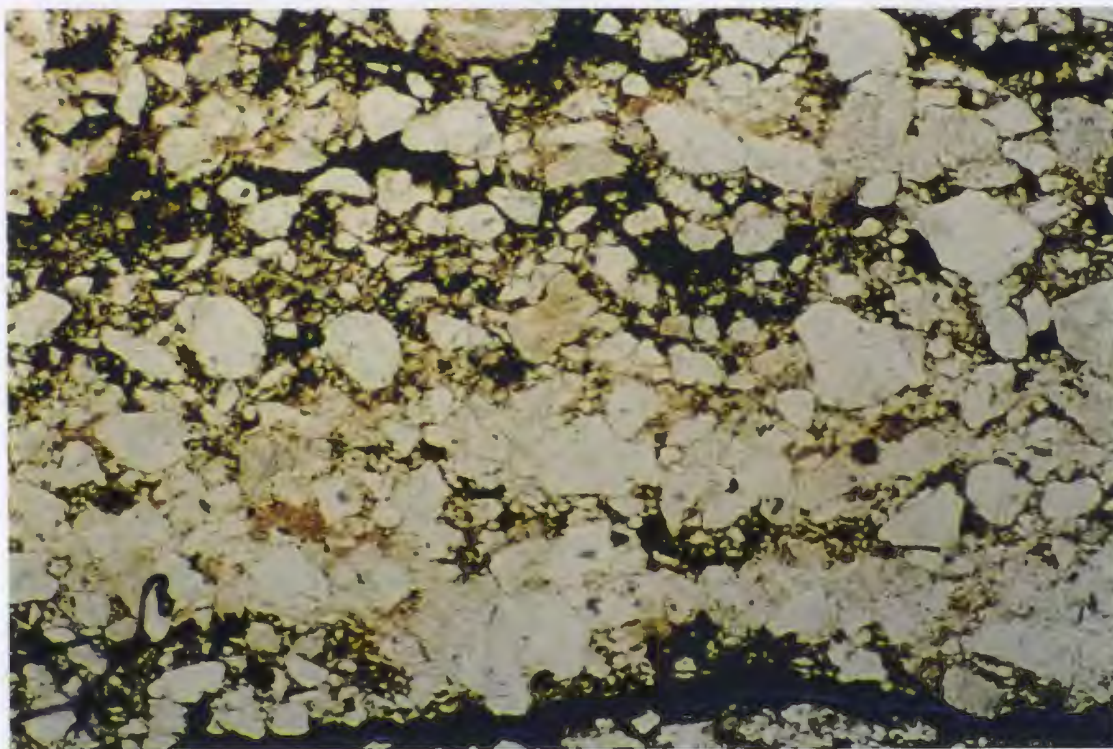
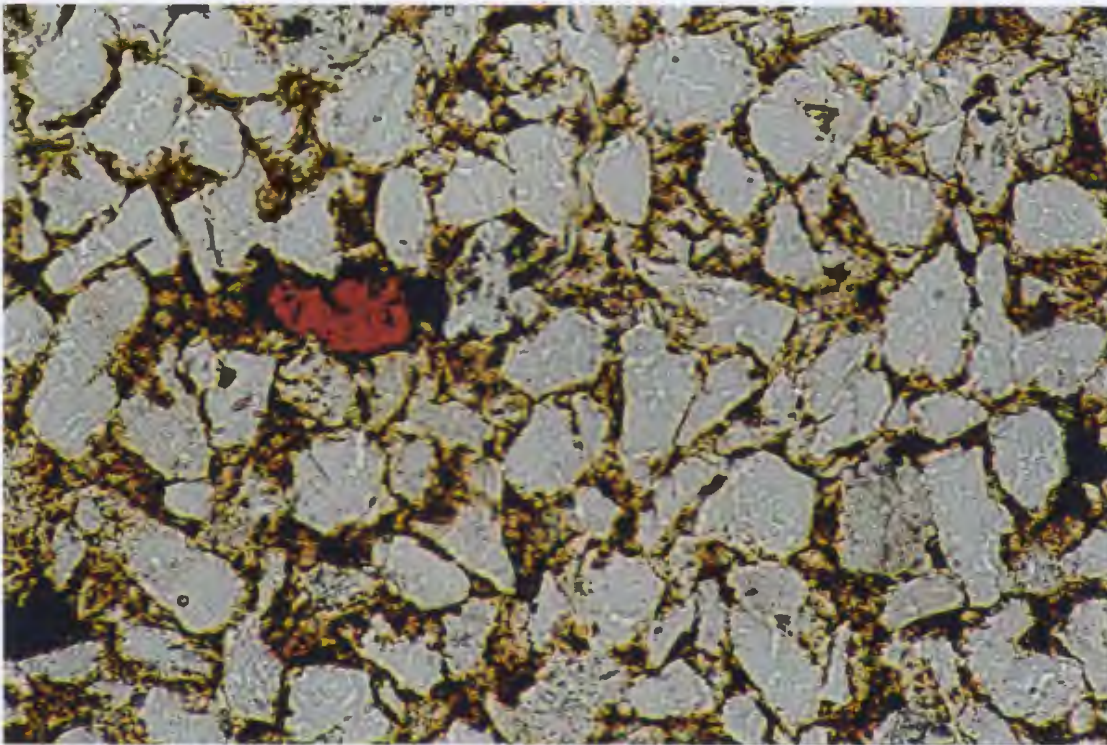


Figure 44a&b: **HF1E1**. Fine- to very fine-grained, carbonaceous sands are poorly-sorted, angular, and rich in organic matter. Complex intergranular matrix makes the clay types unspecifiable. Quartz overgrowths also reduce the pore space. Parallel lamination, in the form of alternating sand and muddy/carbonaceous zones, is abundant. (P137; a): Width of picture=3.2mm; Mag=X2PP; b): Width of picture=0.64mm; Mag=X10PP) ($k=0.13$ mD; $\phi=5.2\%$)

a)

118



b)

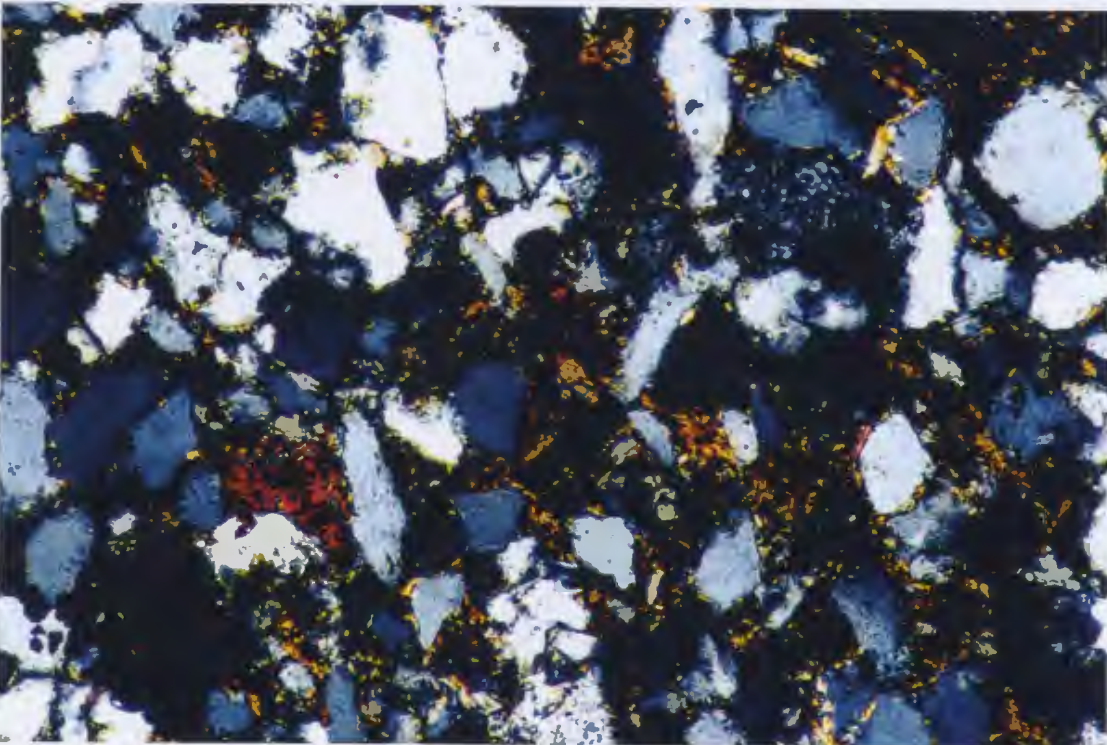
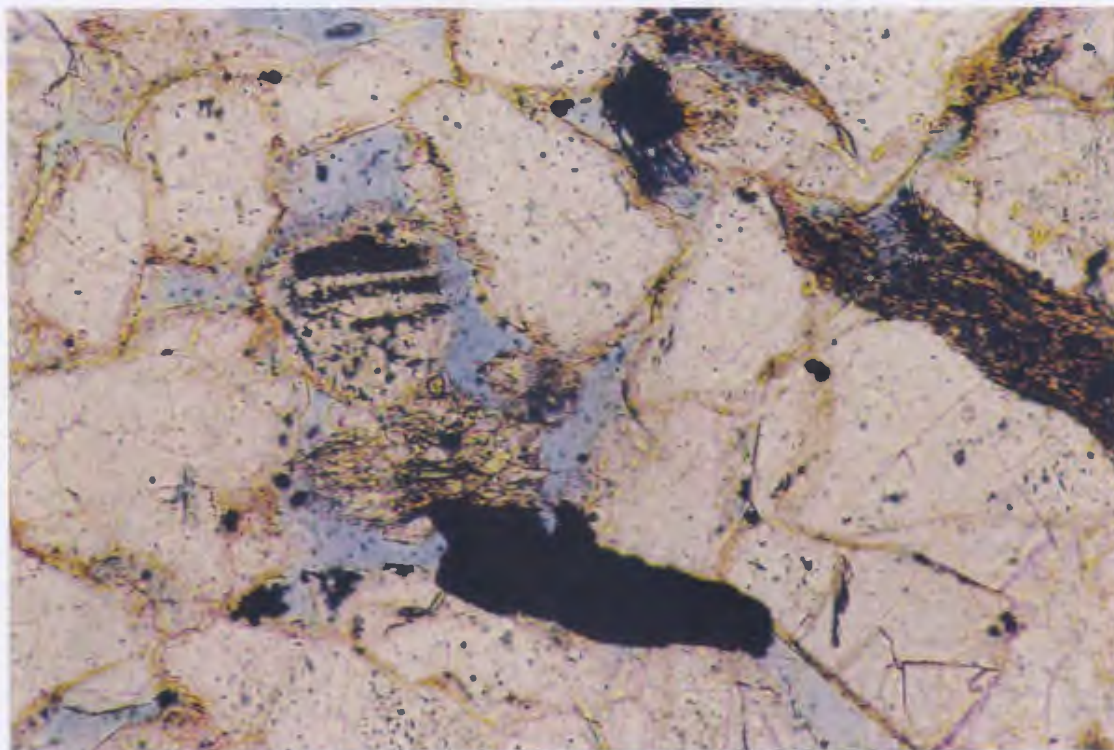


Figure 45a&b: (P203) HF1G photo from were two different locations display a very argillaceous, very fine-grained lithology. Local calcite cement is observed in red stained patches and reduce the porosity. Intergranular matrix is micaceous. The sorting is poor to moderate, and the roundness is angular to subangular. (P203; Mag=a):X10PP&b):10XP)($k=0.67$ mD; $\phi=13.2\%$)

(Width of both of the pictures=0.64mm)

a)



119

b)

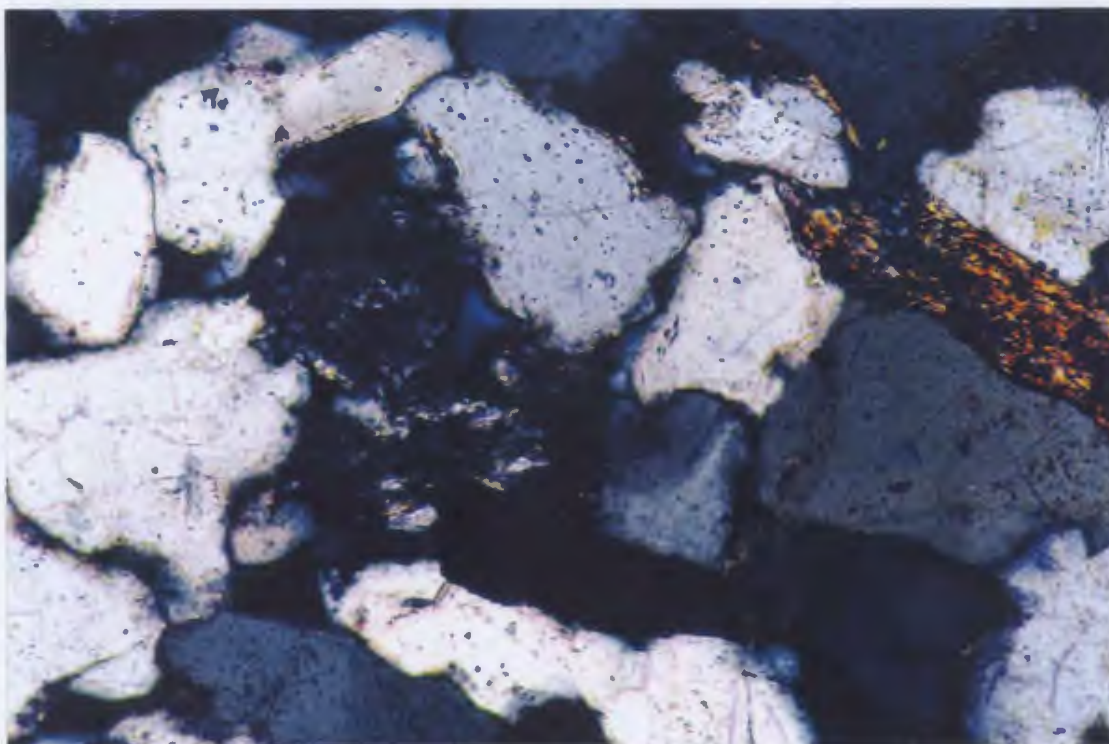


Figure 46a&b: **HF6**. Fine-grained sands of have well-preserved pores. The lithology is moderately-sorted, and subrounded. Organic material is present in the lithology. Organic material-rich mud pellet is evident in the upper right of the photos. Rare quartz overgrowths are observed in the cross-polar mode. (P164; Mag=a): X10PP and b): X10XP)($k=17.0$ mD; $\phi=10.2$ %)

(Width of both of the pictures=0.64mm)

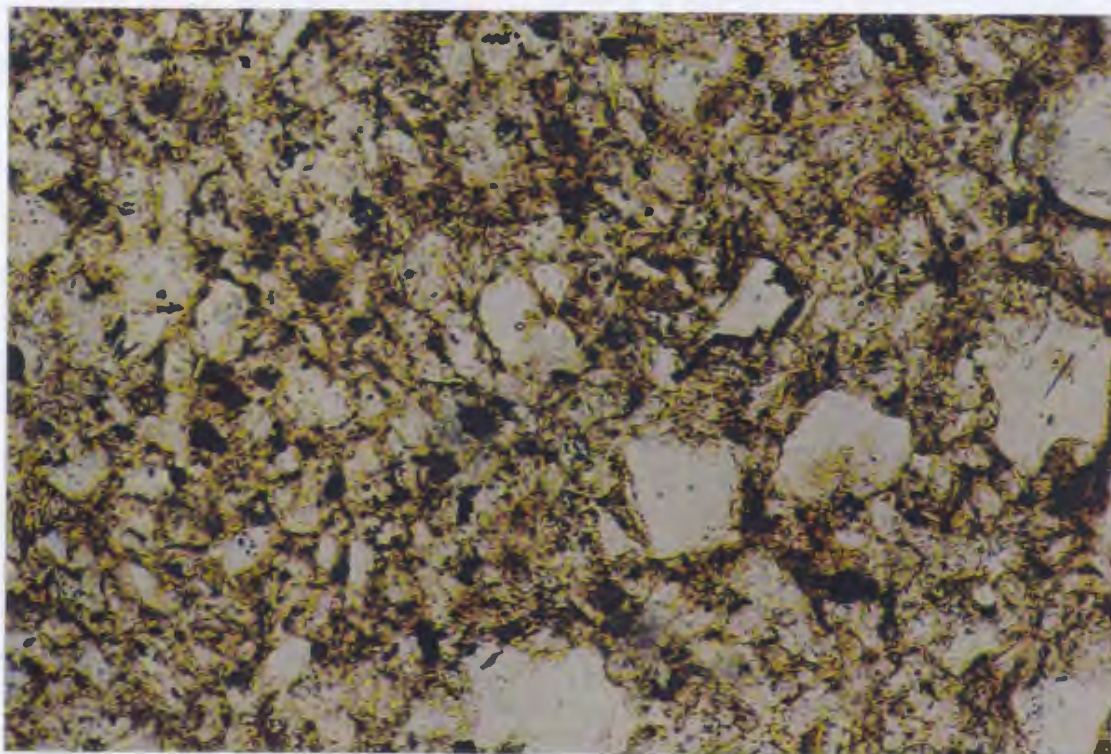


Figure 47: HF2A. Texturally submature lithology consists mainly of very fine sand, silt, and clays. Argillaceous material is abundant. Porosity and pore connectivities are very poor. Quartz overgrowths are rare. Argillaceous matrix material is micaceous. Chaotic texture lithology is controlled by the highly-contorted bedding structures as observed in core. Similar high clay/silt content and submature texture is observed in the thin sections of HF2B and HF2C lithologies. This figure is representative of all three HF2 interstratified lithofacies. (P147; Mag=10PP)($k=0.62$ mD; $\phi = 11.4\%$)

(Width of picture=0.64mm)

VI - INTERPRETATIONS AND APPLICATIONS

VI.1- INTERPRETATIONS

VI.1.1- Assessment of flow capabilities in hydraulic flow units and lithofacies:

Permeability "*is a measure of the ease with which fluid can flow through [rock]*" (Koederitz *et al.* 1989). Permeability is a parameter derived from the integrated effects of porosity, roundness, sorting, cementation, grain size, argillaceous content, and the formation resistivity (function of the way pores are connected). Therefore, permeability is an end product of a complex system, which ultimately defines the optimal drainage points and production rates, permits well completion and perforation design, and identifies future EOR patterns and injection conditions (Alhilali and Shanmugan 1991). As discussed in chapter I the enhanced form of the Kozeny-Carman equation (KCE; equation 7) (Amaefule *et al.* 1993) correlates rock properties and porosity in order to define permeability.

Application of the **KCE-derived RQI, FZI approach** to Hibernia data (Gardner and Albrechtsons 1995) resulted in definition of 5 major FZI clusters (Figure 3) which were ultimately designated to be 5 separate flow units with approximate permeability ranges as follows:

<u>HU</u>	<u>Average k (mD - core)</u>
HU5	0.01-20
HU4	0.5-320
HU3	0.2-650
HU2	4-4000
HU1	400-10000

Figure 4 shows that rocks with the same permeability but different porosities are grouped in separate flow zones. For instance,

<u>k (mD)</u>	<u>ϕ (%)</u>	<u>HU</u>
4.8	3	HU2
4.8	8	HU4
4.8	9	HU4
4.8	12	HU5
4.8	18	HU5

Since the goal is to identify flow paths with different flow rates, the hydraulic flow unit concept becomes misleading. In reality, the ratio between permeability and porosity (RQI) defines the flow quality of a reservoir, not the separate flow paths. As displayed in the example above, even though the permeabilities are the same, the reservoir qualities differ due to the changes in porosity. Another factor influencing FZI frequency is the fact that hydrocarbon-bearing, porous sands were cored more frequently than other lithologies in the formation. Therefore, sampling density biases the distribution of the frequency modes in the histogram, thereby influencing designations of the hydraulic units in a potentially misleading way. It is obvious therefore that "hydraulic flow units" are not different zones each with their own uniform flow potentials.

In this study, Hibernia lithofacies superimposed on a ϕ vs k crossplot also span wide ranges of permeabilities, ranging from <1mD to millidarcies in the order of thousands (Figure 50). Transitional variations between lithofacies produce wide scatter as well. Consequently, lithofacies analysis by itself is not a method for identifying separate flow paths. It solely distinguishes separate rock quality groups based on other criteria. Integration of the available

data sets obtained from the lithofacies and core plug analyses improves the potential for the identification of actual quality zones in the formation.

VI.1.2- Integrated interpretation of the Hibernia lithofacies:

Core, SEM/EDS, and thin section analyses have served to characterize features of the different Hibernia lithofacies. Permeability-controlling components, such as grain size, degree of sorting and roundness, abundance of argillaceous, calcareous, and carbonaceous materials, nature of the clays and diagenetic factors have been evaluated by core, log, SEM/EDS analyses, thin section petrography, and detailed cross plotting techniques (Table 7a&b). By integrating findings of each method, a template in the ϕ vs k was produced (Figure 50).

Figure 50 indicates that increasing grain size is proportional to increasing permeability.

Significant pore space-reductions by quartz overgrowths appeared to bear relationship to grain size and porosity at the time of precipitation. This is consistent with the findings of Berg (1986), McIlreath and Morrow (1990), and Lynch (1996) who evaluated the quartz silicification in sandstone reservoirs. As a result, two distribution patterns were identified:

1. Large-crystal form of overgrowths (~width=100 μ m) in the less argillaceous and porous sands of fine to coarser grain size (HF1B, HF6, HF1C, HF1D, HF1F, and HF3)
2. Micro-size crystal form of numerous overgrowths (~width=3-4 μ m) in the argillaceous sands of very fine to fine grain size (HF1C1, HF1G, HF1E, and HF1E1) which coalesce to produce overgrowth rims forming stepped pore surfaces.

Precise identification of clay types by the thin section analysis is not possible. SEM/EDS-coupled analyses indicate that authigenic smectite occurs ubiquitously in all of porous sands

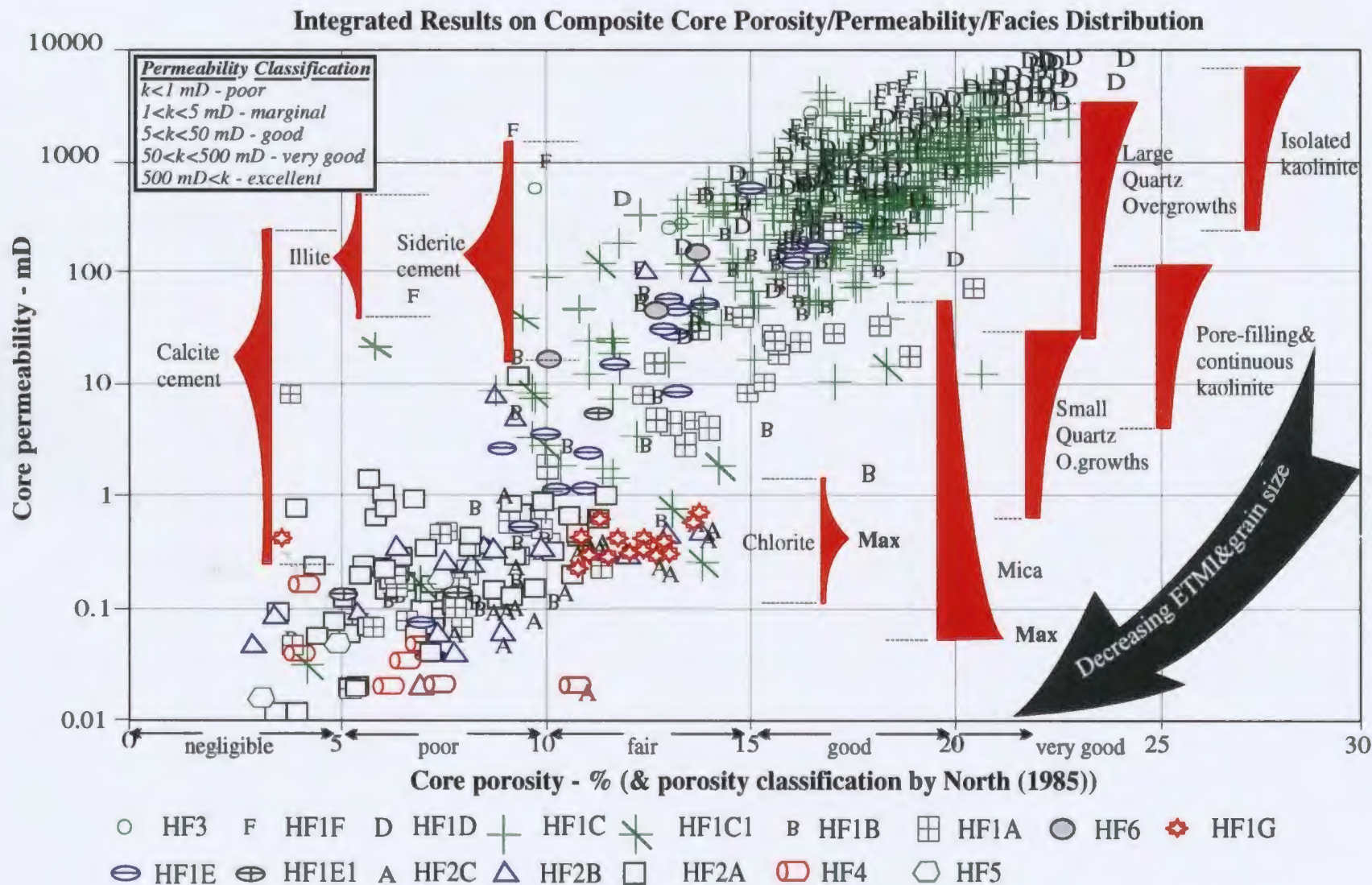


Figure 50: Integrated mineralogic and diagenetic attributes of porosity&permeability-influencing factors derived from core, SEM/EDS, and thin section petrography.

Facies	Definition	Av. Grain Size	k/φ-reducing agents	S.Features	Roundness	Sorting	ETMI
IIF1A	Convolute&wavy bedded ss	very fine	siderite cement& qtz. overgrowth		A-SA	Poor-Moder.	<5
IIF1B	Crossbedded&carbonaceous ss	fine	rare calcite cem. carb. mat & QO		SA-SR	Moderate	7-8
HF1C	Crossbedded&oil-stained ss	medium lower	QO&clays		SA-R	Moder.-well	7-13.5
IIF1C1	Medium-grained sands with high clay&rip-up clasts	medium lower	Arg. content+chl calc.+mud clasts		SA-SR	Poor-Moder.	4.5-8
IIF1D	Poorly-consolidated ss	medium-coarse	rare qtz. overgr.		R-WR	Well	15≤
IIF1E	Basal sandstones	coarse	minor clays		SA-R	Moder.-well	8.75-13
IIF3	Conglomeratic bimodal ss	pebbly medium-coarse	qtz. overgrowths and clays		SR	Poor-Moder.	~6
IIF1E	Rippled&wavy bedded carbonaceous ss	very fine-fine	QO+calc. cem. Car. zones+clays		SA	Poor-Moder.	<5
HF1E1	Horizontally-laminated carbonaceous ss	very fine-fine	Chlorite+car. zones+clays		A	Poor	<5
IIF1G	Argillaceous slightly carbonate-cemented ss	silt-very fine	Chlorite+calcite		A-SA	Poor-Moder.	<5
IIF6	Coaly&carbonaceous ss	fine	QO+clays+ car. material		R	Moderate	8-10
HF2A	Slightly-burrowed silty/shaly ss	silt-clay	qtz. overgrowths and clays		VA	Poor	<5
HF2B	Lenticular-bedded, moderately-burrowed silty/shaly ss	silt-clay	clays+calcite cem.+qtz. overg.		SA-SR	Poor	<5
HF2C	Well-burrowed silty/shaly ss	clay-silt	abundant clays		SA	Poor	<5
HF4	Loose/carbonaceous shales&soil zones	clay	N/A		N/A	N/A	N/A
HF5	Shelly/churned&well-burrowed shales	clay	N/A		N/A	N/A	N/A

Table 7a: Hibernia lithofacies and some of their descriptive features For legends and abbreviations, see table 7b

Sedimentary Structures

	Horizontal bedding
	Crossbedding
	Convolute bedding
	Load cast
≡	Normal grading
	Wavy bedding
	Arkosic
⬢	Pyrite growth
⬢	Siderite growth
⌋	Ball&pillow structure
⊕	Rip-up clast

Roundness

VA	Very angular
A	Angular
SA	Subangular
SR	Subrounded
R	Rounded
WR	Well-rounded

Other Abbreviations

ss	sandstone
ETMI	Enhanced Textural Maturity Index
Moder.	Moderate
N/A	Not available
qtz. overg.	
(QO)	quartz overgrowth
Sid.	sidite
carb. mat.	carbonaceous material
cal.	calcite
cem.	cement

Burrowing

●	Coal growth	⬢	Slightly-burrowed
T	Quartzitic	⬢	Moderately-burrowed
⌋	Ripple xbedding	⬢	Well-burrowed
⌋	Climbing ripples		
⬢	Lenticular bedding		
⌋	Shell fragments		
⬢	Rafted carb. material		
⬢	Vertical carb. material		
C	Churned		
⌋	Plant root tube		

Facies Coding System

- 1 as in "HF1A" stands for ss-dominated facies
- 2 as in "HF2A" stands for interstratified silt/sand/shale facies
- 3 as in "HF3" stands for conglomeratic sands
- 4 as in "HF4" stands for loose shales&soil zones
- 5 as in "HF5" stands for shelly/churned shales
- 6 as in "HF6" stands for coaly/carbonaceous sands

Grain Size Scale

vcU = 1410-2000 μ	mL = 250-350 μ
vcL = 1000-1410 μ	fU = 177-250 μ
cU = 710-1000 μ	fL = 125-177 μ
cL = 500-710 μ	vfU = 88-125 μ
mU = 350-500 μ	vfL = 62-88 μ

Table 7b: Legends and abbreviations used in table 7a. The same facies coding procedure has been used throughout the thesis.

of very fine to coarse grain size. Authigenic illite was only observed in the fine-grained HF1B and HF1E sands (Figure 50). Pore space reduction by authigenic smectite in pore-lining and pore-bridging forms occurred more effectively than that of illite which crystallized as fine clay rims around the pores.

Authigenic kaolinite was identified in a broader range of the lithofacies than the other authigenic clays. Two types of authigenic kaolinite were described:

1. Isolated, discontinuous booklets in the lower medium (mL)- to coarse-grained sands that have minimal to no effect on permeability
2. Pore-filling and continuous kaolinite booklets which reduce pore connectivity occurring in very fine- to lower medium- grained sands.

Secondary kaolinite reduces permeability when it is in the form of patches partially or fully covering the pores (Shelton 1979). Isolated and discontinuous authigenic kaolinite booklets identified in the HF1D sands yielded low Si/Al ratios from EDS. Isolated booklets of kaolinite increase Al detection but have little effect on high permeabilities (P349-HF1D $k=9710$ mD and Si/Al=17)(Figure 10b).

Mud rip-up clasts, which are the characteristics of the HF1C1 lithology, are known to reduce permeability of the zones in which they occur (Cuthiell and Bachu 1991).

Identification of chlorite by thin section petrography is difficult due to highly variable mineral forms unless complementary SEM techniques are used (Wilson and Pittman 1979). Grain-coating chlorite determined in the SEM/EDS technique reduced pore connectivity by producing grain coats and pore-blocking crystals (HF1C1, HF1E1, and HF1G). The crystal

structure of chlorite increases surface friction to fluid flow due to the blade-like crystals standing perpendicular on underlying grains. Therefore lower permeabilities, regardless of grain size of the lithology, are to be expected for sands containing authigenic chlorite. In this regard, on the composite porosity/permeability crossplot (Figure 50) HF1G specimens cluster in the porosity range of 10-13% yet they maintain a permeability range of < 1 mD. This is consistent with the finding of Hutcheon (1990) where he indicated that authigenic clays, depending on their abundance, can create ineffective secondary porosity in sandstone reservoirs. Total porosity increases whereas permeabilities can be reduced due to decreased pore connectivity.

Results of thin section and SEM/EDS analysis indicate that calcite cement reduction of available pore space is common in the very fine- to lower medium (mL)-grained sands of HF1A, HF1B, HF1G, HF1E, and HF1C.

Permeability and porosity decreased with the increasing abundance of argillaceous material composed of mica, feldspars, and blend of silts and clays.

VI.1.3- Assessment of k-reductions by k-vertical (k_v) vs k-horizontal (k_h) crossplots:

The relationship between k_v and k_h , highlights the control of sedimentary structures on permeability. Figure 51 illustrates graphs depicting the relationship between vertical and horizontal permeabilities from three Hibernia wells. Lithofacies of the Hibernia Formation contain a wide range of different sedimentary structures (Table 7a&b). Bedding plane orientations and grain size variations, shale laminations and platy minerals such as mica affect the fluid flow depending on their orientation in respect to the direction of fluid flow. They

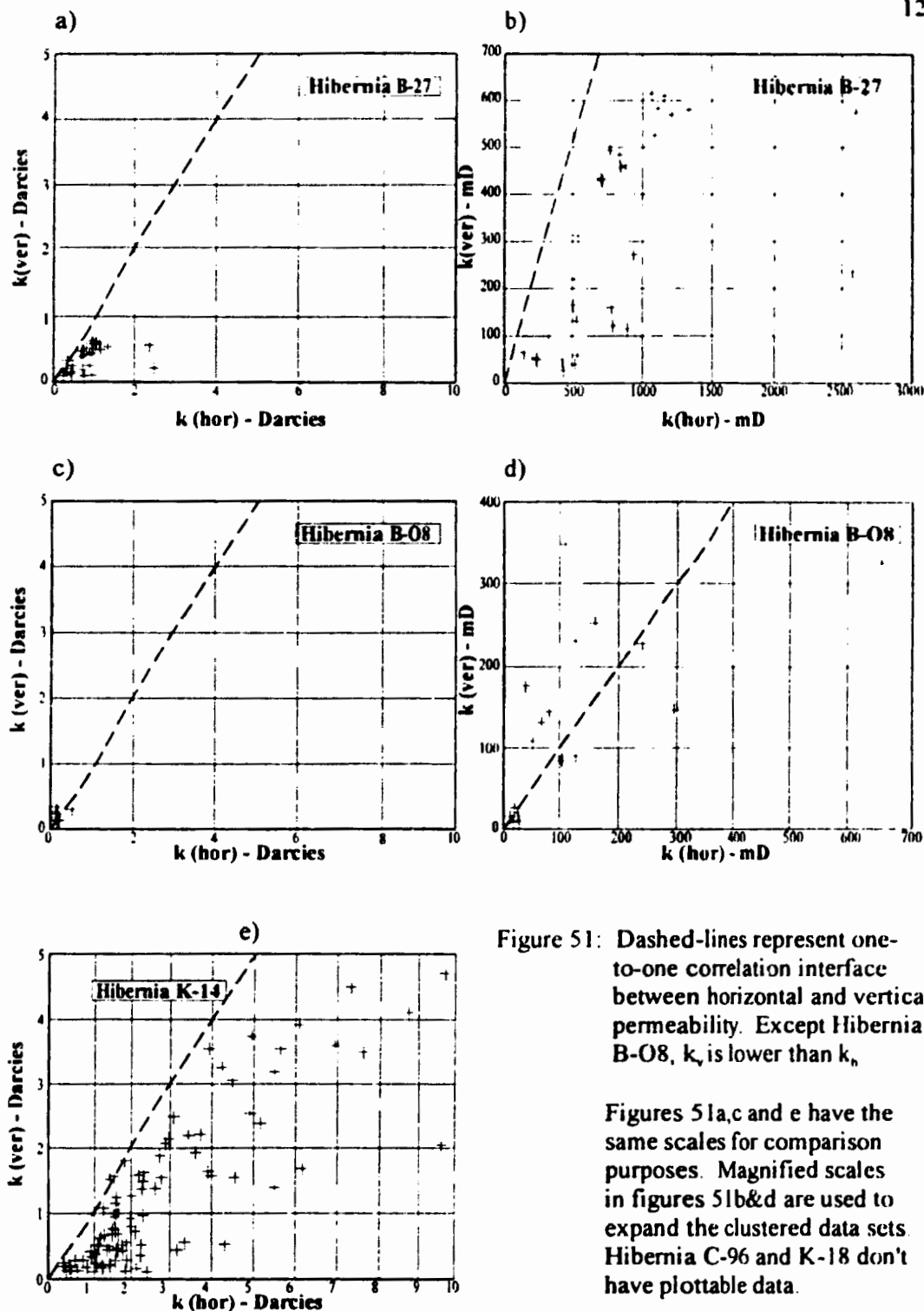


Figure 51: Dashed-lines represent one-to-one correlation interface between horizontal and vertical permeability. Except Hibernia B-08, k_v is lower than k_h .

Figures 51a,c and e have the same scales for comparison purposes. Magnified scales in figures 51b&d are used to expand the clustered data sets. Hibernia C-96 and K-18 don't have plottable data.

may or may not necessarily decrease horizontal permeability, yet can play an obstructive role on the vertical direction. With the exception of Hibernia B-O8, horizontal permeabilities (k_h) are greater than vertical permeabilities (k_v). Reductions in vertical permeability are induced by depositional features of the lithologies. This situation sets an example showing the significance of textural and depositional settings for fluid flow, especially in the sandstone reservoirs.

Core analysis of Hibernia B-O8 identified a relative scarcity of sedimentary structures of the reservoir sands. As a result k_v is high (i.e. see core of B-O8 in depth range of ~3,619-3,623 m, appendix 1). Poor consolidation and coarse grain size in the reservoir sands may also contribute to the greater values of k_v in Hibernia B-O8. Micro-fractures that could act as vertical conduits (North 1985) were not observed in B-O8.

VI.1.4- Si/Al ratio-permeability relationship.

The EDS Si/Al ratio-permeability crossplot illustrates that Si/Al increases with increasing permeability. As a result, the Si/Al ratio is a significant tool in determining the effects of argillaceous content as a k -controlling mechanism. Gies *et al.* (1992) used this crossplot to assess permeability relationship in the Montney Formation of NW Alberta.

Specimens with permeabilities less than ~100 mD and whose grain size attributes range from clay to lower medium ($mL \leq 350\mu$) reflect scattered distributions in the k/ϕ crossplot. The scatter pattern becomes even broader with decreasing grain size. For instance, the fine-grained sands of HF1B and very fine-grained sands of HF1A form two separate clusters of data in figure 50; a) clusters in the "good" and "very good" reservoir quality windows and

b) clusters in the "poor to marginal" quality windows. The major factor placing an HF1A or HF1B specimen into the poor quality section is the abundance of argillaceous material which is consistent with the graph of Si/Al-k in figure 10b.

VI.1.5- ETMI-permeability relationship:

Enhanced Textural Maturity Index (*ETMI*) is a numerical demonstration of the degree of sorting and roundness. Assignment of numerical codes to the *ETMI* allows us to directly relate the textural quality measurements (sorting and roundness) to permeability

Two separate packages were identified (Line A and line B in figure 48) on the *ETMI*-permeability crossplot. The relationship between *ETMI* and permeability is proportional (Increasing *ETMI* = increasing k) Specimens falling around line A have better flow capabilities than those having the same *ETMI* but falling around line B. For instance, in spite of having the same *ETMI* (4.5_n), the permeability of P145 of HF1E is 29.6 mD (around line A) and P208 of HF1C1 has a permeability of 0.32 mD (around line B) This is caused by the abundant clays (chlorite, corrensite, and smectite) and mica, and rare calcite cement in P208 (also refer to Si/Al-k graph - figure 10b).

As a result, cross plotting *ETMI* against permeability allows us to visualize the control of textural maturity over permeability as well as to highlight the presence of other permeability-reducing components.

VI.1.6- Evaluation of the lithofacies and hydraulic flow unit (HU) distributions:

3D graphs of the lithofacies/flow unit (HU) frequencies reveal that a single HU may contain many facies that are distinctly separate from each other (Figure 52&appendix 4). For

example HU5 can be subdivided into 12 lithofacies and HU4 into 9 lithofacies. On the other hand many lithofacies spread over a range of many flow units (e.g HF1C occurs in all five HUs, HF1D in 4 HUs, etc.; figure 52&appendix 5). These 3D-crossplots also highlight general clusters between lithofacies and HMDC flow units. Coarser-grained sandstones, HF3, HF1F, HF1D, and HF1C are never grouped in the section HU5 designated for the weakest flow. Only HF3, HF1F, HF1D, and HF1C coincide with the highest quality flow unit (HU1). HF1C is the lithology bearing majority of the hydrocarbons in the formation and is mainly clustered in HU2 and HU3. None of the interstratified sandstone/siltstone/shale facies are grouped in HU1 and HU2 whereas they are spread over the remaining flow units.

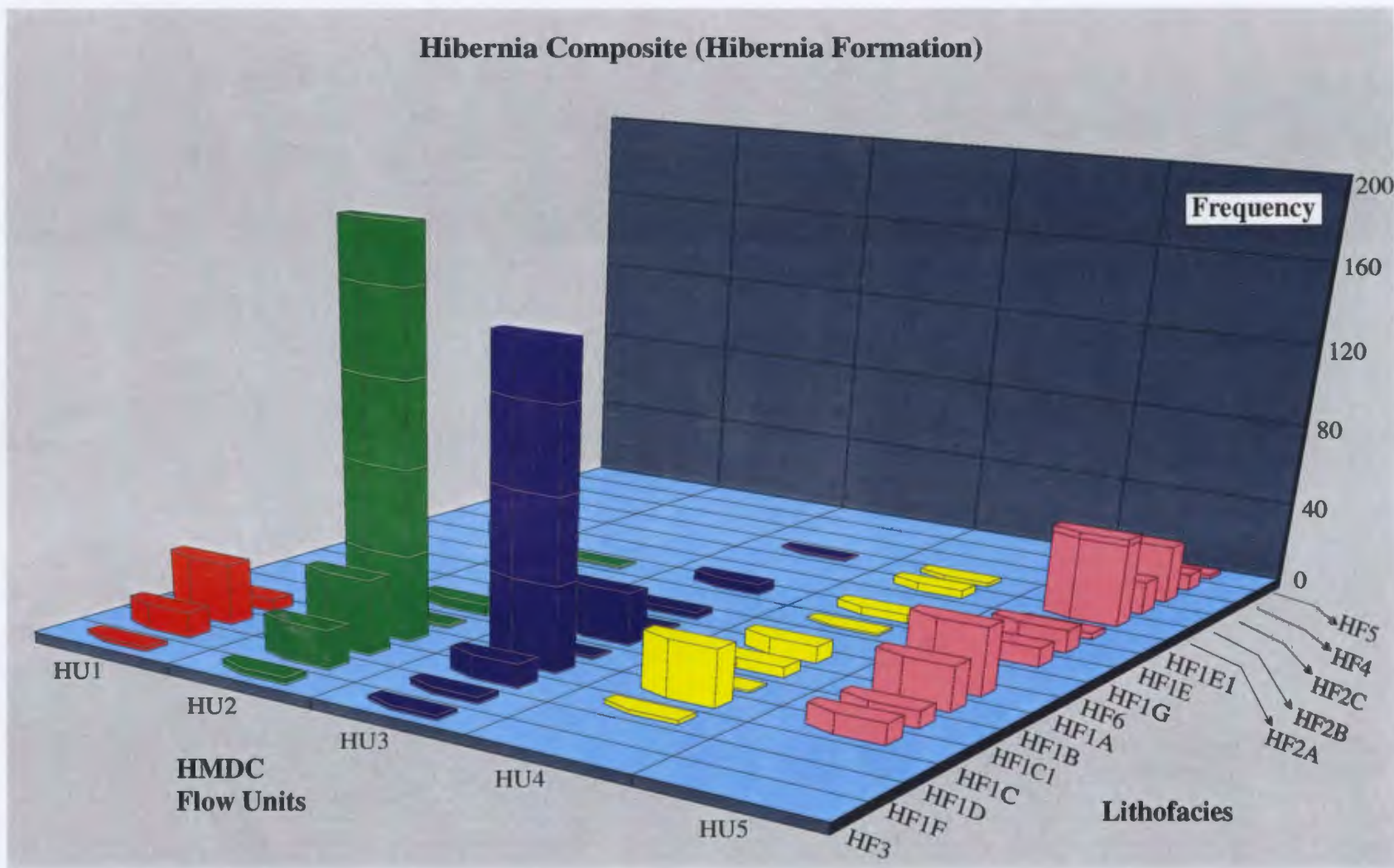


Figure 52: Composite hydraulic flow unit - lithofacies distribution in the Hibernia Formation. Red represents the best and pink represents the weakest flow. Colour designations are adopted from Gardner and Albrechtsons (1995). (For the values of frequency peaks refer to appendix 5)

VI.2- INTERPRETATION OF RESERVOIR QUALITY BASED ON MULTI PARAMETER INTEGRATION

VI.2.1- Identification of the Reservoir Quality Zones (RQZ) in the composite core plug data:

As displayed in this study, neither hydraulic flow units (HUs) nor lithofacies adequately distinguish separate quality zones in the composite data. Textural changes in lithologies are gradational. For example, fining-upward trends of channel systems generate scattered data ranges in the composite graph of porosity and permeability (Figure 50). In order to introduce an effective and meaningful interpretation of the data set, the findings of each method used in this study (core, SEM/EDS, thin section and petrography) are integrated. Lithologies possessing similar ϕ/k data, SEM images, textural, mineralogic, and diagenetic characteristics are grouped as subdivisions of a new multi-parameter concept "*Reservoir Quality Zone (RQZ)*". RQZs can group the specimens of different lithofacies and/or HUs within a specific quality zone. RQZs are the results of the full criteria range (ϕ - k data, depositional structures, grain size, ETMI, Si/Al ratio, mineralogy, diagenetic character, and clay mineralogy) which earlier described lithofacies and HUs. As a result, the composite data set in figure 53 shows 3 general clusters of the data set subdivided into 10 RQZ sub zones. The coding system of RQZs is defined based on the three general clusters, as follows:

1. **Principal Reservoir Zone:** This zone corresponds to that segment of the crossplot (Figure 53) where the majority of the fine- and coarser-grained sands occur within the porosity range of $>\sim 13$, and permeability range of $>\sim 100$ mD (RQZ1a,

RQZ1b, RQZ1c, and RQZ1d).

2. **Transition zone:** This zone corresponds to that segment of the crossplot where the majority of very fine- to lower medium (mL)-grained sands occur within the porosity range of ~8-21%, and permeability range of $1 < k < 100$ mD (Figure 53)(**RQZ2a, RQZ2a', and RQZ2b**).
3. **Tight zone:** This zone corresponds to that segment of the crossplot where the permeability range is < 1 mD (Figure 53)(**RQZ3a, RQZ3b, and RQZ3c**).

Subdivision of 3 general data clusters into **RQZs** are performed based on the following characteristics:

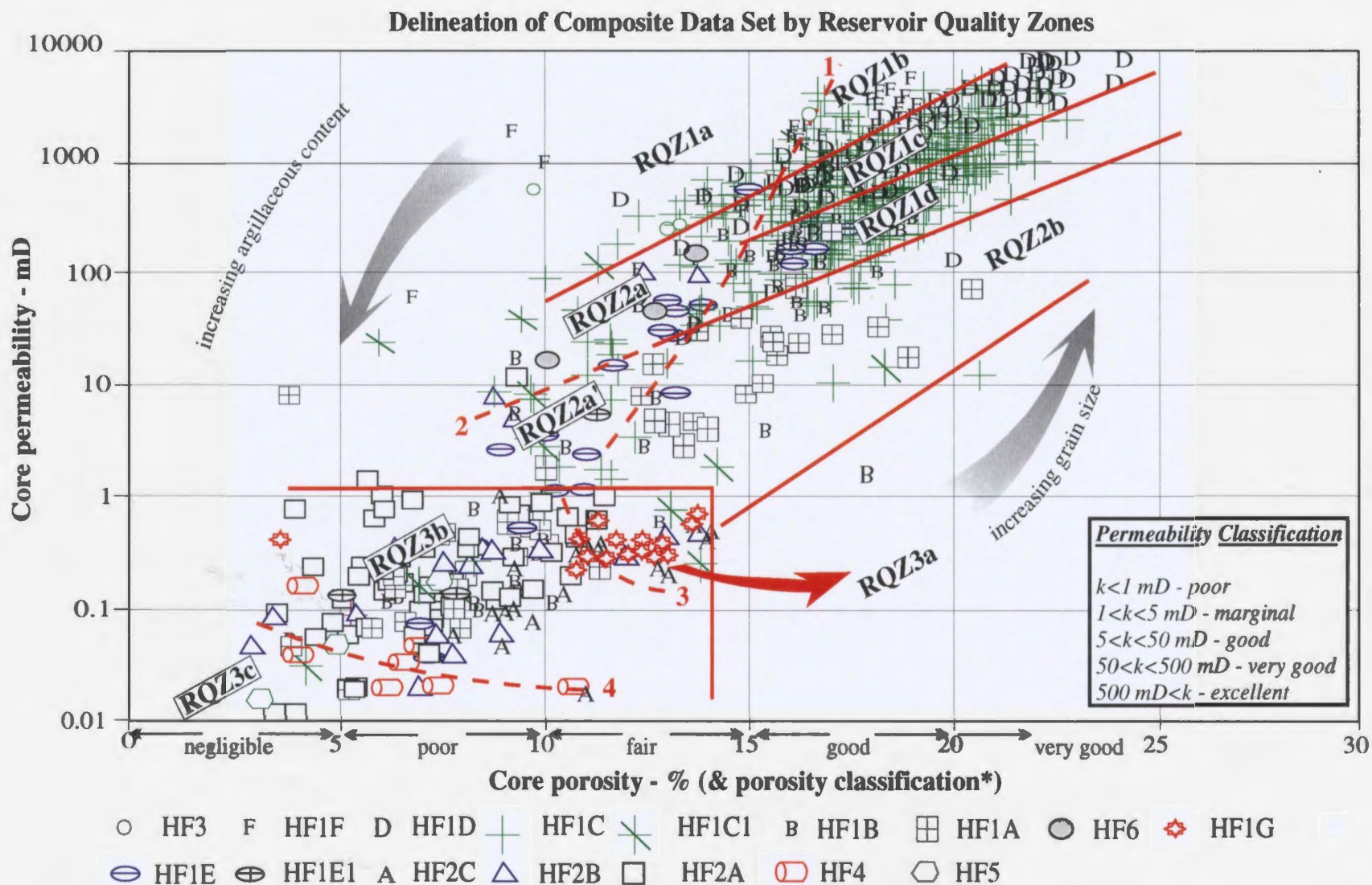
VI.2.1.1. Principal Reservoir Zone

VI.2.1.1.1. RQZ1a

RQZ1a contains pebbie-sized sands of HF3 and part of lower medium- to coarse-grained sands of HF1F, HF1D, and HF1C where the sorting is poor- to moderate and the roundness is subrounded, resulting in lower *ETMI* values (refer to table 6a&6b). The porosity range of RQZ1a is "fair" and permeability range is "very good" to "excellent". Lithologies in this zone are "clean" in terms of their argillaceous content (Figure 53) and can contain isolated kaolinite booklets, large quartz overgrowths, and rare siderite cement.

VI.2.1.1.2. RQZ1b

RQZ1b contains primarily HF1F specimens and part HF1D and HF1C specimens. RQZ1b represents the highest flow quality segment where isolated kaolinite booklets, large quartz overgrowths are observed (Figure 50 and 53). The porosity range of the RQZ1b specimens



* porosity classification by North (1985)

Figure 53: Reservoir Quality Zones in the composite porosity vs permeability crossplot of the Hibernia Formation.

is "good" and the permeability range is "excellent" (Figure 53).

VI.2.1.1.3. RQZ1c

Primarily HF1D specimens, secondarily HF1C and rarely HF1F specimens constitute the RQZ1c. RQZ1c is characterized by decreased grain size and higher argillaceous content relative to RQZ1b, possibility for siderite cement, authigenic pore-lining illite and pore-filling, pore-bridging smectite. In this zone authigenic kaolinite begins to change its character from being isolated and ineffective to being continuous and pore-filling. The RQZ1c specimens have porosity range of "good to very good" and permeability range of "very good to excellent."

VI.2.1.1.4. RQZ1d

The abundant lithology in this zone is the HF1C sands (Figure 53). Argillaceous components, micro size quartz overgrowths (width \approx 3-4 μ) become more abundant, and calcite cement starts to affect the system. Siderite cement is also effective in this zone. Relative to the other RQZs of the "Principal Reservoir Zone", RQZ1d specimens are in "the good porosity" and "very good permeability ranges" in spite of the increased argillaceous content.

VI.2.1.2. Transition Zone

VI.2.1.2.1. RQZ2a

RQZ2a is separated from the other RQZs by a gradual sub-boundary (line 1 in figure 53) Increased carbonaceous material content is the characteristic of this zone. Calcareous cements, authigenic clays, and higher argillaceous components are higher relative to the zones

of the Principal Reservoir (RQZ1s) segment. The majority of the carbonaceous/coaly sands of HF6 and laminated, carbonaceous sands of HF1E are grouped in RQZ2a. The average range for porosity is "fair" and for permeability "good to very good". Specimens from the lithofacies HF1B, HF1C, HF1D, HF2A, and HF2B are rarely present in this section.

VI.2.1.2.2. RQZ2a'

This reservoir quality zone is separated from RQZ2a by line 2 (Figure 53). The main reason for the breakdown is the increased argillaceous content and decreased permeabilities in spite of being in the "fair porosity" range. The average grain size of the carbonaceous sands in this zone is very fine to fine. The abundance of quartz overgrowths decreases to a minimal level whereas calcite cement remains an effective factor in this quality zone. The facies groups in RQZ2a' are the same as those in the RQZ2a. The permeability ranges in this zone are "marginal" and "good".

VI.2.1.2.3. RQZ2b

HF2C, some HF1A, rare HF1C, HF1E, and HF1E1 specimens are grouped in this quality zone (Figure 53). The average grain size is very fine to lower medium. Authigenic kaolinite booklets are in the form of more continuous clay rims, thereby reducing pore connectivity. Quartz overgrowths are micro size crystals (width \approx 3-4 μ) in abundance, generating rough pore walls. Calcite cement, especially in HF1B sands, is another feature of RQZ2b. Porosity range is "fair" to "very good" whereas permeability ranges between "marginal" to "very good".

VI.2.1.3. Tight Zone

VI.2.1.3.1. RQZ3a

RQZ3a is subdivided from the other RQZs by line 3 (Figure 53). The dominant lithofacies cluster in this tight permeability zone is HF1G where chlorite is identified as the grain-coating authigenic clay component. Chlorite, as described in the section IV.2.3.2.3., can decrease permeability by disrupting pore connections and creating ineffective porosity. The average grain size of the lithofacies in this zone is silt to very fine. SEM photomicrographs and thin section photos of the related lithofacies of the specimens in RQZ3a display a high argillaceous content. Porosity and pore connectivity reduction by calcite cement is significant. The average porosity is "fair", and permeability range is "poor".

VI.2.1.3.2. RQZ3b

This quality zone has an extremely mixed internal framework where different lithofacies, especially interstratified lithofacies of HF2A, HF2B, and HF2C are intermixed (between line 3 and 4; figure 53). Clay-rich argillaceous facies as well as interstratified lithofacies with average silt-sized grains mainly occur in RQZ3b. The *ETM* and the Si/Al ratio values are very low (Table 6a & figure 10b). Porosity of the zone ranges from "negligible to fair" and permeabilities remain in the range of <1mD.

VI.2.1.3.3. RQZ3c

This quality zone contains specimens with less than 0.1 mD permeability, and "poor to negligible" porosity (Figure 53). The highest clay content is observed in this group zone. Although the majority of RQZ3c specimens have silt to clay size grain attributes, larger-

grained lithologies are occur in this zone as well. For example, the average grain size of SP99-HF1C1 is lower medium (250-350 μ), a complex blend of clays and micas reduce the flow properties. Shale lithofacies HF4 and HF5 also occur in RQZ3c.

VI.2.2- Comparison of the RQZ to the HMDC hydraulic flow units (HU):

The RQZ boundaries and the HU interfaces are superimposed in the composite porosity-permeability cross plot for the Hibernia Formation (Figure 54). In the Principal Reservoir Zone (RQZ1s) the RQZ boundaries and the HU interfaces show close matches. In the Tight Zone (RQZ3s) there is no available differentiation by the means of HU method, whereas the RQZ method subdivides the data set into distinct populations. The sub-boundaries (lines 1&2) based on mineralogic differences are not defined by the HU method.

3D frequency graphs cross-correlating HMDC flow units and Reservoir Quality Zones for the entire Hibernia Formation are presented in figure 55 and appendix 5. Each HU can be subdivided into 3 to 6 different RQZ, thereby contributing to a higher level of resolution.

Both of the methods, as previously indicated, aim to identify reservoir quality sectors rather than separate drainage paths of different flow rates. The HU method is solely built on the core porosity and permeability values. The RQZ method is based on the integration of k/ϕ , core, log, SEM/EDS, and thin section analyses and therefore, is able to describe subtle differences of lithologies.

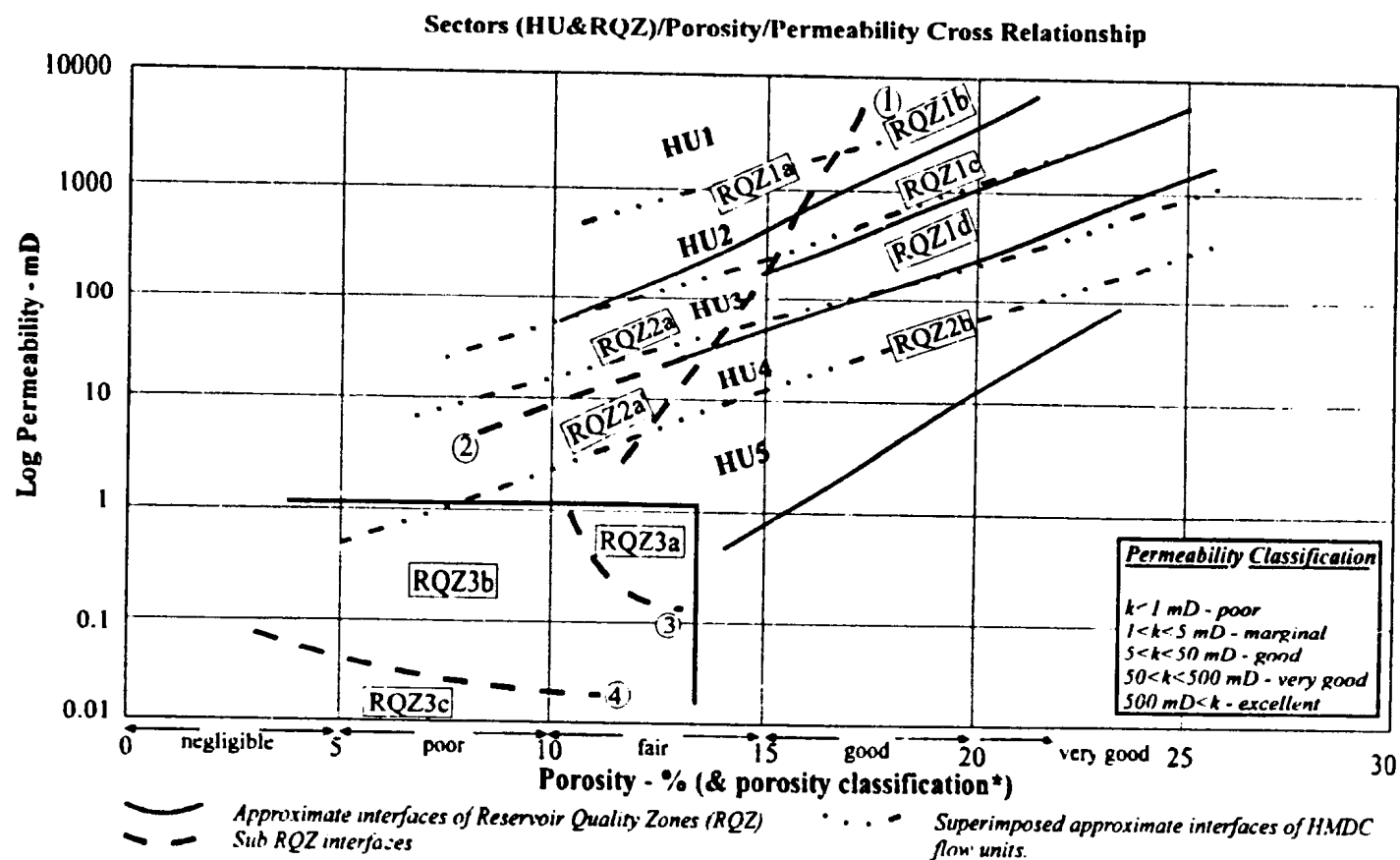


Figure 5-4: HMDC flow unit and RQZ boundaries do not coincide. Partitioning in the lower permeability sectors (good to poor) are defined in more details by RQZ interfaces where only 2 HMDC flow units are described (HU4&HU5). (* porosity classification by North 1985)

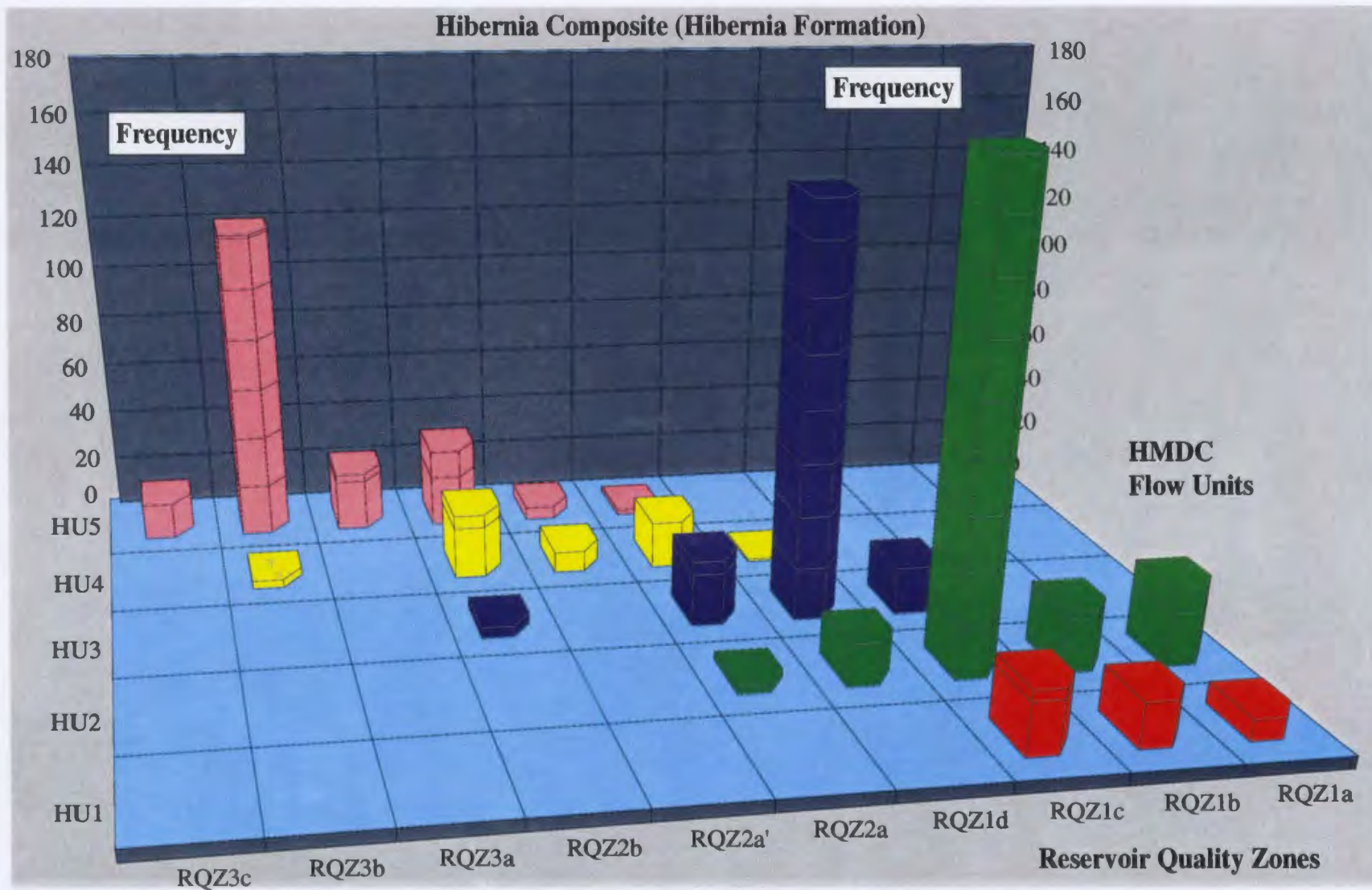


Figure 55: Hydraulic flow unit (HMDC/Core Lab.) - RQZ occurrence frequency graph of the Hibernia Formation. Red is the best quality, pink is the worst quality unit. Colours are adopted from Gardner and Albrechtsons (1995). (For values of the frequency peaks, refer to appendix 5)

VI.2.3. Estimation of the RQZ in the uncored sections:

The RQZ template (Figure 56) can be used to estimate permeability in uncored intervals. Porosity of a given unit can be defined by the integrated use of neutron, density, and sonic logs (Schlumberger Educational Services 1991). Rock properties of cuttings (RQZ) can be determined by the integrated approach of rock, SEM, and thin section analyses. From this information, a permeability value or range can be determined for a given specimen.

When the availability of drill cuttings is restricted or non-existent, porosity and clay (shale) content, carbonate cements, carbonaceous zones, coal and tight zones can be identified from logs in order to estimate an RQZ from a porosity - shale % crossplot. The determined RQZ for the indicated log porosity then permits determination of a permeability range for that specimen from the ϕ/k crossplot.

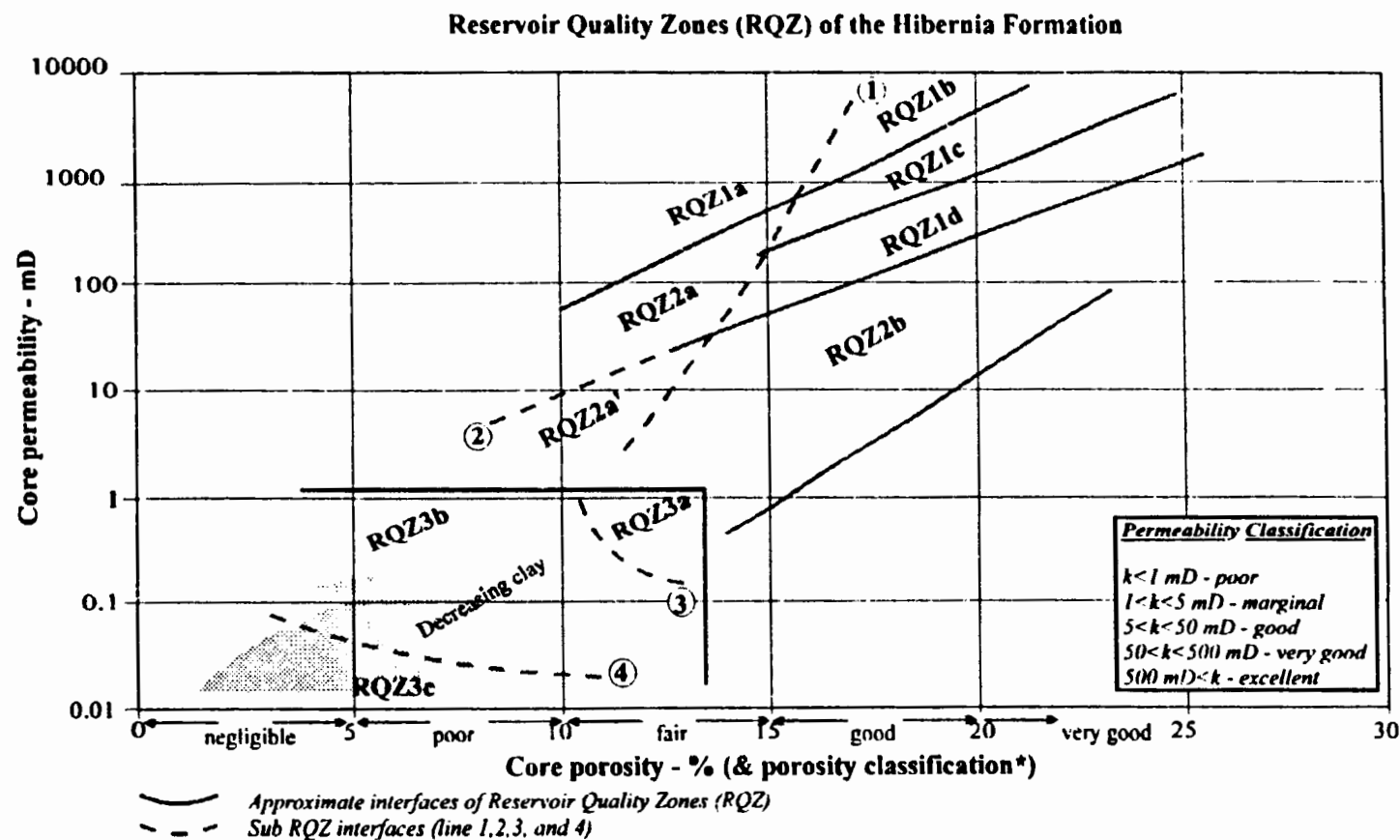


Figure 56: Reservoir Quality Zones (RQZ) of the Hibernia composite core plug data. Composite data is broken into RQZ based on the integration of porosity/ permeability data, facies interpretation, SEM images, SEM/EDS-coupled analyses, thin section petrography and analytically-calculated hydraulic flow units. (* porosity classification by North 1985)

VII - SUMMARY INTERPRETATION & IMPLICATIONS

The Hibernia Formation was deposited as a river-dominated palaeo-deltaic system having abundant distributary channels with minimal marine influence. The main sediment load is distributed within channel complex, as well as in distributary mouth bars where subaqueous levees formed. Crevasse splay deposits occurred with less frequency in the Hibernia Formation. Carbonaceous shales of interchannel marsh sedimentation containing remains of vegetation, rafted material, and coal zones commonly occur in association with the channel sands. Shales in the form of soil zones identify repetitive subaerial exposures formed after the waning of channel deposition. Shales of marsh sedimentation were commonly eroded by coarse-grained to conglomeratic distributary channel sands. Erosion surfaces are marked with basal lag conglomerates, ironstone pebbles and rip-up mud clasts which originated from the underlying shaly strata.

Distributary channel sands in the Hibernia Formation are porous and permeable. Net oil pay, ranging between 29 to 68 m in thickness (Hurley *et al.* 1992), is mainly concentrated within these channel sands. Therefore, an understanding of the internal geometry of the channel sequences controlling fluid transmittance is essential for prediction of reservoir behaviour during the production phase.

Internal channel geometry is controlled by depositional lithofacies, and by partitioning caused by the influences of interbedded and interstratified levee, and crevasse splay sands, and shale sequences. Distributary channels in the Hibernia Formation possess basal lag

conglomerates (HF3) and/or massive lower medium (mL)- to coarse-grained sands (HF1F, HF1D, HF1C) at their base, where the only evidence of any type of sedimentary structure is faint crosslamination. In general, porosity and permeability decrease upsection within the channel sequences with the increasing abundance of silt and clay interstratifications observed in HF1E, HF1E1, HF2A, HF2B, and HF2C.

Crossplotting core porosity and core permeability data relative to the different lithofacies indicates that the distributary channel sand lithofacies in the Hibernia Formation cluster mainly in "good" to "excellent" permeability windows where porosity ranges between "fair" and "very good." (Figure 53). The gradational upward fining trend typical of the channels applies significant control over porosity and permeability, whereas the basal coarsest sands possess the best flow capabilities. Micaceous, very fine- to fine-grained, and ripple-laminated sandstones (HF1G, HF1A, HF1E, HF1E1) grade into lower porosity and permeability units (HF2A, HF2B, and HF2C). Some very fine-grained sands of HF1s and interstratified lithofacies of HF2s are mainly clustered in the Tight Zone (RQZ3s) suggesting that the shallow water channel-fill sediments deposited during channel abandonment and subaqueous levee and crevasse splay phases generate reduced porosity and permeability relationships. Porosity and permeability-reducing components (Figure 50) are common and are very effective in those sands of channel abandonment levee, and crevasse splay deposits (Figure 50).

Different depositional sequences such as channels, channel abandonments, partitioning by interbedded sequences of levee and crevasse splays, and interbedded shales are correlatable

across the field (Pocket). Most channel sequences have lateral continuity and are correlatable in the cross-section as well. The internal complexities of the channel sequences examined in core reflect consistent depositional patterns where they commonly truncate and erode shaly strata and die out as fining upward sections. Therefore having an understanding of those complexities which are addressed as "k-reducing factors" at the lithofacies scale is the most crucial step for Hibernia reservoir characterization and definition of flow zone distribution.

Neither hydraulic flow units (HUs) nor lithofacies define the boundaries of separate quality zones in the reservoir. Textural variations in fining-upward trends of the channel-dominated deposition produce scattered data points in the composite porosity vs permeability crossplots. The method of "Reservoir Quality Zones (RQZ)" introduces a multi-parameter approach which combines the porosity and permeability data, depositional, textural, mineralogic, and diagenetic rock characteristics and creates a template involving separate quality units in the reservoir (Figure 56). The usefulness of the template is significant. It is based on field wide formation data and therefore provides a strong basis for reservoir modelling and cell characterization in the model. This new method has an enhanced resolution relative to the HU and lithofacies methods and can be used as a template to assign an RZQ, and to estimate a permeability range for a given unit of either cored or uncored sections in the Hibernia Formation.

VIII - CONCLUSIONS

1. Lithofacies control porosity and permeability variations as a function of their mineralogical, textural, diagenetic, and depositional characteristics. Facies associations and facies stacking resulting from the nature of deposition and the amount of depositional palaeo-energy produce the actual flow zones in the Hibernia Formation with predictable flow properties.

2. Channel sands in the Hibernia Formation are correlatable between different wells suggesting that actual "flow zones" which are a function of permeability, and "Reservoir Quality Zones (RQZ)" are also correlatable laterally.

3. Both delineation methods, the hydraulic units (HUs) and the lithofacies method (RQZs), create separate reservoir quality zones, not separate flow zones.

4. Proposed permeability ranges for the hydraulic flow units (HUs) are too wide to permit an efficient reservoir delineation. Broad FZI cut-offs in the univariate histogram can generate misleading interpretations of the limits of the hydraulic units. The distribution of frequency peaks is controlled by sampling density. The statistical delineation method does not reflect rock and geological attributes, which are so essential for an effective permeability estimation process.

5. Distinct clusters of lithofacies occur especially in the **Principal Reservoir Zone** of the composite porosity vs permeability crossplot of the Hibernia Formation. Scattered lithofacies distribution becomes dominant with decreasing grain size in the **Transition Zone** and **Tight**

Zone segment of the graph where gradual transitions in rock properties reduced the accuracy of "reservoir delineation". Therefore, the assessment of permeability-controlling mechanisms which permits to identify "**Reservoir Quality Zones (RQZ)**" with internal similarity and consistency is essential.

6. The RQZ delineation method integrates porosity-permeability data, lithofacies characteristics, SEM/EDS and thin section petrography techniques, and log responses. Therefore, this new method is a multi-dimensional process. Similarities in different rock types were assessed and grouped within same **RQZs**.

7. The RQZ method delineates flow data with a higher resolution than the hydraulic unit (HU) approach. Identification of RQZ in the formation has shown that the hydraulic flow unit interfaces neither recognize some of the major boundaries (RQZ3s) nor any of sub-boundaries of the RQZ method. HU and RQZ interfaces in the Principal Reservoir Zone (RQZ1s) closely correspond to one another where internally less complex channel sands occur. In more complex lithologies ("Transition Zone" and "Tight Zone" lithofacies) HU methods ignore the actual porosity and permeability-affecting rock properties.

8. In general, hydraulic flow units (HUs) do not introduce any way of assessing geologic factors whereas RQZ makes the geologic components assessable and provides a visual appreciation of the reservoir quality and heterogeneity.

9. The RQZ template generated from the core data can be used as a standard comparator to estimate permeability ranges for given units of the uncored sections. Using log-derived volume of shale and porosity it is possible to determine both RQZ for a particular segment

of the formation and a permeability range. Therefore, the RQZ model can be used to predict permeability by using logs, with or without cuttings.

IX - REFERENCES

- Abid, I., 1996, Mixed-layer illite/smectite diagenesis in the rift and post-rift sediments of the Jeane d'Arc basin, offshore Newfoundland, Canada. Unpubl. Ph.D. dissertation, Memorial University of Newfoundland, St John's, p. 21-26.
- Adams, A.E., Mackenzie, W.S., and Guilford, C., 1984, Atlas of Sedimentary Rocks under the Microscope, first edition: Longman, Essex, p. 1-104.
- Alhilali, K.A., and Shanmugam, G., 1991, Utility of mechanical facies for rock classification, characterization, and correlation, *in* R. Sneider, W. Massell, R. Mathis, D. Loren, and P. Wichmann, conveners, The integration of geology, geophysics, petrophysics and petroleum engineering in reservoir delineation, description and management: AAPG, proceedings of the 1st Archie conference, Tulsa, Oklahoma, p. 80-85.
- Amaefule, J.O., Altunbey, M., Tiab, D., Kersey D.G., and Keelan, D.K., 1993, Enhanced reservoir description: Using core and log data to identify hydraulic flow units and predict permeability in uncored intervals/wells; a paper prepared for presentation at the 66th annual conference of Society of Petroleum Engineers, Houston, Texas, October 1993, p. 1-16.
- Arthur, K.R., Cole, D.R. Henderson, G.G.L., and Kushnir, D.W., 1982, Geology of the Hibernia discovery, *in* M.T. Halbouty, ed., the deliberate search for the subtle trap: AAPG, Memoir no. 32, p. 181-195.
- Berg, R.R., 1986, Reservoir sandstones: Prentice-Hall, Inc., Englewood Cliffs, New Jersey, p.24-25.
- Blatt, H., Middleton, G., and Murray R., 1980, Origin of sedimentary rocks: Prentice Hall, Inc., Englewood Cliffs, New Jersey, p. 343-344.
- Boles, J.R., and Franks, S.G., 1979, Clay diagenesis in Wilcox sandstones of Southwest Texas: Implication of smectite diagenesis on sandstone cementation: Journal of Sedimentary Petrology, v.49, p. 55-70.
- Brown, D.M., McAlpine, K.D., and Yole, R.W., 1986, Sedimentology and sandstone diagenesis of Hibernia Formation in Hibernia oil field, Grand Banks of Newfoundland: AAPG, Bulletin 73, p. 557-575.

- Carman, P. C., 1937, Fluid flow through granular beds, *Trans. AIChE*, v. 15, p. 150-166.
- Chilingarian, G. V., and Vorabutr, P., 1983, *Drilling and drilling fluids: Updated textbook edition*, Elsevier, Amsterdam, p. 62-63.
- CNOPB (Canada Newfoundland Offshore petroleum Board), 1986, Decision 86.01, Application for approval, Hibernia, Canada-Newfoundland benefits plan, Hibernia development plan.
- CNOPB, 1990, Schedule of wells, Newfoundland offshore area
- Cuthiell, D. L., and Bachu, S., 1991, Characterizing shale clast heterogeneities and their effect on fluid flow, *in* L. W. Lake, H. B. Carroll, Jr., and T. C. Wesson, eds., *Reservoir characterization II*: Academic Press, Inc., San Diego, California, p. 226-231.
- Degens, E. T., 1965, *Geochemistry of sediments (a brief survey)*: Prentice Hall, Englewood Cliffs, New Jersey, p. 66-91.
- Driscoll, N. W., and Hogg, J. R., 1995, Stratigraphic response to basin formation: Jeanne d'Arc Basin, offshore Newfoundland, *in* J. J. Lambiase, ed., *Hydrocarbon habitat in rift basins*: Geological society special publication, no. 80, p. 145-163.
- Emerson, C., 1995, Personal communication: Department of Science, Memorial University of Newfoundland, St. John's, Canada.
- Finley, R. J., and Tyler, N., 1986, Geological characterization of the sandstone reservoirs, *in* L. W. Lake, and H. B. Carroll, Jr., eds., *Reservoir characterization*: Academic Press, Orlando, Florida, p. 1-36.
- Fitzgerald, C. E., 1987, Deposition and diagenesis of the Hibernia Member, Jeanne d'Arc basin, offshore Newfoundland, Unpubl. M.Sc. thesis, Dalhousie University, Halifax, 146 p.
- Folk, R. L., 1980, *Petrology of sedimentary rocks*: Hemphill Publishing Company, Austin, Texas, p. 127-131.
- Franks, S. G., and Forester, R. W., 1984, Relationships among secondary porosity, pore-fluid chemistry and carbon dioxide, Texas Gulf Coast, *in* D. A. McDonald, and R. C. Surdam, eds., *Clastic diagenesis*: AAPG, Memoir no. 37, 2nd printing, p. 63-80.
- Galloway, W. E., 1985, Hydrogeologic regimes of sandstone diagenesis, *in* D. A.

- McDonald, and R.C. Surdam, eds., *Clastic diagenesis*: AAPG, Memoir no. 37, 2nd printing, p. 3-13
- Gardner, R.I., and Albrechtsons, E.A., 1995, Hydraulic zonation and permeability modelling of the Hibernia Formation using an integrated mathematical, petrophysical and geological approach: The Petroleum Society of CIM. Paper 95-02, p. 1-16
- Gies, R.M., King, H.R., and Dawson, S., 1992, Petrographic evolution of the Triassic Montney Formation in the ring/border field of the NE BC & NW Alberta, Hycal Energy Research Laboratories: Unpubl. report, 151 p.
- Goldstein, J.I., Newbury D.E., Echlin, P., Joy, D.C., Fiori, C., and Lifshin, E., 1981, *Scanning electron microscopy and X-ray microanalysis*: Plenum Press, New York, p. 338-351.
- Grant, A.C., McAlpine, K.D., and Wade, J.A., 1986, The continental margin of eastern Canada: Geological framework and petroleum potential, *in* Halbouty, M.T., ed., *Future petroleum provinces of the world*: AAPG, Memoir no. 40, p. 177-205.
- Handyside, D.D. and Chipman, W.I., 1983, A preliminary study of the Hibernia field: Petroleum Society of CIM,
- Hayes, J.B., 1979, Sandstone diagenesis - the hole truth, *in* P.A. Scholle and P.R. Schluger, eds., *Aspects of diagenesis - symposia*, Society of Econ. Paleontologists and Mineralogists, Special publ. 26.
- Hietala, R.W., 1991, The process and value of petrophysical interpretation, The integration of geology, geophysics, petrophysics and petroleum engineering in reservoir delineation, description and management: AAPG, Tulsa, Oklahoma, p. 72-78.
- Hiscott, R.N., Wilson, R.C.L., Gradstein, F.M., Pujalte, V., Garcia-Modejar, J., Boudreau, R.R., and Wishart H.A., 1990, Comparative stratigraphy and subsidence history of Mesozoic rift basins of North Atlantic: AAPG Bulletin, v. 74, p. 60-76.
- Hurley, T.J., Kreisa R.D., Taylor G.G., and Yates, W.R.L., 1992, The reservoir geology and geophysics of the Hibernia field, Offshore Newfoundland, *in* M.T. Halbouty, ed., *Giant oil and gas fields of the decade 1977-88*: AAPG, Memoir 54, p. 35-54.
- Hurst, A., and Rosvoll, K.J., 1991, Permeability variations in sandstones and their relationship to sedimentary structures, *in* L.W. Lake, H.B. Carrol, Jr., and T.C. Wesson, eds., *Reservoir characterization II*: Academic Press Inc, p. 166-196.

- Hutcheon, I., 1990, Aspects of diagenesis of coarse-grained siliciclastic rocks, *in* I.A. McIlreath and D.W. Morrow, eds., *Diagenesis: Geoscience Canada reprint series 4*, p. 165-176.
- Kozeny, J., 1927, Über kapillare leitung des wassers im baden, *Sitzungsberichte, Royal Academy of Science, Vienna, Proc. Class I*, v. 136, p. 271-306.
- Koederitz, L.F., A.H. Harvey, and Honarpour M., 1989, *Introduction to petroleum reservoir analysis*, v. 6: Gulf Publishing Company, Houston, Texas, p. 34-35.
- Kramers, J.W., Bachu, S., Cuthiell, D.L., and Yuan, L.P., 1989, Reservoir characterization case study: The Porovost Upper Mannville B pool, Alberta Geological Survey, Alberta Research Council, Alberta, p. 76-80.
- Lake, W.L., 1989, *Enhanced oil recovery*: Prentice-Hall, Englewood Cliffs, New Jersey, p. 43-47.
- Lynch, F.L., 1996, Mineral/water interaction, fluid flow, and Frio sandstone diagenesis, Evidence from the rocks: *AAPG bulletin*, v.80/4, April 1996, p. 486-504.
- McAlpine, K.D., 1990, Mesozoic stratigraphy, sedimentary evolution and petroleum potential of the Jeanne d'Arc basin, Grand Banks of Newfoundland: Geological Survey of Canada, paper no. 89-17, 50 p.
- McIlreath, I. and Morrow, D.W. (eds.), 1990, *Diagenesis general introduction*, *in* I. McIlreath, and D.W. Morrow, eds., *Diagenesis*, pp. 1-8.
- North, F.K., 1985, *Petroleum geology*: Allen and Unwin, Inc., Winchester, Mass., p. 121-124.
- Pettijohn, F.J., Potter P.E., and Siever, R., 1973, *Sand and Sandstone*: Springer, Berlin.
- Pittman, E.D., Larese, R.E., Heald, M.T., 1992, Clay coats: Occurrence and relevance to preservation of porosity in sandstones, *in* D.W. Houseknecht and E.D. Pittman, eds., *Origin, diagenesis, and petrophysics of clay minerals in sandstones: SEPM special publication*, no. 47, p. 241-255.
- Powell, T.G., 1984, Hydrocarbon source relationships; Jeanne d'Arc and Avalon basins, offshore Newfoundland: Geological Survey of Canada, open file 1094.

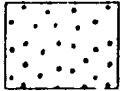
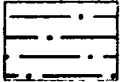
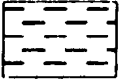
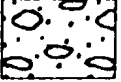

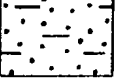
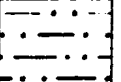
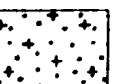
- Reineck, H.E., and Singh, I.B., 1973, *Depositional sedimentary environments*: Springer-Verlag, Berlin, Heidelberg, p. 109-110.
- Rogers, S.J., Chen, H.C., Kopaska-Merkel, D.C., Fang, J.H., 1995, Predicting permeability from porosity using artificial neural networks: *AAPG Bulletin*, v. 79/12, p. 1786-1796.
- Schlumberger, 1991, *Log interpretation principles/applications*: Schlumberger educational services, Schlumberger, 3rd printing, Houston, Texas. Sections 6-1, 6-2, 6-3, and 6-4.
- Shelton, J.W., 1979, Authigenic kaolinite in sandstone, in E.F. McBride, compiler, *Diagenesis of sandstone: Cement-porosity relationship*: Society of Economic Paleontologists and Mineralogists, reprint series #9. pp.34-42.
- Sinclair, I.K., 1988, Evolution of Mesozoic-Cenozoic sedimentary basins in the Grand Banks area of Newfoundland and comparison with Falvey's (1974): *Canadian Petroleum Geology Bulletin*, v. 36, no. 3, p. 255-273.
- Sinclair, I.K., 1993, Tectonism: the dominant factor in mid-Cretaceous deposition in the Jeanne d'Arc Basin, Grand Banks: *Marine and Petroleum Geology*, v. 10, p. 530-549.
- Slingerland, R., Harbaugh, J.W., and Furlong, K.P., 1994, *Simulating clastic sedimentary basins*: Prentice Hall, Englewood Cliffs, New Jersey, p. 161-162.
- Sneider, R.M., King, H.R., Hietala, R.W. and Connolly E.T., 1984, Integrated rock log correlation in the Elsworth Field, Alberta, Canada, *in* J.A Masters, ed., *Elsworth-Case study of a deep basin gas field*: AAPG, Memoir no.38, p. 205-282.
- Soliman, O.M., 1995, *Depositional facies and calcite cementation in the Avalon Formation, Hibernia Oil Field, Jeanne d'Arc Basin, Grand Banks of Newfoundland*: Unpubl. Ph.D. Dissertation, Department of Earth Sciences, Memorial University of Newfoundland, 282 p.
- Swanson, R.G., 1981, *Sample examination manual*: AAPG Appendix IV, p. IV/1-37.
- Tankard A.J., and H.J. Welsink, 1989, Mesozoic extension and styles of basin formation in Atlantic Canada, *in* A.J. Tankard and H.R. Balkwill, eds., *Extensional tectonics and stratigraphy of the North Atlantic margins* by : AAPG Memoir 46, p. 175-195.
- Tankard A.J., and H.R. Balkwill, 1989, *Introduction, Extensional tectonics and*

- stratigraphy of the North Atlantic margins: AAPG Memoir 46, p. 1-6.
- Tankard A.J., H.J. Welsink, and W.A.M. Jenkins, 1989, Structural styles and stratigraphy of the Jeanne d'Arc Basin, Grand Banks of Newfoundland, *in* A.J. Tankard and H.R. Balkwill, eds., Extensional tectonics and stratigraphy of the North Atlantic margins: AAPG Memoir 46, p. 265-282.
- Vavra, C.L., Scheihing, M.H., and Klein, J.D., 1991, Reservoir geology of the Taylor sandstone in the Oak Hill Field, Rusk County, Texas: Integration of petrology, sedimentology, and log analysis for delineation of reservoir quality in a tight gas sand, *in* R. Sneider, W. Massell, R. Mathis, D. Loren, and P. Wichmann, conveners, The integration of geology, geophysics, petrophysics and petroleum engineering in reservoir delineation, description and management: AAPG, proceedings of the first Archie Conference, Tulsa, Oklahoma, p. 130-158.
- von der Dick, H., 1989, Environment of petroleum source rock deposition *in* the Jeanne d'Arc Basin off Newfoundland, *in* A.J. Tankard and H.R. Balkwill, eds., Extensional tectonics and stratigraphy of the North Atlantic margins: AAPG Memoir 46, p. 295-303.
- Well Summary, 1983, Well summary of Hibernia K-14, End of mud recap for Mobil Oil Canada, Ltd., by Baroid of Canada, Ltd.
- Welsink H.J., S.P. Srivastava, and A.J. Tankard, 1989, Basin architecture of the Newfoundland continental margin and its relationship to ocean crust fabric during extension, *in* A.J. Tankard and H.R. Balkwill, eds., Extensional tectonics and stratigraphy of the North Atlantic margins: AAPG Memoir 46, p. 197-212.
- Welton, J.E., 1984, SEM petrology atlas: AAPG, Methods in Exploration Series, p. 9-225.
- Wilson, M.D. and Pittman, E.D., 1979, Authigenic clays in sandstones, *in* E.F. McBride (compiler), Diagenesis of sandstone: Cement-porosity relationship: Society of Economic Paleontologists and Mineralogists, Repr. Series #9, p. 60- 63.



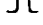




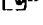
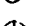











**APPENDIX I- Grain size logs and facies identification of the cored wells of the
Hibernia Formation (Hibernia B-27, Hibernia B-O8, Hibernia C-96,
Hibernia K-18, and Hibernia K-14).**

LEGEND (Legend is modified and/or adopted from Swanson (1981))



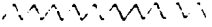
Lithologies

	Sandstone
	Siltstone
	Shale
	Conglomerate
	Coal
	Shaly Sandstone
	Silty sandstone
	Silty shale


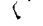


Sedimentary Structures

	Horizontal bedding
	Crossbedding
	Convolute bedding
	Load cast
	Normal grading
	Wavy bedding
	Arkosic
	Pyrite growth
	Siderite growth
	Ball and pillow structure
	Rip-up clast
	Coal growth
	Quartzitic
	Ripple crossbedding
	Climbing ripples
	Carb. rafted material
	Lenticular bedding
	Vertical carb. material
	Churned
	Shell fragments






Boundaries

	Sharp bound.
	Gradational bound.
	Erosion surface





Visual Oil-Show Descriptions

	No oil-show
	HC Odor
	Poor oil stain
	Excellent oil stain






Visual Porosity Descriptions

	Not predictable
	Poor (1-5%)
	Fair (5-10%)
	Good (10-15%)
	Excellent (>15%)



Burrowing

	Slightly burrowed
	Moderately burrowed
	Well-burrowed
	Plant root tubes

Palaeo-environments

	DCD Distributary channel deposits
	LCSD Levee and proximal crevasse splay deposits
	DFF Delta front facies
	SLDF Subaqueous levee of delta front deposits
	MSD Marsh and swamp deposits

Sample location mark

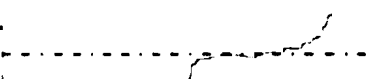
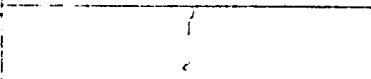

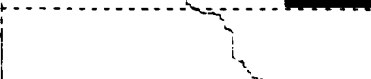
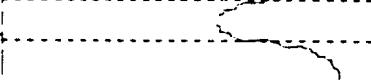

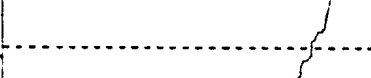
	SEM/EDS analysis
	Thin section analysis

Core Box#	Core Depth(m)	Lithology/Grain Size Log										Sedimentary Structures	Oil Show	Plugs	Perc	SEM TS	
		A	B-14	4-8	2-4	VC	U	Z	VF	Silt	Shale						
Hibernia B-27(#92)																	
Core 5 1/9	3841.00																Beginning of cored section
	3842.00	SOIL ZONE										COAL					
	3843.00											HF4					MSD
	3844.00																
	3845.00											HF1C					MSD
	3846.00																
	3847.00																
	3848.00											HF6	Carbonaceous				MSD
	3849.00																
	3850.00											HF1C					MSD
Core 6 1/15	3851.00											HF2					MSD
	3852.00											HF2B					MSD
	3853.00											HF1C					MSD
	3854.00											HF2B					MSD
	3855.00											HF1C					MSD
	3856.00											HF1B					MSD
	3857.00											HF2B					MSD
	3858.00											HF2B					MSD

Core Box#	Core Depth(m)	Lithology Grain Size Log										Shale	Facies	Sedimentary Structures	Oil Show	Ø	Plug#	Palaeo env.	SEM IS	
		>6	8-16	4-8	2-4	VC	C	M	F	V	Silt									
Core 6 4/15	3858.00																	183 SCA20 185		
	3859.00													C				186 187		
5/15	3860.00																	188 189		
6/16	3861.00											HF2C		C				190 191		
7/15	3862.00																	192 193		
	3863.00														c	?		194 SLDF		
8/15	3864.00																	195 196 197 198 199 200 201 202 203 204 205		X
9/15	3865.00													C						
10/15	3866.00																	206 207		
	3867.00																	208 209		
11/15	3868.00																	210 211 212 SCA25 213 214		
12/15	3869.00											HF1G						DFF		
13/15	3870.00																	215 SCA26 216 217		X
14/15	3871.00																	218 219		✓
15/15	3872.00													Carbonaceous				220 SLDF		
Core 7 1/10	3873.00																	221 MSD		✓
	3874.00																	222		
2/10	3875.00											HF2A						223 SLDF		
	3876.00																	224		
3/10	3877.00																	225		

Core Box#	Core Depth(m)	Lithology Grain Size Log										Shale	Facies	Sedimentary Structures	Oil Show	Ø	Plug#	Palaeo env	SFM IS
		A	B	C	D	E	F	G	H	I	J								
Core 7 4/10	3877.00																322		
	3878.00												HF2A	C			SP213 SP213	SLDP	
	3879.00												HF1C				SP214		
	3880.00												HF2C	C			SP217 SP218		✓
	3881.00												HF2A	C			SP219 SP220 SP221 SP222	SLDP	
Core 8 1/2	3882.00																		
	3883.00												HF4					MND	
	3884.00																SP233 SP234		
	3885.00												HF2B	C			SP235 SP236 SP237	SLDP	✓
	3886.00	LOST CORE																	
Core 9 1/4	3887.00																		
	3888.00																		
	3889.00																SP238	MND	
	3890.00												HF2B				SP239	SLDP	
	3891.00																ANT239 SP240 SP241		
Core 9 1/4	3892.00																		
	3893.00												HF1C	T			SP242 SP243	DC D	
	3894.00												HF1E4	Carbonaceous			SP244	LCSD	✓
	3895.00												HF1C	T			SP245 SP246 SP247	DC D	
	3896.00												HF4	Pgs			SP248 SP249 SP250	MND	

Libermia B-27(#92)

Core Box#	Core Depth(m)	Lithology Grain Size Log										Facies	Sedimentary Structures	Oil Show	Ø	Plug#	Palaeo env.	SEM TS
		Gr	Co	Ar	Ca	Fe	Mn	Si	Al	Shale								
Core 9 4/4	3896.00											HF4			?		MSD	
	3897.00											HF1G			oo	SP252 SP254	DCD	
	3898.00	LOST CORE																
	3899.00																	
	3900.00																	
Core 10 1/11	3901.00															SCA35 a255		
	3902.00											HF1C			oo	a259	DCD	
2/11	3903.00															a263		
	3904.00											COAL				SP258 a272		
3/11	3905.00											COAL				SP259 a273		
	3906.00											HF1E			o	SP260 SP261	LCSO	✓
4/11	3907.00	SOIL ZONE																
5/11	3908.00											HF4	Carbonaceous		?		MSD	
6/11	3909.00																	
7/11	3910.00											HF1B			o	SP262 a280	DCD	
8/11	3911.00																	
9/11	3912.00											HF4			o	?		
	3913.00																	✓
10/11	3914.00																	
	3915.00											HF2A			o	?	SLDP	
11/11																	End of cored section	

Hibernia B-27(#92)

Core Box#	Core Depth(m)	Lithology Grain Size Log										Facies	Sedimentary Structures	Oil Show	ϕ	Plug#	Palaeo env.	SFM TS								
		A 16	8-16	4-8	2-4	VC	C	M	L	VF	Silt								Shale							
	3479.00	Beginning of cored section																								
Core 2 9/16	3480.00											HF2A	o	o	o	?		SP10								
	3481.00											HF1C													SP11	DCD
2/16	3482.00											HF1C													SP12	
	3483.00											HF1C													SP13	MSD
3/16	3484.00											HF1C													SP14	
	3485.00											HF1A													SP15	DCD
4/16	3486.00											HF1A													SP16	
5/16	3487.00											HF1A													SP17	DCD
	3488.00											HF1A													SP18	
6/16	3489.00											HF1A													SP19	DCD
7/16	3490.00											HF1A													SP20	
8/16	3491.00											HF1A													SP21	MSD
9/16	3492.00											HF1A													SP22	
10/16	3493.00											HF1A													SP23	DCD
11/16	3494.00											HF1A													SP24	
12/16	3495.00											HF1A													SP25	DCD
13/16	3496.00	HF1A													SP26	MSD										
14/16	3497.00	HF1A													SP27	DCD										
15/16	3498.00	HF1A													SP28											
16/16	3499.00	HF1A													SP29	DCD										
	3500.00	LOST CORE																								

Iliberia B-08(#67)

Core Box #	Core Depth (m)	Lithology/Grain Size Log										Sedimentary Structures	Oil Show	ϕ	Plug #	Palaeo env.	SEM TS
		A	B	C	D	E	F	G	H	I	J						
	3546.00																
	3547.00																
	3548.00																
	3549.00																
	3550.00																
	3551.00																
	3552.00																
	3553.00																
	3554.00																
Core 3 1/3	3555.00																
	3556.00																
	3557.00																
2/3	3558.00																
3/3	3559.00																
	3560.00																
Core 4 1/5	3561.00																
	3562.00																
	3563.00																
2/5	3564.00																
3/5	3565.00																
4/5																	
5/5																	

Hibernia B-O8 (#67)

UNCORED SECTION

LOST CORE

LOST CORE

HF1E

HF1E

HF1D

HF1B

HF2A

HF4

 NP4-5
 SP52
 SP53
 SP54
 NP55
 SP56
 SP57
 SP58
 A
 59
 60
 SP61
 NP62
 SP63
 SP64

 65
 SP66
 67
 SP68
 SP69
 70
 71
 SP72

LCSB

DCD

DCD

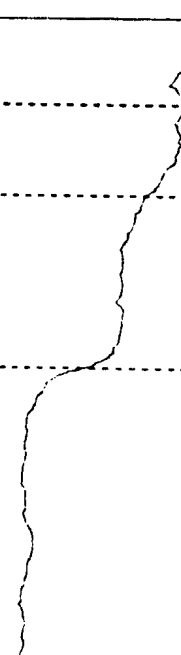
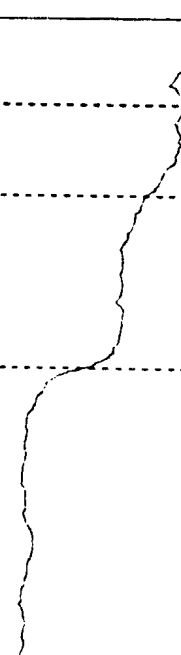
SLDF

MSD

Core Box#	Core Depth(m)	Lithology Grain Size Log										Sedimentary Structures	Oil Show	Plug#	P. den	SEM IS		
		>16	8-16	4-8	2-4	VC	C	M	F	V	Silt							
	3590.00																	
	3591.00																	
	3592.00																	
	3593.00																	
	3594.00																	
	3595.00																	
	3596.00																	
	3597.00																	
	3598.00																	
	3599.00																	
	3600.00																	
	3601.00																	
	3602.00																	
	3603.00																	
	3604.00																	
	3605.00																	
	3606.00																	
Core 1/3	3607.00											HF4	Unconsolidated	00	1	SP73 SP74 75	DCD	√ X
2/3	3608.00											HF2A		0	2		SLDP	
3/3	3609.00											HF4		0	2		SLDP	
	3609.00											HF2A		0	2		SLDP	

Hibernia B-08(#67)

UNCORED SECTION

Core Box#	Core Depth(m)	Lithology/Grain Size Log										Facies	Sedimentary Structures	Oil Show	Ø	Plug#	Palsen env	SEM TS
		A-16	B-16	4-8	2-4	VC	L	Σ	L	VF	Stl							
LC	3609.00	UNCORED SECTION																
	3610.00																	
	3611.00																	
	3612.00																	
	3613.00																	
Core 6 1/9	3614.00											HF5		°	?	SP76	SLDP	
2/9	3615.00											HF4		°	?		MSD	
	3616.00															SP77		
3/9	3617.00											HF2A		°	?		SLDP	
4/9	3618.00															SP78		
5/9	3619.00															SP79		
	3620.00															SP80		
6/9	3621.00											HF1C		°		SP81		
	3622.00															SP82		
7/9	3623.00															SP83		
8/9	3624.00											HF2B		°	?	SP84		
												HF1B		°	?	SP85	SLDP	
9/9	3625.00											HF2B		°	?	SP86	DCD	✓ X
		End of cored section														SP87	SLDP	✓ X
	3626.00															SP88		
	3627.00															SP89		
																SP90		
	3628.00															SP91		

Hibernia B-O8(#67)

Core Box#	Core Depth(m)	Lithology/Grain Size Log										Facies	Sedimentary Structures	Oil Show	Ø	Plug#	Palaeo env.	SEM TS
		Al	Si	Ca	Mg	Fe	Mn	Zn	Shale									
Core 9 2/10	3883.00																	
3/10	3884.00										HF4	Carbonaceous		?		MSD		
4/10	3885.00										COAL							
	3886.00										HF2A			?	SPN 90	SLDF		
5/10	3887.00										HF4	Carbonaceous		?		MSD		
6/10	3888.00										HF2A			?	SPN 91	SLDF		
	3889.00										HF4			?		MSD		
7/10	3890.00										COAL							
	3891.00										HF1B			?	92	DCD		
8/10	3892.00										COAL				93			
	3893.00										HF2A			?	94	SLDF		
9/10	3894.00										HF1E			?	95			
10/10	3895.00	LOST CORE										HF1C			?	96	DCD	
Core 10 1/11	3896.00														100			
	3897.00														101			
2/11	3898.00										HF1C			?	102	DCD		
3/11	3899.00													?	103			
4/11	3900.00										HF4			?	104	MSD		
	3901.00										HF1D			?	105	DCD		
5/11	3902.00	SOIL ZONE										HF4			?	106	MSD	

Hibernia C-96(#95)

Core Box#	Core Depth(m)	Lithology/Grain Size Log										Facies	Sedimentary Structures	Oil Show	Ø	Plug#	Palaeo env.	SUM TS
		Δ 10	8-16	4-8	2-4	VC	U	Z	L	VP	Silt	Shale						
Core 10 5/11	3902.00	SOIL ZONE											HF1	SUBAERIAL EXPOSURE	?		MSD	
6/11	3903.00												HP2A		?	116 117 SP118	SLDF	
	3904.00															119 120		
7/11	3905.00												HF1A			121	DCD	
	3906.00															122 123 124		
8/11	3907.00												HF1C		..	125 126	DCD	
	3908.00															SP127 128 129		
9/11	3909.00												HP2A		?		SLDF	
	3910.00												HF1C		..	SP130 131 132	DCD	
10/11	3911.00												HF3		..	133-4	DCD	√ X
11/11	3912.00												HP1F		..	135 136	DCD	
	3913.00	LOST CORE																
	3914.00												HF1P		..	137 138 139 140	DCD	
1/7	3915.00															141 142		
2/7	3916.00												HF3			143 144	DCD	
	3917.00												HF3	SUBAERIAL EXPOSURE	?		MSD	
3/7	3918.00	SOIL ZONE											HF2A		?	145 146	SLDF	
4/7	3919.00												HF2A	SUBAERIAL EXPOSURE	?		MSD	
5/7	3920.00	SOIL ZONE											HF2A		?	147 148	SLDF	√ X
	3921.00												HF1A			149 150 151 SP152 153	DCD	

Hibernia C-96(#95)

Core Box#	Core Depth(m)	Lithology/Grain Size Log										Facies	Sedimentary Structures	Oil Show	ϕ	Plug#	Palaeo env.	SEM TS
		A/C	B/C	4-8	2-4	VC	C	Z	F	VF	Silt	Shale						
	3921.00																	
7/7	3922.00												HFIC		00	SP154	DCD	
													HF1A		00	SP156	SLDP	
													HF1F		00	SP157	DCD	
																SP158		
Core 13	3923.00															159		
Core 13																160		✓X
1/13	3924.00															161		
																162		
2/13	3925.00												HF1P		00	163	DCD	
																164		
																165		
3/13	3926.00															166		
																167		
																168		
	3927.00															169		
																170		
4/13	3928.00												HF1A		00	SP172	SLDP	
													HF1C		00	173	DCD	
																174		
5/13	3929.00												HF1A		00	175	DCD	
																176		
													HF1C		00	177	DCD	
																178		
6/13	3930.00															179		
	3931.00												HF1C		00	180	DCD	
																181		
7/13	3932.00												HF2B		00	182	SLDP	
													HF4		00		MSD	
	3933.00												HF2A		00		SLDP	
8/13	3934.00															183		
																184		
																185		
9/13	3935.00															186		
																187		
																188		
	3936.00												HF1C		00	189	DCD	
10/13	3937.00															190		
																191		
																192		
11/13	3938.00															193		
																194		
																195		
																196		
12/13	3939.00												HF1F		00	197	DCD	
																198		
																199		
13/13	3940.00												HF1C		00	200	DCD	
													HF4		00		MSD	

Core Box#	Core Depth(m)	Lithology Grain Size Log										Sedimentary Structures	Oil Show	ϕ	Plug#	Palaeo ent.	SEM IS
		A	B	C	D	E	F	G	H	I	J						
Core 13 13/13	3940.00											HF4		?		MSD	
Core 14 1/13	3941.00											HF5		?		SLDF	
	3942.00																
2/13	3943.00											HF4		?		MSD	
3/13	3944.00											HF2A		?		SLDF	
4/13	3945.00											HF4		?		MSD	
	3946.00											HF5		?		SLDF	
5/13	3947.00																
	3948.00																
6/13	3949.00											HF4		?		MSD	
7/13	3950.00																
	3951.00											HF5		?		SLDF	
8/13	3952.00																
	3953.00																
9/13	3954.00																
	3955.00											HF4		?		MSD	
10/13	3956.00																
11/13	3957.00																
12/13	3958.00																
13/13	3959.00																
												End of cored section					

Hibernia C-96(#95)

Core Box#	Core Depth(m)	Lithology Grain Size Log										Sedimentary Structures	Oil Show	ϕ	Plug#	Palaeo env	SEM TS
		2	4	8	16	32	64	128	256	512	Shale						
	3796.00																
	3797.00																
Core 3 1/13	3797.00														SP102	MSD DCD	√ X
	3798.00																
2/13	3799.00														SP103 SP104	MSD	
3/13	3800.00														SP105	DCD	
Core 5 4/13	3801.00																
	3802.00																
5/13	3803.00																
6/13	3804.00																
7/13	3805.00																
	3806.00																
8/13	3807.00																
	3808.00																
9/13	3809.00																
10/13	3810.00																

Hibernia K-18(#76)

Beginning of
cored section

Core Box#	Core Depth(m)	Lithology Grain Size Log										Facies	Sedimentary Structures	Oil Show	ϕ	Plug#	Palaeo env.	SEM TS
		Δ 16	R-16	4 R	2-4	VC	U	Z	L	VT	S	Shale						
Core 3 10/13	3810.00															SP116 SP117 SP118		
	3811.00															SP119		
	3812.00															SP121 SP122		
12/13	3813.00															SP124 SP125 SP126 SP127 SP128	D/D	
	3814.00															SP129 SP130		
	3815.00															SP131 SP132 SP133		
Core 4 1/2	3816.00															SP134 SP135 SP136 ANT138	D/D	
2/2	3817.00																	
	3818.00																	
	3819.00																	
	3820.00															SP137 SP138 SP139 SL140	LCND	✓X
Core 5 1/14	3821.00															SP141 SP142 SP143	MND	
2/14	3822.00															SP144 SP145 SP146 SP147	LCND	✓X
3/14	3823.00															SP150 SP151		
4/14	3824.00															SP152 SP153	SLDP	
5/14	3825.00															SP154 SP155 SP156 SP157 SP158	D/D MND	
6/14	3826.00															SP159 SP160 SP161 SP162 SP163 SP164 SP165		
7/14	3827.00																	
8/14	3828.00																	
	3829.00																	

Hibernia K-18(#76)

LOST CORE

Core Box#	Core Depth(m)	Lithology/Grain Size Log										Facies	Sedimentary Structures	Oil Show	Ø	Plugs	Palaeo env	SFM TS
		Δ	1	2	3	4	5	6	7	8	9							
Core 6 7/13	3848.00																	
8/13	3849.00											HF2A					MSD	
9/13	3850.00																	
	3851.00																	
10/13	3852.00											HF1C HF2B		00	11	SP130 SP131 SP132 SP133 SP134 SP135	DM D SLDF	
11/13	3853.00																	
	3854.00											HF1C		00	11	SP136 SP137 238 239 240 241 242 243 SP146 SP147 SP148 SP149 SP150 SP151	DM D	
12/13	3855.00																	
13/13	3856.00												Rhythmites					✓X
Core 7 1/8	3857.00											HF2B					SLDF	
	3858.00																	
2/8	3859.00											HF1C		00	11	SP152 SP153 SP154 SP155 SP156 SP157 SP158 SP159 SP160	DM D	
3/8	3860.00											HF4					MSD	
4/8	3861.00											HF3A					SLDF	
	3862.00																	
5/8	3863.00											HF4 HF2A					MSD SLDF	
6/8	3864.00											HF4					MSD	
7/8	3865.00											HF2A					SLDF	
8/8	3866.00																	
	3867.00											HF4					DM D	
													End of core 7					

Hibernia K-18 (#76)

Core Box#	Core Depth(m)	Lithology Grain Size Log										Facies	Sedimentary Structures	Oil Show	ϕ	Plug#	Palaeo. env.	SEM TS
		>10	8-16	4-8	2-4	VC	C	S	L	>1	Silt							
Core 7 8/13	3858.00											HF2B	ϕ \approx A		?			
	3859.00																	
9/13	3860.00											HF2			?		MSD	
	3861.00																	
10/13	3862.00											HF1C	ϕ ϕ			206 207 M A1 ANT208 208 209	DC D	X
	3863.00																	X
11/13	3864.00											HF2B HF1C	ϕ ϕ ϕ		?	210	SLDF DC D	
	3865.00											HF2A	ϕ ϕ		?	211	SLDF DC D	
12/13	3866.00																	
	3867.00																	
13/13	3868.00																	
	3869.00																	
Core 8 1/14												HF2	ϕ ϕ		?			
2/14	3870.00											HF1B	ϕ (?)		?	214	MSD DC D	
	3871.00											HF1	ϕ		?		MSD	
3/14	3872.00											HF1C	ϕ (?)		?	215 M A2 ANT216 M216 M A3 M217	DC D	
	3873.00											HF2	ϕ		?		MSD	
4/14	3874.00											HF1B	ϕ (?)		?		DC D	
	3875.00											HF1	ϕ		?		MSD	
5/14	3876.00											HF1B	ϕ (?)		?	218 219	DC D	/ X
	3877.00											HF2A	ϕ ϕ ϕ		?		SLDF	

Hibernia K-14 (#93)

Core Box#	Core Depth(m)	Lithology/Grain Size Log										Facies	Sedimentary Structures	Oil Show	Ø	Plug#	Palaeo env.	SEM TS
		Δ	8-16	4-8	2-4	VC	C	M	L	VL	Silt	Shale						
Core 8 8/14	3877.00												HF2A	φ ≈ Λ	o	?	SLDF	
	3878.00												HF1A	Λ (?)	o	?	DCD	
	3879.00												HF2A	φ ≈ Λ	o	?	SLDF	
	3880.00												HF1B		o	210	DCD	
	3881.00												HF2A		o	211	DCD	
	3882.00												HF1B		o	212	DCD	
	3883.00												HF2A	φ ≈ Λ	o	?	SLDF	
	3884.00												HF1B	Λ (?)	o	SP213 SP214 SCA4 215	DCD	
	3885.00												HF2A	φ ≈ Λ	o	?	SLDF	
	3886.00												HF1B	Λ (?)	o	216 SCA5 AST216 SCA6 217	DCD	
	3887.00												HF2A	φ ≈ Λ	o	218 219 220	DCD	
	3888.00															221 222	SLDF	
	3889.00																	
	3890.00																	
Core 9 1/11	3891.00												HF4		o	?	MSB	
	3892.00																	
	3893.00																	
	3894.00																	
	3895.00												HF2C	φ ≈ Λ	o	?	SLDF	
	3896.00																	

Hibernia K-14(#93)

Soil zone
subaerial exposure

Core Box#	Core Depth(m)	Lithology/Grain Size Log										Sedimentary Structures	Oil Show	ϕ	Plug#	Palaeo env.	SFM TS
		>16	8-16	4-8	2-4	VC	C	M	F	VF	Silt						
Core 9	3896.00																
9/11	3897.00																
10/11	3898.00																
11/11	3899.00	LOST CORE															
Core 10	3900.00																
1/9	3901.00																
2/9	3902.00																
3/9	3903.00																
4/9	3904.00																
5/9	3905.00																
6/9	3906.00																
7/9	3907.00																
8/9	3908.00																
9/9	3909.00																
	3910.00																
	3911.00																
	3912.00																
	3913.00	LOST CORE															
	3914.00																
	3915.00																

Iliberia K-14 (#93)

Core Box#	Core Depth(m)	Lithology/Grain Size Log										Facies	Sedimentary Structures	Oil Show	Ø	Plug#	Petro env.	SEM TS											
		> 6	8-16	4-8	2-4	VC	C	M	F	VF	Silt								Shale										
	3915.00	LOST CORE																											
	3916.00											LOST CORE																	
	3917.00																					LOST CORE							
Core 1 1/13	3918.00											HF2B	Δ	h	≈	o	?												
	3919.00																												
Core 2 1/13	3920.00																												
2/13	3921.00																												
3/13	3922.00											HF1D			..				DCD										
	3923.00																												
4/13	3924.00																												
5/13	3925.00																												
	3926.00											HF4							MSD										
6/13	3927.00											HF2B HF1C	≈	□	⊙					SLDF									
7/13	3928.00											HF4								DCD									
	3929.00																												
8/13	3930.00																												
9/13	3931.00																												
	3932.00											HF1B							SLDF										
10/13	3933.00																			DCD									
11/13	3934.00																												

Hibermia K-14(#93)

Core Box#	Core Depth(m)	Lithology Grain Size Log										Facies	Sedimentary Structures	Oil Show	Plug#	Palcen env.	SFM TS
		A-16	8-16	4-8	2-4	VC	C	M	F	VF	Silt	Shale					
Core 12	3934.00												T				
11/13	3935.00												HFIC			IX D	
12/13	3936.00																5 X
13/13	3937.00																
Core 13	3938.00												T				
1/14	3939.00																
2/14	3940.00																
3/14	3941.00																
4/14	3942.00												HFJG			IX D	
5/14	3943.00																
6/14	3944.00																
7/14	3945.00																
8/14	3946.00																
9/14	3947.00																
10/14	3948.00																
11/14	3949.00																
12/14	3950.00																
	3951.00																
	3952.00																
	3953.00																

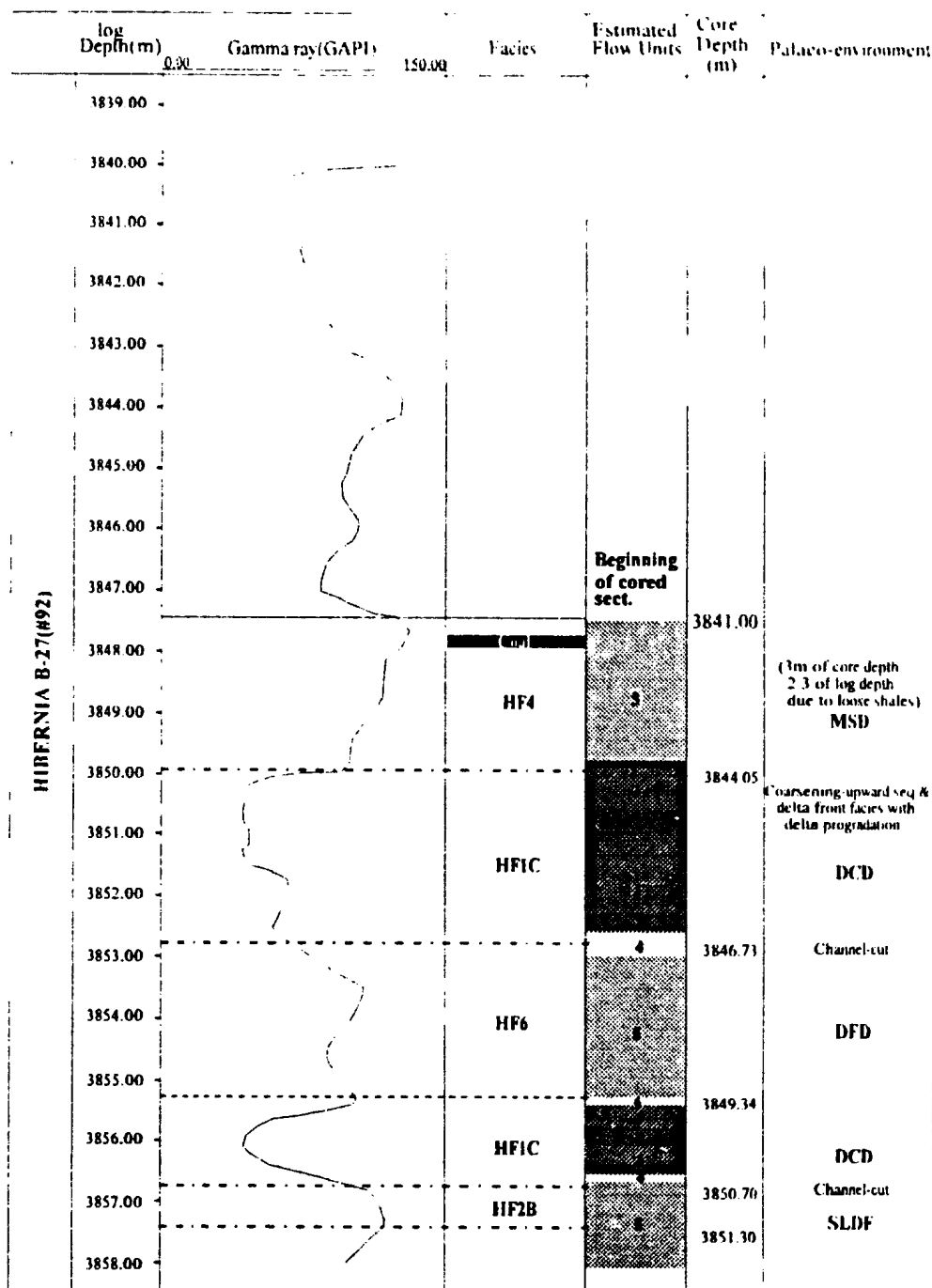
Hibernia K-14(#93)

Core Box	Core Depth(m)	Lithology	Grain Size Log	Shale	Facies	Sedimentary Structures	Oil Show	Plug#	Palaeo	SEM TS
Core 13 12/14	3953.00-									
	3954.00									
13/14	3955.00-				HF5				Marine Shales	
Core 14 1/12	3956.00-									
	3957.00									
2/12	3958.00									
3/12	3959.00-				HF2A				SLDF	
	3960.00				HF1B			3454 3458 3456	DCD	
4/12	3961.00				HF2B				SLDF	
5/12	3962.00				HF3			3450 3451 3452 3453 3454	DCD	✓ X
6/12	3963.00	SOIL ZONE			HF4				SLDF	
	3964.00				HF2C				SLDF	
7/12	3965.00				HF2A			3450 3451	SLDF	
8/12	3966.00				HF1B			3452 3453 3454 3455 3456 3457 3458 3459	DCD	
9/12	3967.00									
	3968.00				HF2A HF2B			3455	SLDF	
10/12	3969.00							3456 3457 3458 3459 3460 3461 3462 3463 3464 3465 3466 3467 3468 3469 3470 3471 3472 3473 3474 3475 3476 3477 3478 3479 3480 3481 3482 3483 3484 3485 3486 3487 3488 3489 3490 3491 3492 3493 3494 3495 3496 3497 3498 3499 3500 3501 3502 3503 3504 3505 3506 3507 3508 3509 3510 3511 3512 3513 3514 3515 3516 3517 3518 3519 3520 3521 3522 3523 3524 3525 3526 3527 3528 3529 3530 3531 3532 3533 3534 3535 3536 3537 3538 3539 3540 3541 3542 3543 3544 3545 3546 3547 3548 3549 3550 3551 3552 3553 3554 3555 3556 3557 3558 3559 3560 3561 3562 3563 3564 3565 3566 3567 3568 3569 3570 3571 3572 3573 3574 3575 3576 3577 3578 3579 3580 3581 3582 3583 3584 3585 3586 3587 3588 3589 3590 3591 3592 3593 3594 3595 3596 3597 3598 3599 3600	DCD	✓ X ✓ X
11/12	3970.00				HP1D	Carbonaceous				
12/12	3971.00									
	3972.00									
					End of cored section					

Hibernia K-14 (#93)

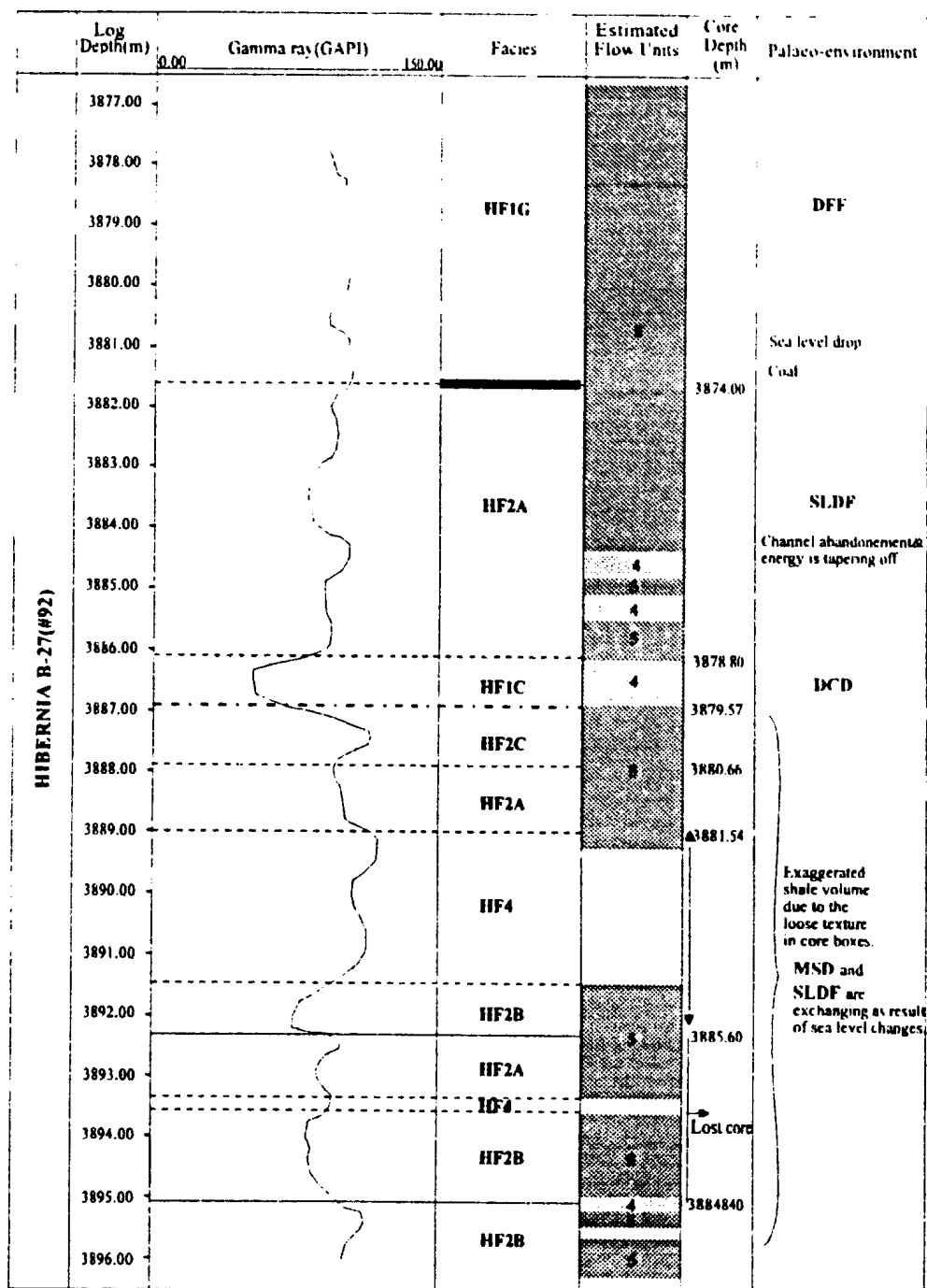
APPENDIX II

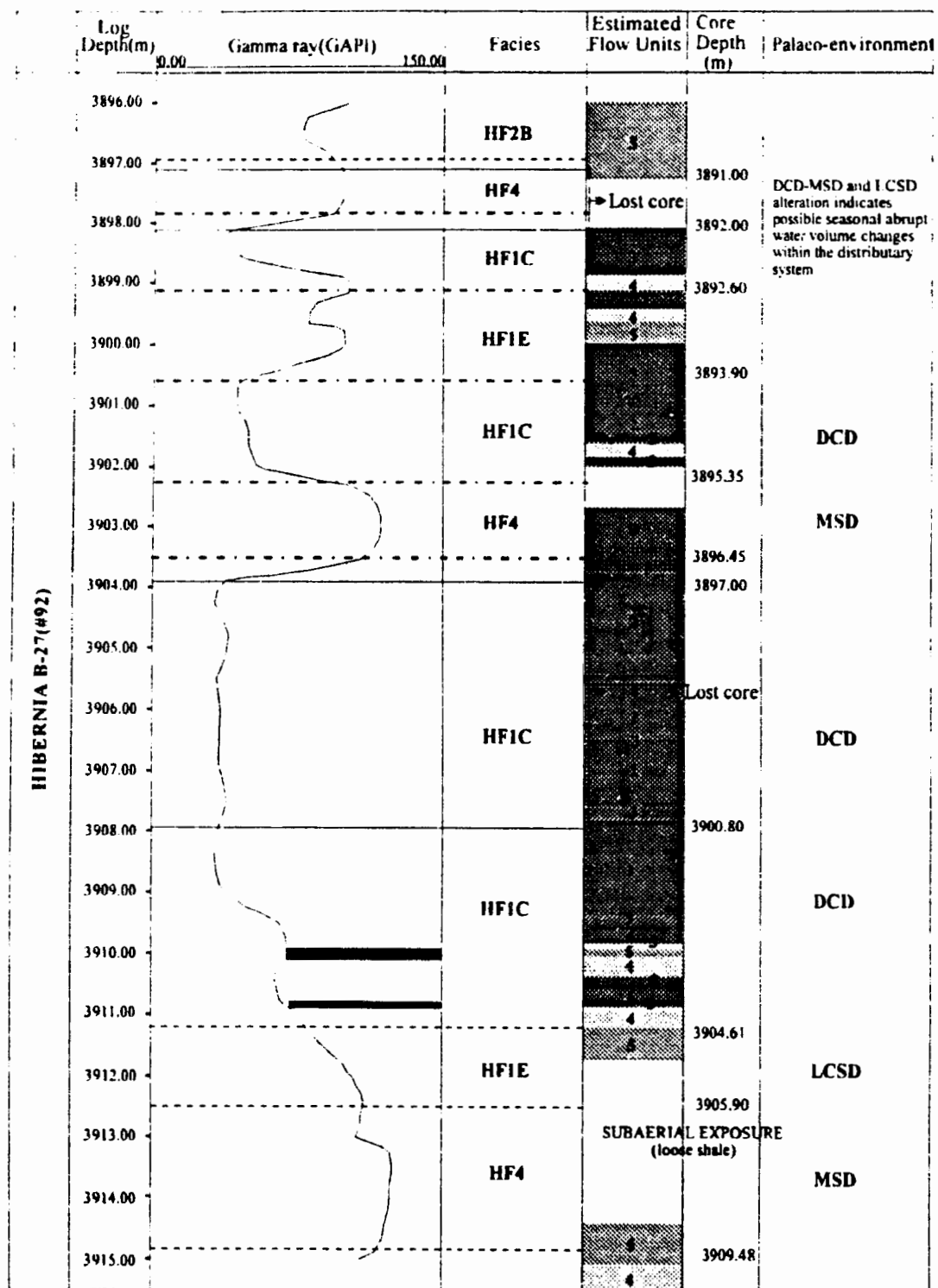
- 1- Deviations between the core and log depths had to be corrected to determine the exact locations of the Hibernia core plugs for correlating the lithofacies associations with the designated hydraulic flow units. Depth deviations were caused by the core units which expand during storage procedure.
- 2- Gamma-ray log of Hibernia B-O8 was not available. Therefore the grain size log of Hibernia B-O8 was with the volume of shale-hydraulic unit composite of HMDC.
- 3- Types of the lithofacies contacts (erosional, sharp, and gradational) in gamma-ray logs are adopted from the grain size logs in appendix I.




Log Depth(m)	Gamma ray(GAPI)	Facies	Estimated Flow Units	Core Depth (m)	Palaeo-environment
3858.00	0.00			3852.10	Progradation of fluvially-dominated distrib. channels.
3859.00		HF1C			DCD
3860.00		HF4		3853.80	MSD
3861.00		HF1C			DCD
3862.00		HF4		3854.66	Coarsening-upward
3863.00		HF1B		3855.94	Abrupt energy cut-off
3864.00		HF2B		3856.67	Lower energy channel-cut
3865.00				3858.03	
3866.00					Gradual sea level drop
3867.00					
3868.00					
3869.00					
3870.00		HF2C			SLDF
3871.00					
3872.00				3865.10	
3873.00					
3874.00		HF1G			
3875.00					Gradual transgression with increasing marine influence.
3876.00					DFF
3877.00					

HIBERNIA B-27(#92)





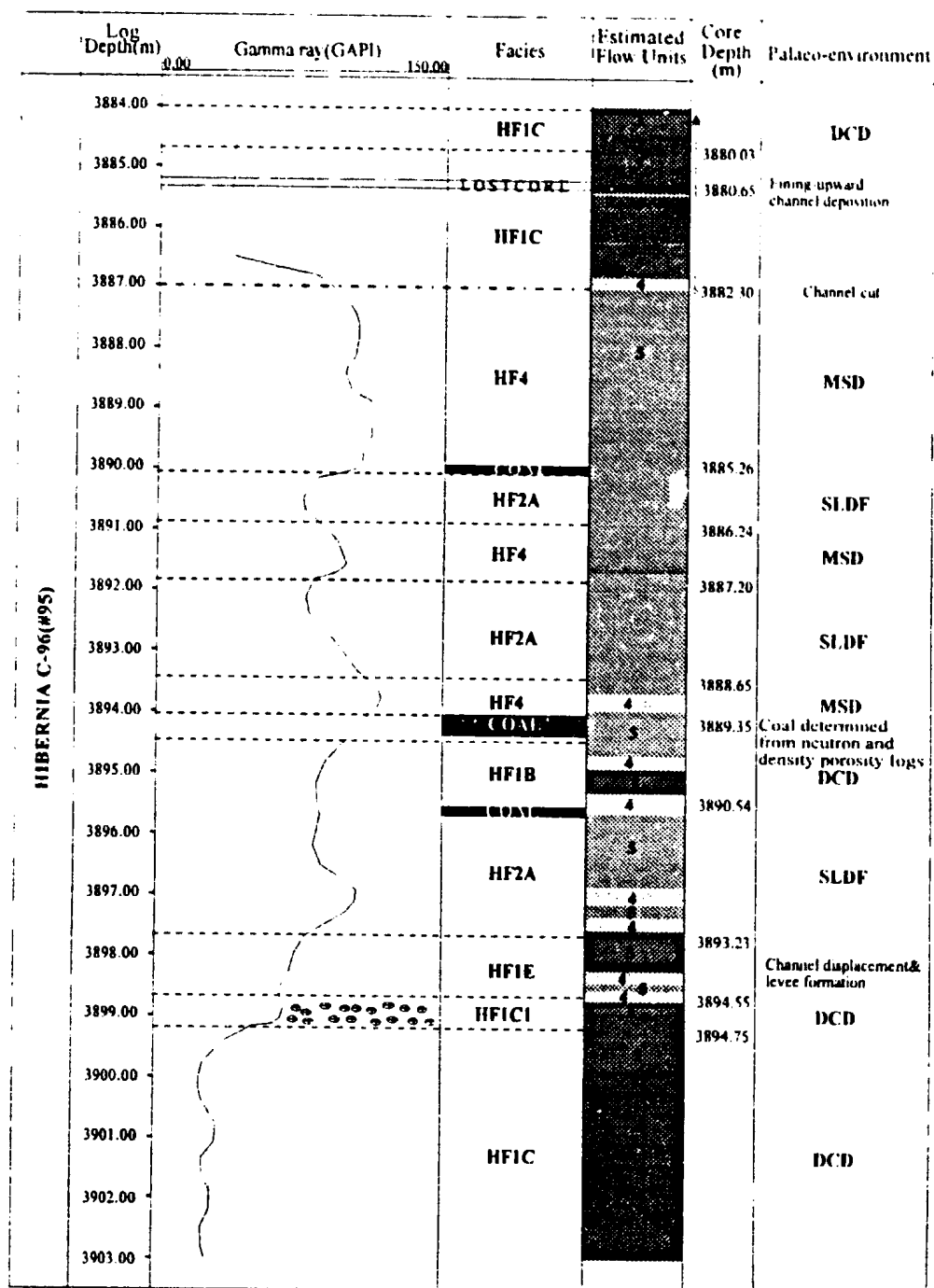
	log	Gamma ray (GAPI)		Facies	Estimated Flow Units	Core Depth (m)	Palaeo-environment
	Depth(m)	0.00	150.00				
HIBERNIA B-27(#92)	3915.00			HF4	2	3909.50	MSD
	3916.00			HF1B	4		DCD
	3917.00				5	3910.10	
	3918.00			HF4			MSD
	3919.00						
	3920.00						
	3921.00			HF2A	1	3913.95	SLDF
	3922.00				End of cored sect.	3915.00	
	3923.00						

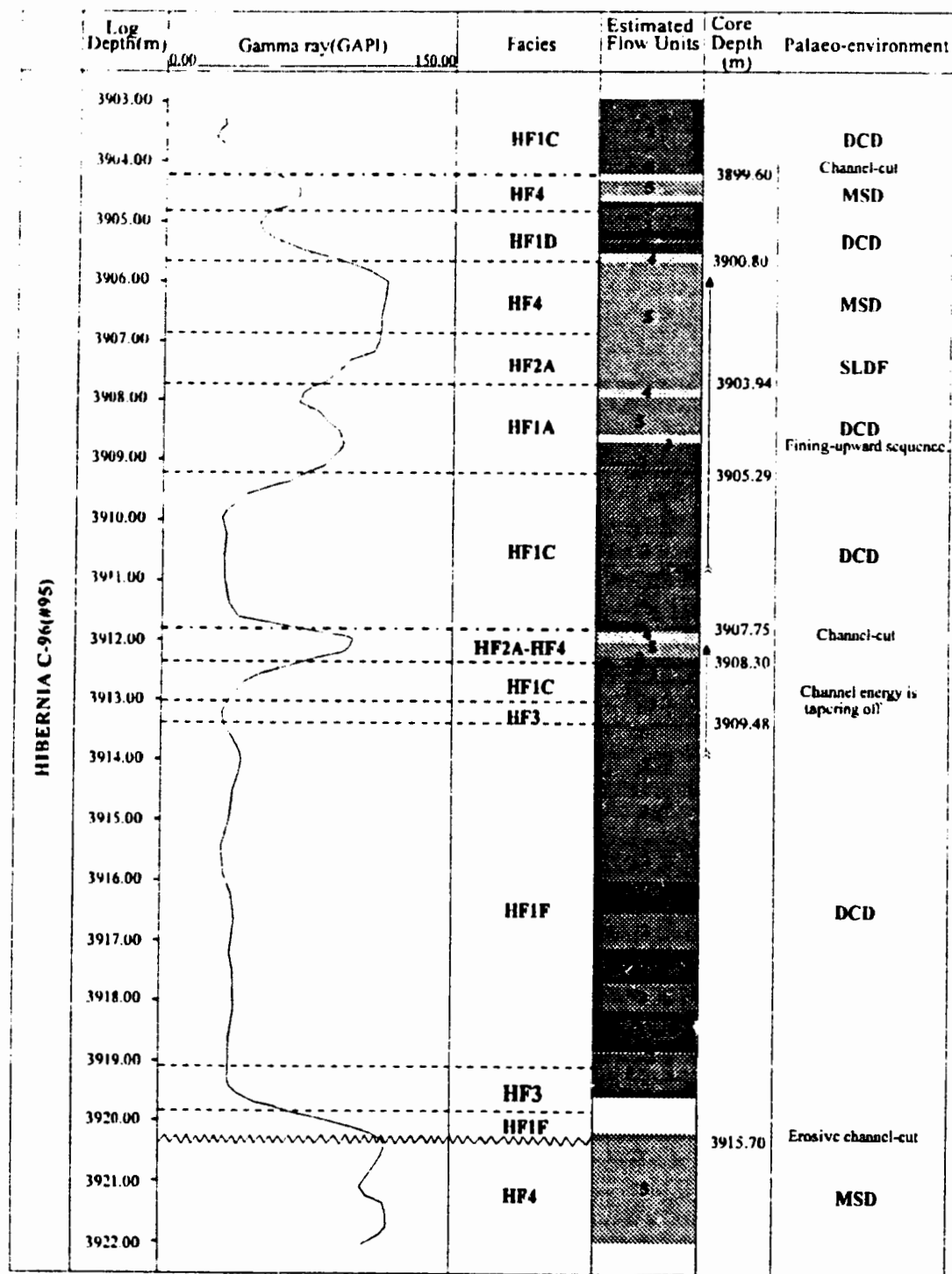
Log Depth(m)	Gamma ray(GAPI)	Facies	Estimated Flow Units	Core Depth (m)	Palaeo-environment
3865.00					
3866.00		HF4			MSD
3867.00					
3868.00		HF1A			DCD
3869.00		HF1B			DCD
3870.00					
3871.00					
3872.00		HF1C			DCD
3873.00					
3874.00					
3875.00		HF1E		3869.70	LCSD
3876.00		HF2A			SLDF
3877.00		HF1A			DCD
3878.00		HF4		3872.46	MSD
3879.00		HF2A		3873.83	Less fluvial influence during sea level changes
3880.00				3874.90	SLDF
3881.00		HF4			MSD
3882.00				3877.14	Significant & sudden relative sea level drop
3883.00		HF1C		3877.60	DCD
3884.00					

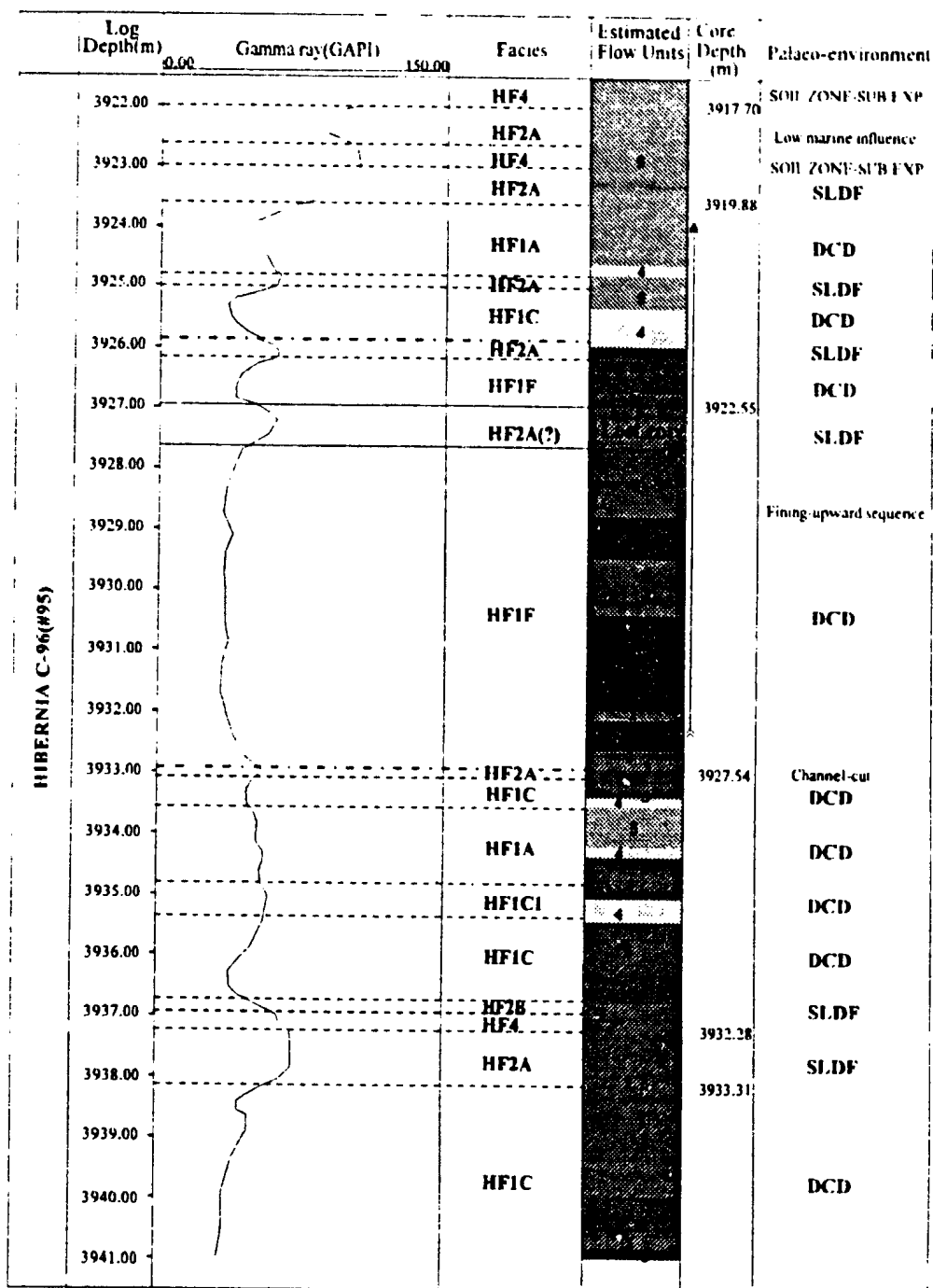
HIBERNIA C-96(#95)

Extrapolated section

Beginning
of cored
section



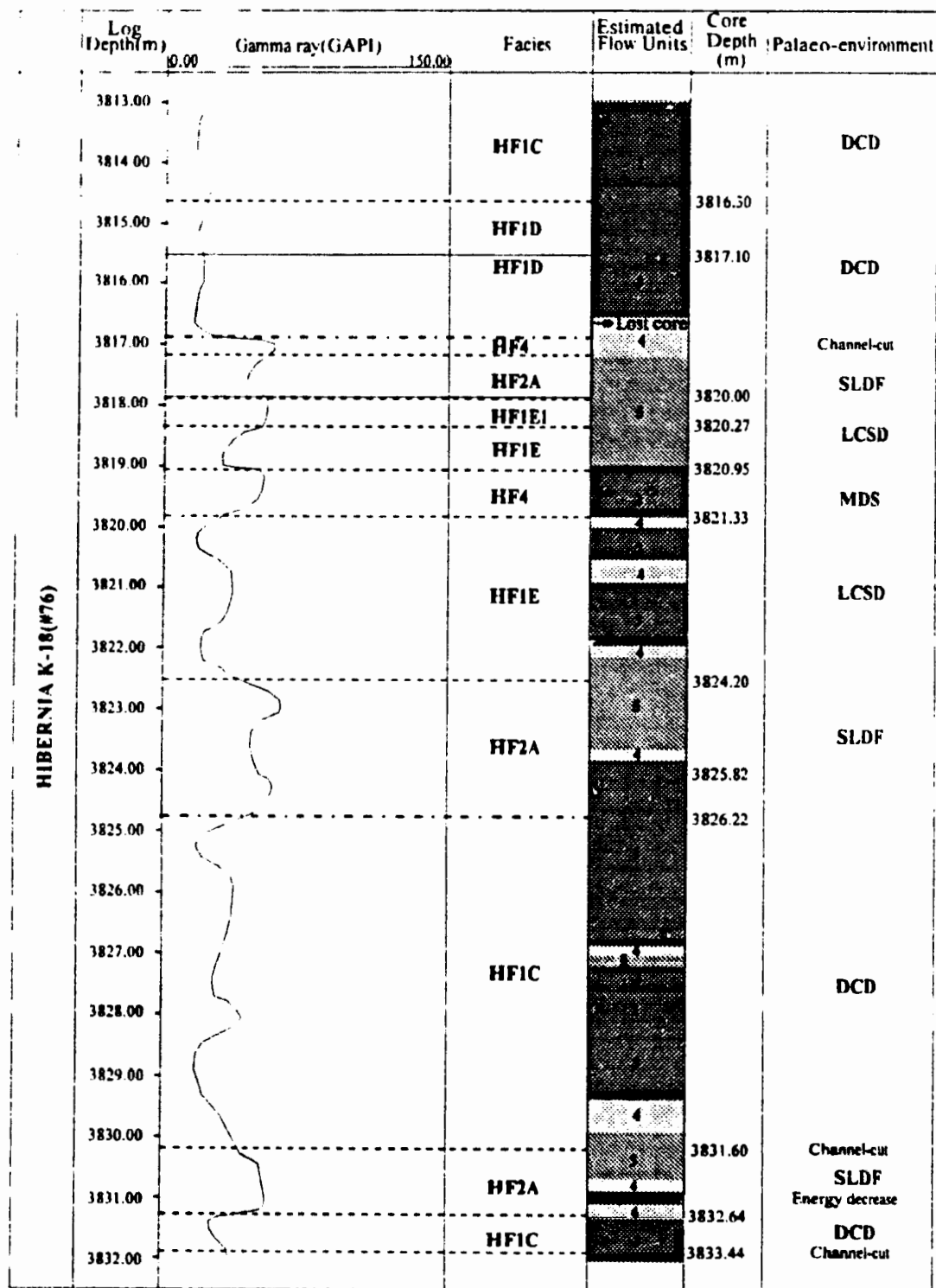


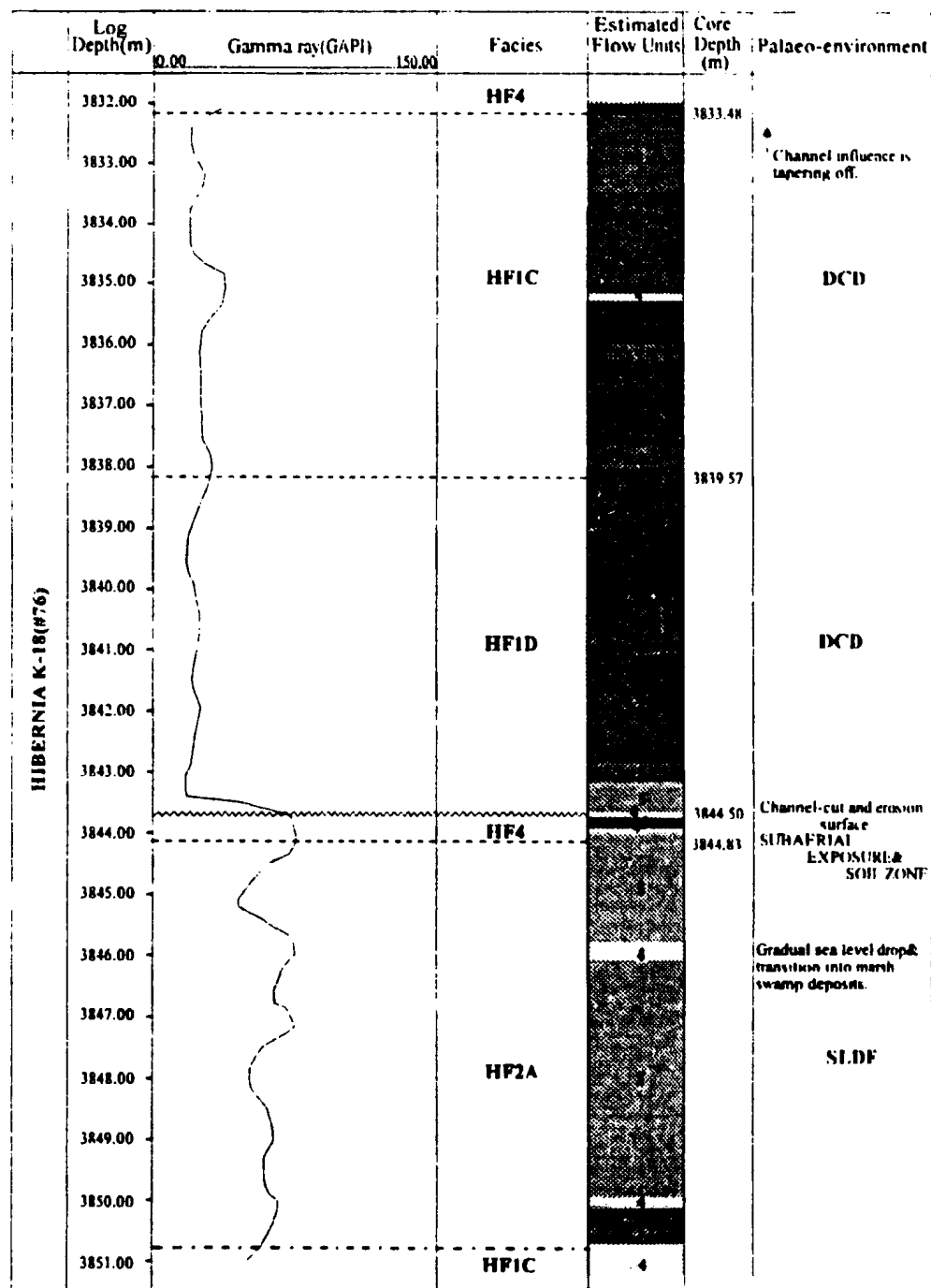


Log Depth(m)	Gamma ray(GAPI)		Facies	Estimated Flow Units	Core Depth (m)	Palaeo-environment
	0.00	150.00				
3941.00			HF1C- HF1F(?)			DCD
3942.00						
3943.00						
3944.00			HF1F		3938.52	
3945.00			HF1C1		3939.70	Channel-cut&erosion surface
			HF4		3940.60	MSD
3946.00			HF2A			SLDF
3947.00					3941.70	
3948.00			HF4			MSD
3949.00					3943.50	Sea level changes generate prodeltaic shales, marsh and subaqueous levee deposits.
3950.00			HF2A			SLDF
3951.00			HF4		3945.48	
			HF5		3946.10	MSD
3952.00					3946.80	SLDF
3953.00						
3954.00			HF4			MSD
3955.00						
3956.00			HF5		3950.80	
					3951.20	SLDF
3957.00						
3958.00			HF4			MSD
3959.00				End of cored section		
3960.00						

HIBERNIA C-96(#95)

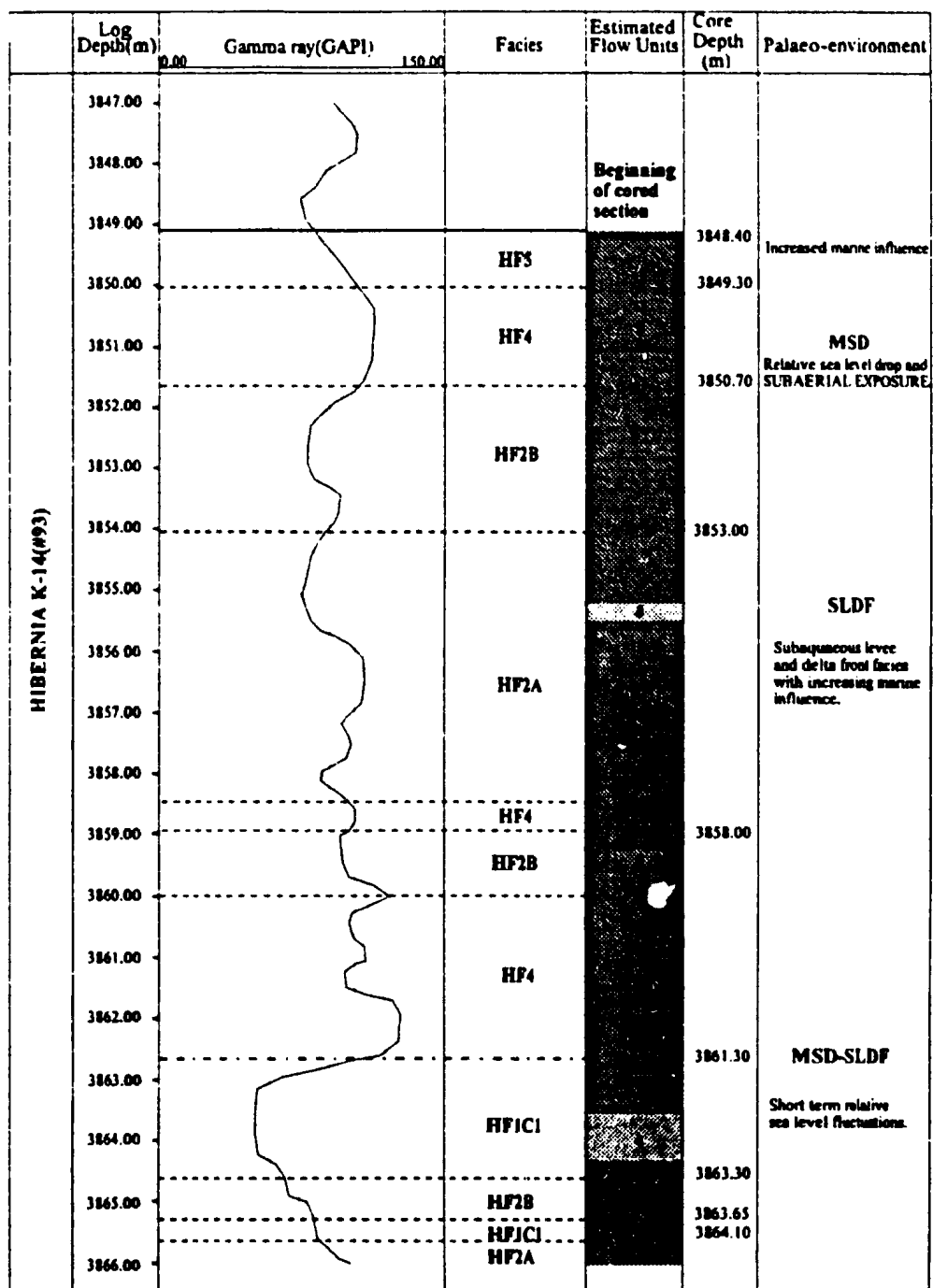
	Log Depth(m)	Gamma ray(GAPI)	Facies	Estimated Flow Units	Core Depth (m)	Palaeo-environment
	0.00	150.00				
HIBERNIA K-18(W76)	3794.00			1	3796.90	Beginning of cored section
	3795.00		HF1A	4	3797.34	DCD
	3796.00		HF4		3798.87	
	3797.00		HF1A		3800.75	
	3798.00		HF4		3800.90	DCD
	3799.00		HF1A		3801.10	
	3800.00		HF4			MSD
	3801.00					
	3802.00				3803.95	
	3803.00		HF2C			SLDF
	3804.00					
	3805.00				3807.21	
	3806.00					
	3807.00		HF1B			DCD
	3808.00					
	3809.00					
	3810.00				3811.11	
	3811.00		HF1C			DCD
	3812.00					
	3813.00					



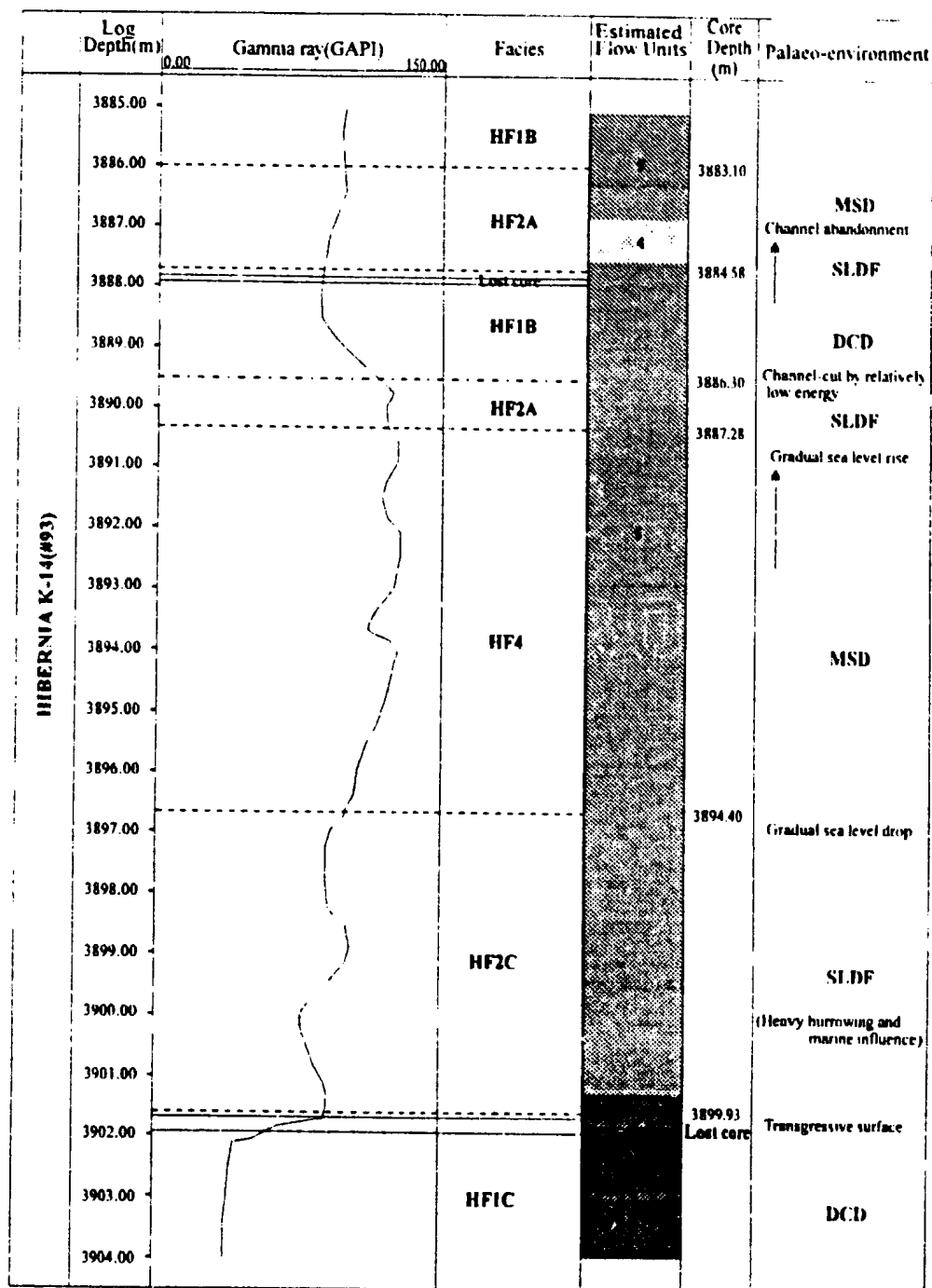


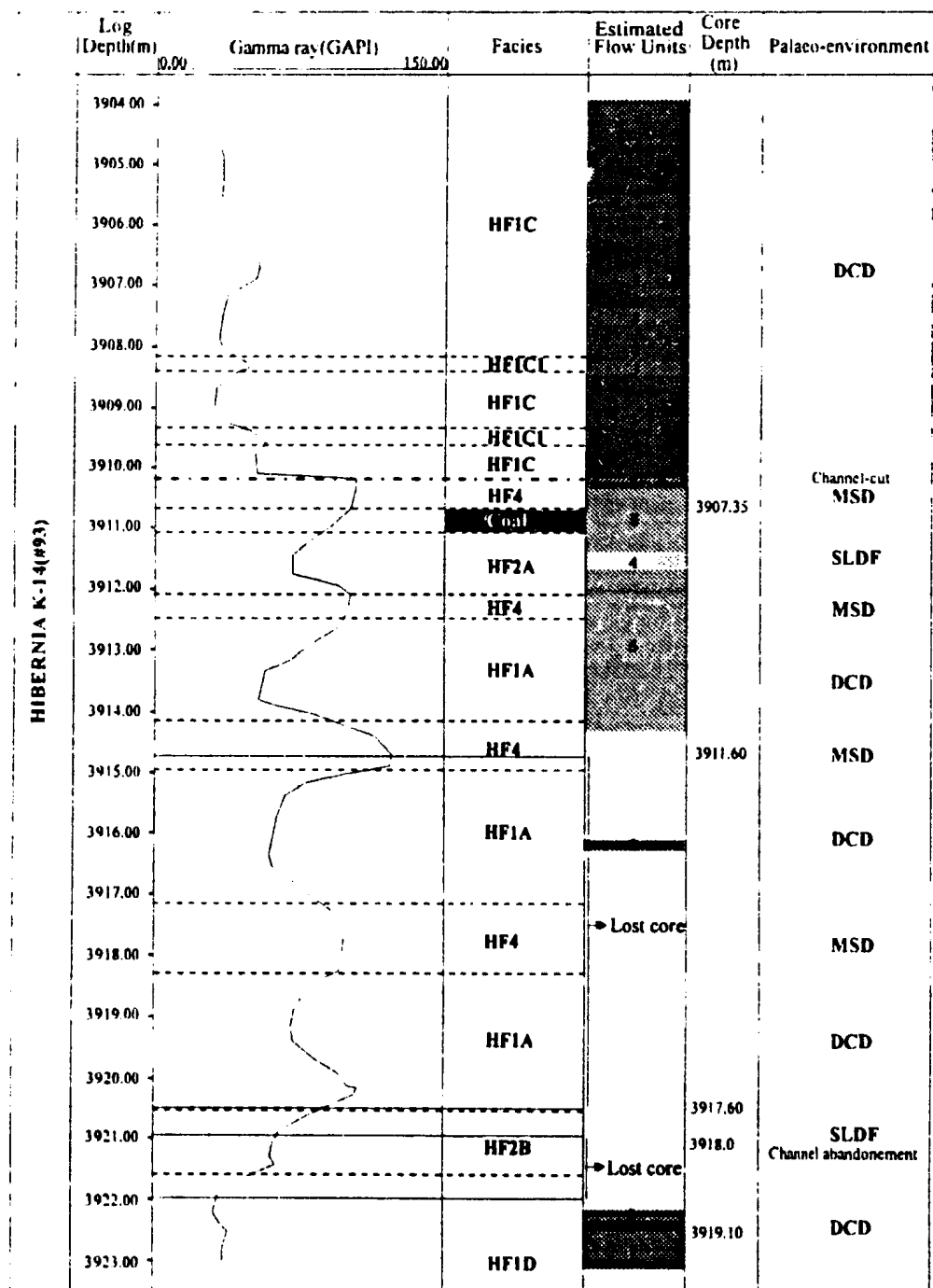
Log Depth(m)	Gamma ray(GAPI)	Facies	Estimated Flow Units	Core Depth (m)	Palaeo-environment
3851.00		HF2B		3851.75	Abrupt sea level rise and transgressive surface.
3852.00					
3853.00		HF1C			DCD
3854.00					
3855.00		HF2B		3856.00	Channel-cut SLDF
3856.00				3857.43	
3857.00		HF1C			DCD
3858.00					
3859.00		HF4		3859.39	Channel-cut MSD
3860.00		HF2A		3860.10	SLDF
3861.00		HF4		3861.82	MSD
3862.00		HF2A		3862.25	SLDF
3863.00		HF4		3862.58	MSD
3864.00		HF2A		3863.74	Marsh-swamp deposits and subaqueous delta front facies with short term sea level changes.
3865.00					
3866.00		HF4		3866.00	MSD
3867.00		HF2A	End of cored section.	3866.70	SLDF
		HF4			MSD
		HF2A			SLDF
		HF4			MSD
		HF2A			SLDF
		HF4			MSD
3869.00					
3870.00					

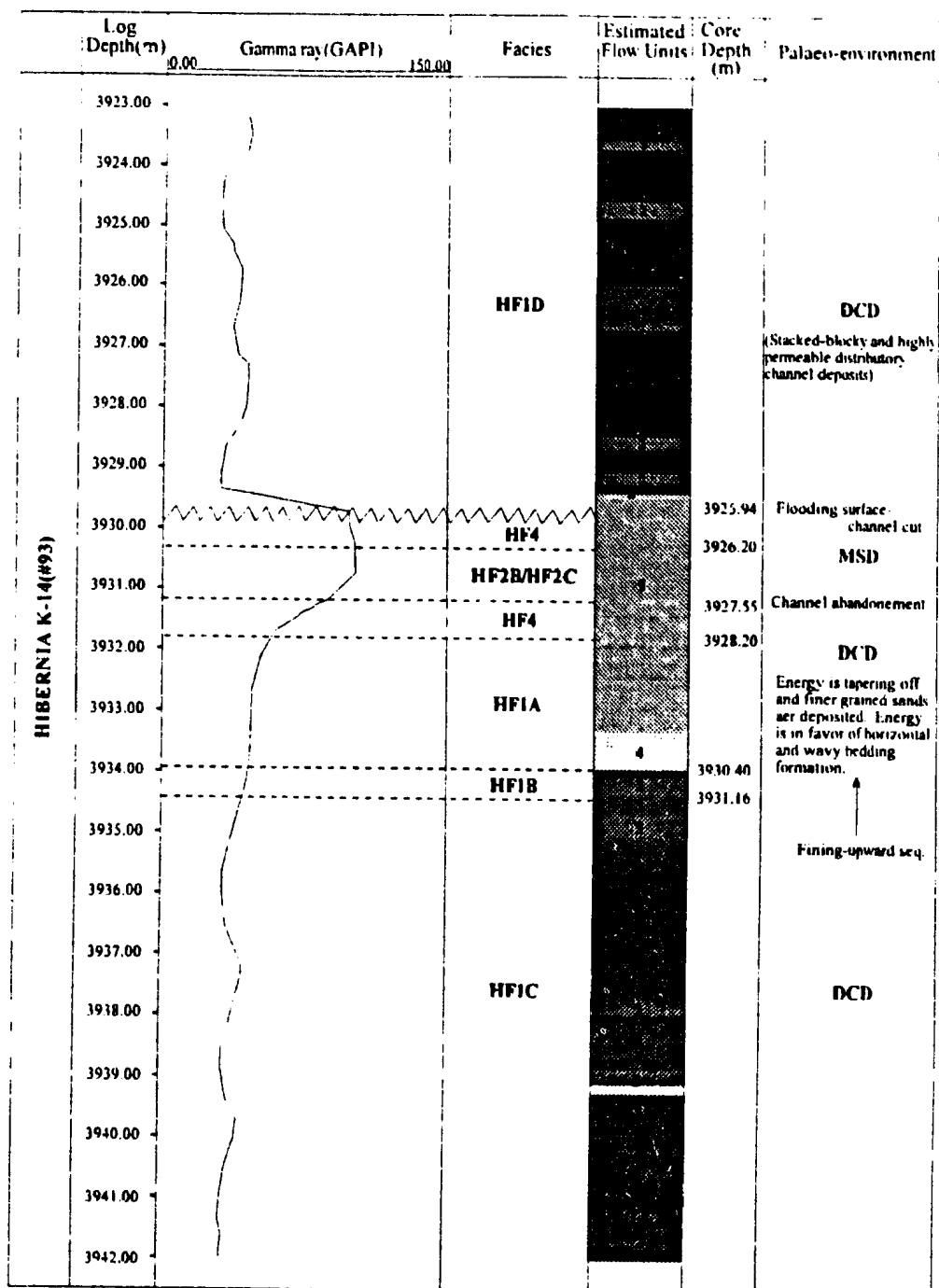
HIBERNIA K-18(#76)

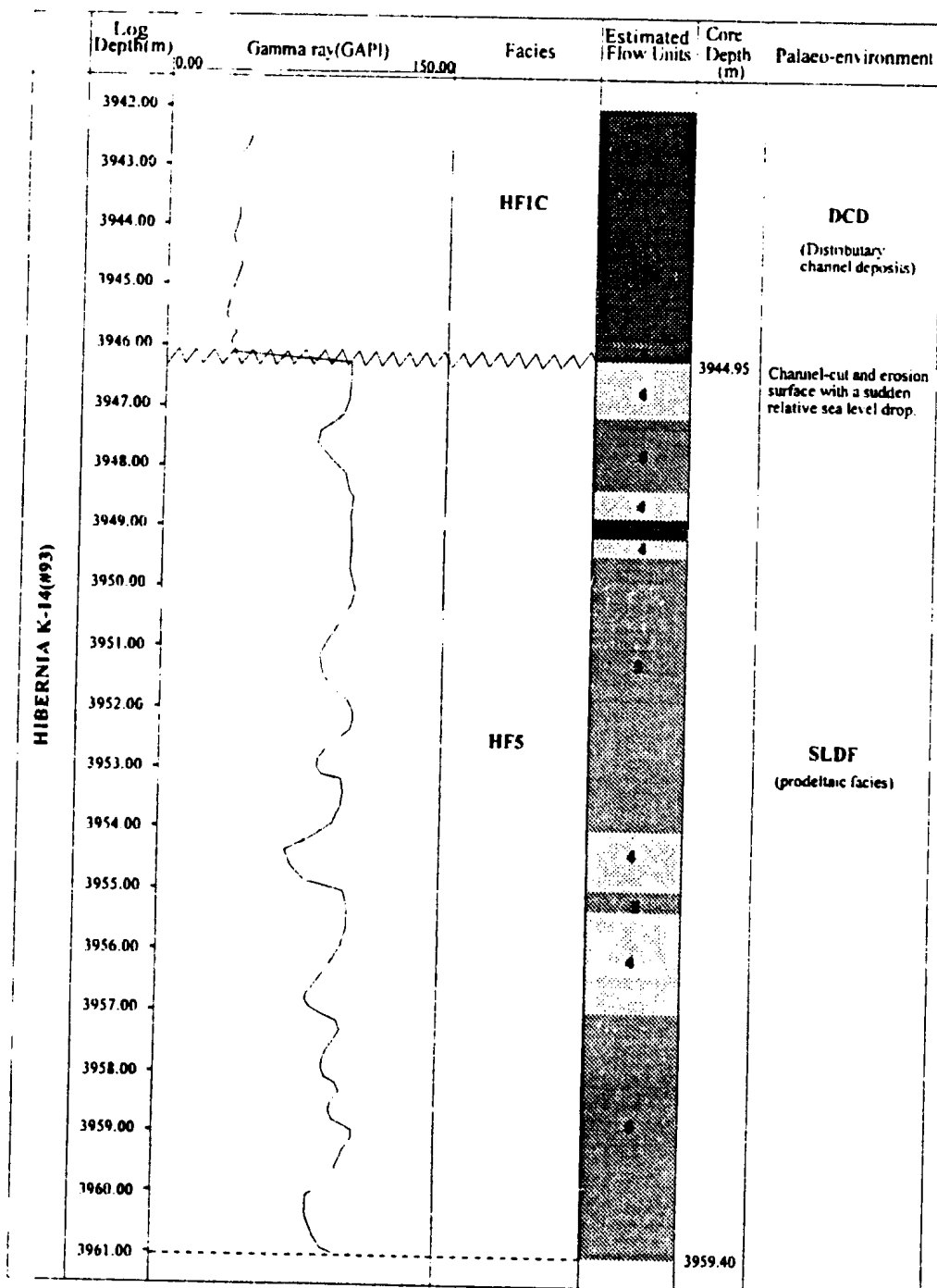


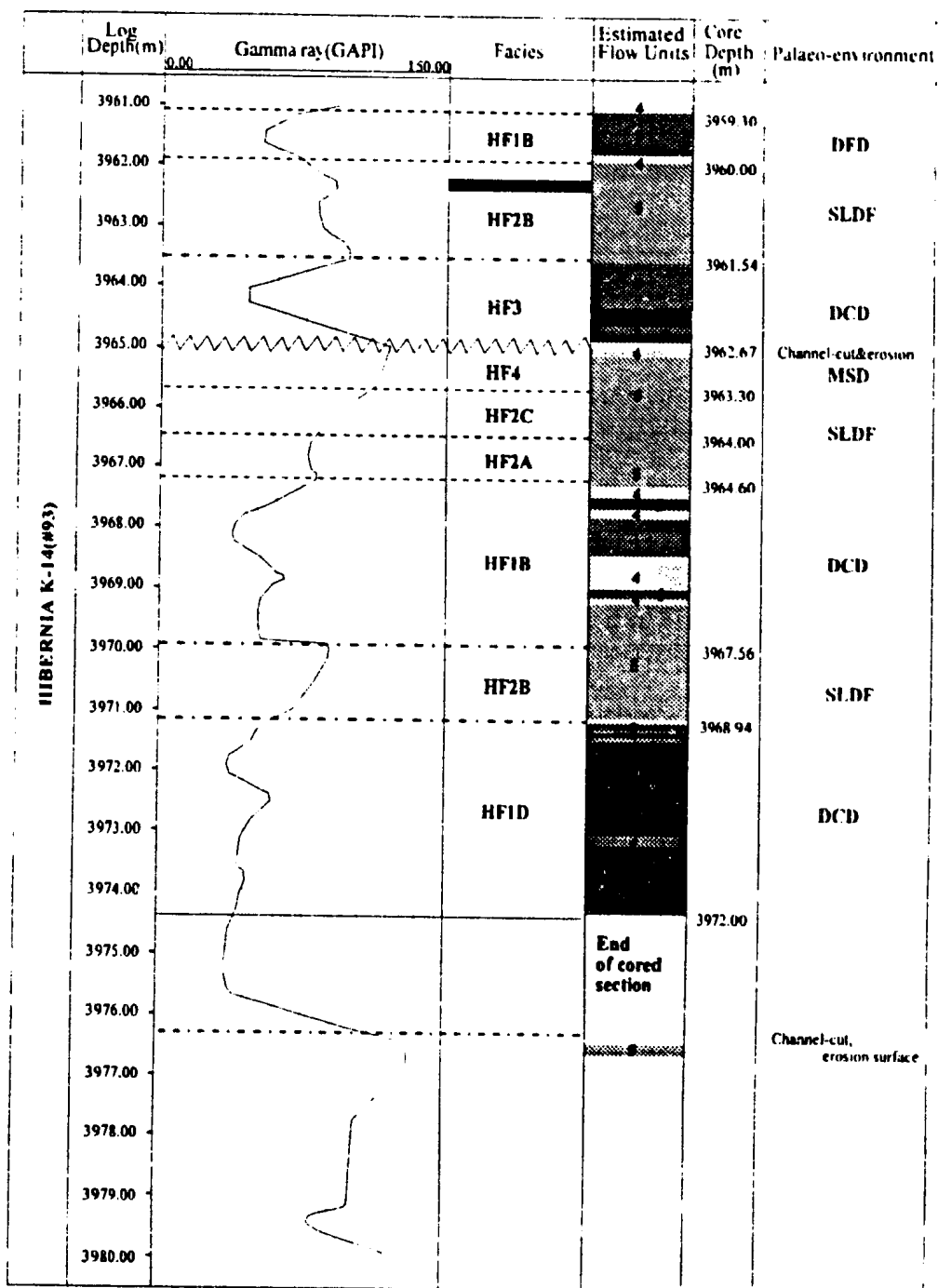
	Log Depth(m)	Gamma ray(GAPI)	Facies	Estimated Flow Units	Core Depth (m)	Palaeo-environment
	0.00	150.00				
HIBERNIA K-14(#93)	3866.00		HF2A			
	3867.00		HF5	→ Log core	3865.80	
	3868.00		HF4		3866.70	
	3869.00		HF1B		3867.80	
	3870.00		HF4			
	3871.00		HF1B			
	3872.00		HF4		3870.35 3871.20	
	3873.00		HF1C			
	3874.00		HF4	4	3872.95	Distributary channel, delta plain, subaqueous levee of delta plain and marine bay deposits, and marsh and swamp deposits generate a serrate log response due to short term sea level changes under a low-energy fluvial influence.
	3875.00		HF1C		3874.00	
	3876.00		HF4			
	3877.00		HF1B			
	3878.00		HF2A	3	3876.05 3877.90	
	3879.00		HF1A			
	3880.00		HF2A			
	3881.00		HF1B		3880.00	
	3882.00		HF4			
	3883.00					
	3884.00		HF1B			
	3885.00					











Appendix III: Distinct mineralogies determined by the beam-spot mode analyses during the SEM/EDS-coupled analysis. For sample and analysis coding system see page 49, chapter 4. *Min*=Mineral, *Q*=Quartz, *K*=Kaolinite, *Sd*=Siderite, *Sm*=Smectite, *I*=Illite, *M*=Muscovite, *Bi*=Biotite, *Dol*=Dolomite, *C*=Calcite, *R*=Rutile, *Syl*=Sylvite, *Ilm*=Ilmenite, *Alb*=Albite, *Pl*=Plagioclase

SP102-HF1A				P269-HF1A	
	1-A-1	1-A1-3	2-A1-2	1-3	1-4
Mg	0	0	1.34	0.93	0
Al	23.32	0.72	21.45	14.32	4.33
Si	43.99	24.81	53.82	61.81	22.06
K	1.41	0	2.84	9.89	4.04
Ca	0	0	0.76	0.98	0
Fe	0.72	65.97	6.37	11.04	69.57
Cr	0	8.50	0.46	0	0
Na	0.12	0	0.70	1.02	0
Cl	0	0	0.14	0	0
P	13.61	0	7.08	0	0
Ti	8.61	0	0.30	0	0
S	8.23	0	4.74	0	0
Cd	0	0	0	0	0
Min	K	Sd	Sm/Bi	Sm/Bi	Sd

P218-HF1B					SP102-HF1B		
	1-A-2	1-A-3	1-A1-1	2-A-2	1-A-1	1-A1-1	1-A1-3
Mg	1.36	19.81	1.65	1.31	2.11	0.28	2.15
Al	7.11	7.84	24.90	22.79	3.1	22.41	3.16
Si	49.54	7.27	40.42	55.79	10.94	47.80	5.34
K	6.43	0.64	6	6.59	0.31	1.98	0
Ca	0.77	6.52	0.61	0.61	66.14	18.56	68.85
Fe	1	33.43	8.98	3.43	1.53	0.84	0.94
Cr	0	0	0	0.06	0.13	0.09	0
Na	2.72	9.05	0.36	0	4.83	0.21	6.03
Cl	3.03	0.81	0.61	0.45	0.45	0.36	0
P	15.29	8.84	3.03	6.18	5.99	4.6	8.79
Ti	0.21	0.07	0.24	0.32	0.21	0.04	0
S	12.32	5.57	12.93	2.36	4.02	2.71	4.74
Cd	0.23	0.15	0.27	0.09	0.23	0.11	0
Min	(I)+Sm	Sd+Dol	Sm/I	I	C	C+K	C

SP249-HF1C P85-HF1C P315-HF1C

	L-2	L-A1-3	2-A1-1	2-A1-2	L-A-1	1-A-2	2-A-1	L-2	L-5	2-A-2
Me	2.55	1.19	0.49	0.07	0.01	0	10.85	0	2.54	0.71
Al	6.65	19.10	9.44	1.10	1.99	0.08	15.75	3.32	39.99	29.56
Si	25.31	65.99	75.02	89.49	80.19	16.44	12.51	94.54	47.88	52.57
K	0.28	6.31	3.27	0.21	0.64	30.00	1.34	0.59	0	2.70
Ca	0	0	0.24	0.31	0.04	19.57	0.31	1.55	0	0.32
Fe	61.03	3.01	1.65	0.21	0.15	0.40	1.01	0	0	0.74
Cr	0.51	0	0.22	0.03	0.18	0	3.10	0	3.79	0.11
Na	2.04	0	0.39	0.02	0.41	0	11.21	0	5.80	0.45
Cl	0.23	0.42	1.10	0.71	0.70	0	4.15	0	0	3.91
P	1.21	3.62	7.83	7.57	9.70	0	8.00	0	0	8.65
Ti	0.17	0.36	0.23	0.07	0.04	0	25.44	0	0	0.27
S	0	0	0	0	5.95	33.51	6.21	0	0	0
Ca	0	0	0	0	0	0	0	0	0	0
Min	Si-Me	BUCH-2	Qtz-Sm	Quartz	Quartz	Amh	Hbl-Me	Quartz	K	Sm+K-2

P208-HF1C1										SP99-HF1C1									
	1-A-1	1-A-2	1-A-3	1-A-1	1-A-3	1-A-1	1-A-3	2-A-1	2-A-3	1-A-1	1-A-3	1-A-1	1-A-3	2-A-1	2-A-3				
Mg	3.87	0.86	0	2.27	0	1.84	1.84	3.98	0	0.68	1.61	0.68	1.61	0	0				
Al	11.83	25.68	14.71	21.98	14.71	4.18	4.18	26.70	14.71	21.74	1.68	21.74	1.68	14.51	14.51				
Si	13.40	46.43	59.12	47.68	59.12	14.69	14.69	45.25	59.12	60.60	4.26	60.60	4.26	68.87	68.87				
K	35.83	10.70	0.27	4.06	0.27	33.59	33.59	4.55	4.06	2.16	0.13	2.16	0.13	0	0				
Ca	0.96	0.04	0	0.25	0	0.90	0.90	0.17	0.25	0.72	0.12	0.72	0.12	0	0				
Fe	5.50	3.17	0.75	3.40	0.75	0.50	0.50	5.22	3.40	1.43	30.79	1.43	30.79	0.30	0.30				
Cr	0.64	0.02	0	0.29	0	0.08	0.08	0	0.29	0	0.05	0	0.05	0	0				
Na	5.87	0	4.06	1.50	4.06	2.88	2.88	2.03	1.50	1.20	2.72	1.20	2.72	0	0				
Cl	15.59	0.16	0.27	0.68	0.27	30.09	30.09	0.56	0.68	0.46	0.75	0.46	0.75	0	0				
P	4.37	7.89	12.64	10.68	12.64	5.29	5.29	6.62	10.68	11.02	3.37	11.02	3.37	9.59	9.59				
Ti	0	0	0	0.03	0	0.37	0.37	0.39	0.03	0	0	0	0	0	0				
S	2.45	4.86	8.19	7.01	8.19	3.90	3.90	4.23	7.01	0	54.51	0	54.51	6.06	6.06				
Cd	0.48	0.19	0	0.16	0	1.50	1.50	0.28	0.16	0	0	0	0	0	0				
Mn	Spinel	Cr-Mn	Al-Mn	Blende	Spinel	Spinel	Spinel	Blende	Blende	Smectite	Pyrite	Smectite	Pyrite	Kaolinite	Kaolinite				

P347-HF1D

P349-HF1D

	1-3	1-4	1-A-1	1-A-2	1-A-1	2-A1-1
Me	0	2.56	0	0.47	0	0.86
Al	0.18	3.58	9.97	5.33	6.63	31.92
Si	32.75	10.24	49.02	14.55	52.92	56.10
K	31.12	14.56	3.12	10.85	0	2.65
Ca	0	3.31	2.88	3.72	0	0.10
Fe	0.23	16.65	12.62	18.69	1.33	0.45
Cr	0	0	0	0.67	0	0
Na	0	6.99	0	0.91	0	0.91
Cl	29.91	34.13	0	32.85	0	0.83
P	2.70	2.77	0	5.32	7.01	6.07
Ti	0.23	0.97	22.03	0.84	32.11	0.02
S	2.85	4.24	1.26	5.80	0	0
Cd	0.02	0	0	0	0	0
Min	Sphcle	Micst+Spd	Ilm	Micst+Spd	K+P+R	Kaolinite

SP74-HF1F

P160-HF1F

SP74-HF1F

P160-HF1F

	1-A-1	1-A-2	1-A1-2	1-A-1		1-A-1	1-A-2	1-A1-2	1-A-1
Me	0	1.12	1.02	7.87	Na	0	0	0.54	11.23
Al	0	11.87	19.38	17.79	Cl	0	0	0	3.18
Si	29.58	62.14	55.06	17.87	P	N/A	9.01	4.65	18.95
K	0	2.47	3.70	1.63	Ti	52.73	1.41	2.22	0.19
Ca	0	0	0.92	0.84	S	2.51	8.98	8.32	13.39
Fe	15.18	3.01	4.13	0	Cd	0	0	0	6.34
Cr	0	0	0	0.71	Min	Ilm	Qtz+R	Qtz+Sm	K

P134-HF3

P345G-HF3

	1-A1-1	2-1	2-A1-1	1-A-1	1-A-2	2-A-2
Me	3.71	0	0	4.90	3.68	0
Al	7.62	2.30	0	15.07	3.40	31.30
Si	72.44	24.64	1.54	55.84	3.67	50.39
K	1.40	0.60	0	1.10	1.34	0
Ca	0.76	0	0	0	0.18	0
Fe	0.43	0	0	0	24.43	0.51
Cr	0	0.03	0	0.70	0	0.54
Na	4.75	21.26	0	5.72	7.90	0
Cl	2.36	50.02	0	1.87	4.56	0
P	6.36	1.15	0	9.06	4.36	10.35
Ti	0.19	0	98.46	0	0.08	0.04
S	0	0	0	5.74	46.40	6.87
Cd	0	0	0	0	0	0
Min	Na-rich Sm	Qtz+H	Rutile	Qtz/K(2)	Pyrite	Kaolinite

SP277-HF1E

P145-HF1E

	1-1	1-A-1	2-A1-1	1-1	1-A-1	1-A1-1	2-A1-2
Mg	0.80	1.41	0.92	1.05	0.85	5.86	1.46
Al	31.07	23.54	6.93	7.04	2.02	7.13	14.48
Si	49.64	47.89	73.97	64.10	64.68	31.21	39.45
K	0.79	0.99	1.63	1.37	0.66	0.51	5.04
Ca	0.11	0.25	1.06	0	0.42	0.27	0.51
Fe	0.78	1.82	1.72	0.64	0.30	32.74	1.29
Cr	0.31	0.18	0	0	0	0.20	0
Na	0.59	1.71	1.22	0.85	1.02	8.79	0.68
Cl	0.73	0.66	0.46	0.73	0.30	1.80	0.61
P	8.83	12.46	11.60	15.03	17.87	6.21	20.36
Ti	0.02	0.50	0.48	0	0.23	0	0.66
S	6.18	8.43	0	9.20	11.46	4.30	14.91
Cd	0.13	0.16	0	0	0.19	0.97	0.55
Min	K	K+Sm	Q+Sm/Bv	Q	Q	Ch	I

SP244-HF1E1

P137-HF1E1

SP244-HF1E1

P137-HF1E1

	1-1	1-A-1	2-A1-1	2-A1-2		1-1	1-A-1	2-A1-1	2-A1-2
Mg	5.63	1.46	3.10	2.66	Na	6.89	2.36	0	0
Al	7.16	13.62	23.14	26.52	Cl	0.26	0	0	0
Si	8.80	62.03	45.04	53.50	P	2.92	10.07	6.00	1.27
K	0.17	4.71	11.57	5.80	Ti	0	0	1.50	0.80
Ca	59.21	1.18	0	0	S	0	0	0	0
Fe	8.97	4.56	9.28	8.61	Cd	0	0	0	0
Ca	0	0	0.36	0.84	Min	C	Ch+M	K/Ch	K/Ch

SCA29-HF1G

	1-A-2	1-A-3	1-A1-1
Mg	10.41	0	1.32
Al	26.55	1.58	18.14
Si	31.10	88.69	57.11
K	0.75	0	1.97
Ca	0.06	0	0.05
Fe	15.62	1.39	0.98
Cr	0.07	0.24	0.04
Na	4.44	0	7.54
Cl	0.60	0	0.41
P	6.47	5.57	7.94
Ti	0	0	0.08
S	3.79	2.53	4.25
Cd	0.10	0	0.18
Min	Blotite	Quartz	Albite

SP162-HF6

	1-A-2	1-A-3	2-A-1	2-A-2		1-A-2	1-A-3	2-A-1	2-A-2
Mg	0.21	10.24	1.56	1.57	Na	0.92	11.57	1.60	0.68
Al	27.10	12.08	11.50	23.71	Cl	0.54	5.40	1.23	1.49
Si	40.71	12.24	59.77	50.54	P	17.25	8.10	11.59	8.68
K	0.42	2.26	3.49	6.17	Ti	0.03	0.39	0.27	0.06
Ca	0.17	1.92	0	0.12	S	12.26	6.81	7.86	5.61
Fe	0	26.39	0.62	1.06	Cd	0.20	2.61	0.38	0.32
Cr	0.18	0	0.12	0	Min	K	Sd	Qtz	Kz

P147-HF2A

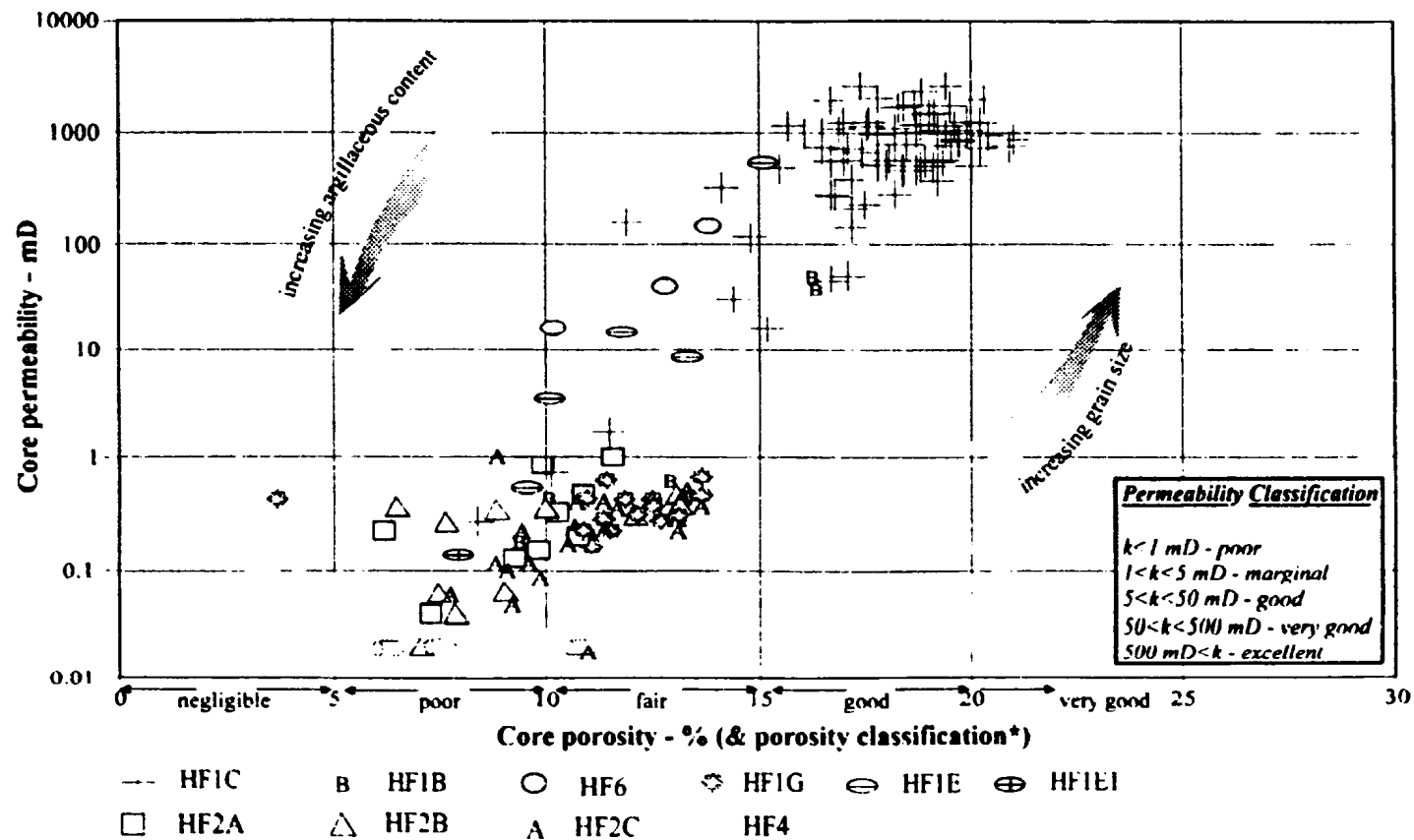
SP103-HF2B

SP228-HF2C

	1-A-2	1-A1-2	2-A-3	1-A1-2	1-A1-3	1-A2-1	2-1	2-A1-1	2-A1-1
Mg	2.77	8.89	0	1.63	0	0.91	0	0.30	0.39
Al	23.12	12.12	11.03	28.58	38.00	27.92	20.59	35.19	19.17
Si	42.34	20.44	34.62	49.13	56.44	55.27	44.98	58.88	56.33
K	6.61	2.40	0	10.31	0.47	7.74	16.02	0.66	1.69
Ca	0.15	5.28	2.65	0.14	0.08	0.10	0.76	0	0.96
Fe	2.16	37.56	0.47	5.18	0.40	1.60	13.54	0.20	1.38
Cr	0	0	0	0	0.10	0.06	1.41	0	0
Na	3.13	2.70	0	0	0	0.66	0	0	5.10
Cl	1.14	0.35	0	0	0	0.21	0	0.22	0.32
P	11.10	6.11	3.14	7.70	4.17	5.90	0	4.37	11.45
Ti	0.41	0	39.10	2.33	0.35	0.12	2.69	0	1.01
S	6.62	4.17	8.98	0	0	0	0	0	0
Cd	0.44	0	0	0	0	0	0	0	0
Min	M	Bt	Pl:R	*	K	M	M	K	Alb(?)

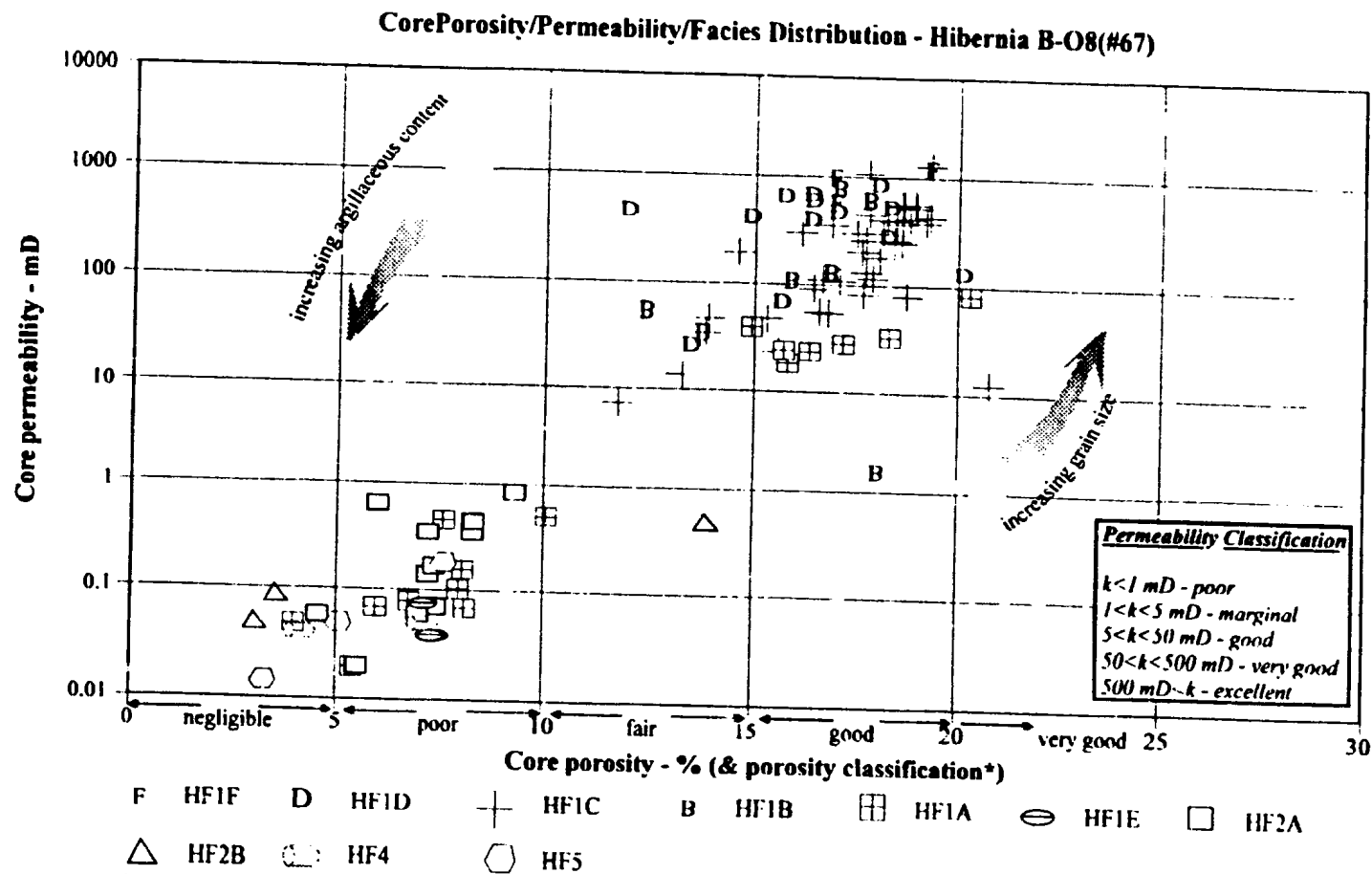
APPENDIX IV- Core porosity - core permeability/lithofacies distribution crossplots of the Hibernia Formation in 5 Hibernia wells (Hibernia B-27; Hibernia B-08; Hibernia C-96; Hibernia K-18; Hibernia K-14).

Core Porosity/Permeability/Facies Distribution - Hibernia B-27(#92)



* porosity classification by North (1985)

Figure IV-1: Composite porosity/permeability facies relationship in the plugged section of the cored interval of Hibernia B-27(#92).



* porosity classification by North (1985)

Figure IV-2: Composite porosity/permeability/facies relationship in the plugged sections of the cored interval of Hibernia B-O8(#67).

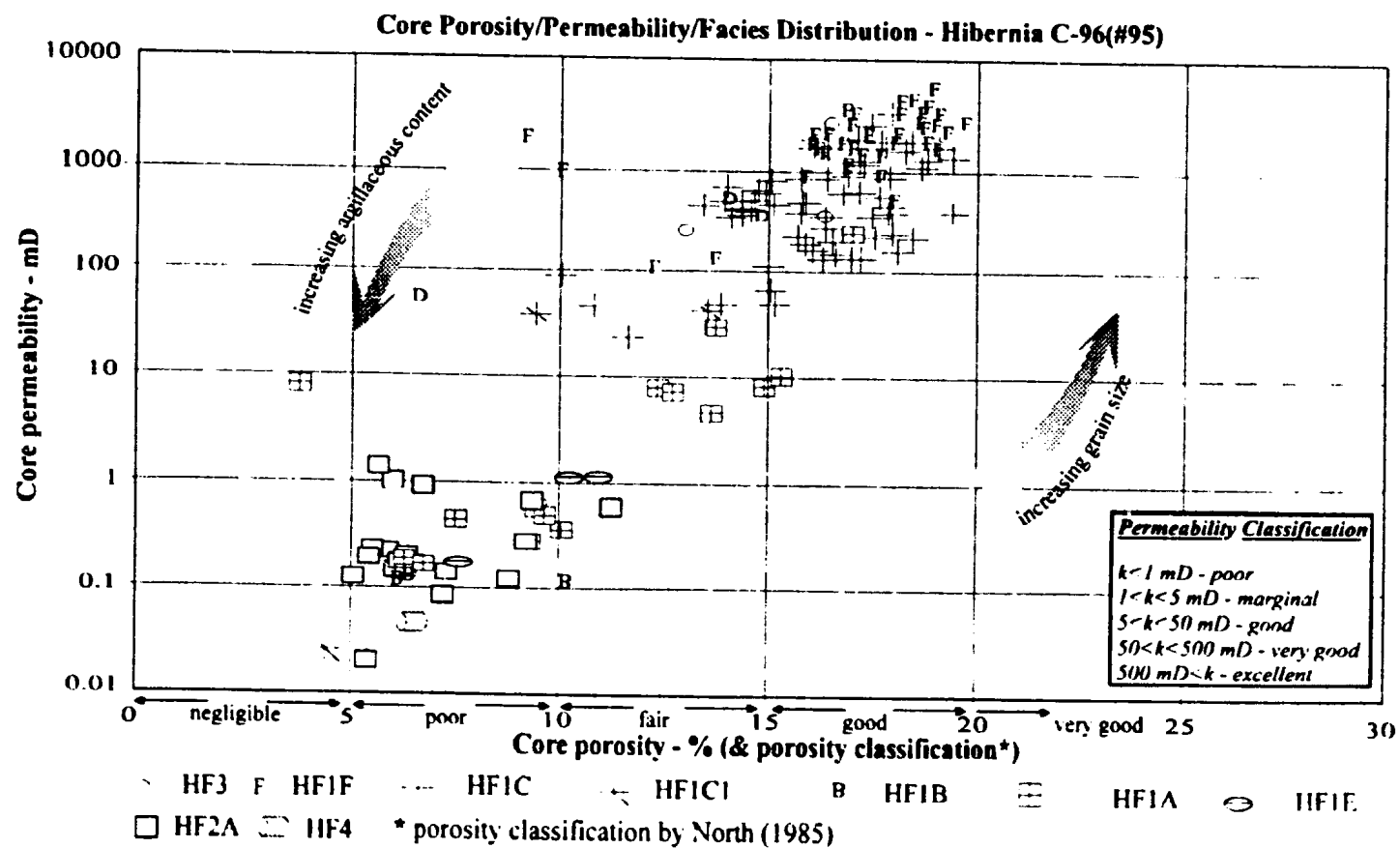


Figure IV-3: Composite porosity/permeability/facies relationship in the plugged sections of the cored interval of Hibernia C-96(#95).

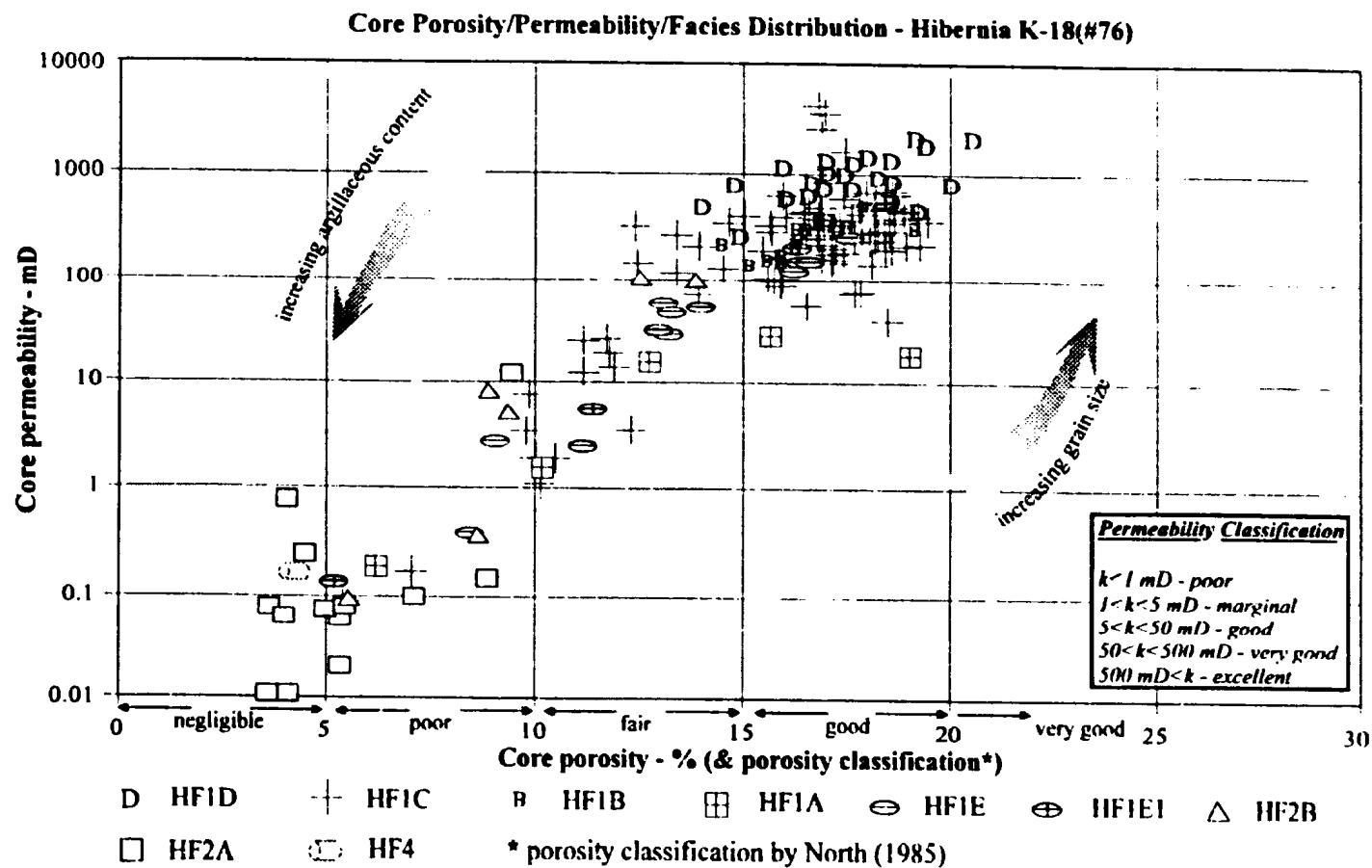


Figure IV-4: Composite porosity/permeability/facies relationship in the plugged sections of the cored interval of Hibernia K-18(#76).

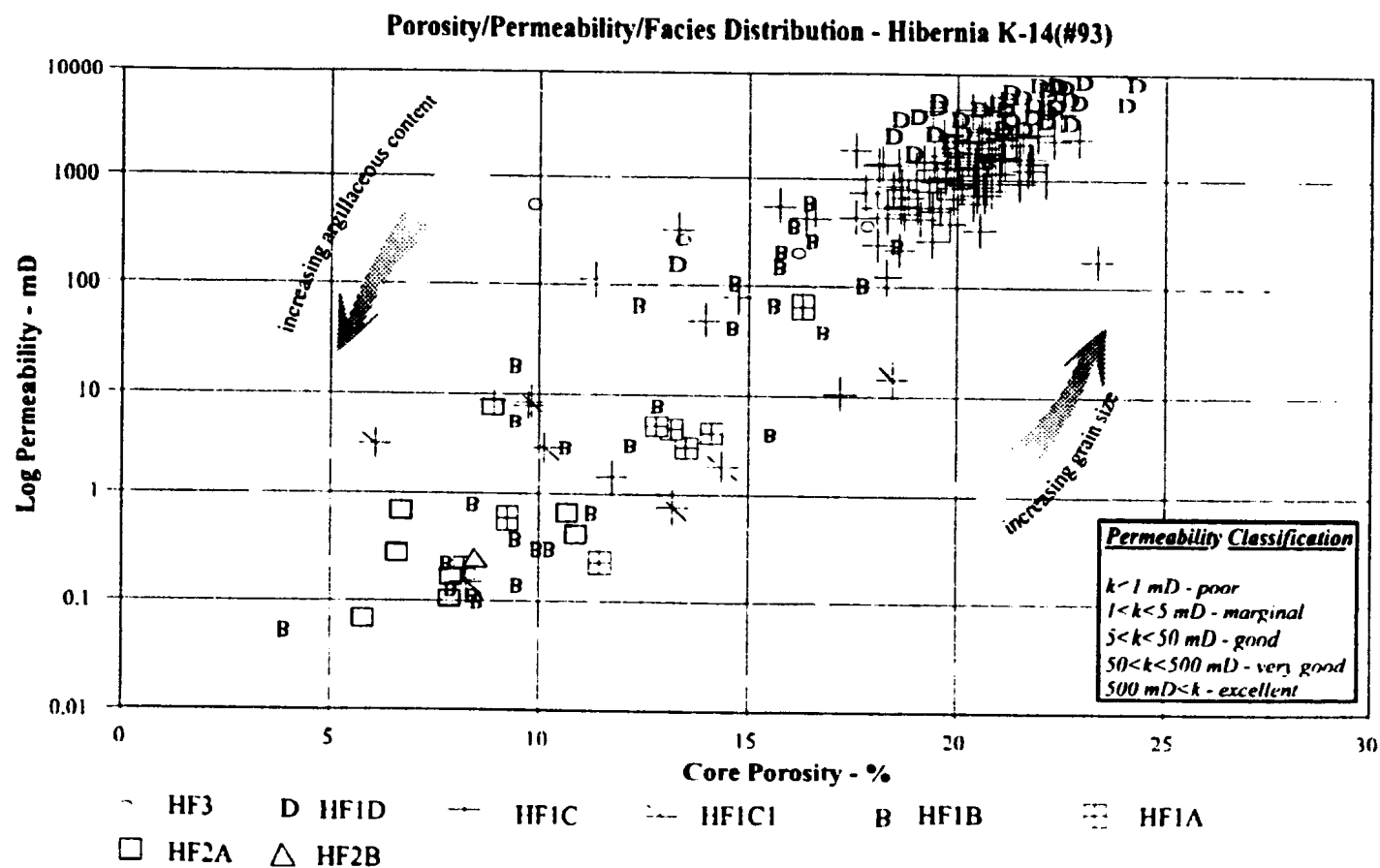


Figure IV-5: Composite porosity/permeability/facies relationship in the plugged section of the cored interval of Hibernia K-14(#93).

APPENDIX V- 3-dimensional comparisons of

- a) hydraulic flow units (HU) - lithofacies distributions**
- b) hydraulic flow units (HU) - reservoir quality zones (RQZ)**

In the Hibernia Formation.

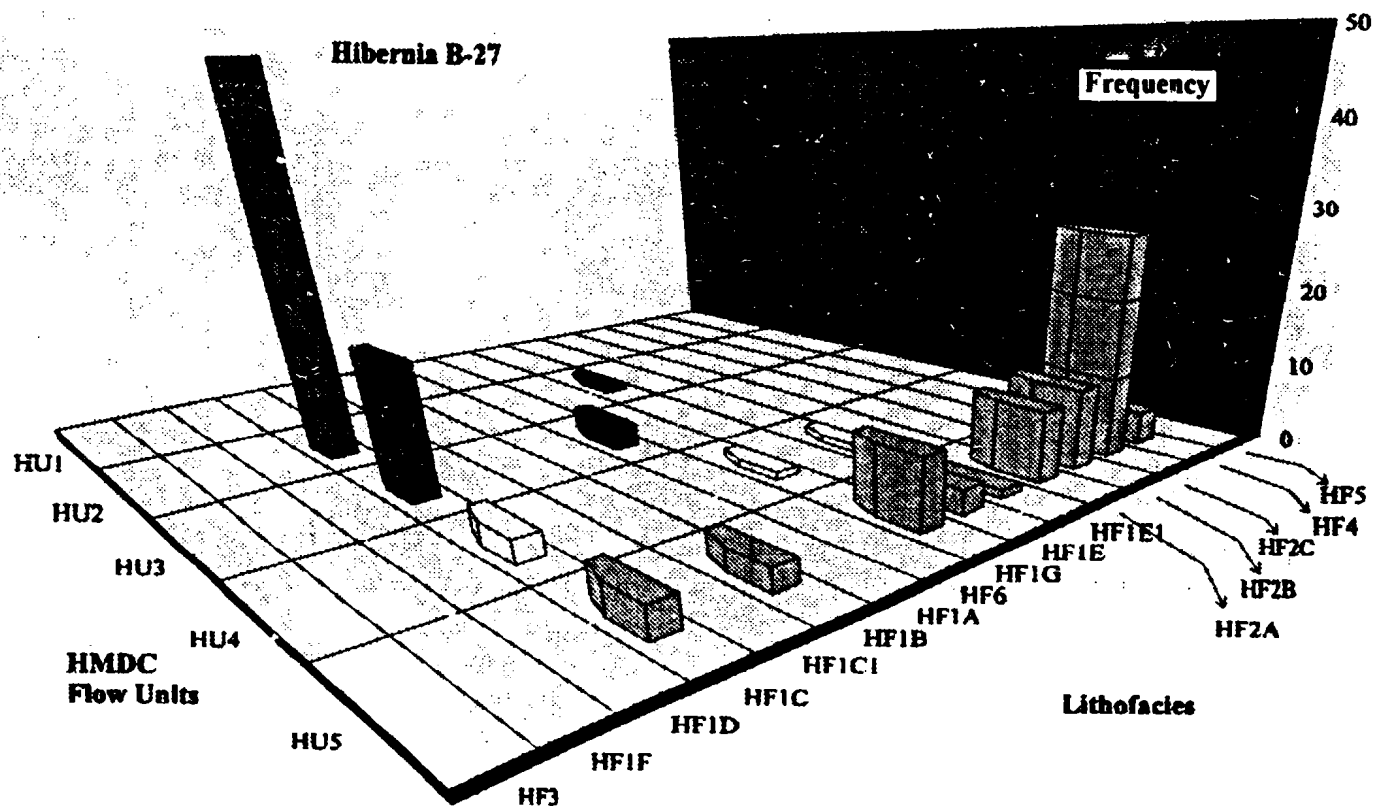


Figure Va-1: Hydraulic flow units - lithofacies distribution of the Hibernia Formation in Hibernia B-27.

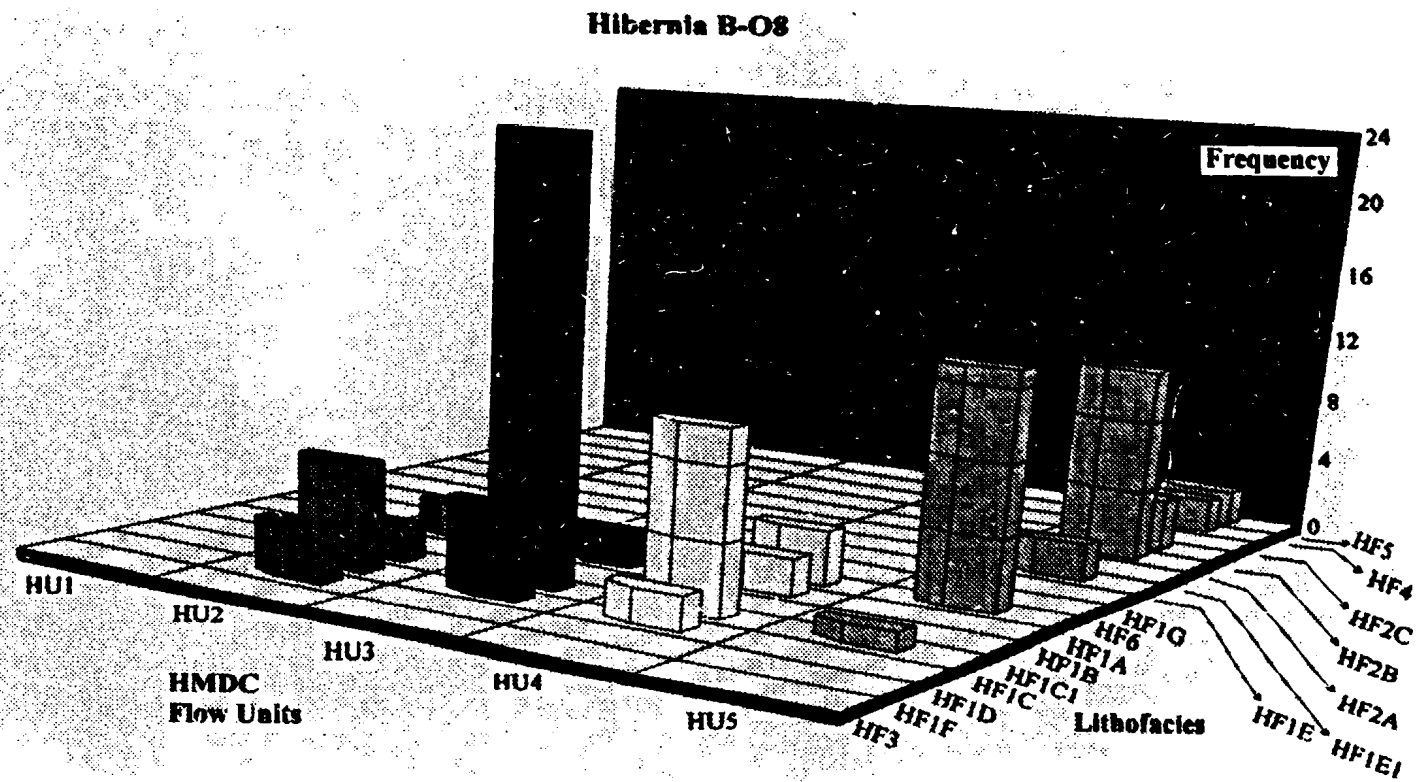


Figure Va-2: Hydraulic flow units - lithofacies distribution of the Hibernia Formation in Hibernia B-08.

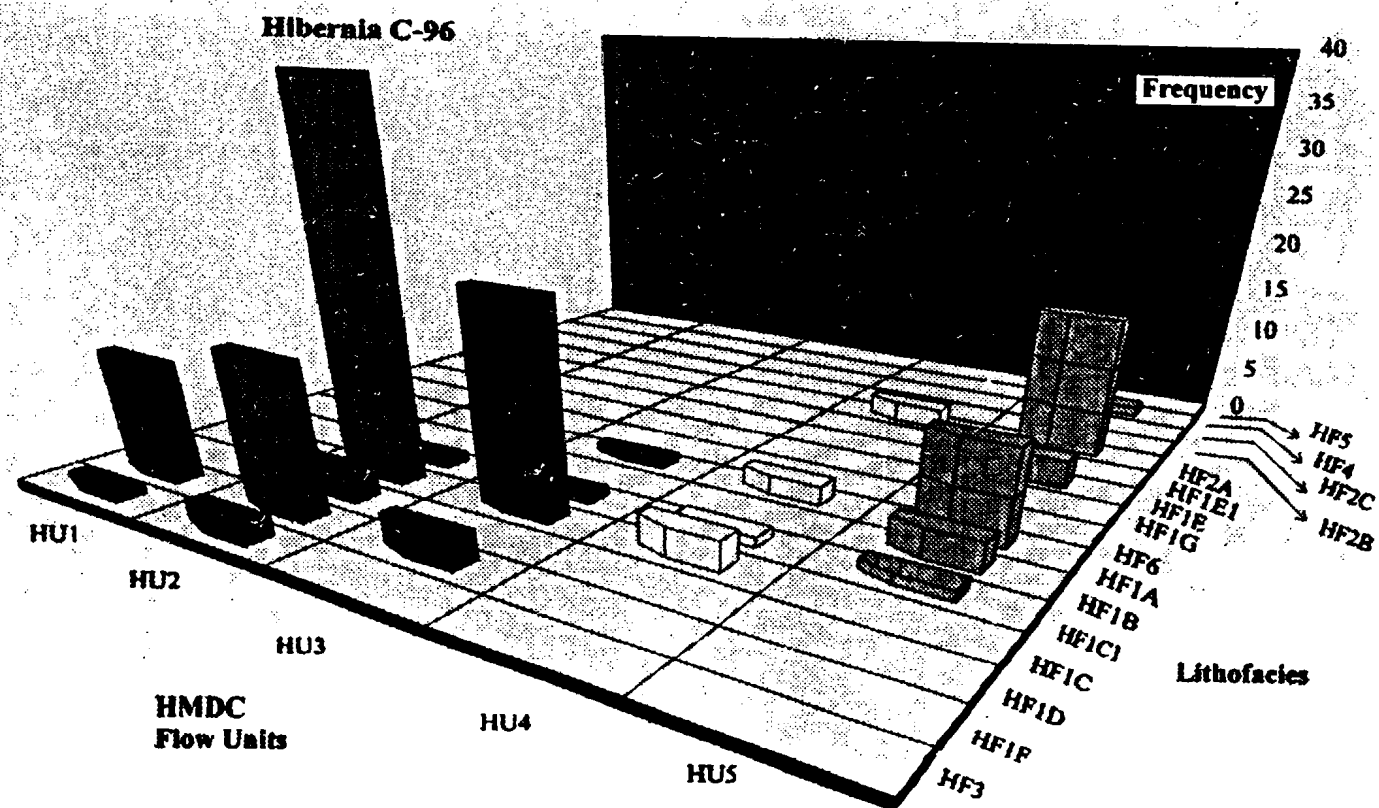


Figure Va-3: Hydraulic flow units - lithofacies distribution of the Hibernia Formation in Hibernia C-96.

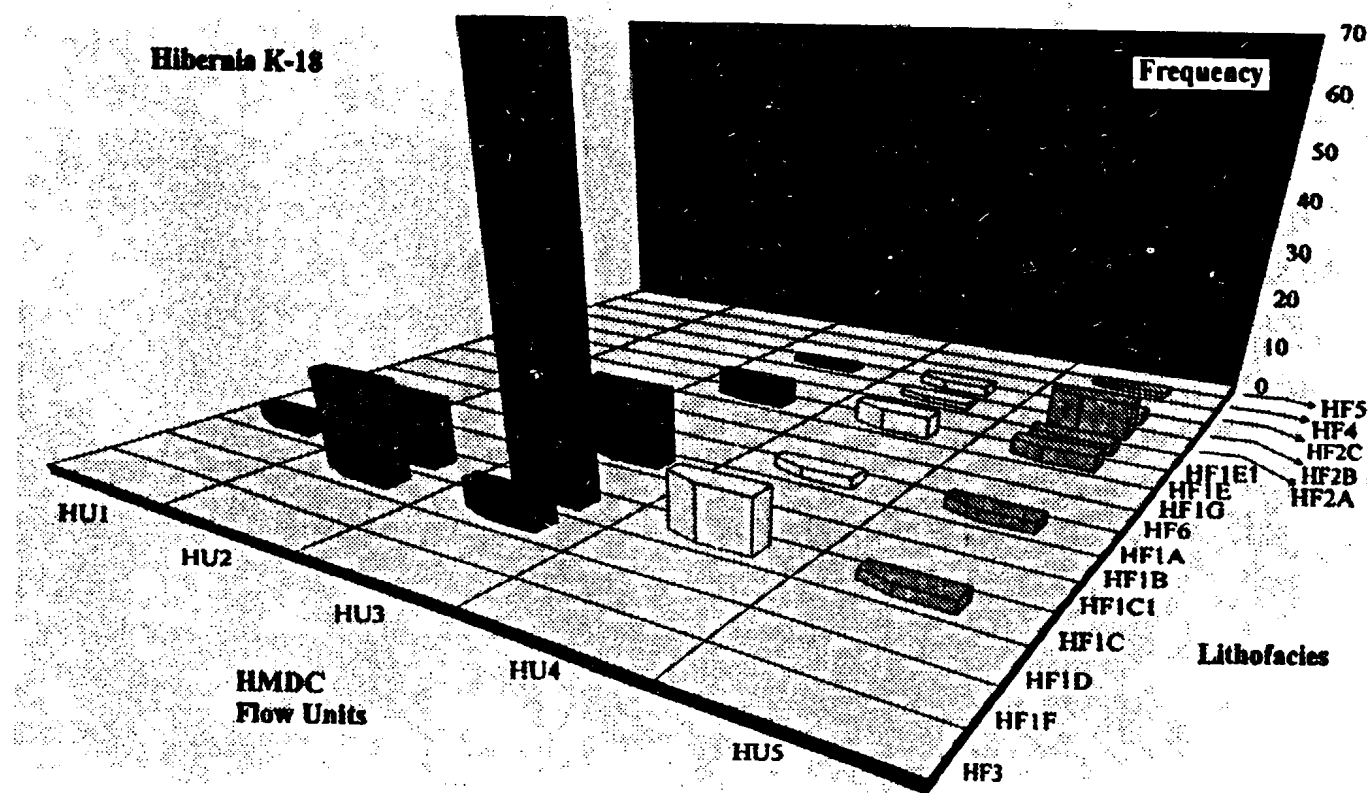


Figure Va-4: Hydraulic flow units - lithofacies distribution of the Hibernia Formation in Hibernia K-18.

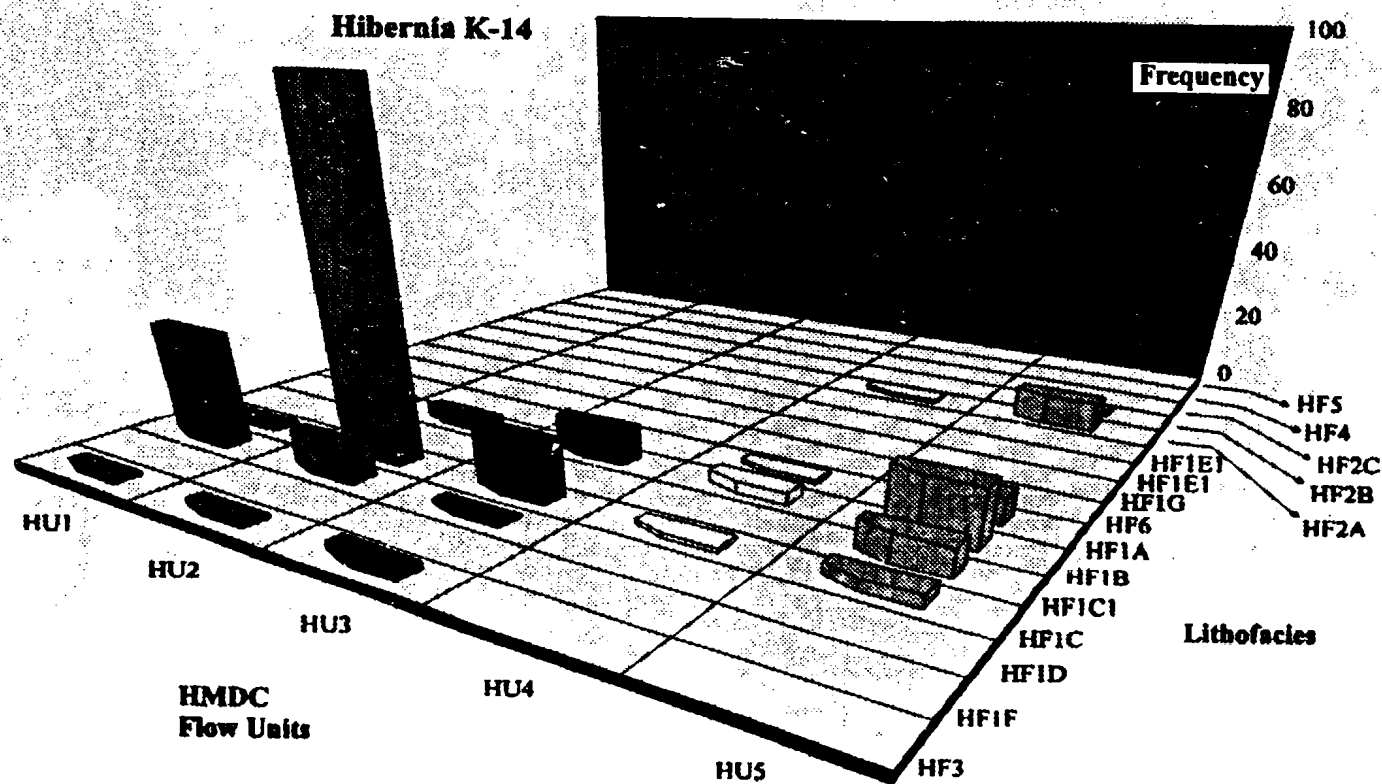


Figure Va-5: Hydraulic flow units - lithofacies distribution of the Hibernia Formation in Hibernia K-14.

Hibernia B-27

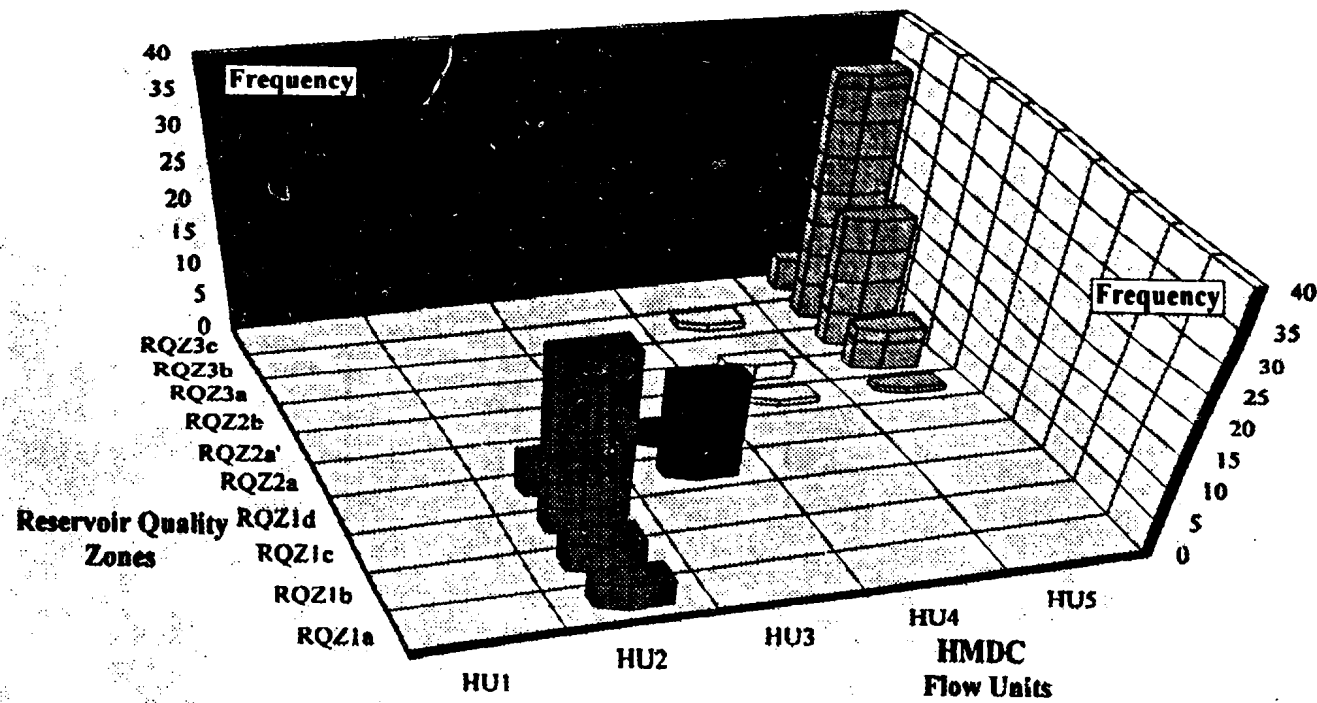


Figure Vb-1: Hydraulic flow units - reservoir quality zone (RQZ) distribution of the Hibernia Formation in Hibernia B-27.

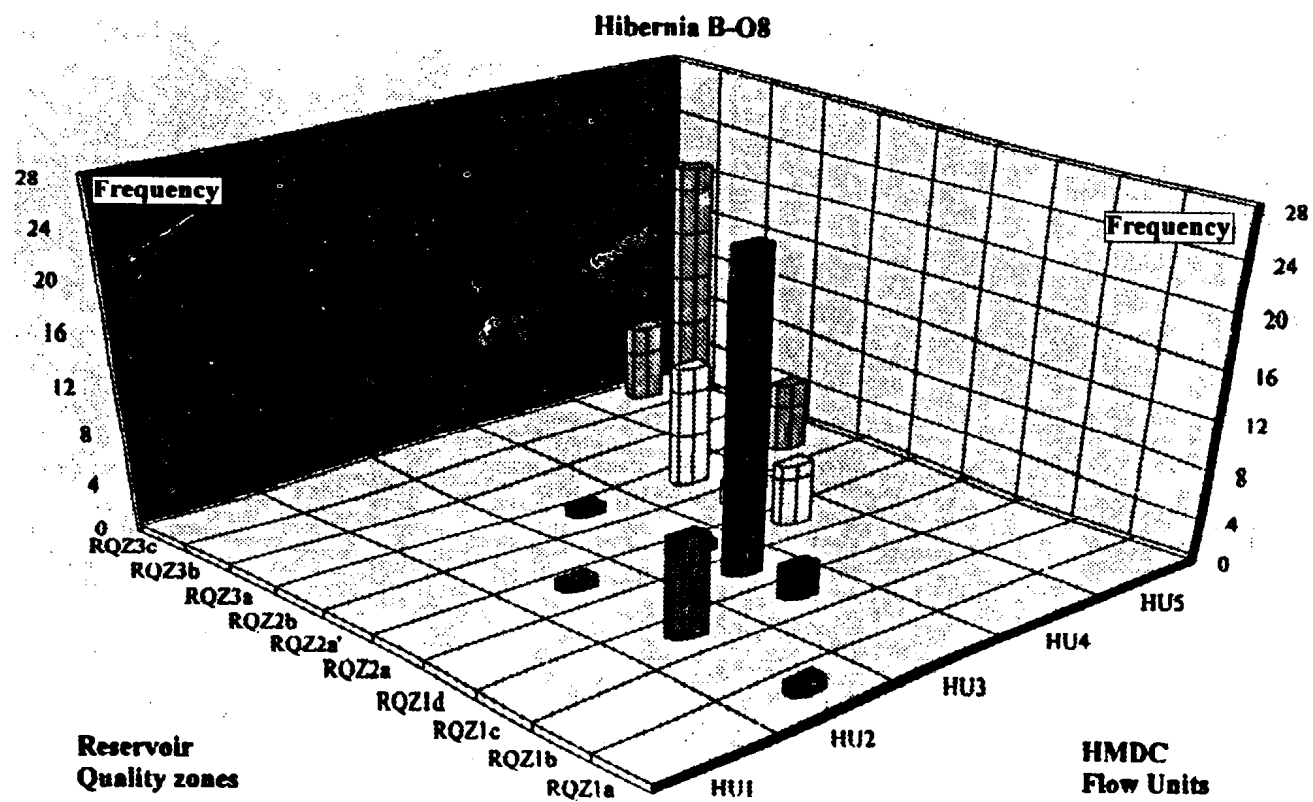


Figure Vb-2: Hydraulic flow units - reservoir quality zone (RQZ) distribution of the Hibernia Formation in Hibernia B-O8.

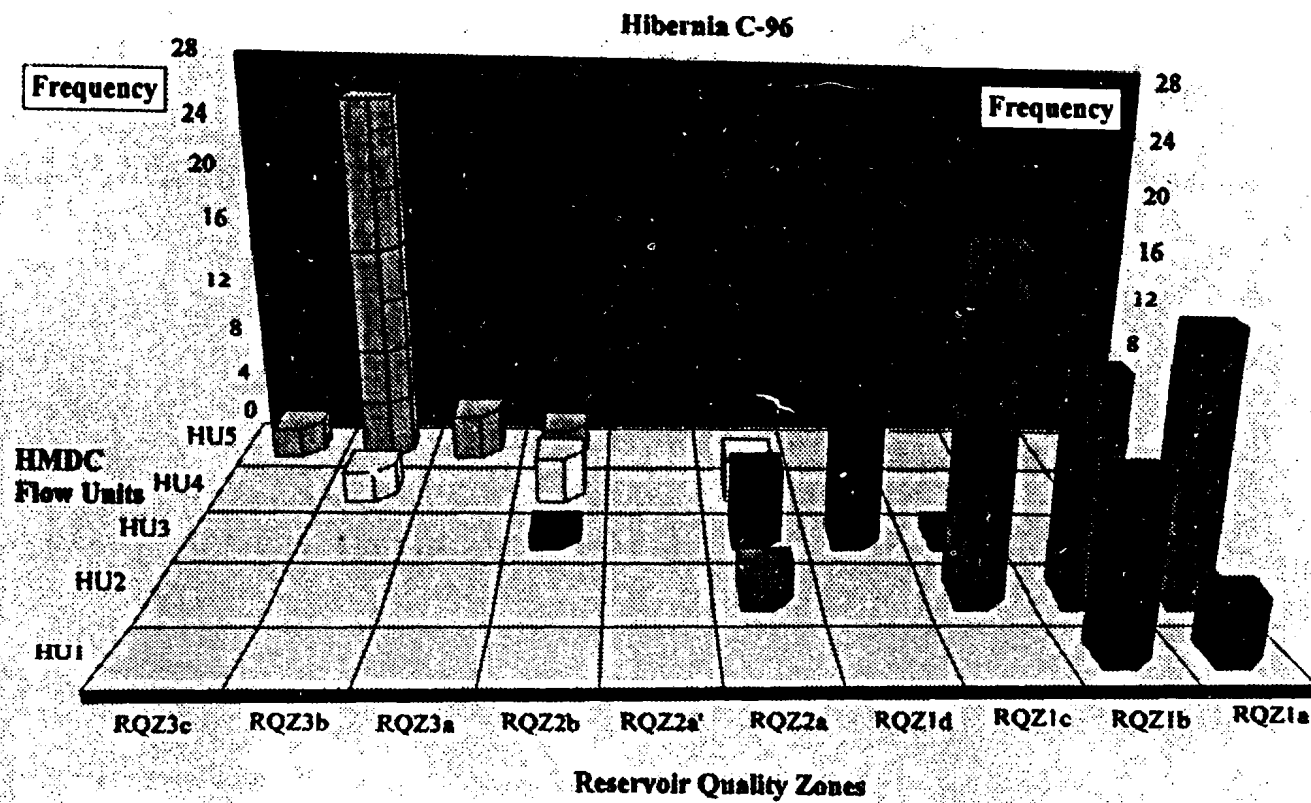


Figure Vb-3: Hydraulic flow units - reservoir quality zone (RQZ) distribution of the Hibernia Formation in Hibernia C-96.

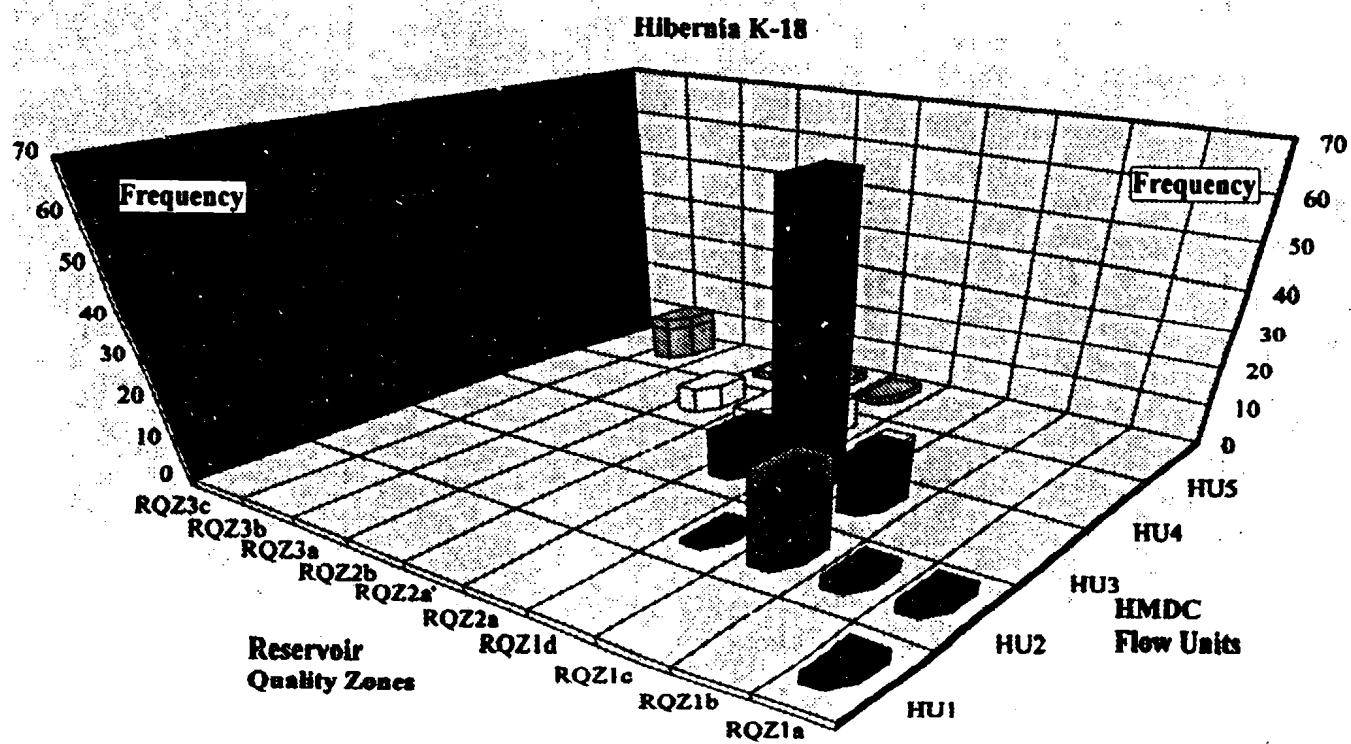


Figure Vb-4: Hydraulic flow units - reservoir quality zone (RQZ) distribution of the Hibernia Formation in Hibernia K-18.

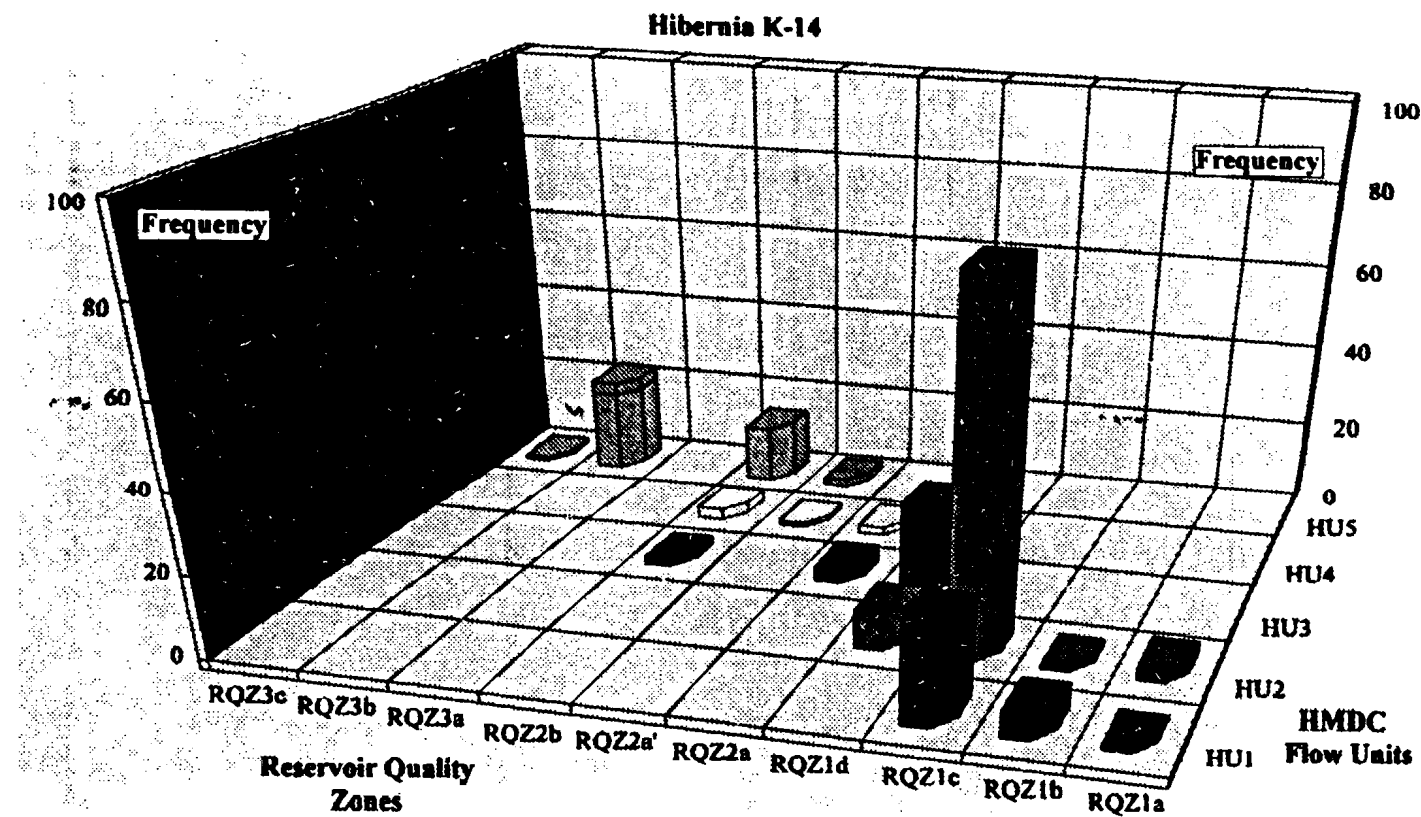
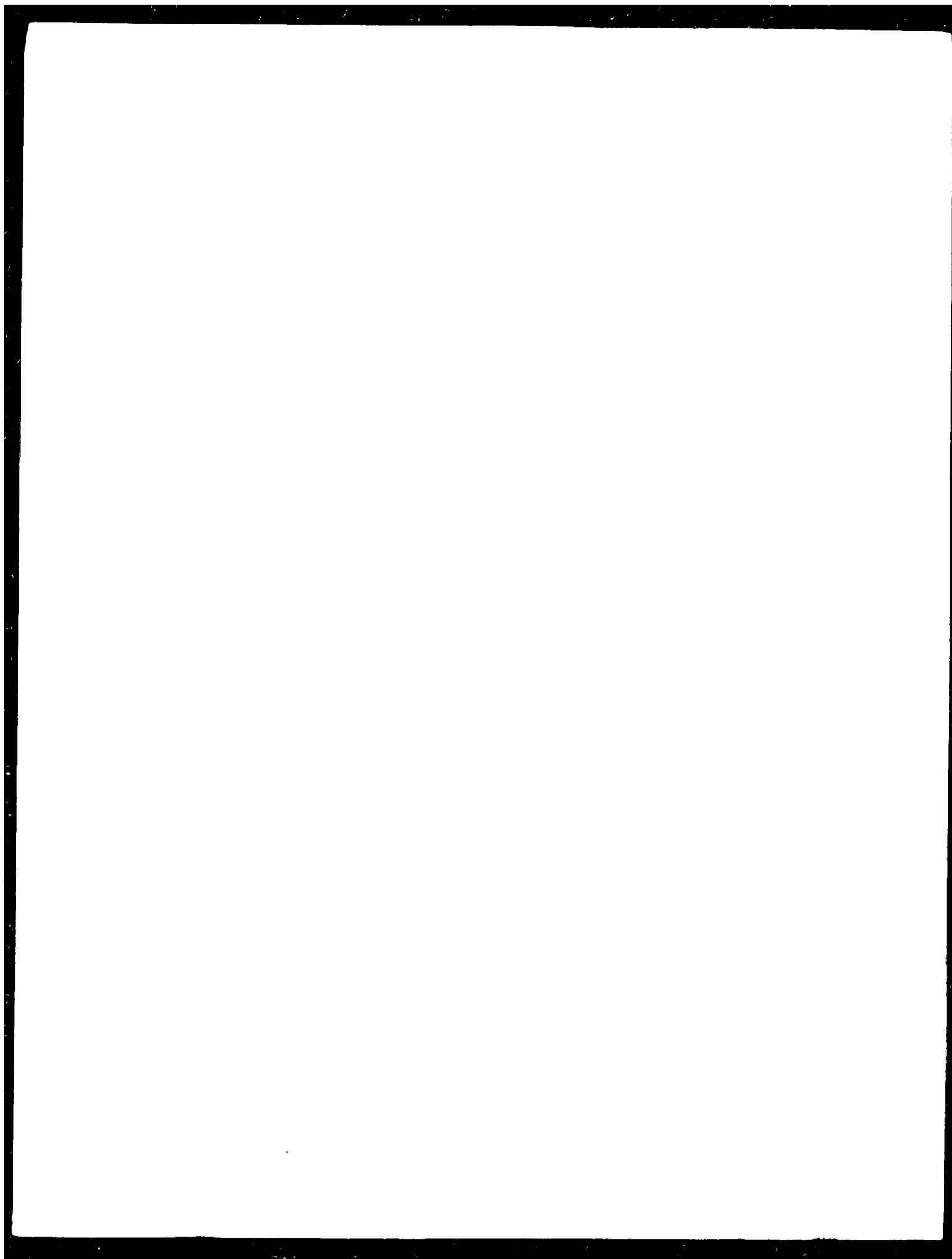


Figure Vb-5: Hydraulic flow units - reservoir quality zone (RQZ) distribution of the Hibernia Formation in Hibernia K-14.

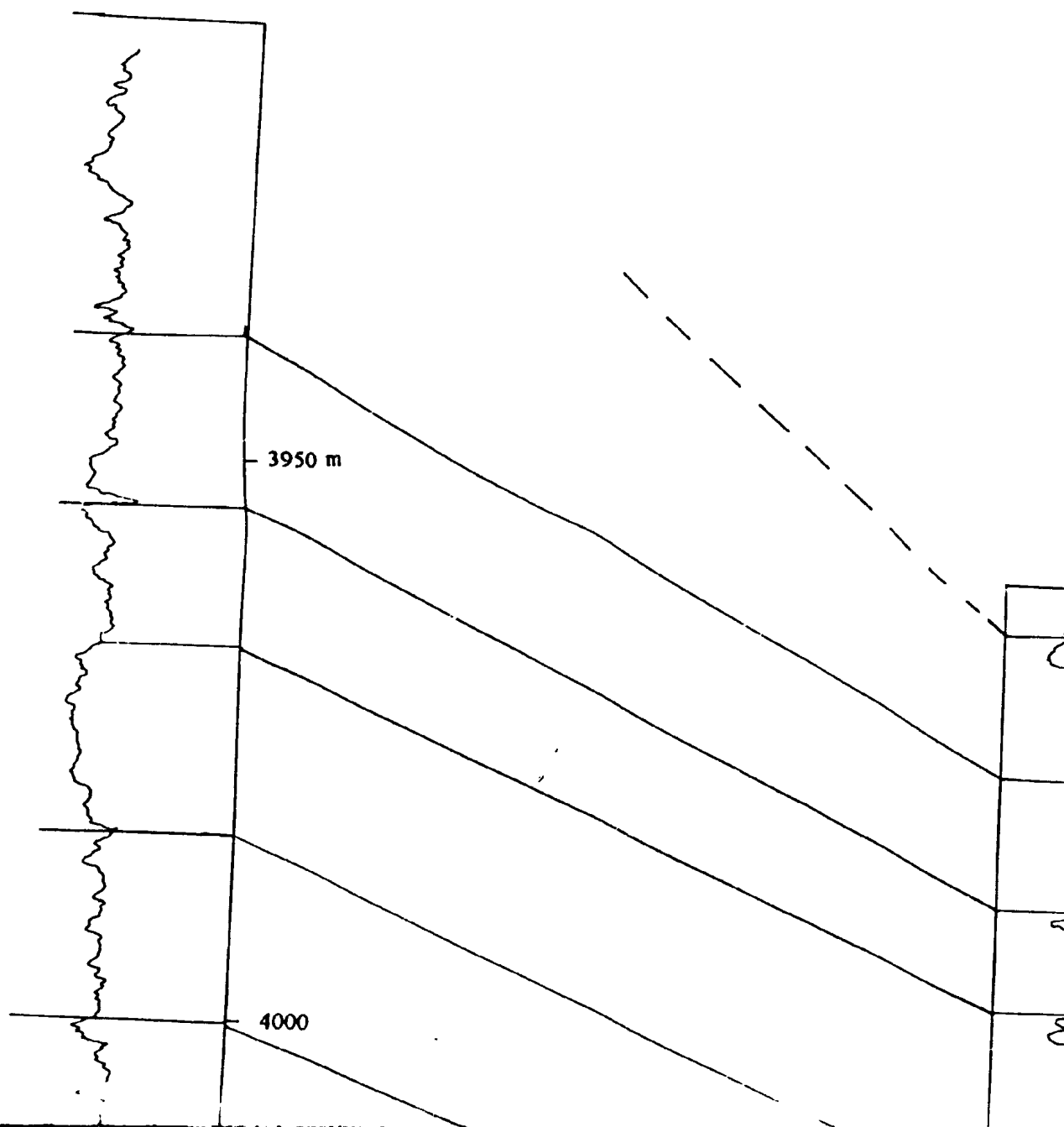


O-35

KB.4788.5 m



3.7 km



K-14

KB.4462.0 m

P-15

KB.4406.8 m

2.6 km

HIBER

3850m

3750m

P-15

KB.4406.8 m

C-96

KB.4420.0 m

2.9 km

HIBERNIA OIL FIELD

3750m

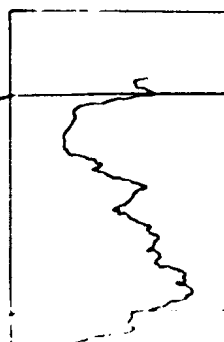
B-27

KB.4380.0 m

5.3 km



2.9 km



386.0m

C-96
KB.4420.0 m

B-2
KB.4380

5.3 km

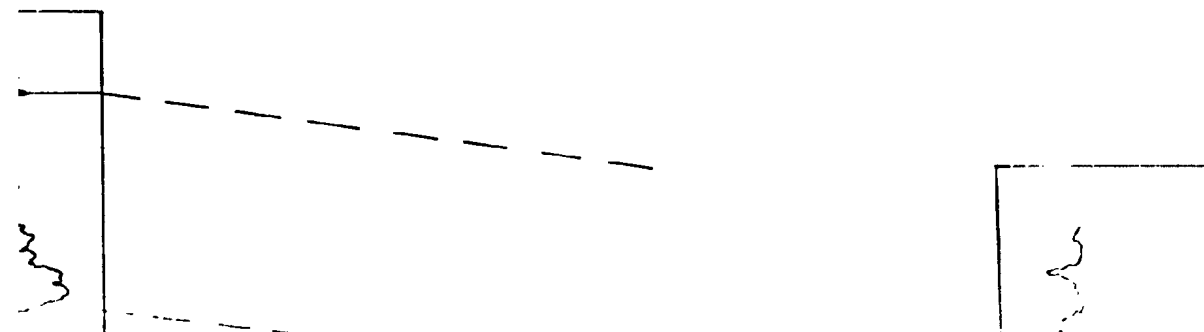
FIELD



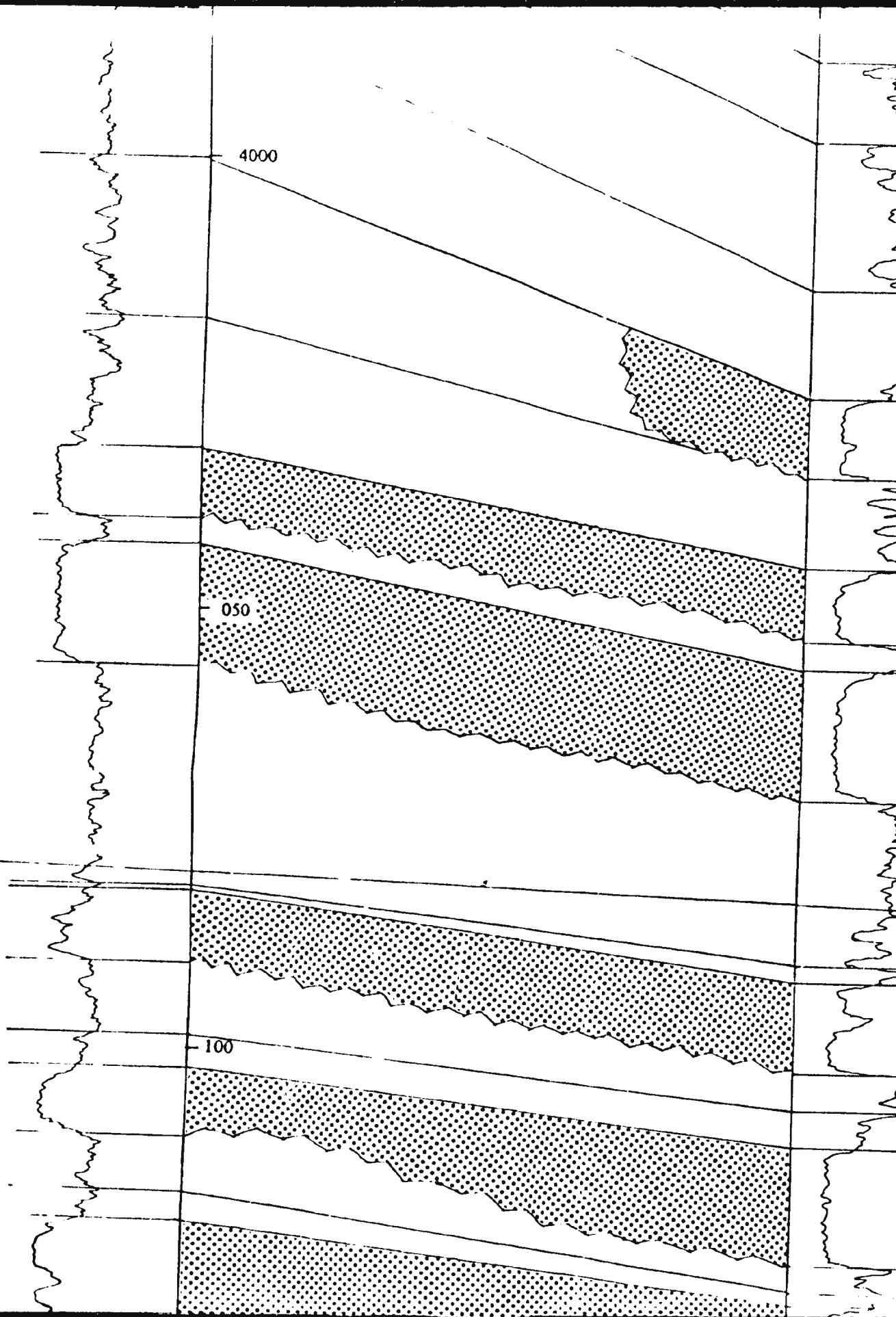
-27
180.0 m

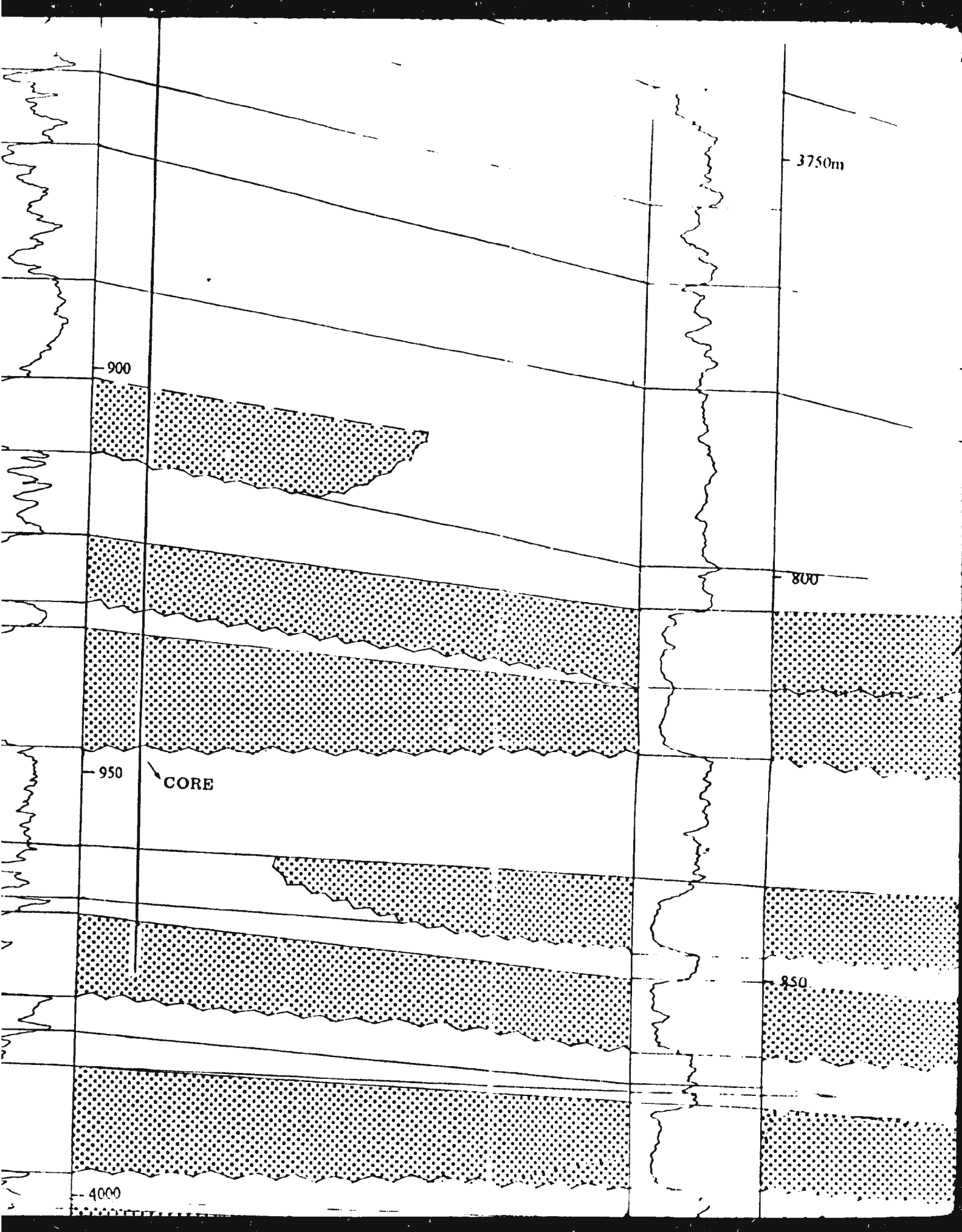
K-18
KB.5093.3m

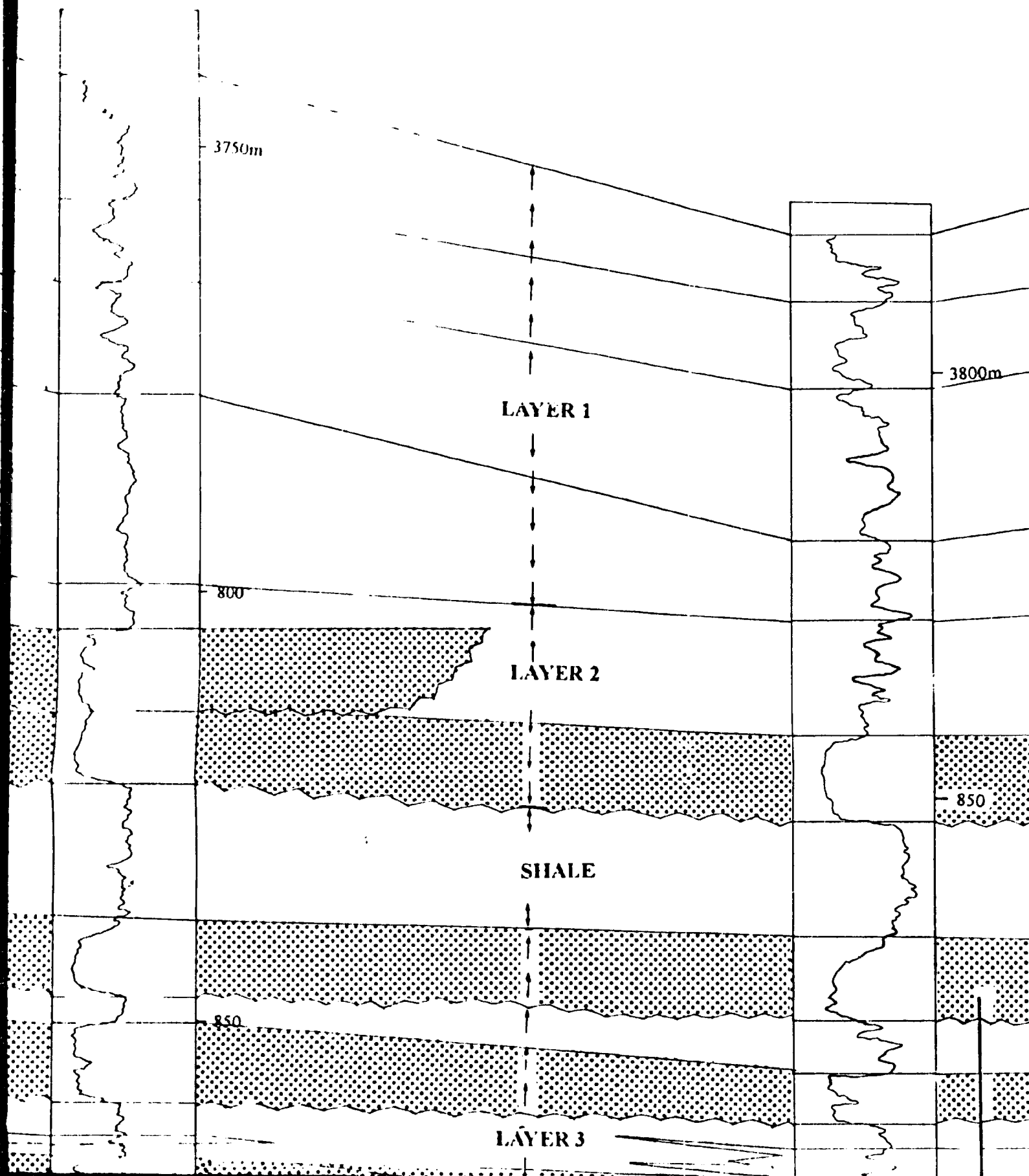
2.9 km

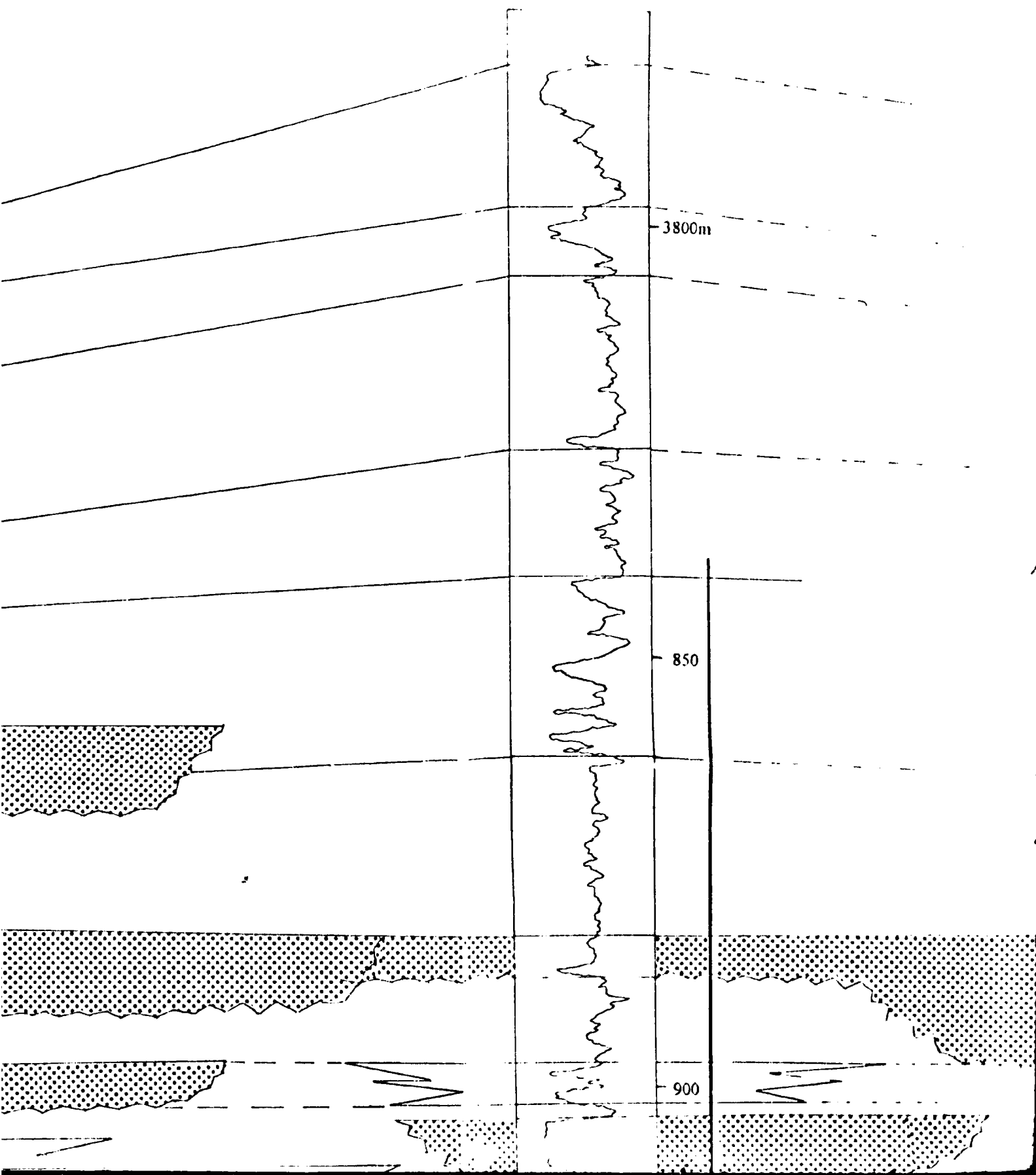


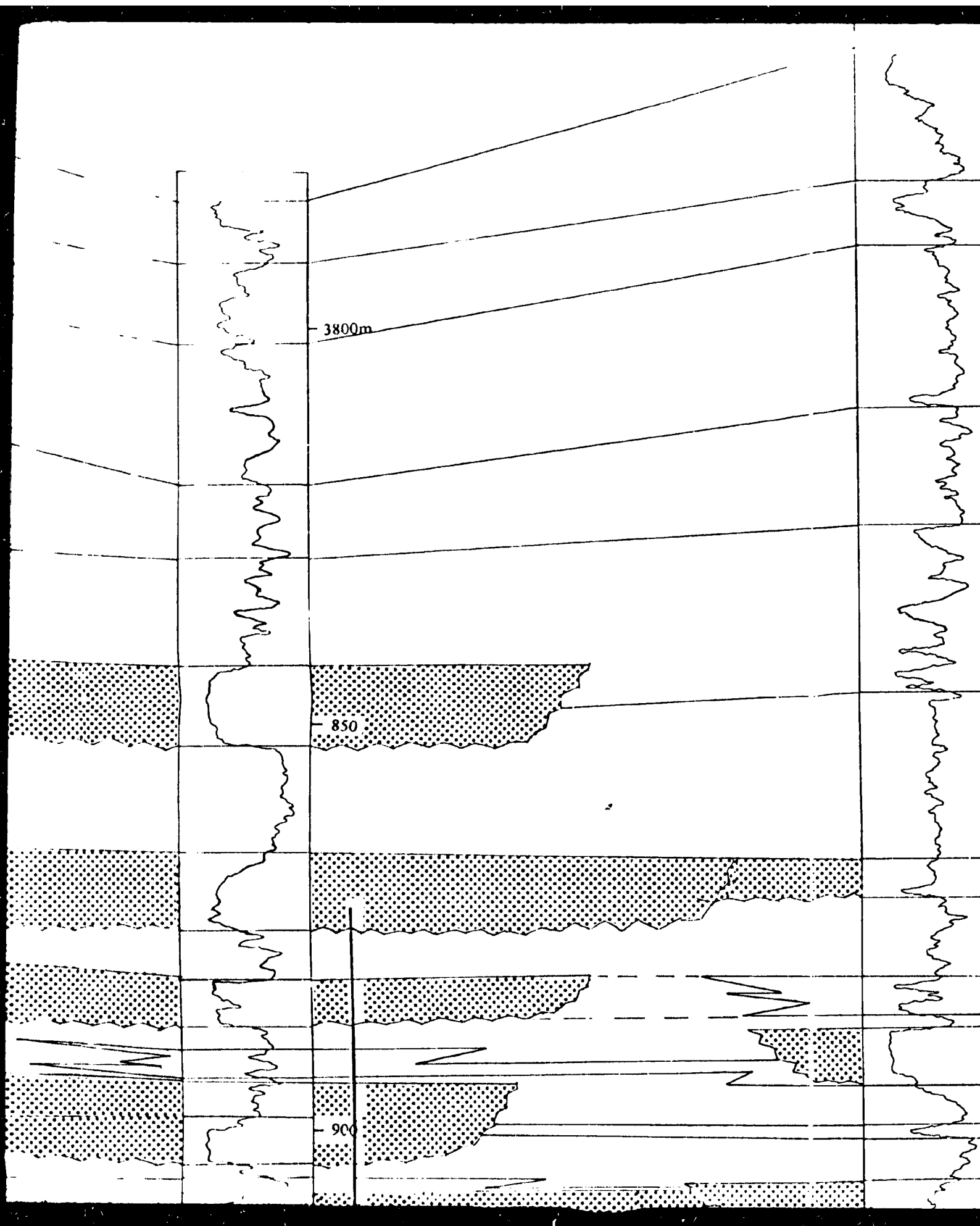
A

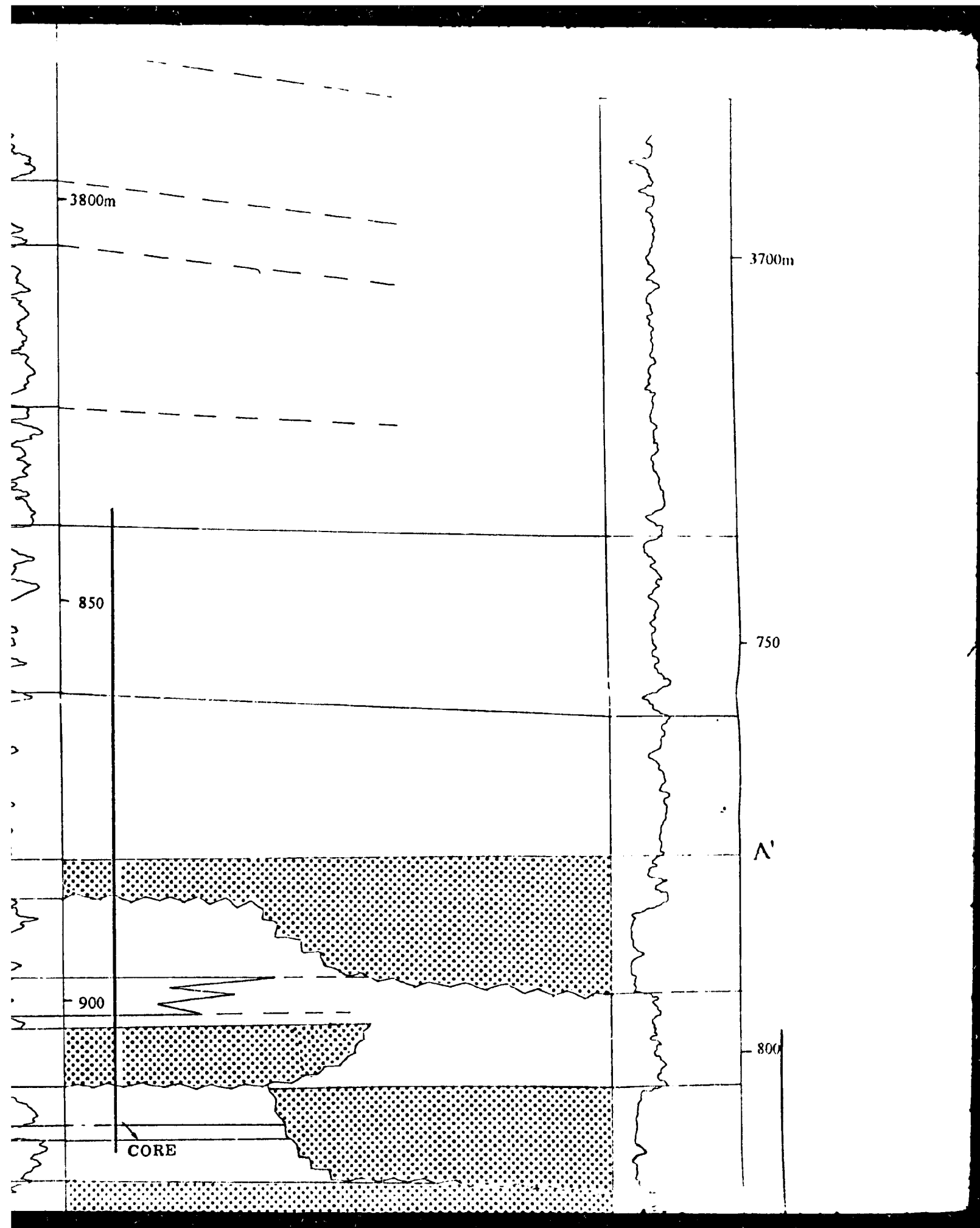


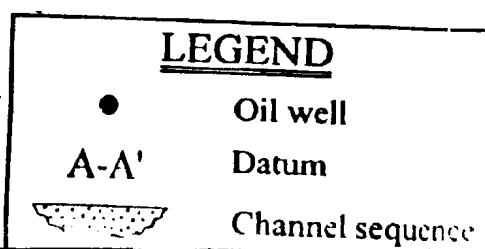
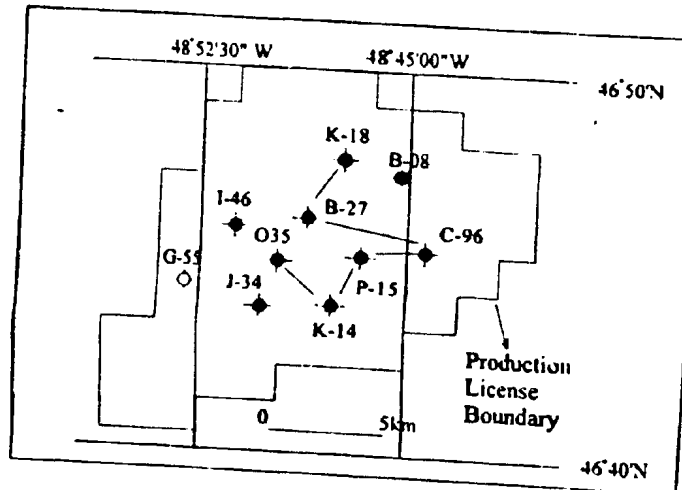
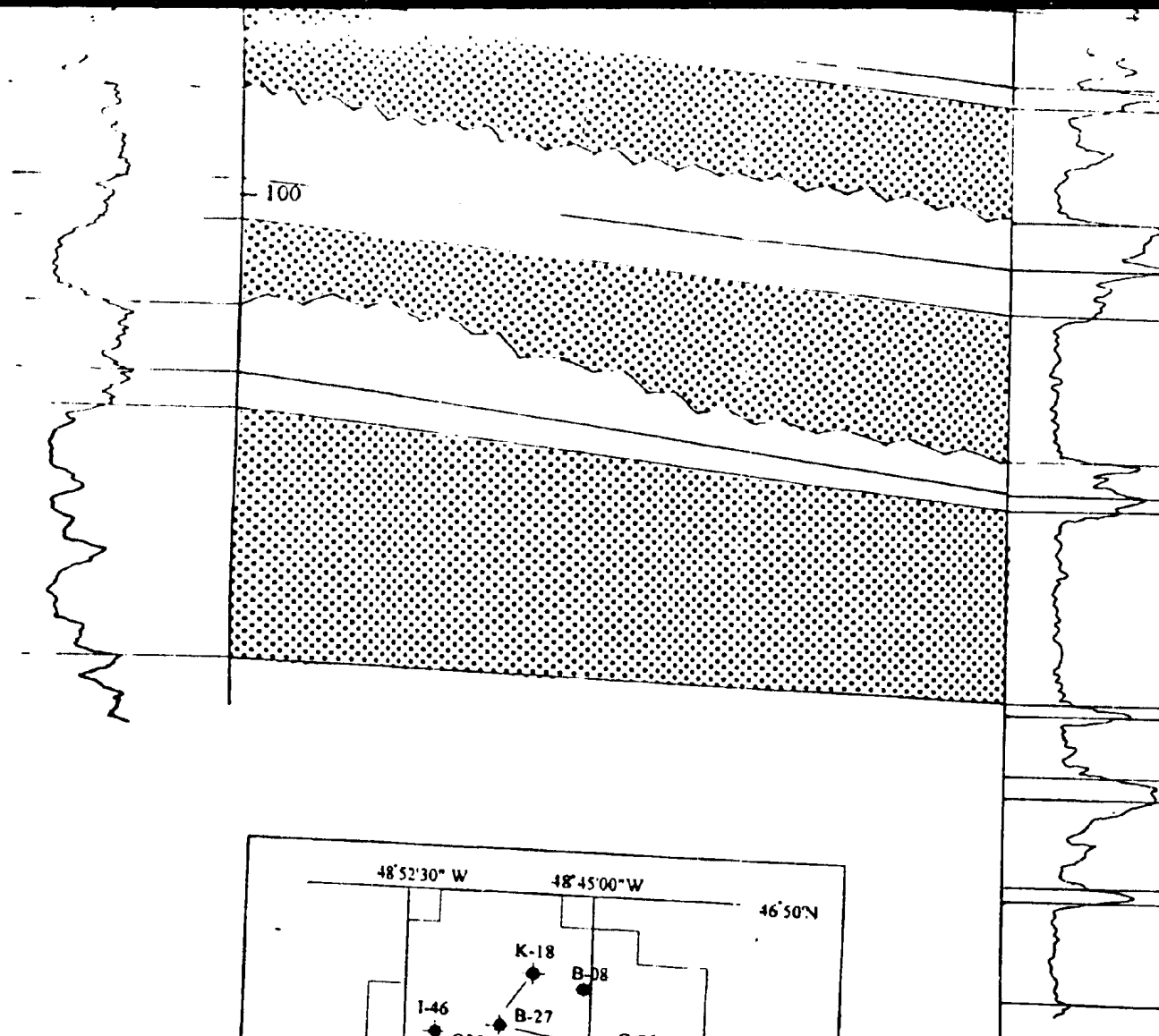


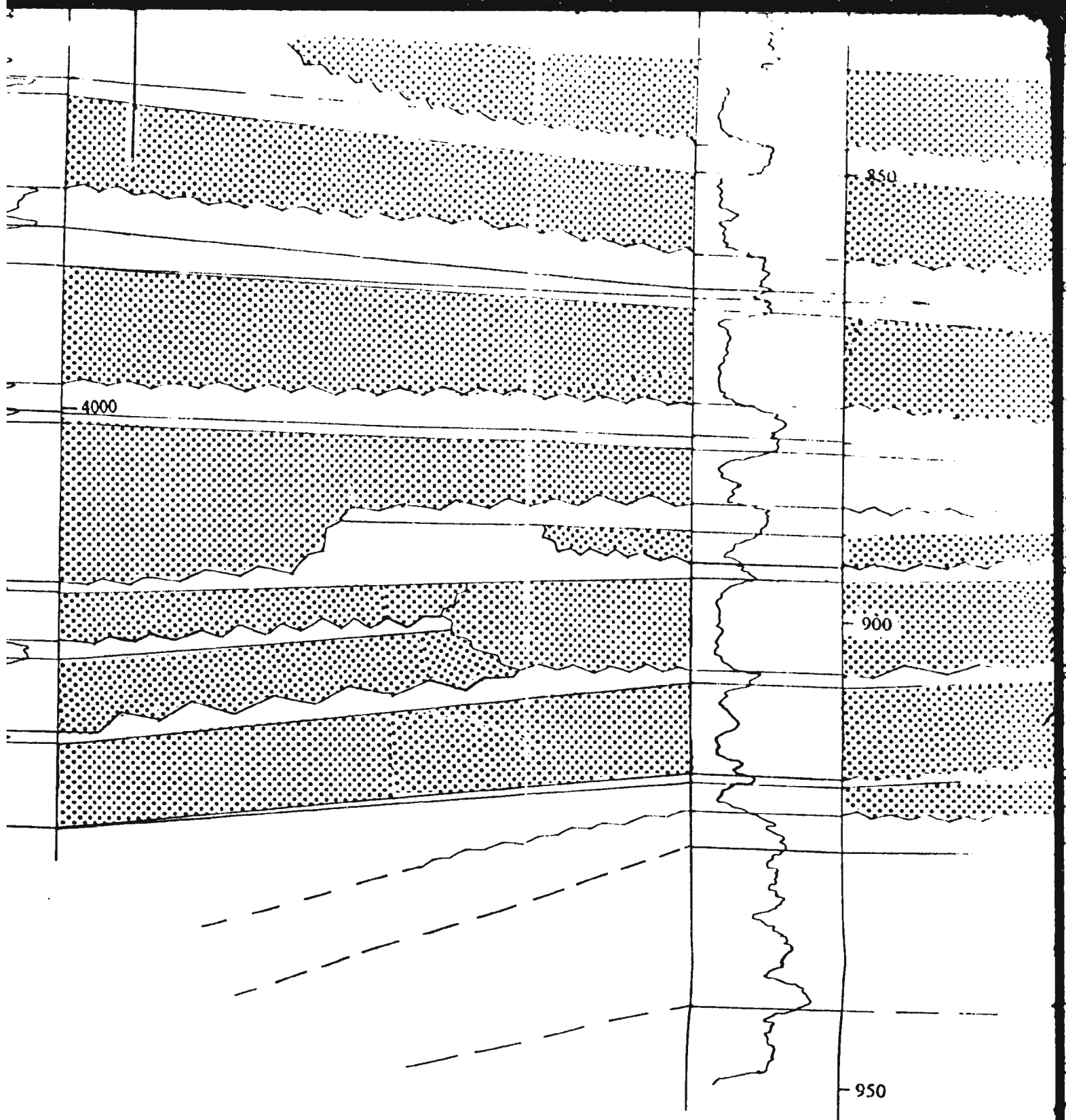




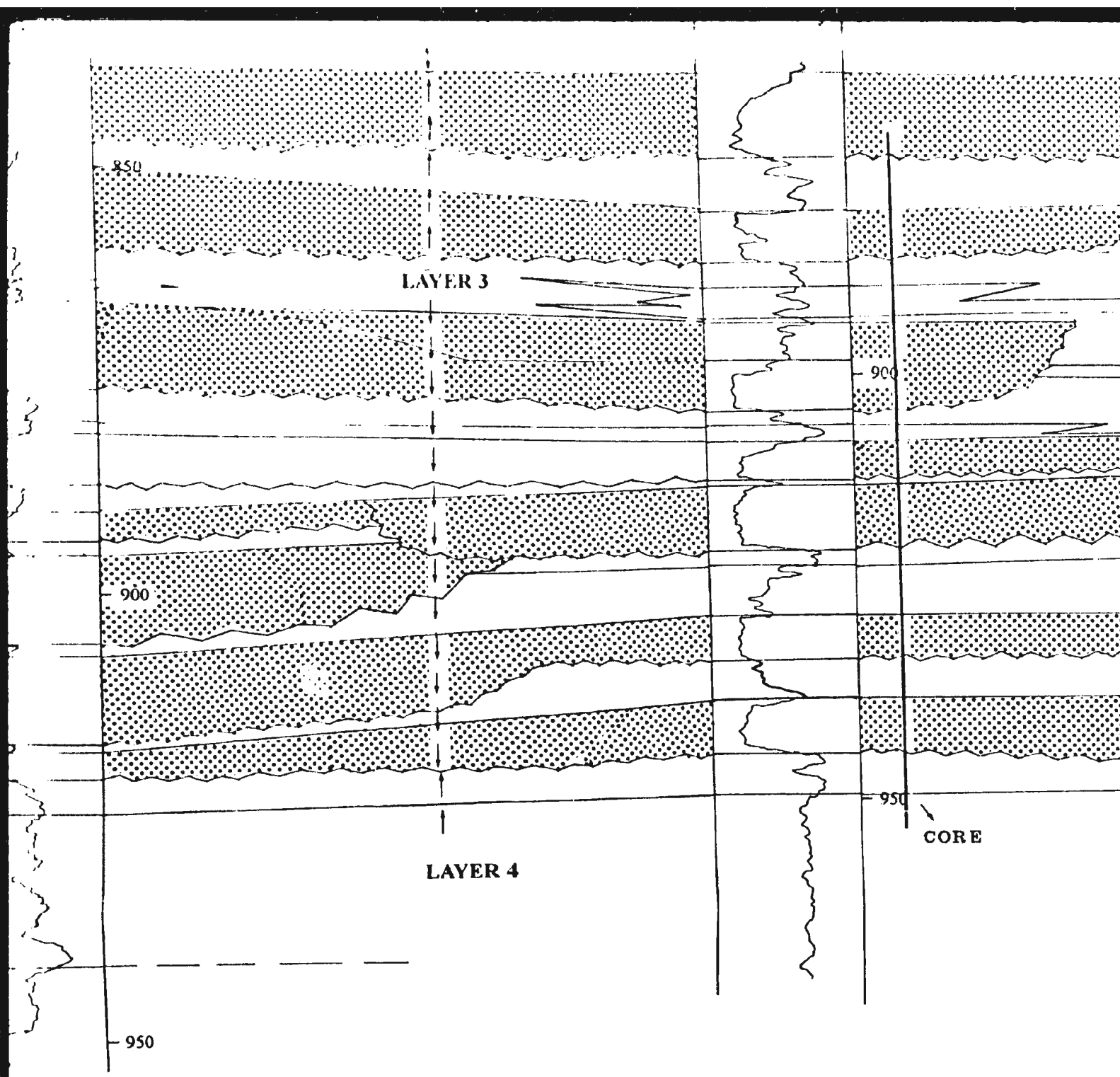




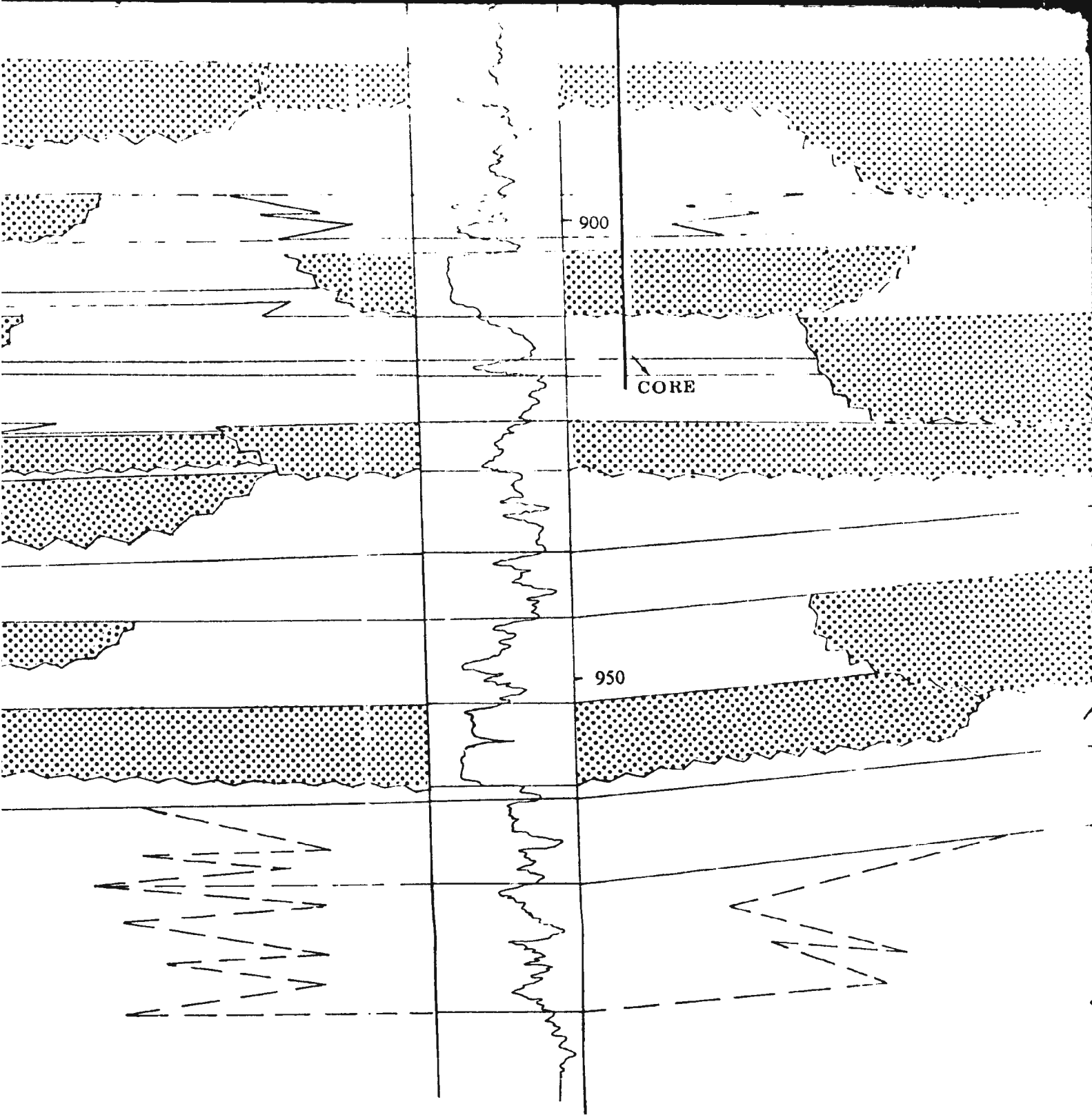




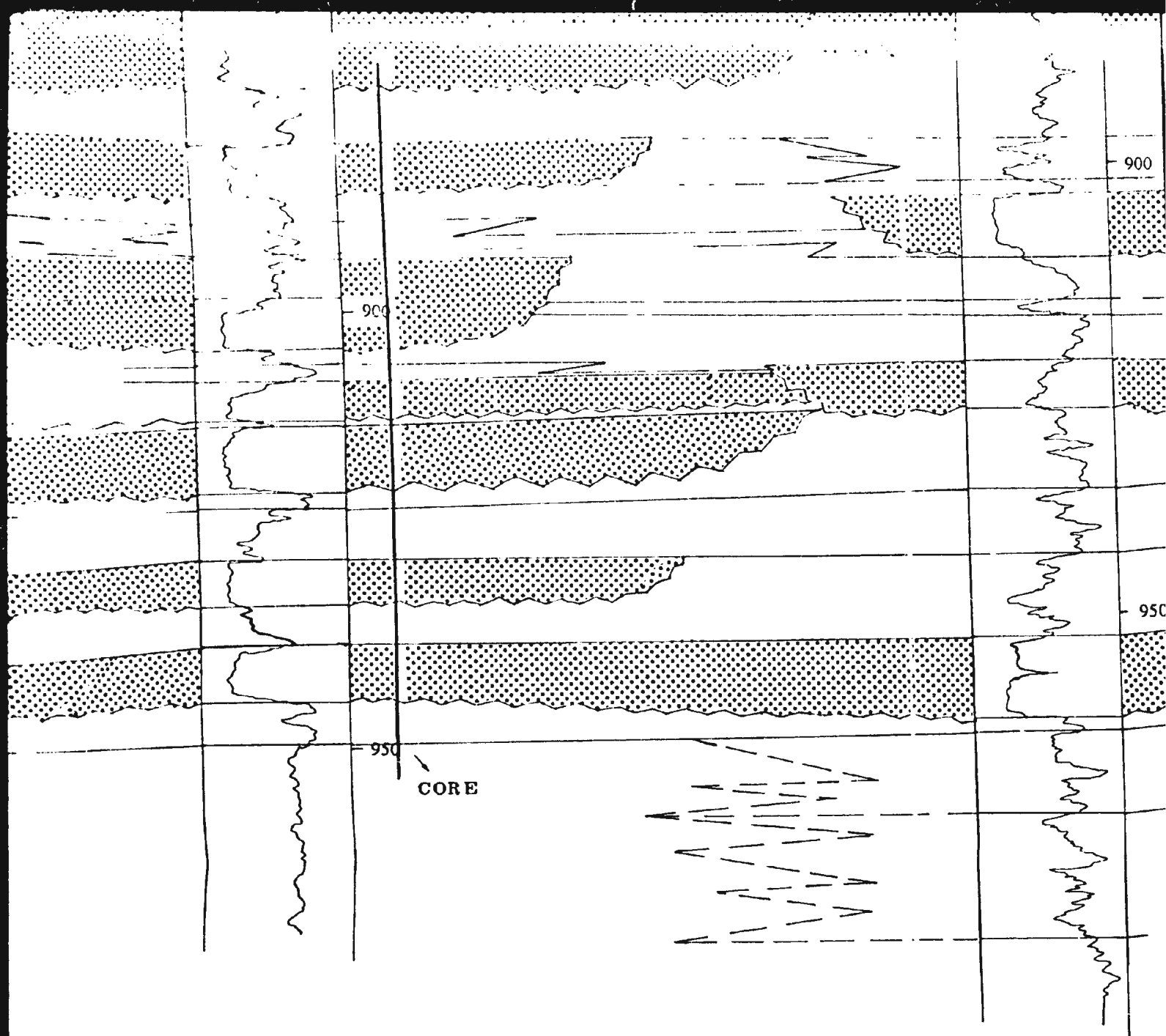
SW-NE CROSS SECTION
HIBERNIA C



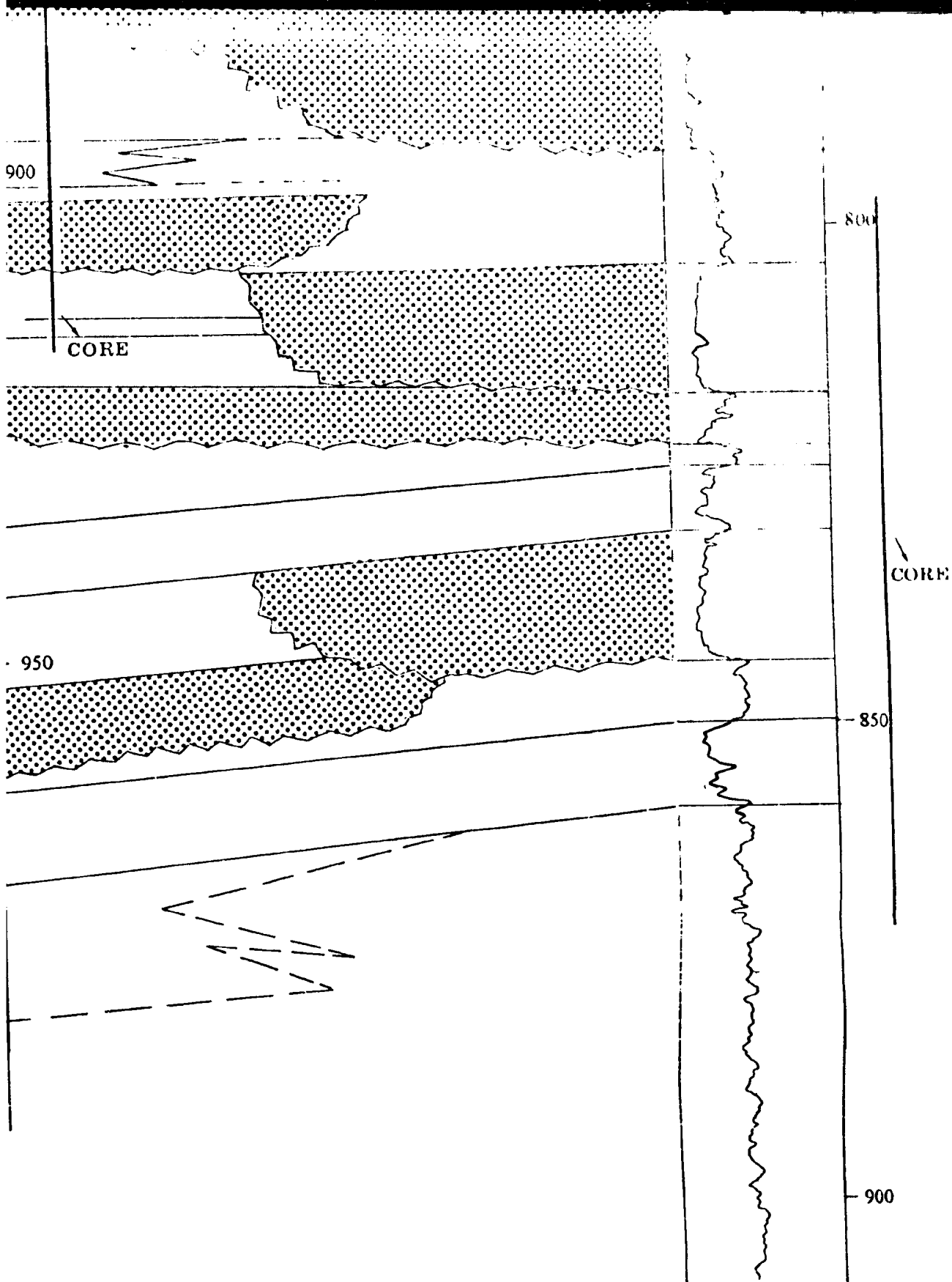
SW-NE CROSS SECTION OF THE HIBERNIA FORMATION
HIBERNIA OIL FIELD, GRAND BANKS



Pocket Enclosure

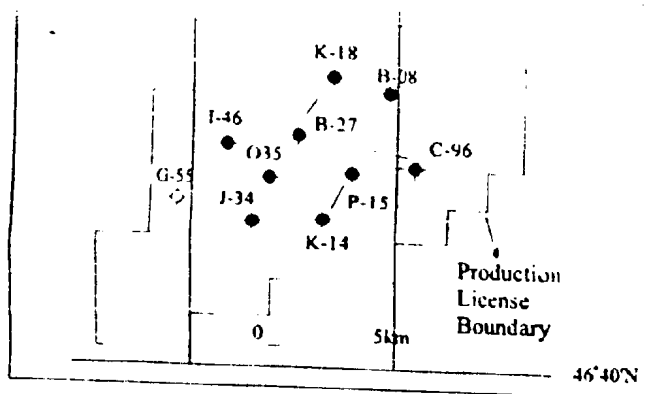


RNIA FORMATION
BANKS

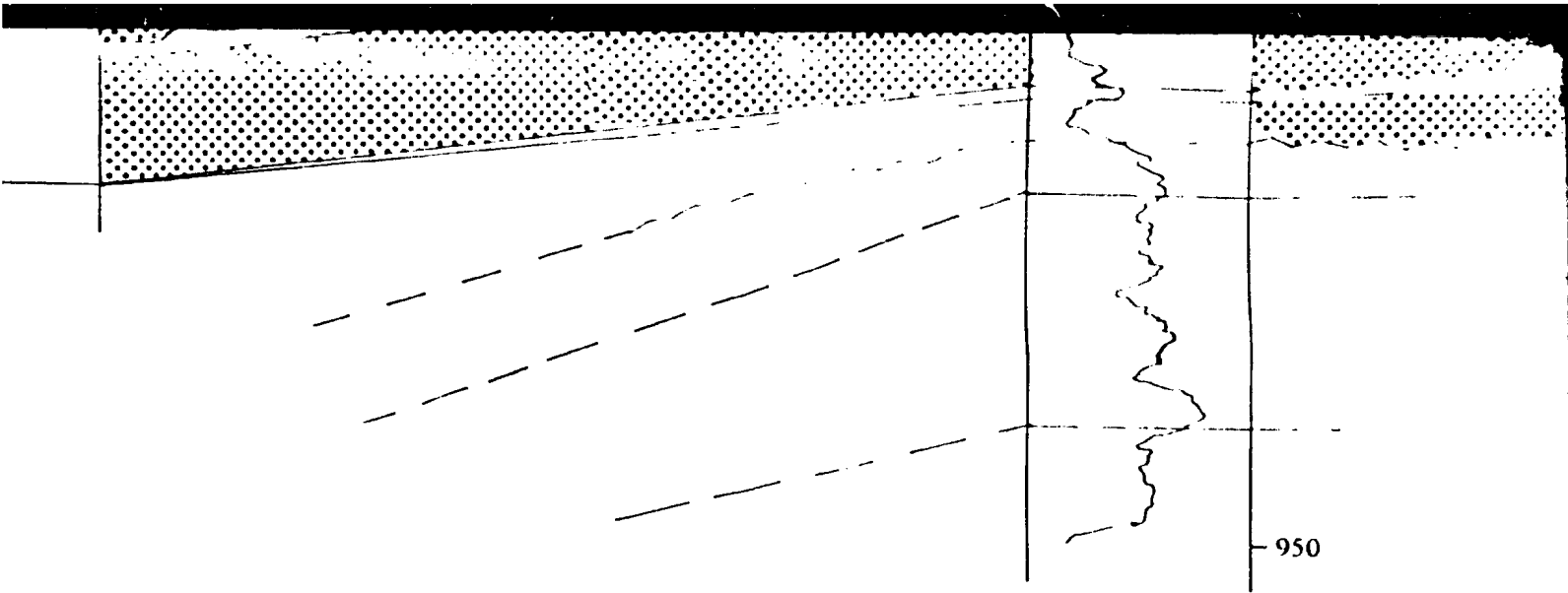


Pocket Enclosure
M.Sc. thesis

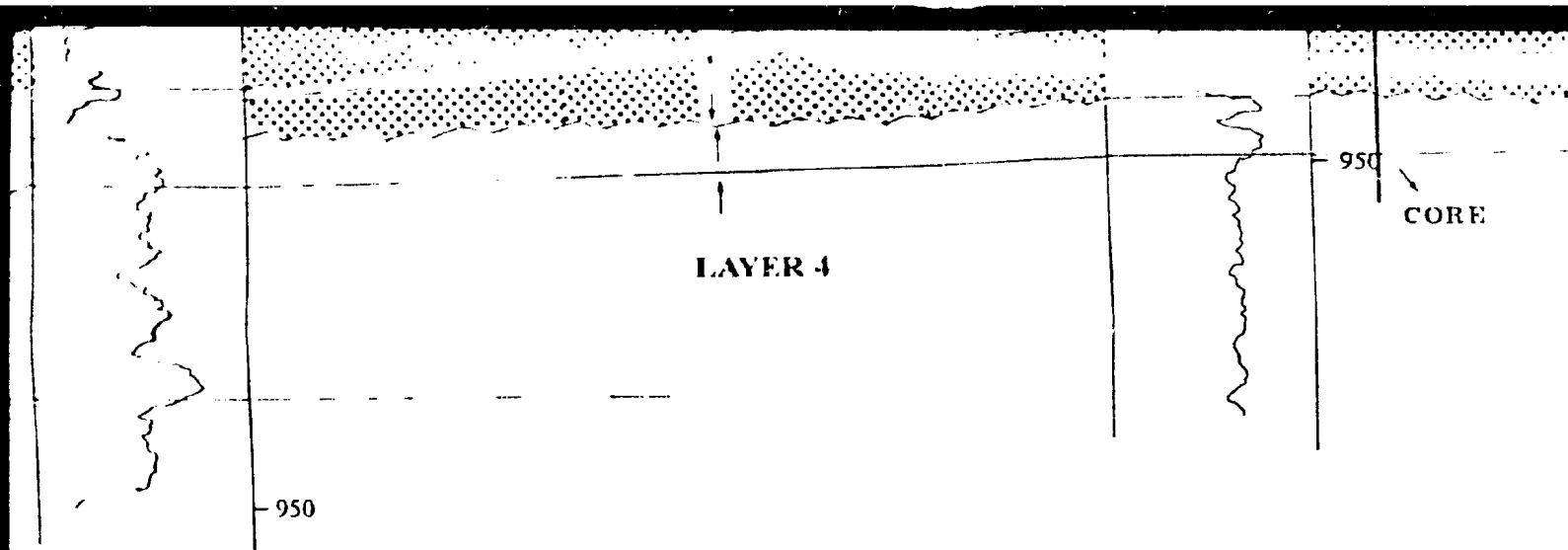
ERKAN ELDAN



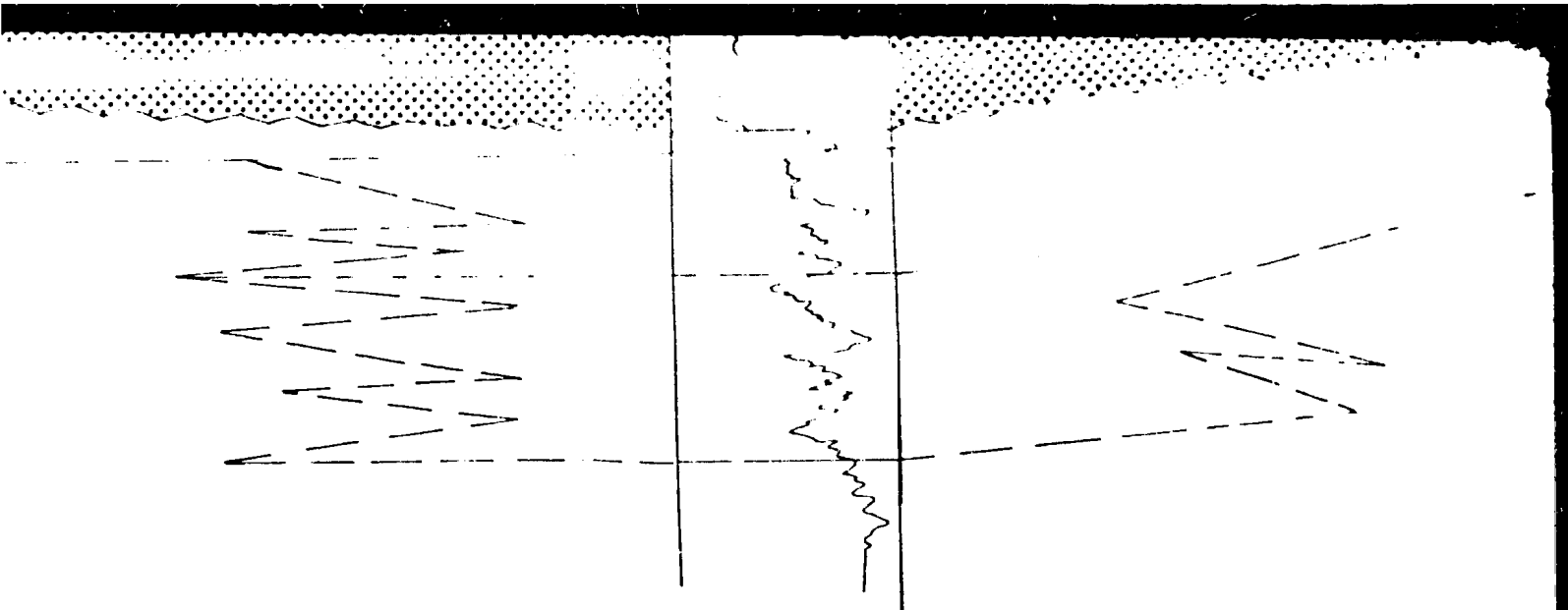
<u>LEGEND</u>	
●	Oil well
A-A'	Datum
	Channel sequence
	Sandstone
Boundaries:	
	Erosional b.
	Sequence b.
	Undefined b.
	Undefined closure
	Defined closure



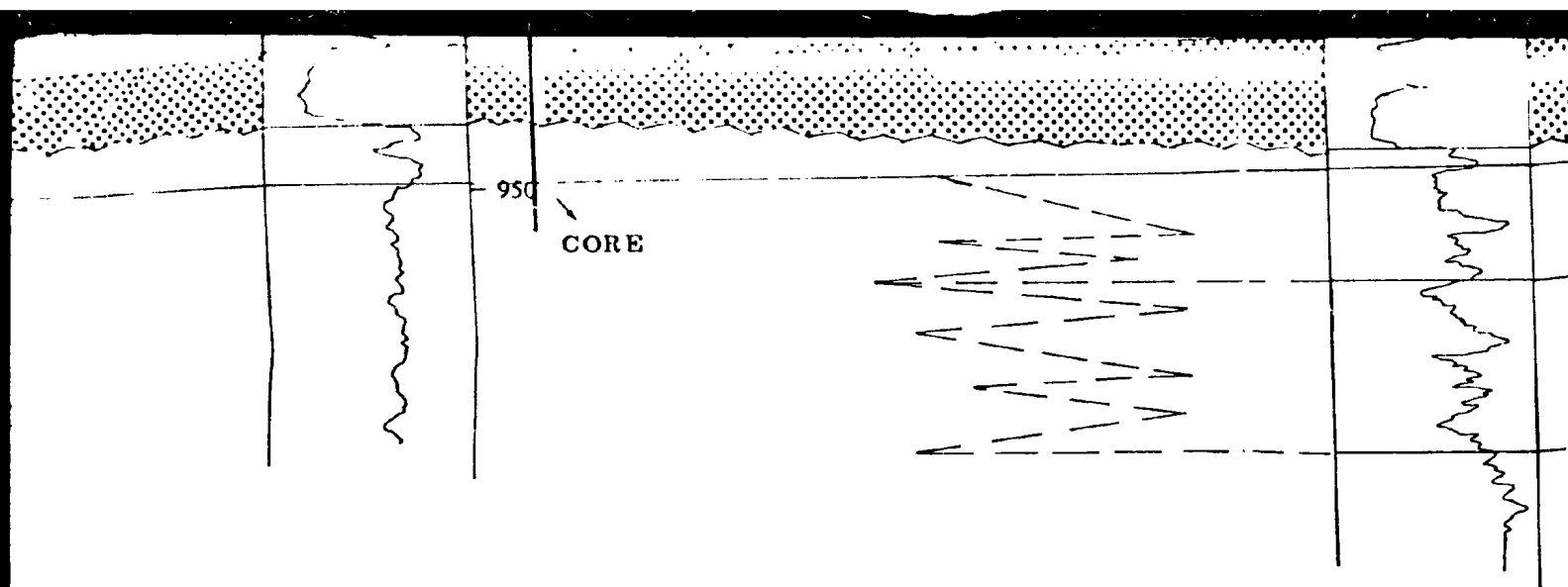
SW-NE CROSS SECTION
HIBERNIA C



SW-NE CROSS SECTION OF THE HIBERNIA FORMATION
HIBERNIA OIL FIELD, GRAND BANKS

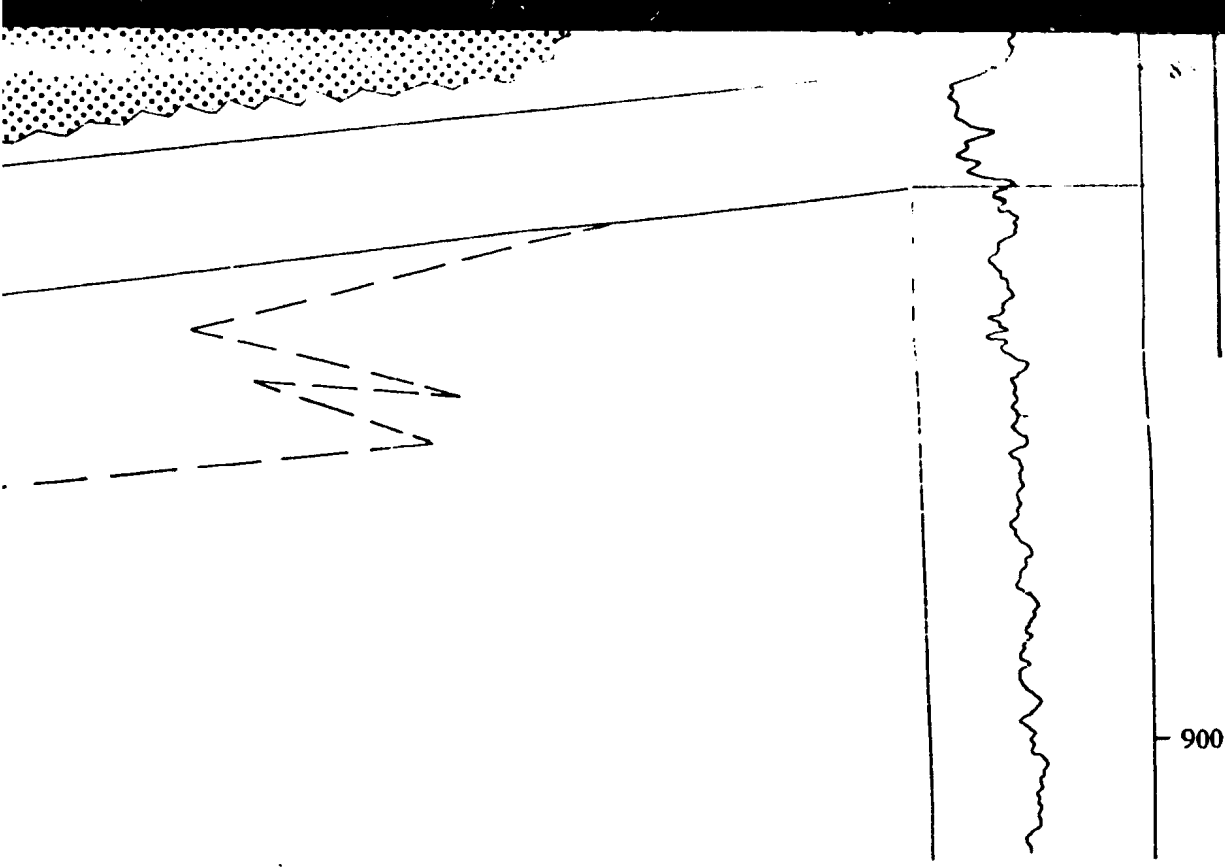


Pocket Enclosure
M.Sc. thesis
ERKAN FIDAN
1996



RNA FORMATION
BANKS

[



Pocket Enclosure
M.Sc. thesis
ERKAN FIDAN
1996

